SWASH: A robust numerical model for shallow water coastal engineering applications

by
Frans van Eeden

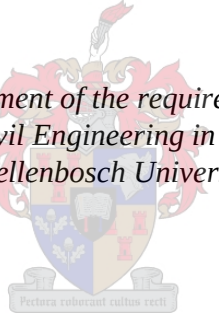

Thesis presented in fulfilment of the requirements for the degree of Master of Engineering in Civil Engineering in the Faculty of Engineering at Stellenbosch University

Supervisor: Prof J.S. Schoonees

March 2017

Declaration

By submitting this thesis electronically, I declare that the entirety of the work contained therein is my own, original work, that I am the sole author thereof (save to the extent explicitly otherwise stated), that reproduction and publication thereof by Stellenbosch University will not infringe any third party rights and that I have not previously in its entirety or in part submitted it for obtaining any qualification.

Date: March 2017

Abstract

SWASH: A robust numerical model for shallow water coastal engineering applications

F. van Eeden

Department of Civil Engineering,
University of Stellenbosch,
Private Bag X1, Matieland 7602, South Africa.

Thesis: M.Eng Port and Coastal Engineering

March 2017

Integral to coastal engineering design is the understanding and analysis of the wave climate at an arbitrary site under consideration. In most cases, these wave climate and extreme conditions are simulated by means of numerical computer models. These models afford the coastal engineer the tools to test a wide range of climatic and extreme conditions applicable to the design. The output from these models is used as input into the design formulas for the various structural elements. However, in order for these numerical models to be reliable, some form of calibration is needed.

The surf zone is an area of coastal engineering that is generally difficult to simulate numerically, as this is a highly dynamic zone with numerous interactive processes. The nature of the surf zone makes collecting calibration data to use in numerical models fairly difficult to nearly impossible. Researchers and coastal engineers turn to laboratory measurements to quantify surf zone processes and to calibrate numerical models.

A non-hydrostatic numerical model SWASH (Simulating WAves till SHore) is analysed in terms of its numerical capability to simulate wave breaking, in particular, spilling and plunging waves.

Laboratory data were made available for calibration purposes. The data describe regular spilling and plunging breakers on plane slopes of 1:20 and 1:35. Water levels and instantaneous horizontal and vertical velocities at various positions pre- and post-wave breaking were measured using particle image velocimetry and laser-Doppler velocimetry.

The laboratory data are used to test the sensitivity of the SWASH model in terms of numerical parameters; i.e. the explicit conservation of momentum, bed friction and various discretisation and interpolation schemes that

influence the stability and accuracy of the numerical model. The sensitivities are compared to the laboratory measured data sets in terms of the incipient breaking point, phase averaged water levels and the phase averaged horizontal and vertical particle velocities.

The results of the sensitivity analysis are subsequently used to test the robustness of the SWASH model by comparing three modes of the SWASH model: a calibrated wave model, an uncalibrated model (using default or recommended parameters) and the hydrostatic front approximation. The three modes are compared to the measured data and to each other in terms of breaker depth index, wave setup, phase averaged water levels and the phase averaged horizontal and vertical particle velocities and modelled turbulence. The root mean squared error is calculated between the model data and the measured data in order to gauge the accuracy of the three modes.

It can be concluded that the SWASH model is capable of numerically representing surf zone processes that can assist the engineer in his designs. In addition, the model performs very well in most areas when an uncalibrated SWASH model is employed with accuracy limited to that of the preliminary design stage.

The SWASH model offers a vivid array of numerical schemes and parameters that can be used for calibration purposes. However, the flexibility of the model does not overshadow the robustness and simplicity with which the model can be set up. Regardless, the model does live up to its claim of robustness and accuracy without specifying external parameters to a preliminary design level. Beyond this design level, proper calibration of the model is necessary before the model results can be utilised in detailed design.

Uittreksel

SWASH: 'n Robuuste numeriese model vir toepassings in kusingenieurswese in vlak water

("SWASH: A robust numerical model for shallow water coastal engineering applications")

F. van Eeden

Departement Siviele Ingenieurswese,
Universiteit van Stellenbosch,
Privaatsak X1, Matieland 7602, Suid Afrika.

Tesis: M.Ing Hawe en Kus Ingenieurswese

Maart 2017

'n Deel van kusingenieursontwerp is die begrip en ontleding van die golfklimaat van toepassing op 'n bepaalde terrein onder oorweging. In die meeste gevalle word hierdie golfklimaat en uiterste toestande gesimuleer met behulp van numeriese rekenaarmodelle. Hierdie modelle laat die kusingenieur toe om 'n wye verskeidenheid van klimaatstoestande en uiterstes van toepassing op die ontwerp te toets. Die uitvoer van hierdie modelle word gebruik as insette in die ontwerpformules vir die verskillende strukturele elemente. Ten einde die resultate van hierdie numeriese modelle te vertrou, is 'n vorm van yking nodig.

Die brandersone is 'n studiegebied van kusingenieurswese wat oor die algemeen moeilik is om numeries te simuleer omrede dit 'n baie dinamiese gebied met talle interaktiewe prosesse bevat. Die aard van die brandersone maak die meting en versameling van ykingsdata om te gebruik in numeriese modelle baie moeilik of selfs bykans onmoontlik. Navorsers en kusingenieurs moet hulle dus wend na laboratoriummetings om die brandersone-prosesse te kwantifiseer en die numeriese modelle te kan yk.

'n Nie-hidrostatiese numeriese model SWASH (Simulating WAves till SHore) word ontleed in terme van sy numeriese vermoë om golfbreking te simuleer, spesifiek met betrekking tot rollende- en plonsende branders.

Laboratoriumdata vir yking is beskikbaar gemaak. Die data beskryf reëlmatige rollende- en plonsendebranders wat oor reëlmatige hellings van 1:20 en 1:35 beweeg. Watervlakke en oombliklike horisontale en vertikale snelhede by

verskeie posisies voor- en na golfbreking is deur "Particle Image Velocimetry" en "Laser Doppler Velocimetry"-tegnieke gemeet.

Die laboratoriumdata word gebruik om die sensitiwiteit van die SWASH-model in terme van numeriese verandelikes te toets; met betrekking tot die eksplisiete behoud van momentum, bodemwrywing en verskeie diskretisasie- en interpolasieskemas wat die stabiliteit en akkuraatheid van die numeriese model beïnvloed. Die sensitiwiteit van die model word vergelyk met die laboratorium-gemete datastelle in terme van breekpunt, fase-gemiddelde watervlakke en die fase-gemiddelde horisontale en vertikale snelhede.

Die resultate van die sensitiwiteitsontleding is gebruik om die robuustheid van die SWASH-model te toets deur dit te vergelyk met drie tipes SWASH-modelle: 'n "geykte" golfmodel, 'n "ongeykte" model (met behulp van standaard of aanbevole veranderlikes) en die "hidrostatic front approximation". Die drie tipes word vergelyk met die gemete data en met mekaar in terme van brander indeks, golfopstuwing, fase-gemiddelde watervlakke en die fase-gemiddeld horisontale en vertikale snelhede en turbulensie. Die standaardafwyking is bereken tussen die modeldata en die gemete data ten einde die akkuraatheid van die drie tipes modelle te meet.

Dit kan afgelei word dat die SWASH-model in staat is om numeries brandersone prosesse te simuleer wat die ingenieur in sy ontwerpe kan help. Daarbenewens presteer die model baie goed in die meeste gebiede wat getoets is. Die ongeykte SWASH-model kan gebruik word met 'n akkuraatheid wat tot diè van die voorlopige ontwerp-stadium beperk is.

Die SWASH-model bied 'n wye verskeidenheid van numeriese skemas en veranderlikes wat vir ykings doeleindes gebruik kan word. Dit oorskadu egter nie die robuustheid en eenvoud waarmee die model kan opgestel en gebruik word nie. Ongeag, die SWASH-model bewys sy aanspraak van robuustheid en akkuraatheid sonder om eksterne ykingsveranderlikes hoef in te voer; natuurlik is die aanspraak geldig op 'n voorlopige ontwerp-vlak. Vir detailontwerp is behoorlike yking van die model nodig voordat die modelresultate kan gebruik word.

Acknowledgements

I would like to express my sincere gratitude to the following people and organisations:

To my employer WSP | Parsons Brinckerhoff for the sponsorship to read for this degree and the financial support that made it possible. I would especially like to thank Andre van Tonder and Geoff Smith who gave valuable advice and supported me in this effort.

To the following researchers that made their data available to use in this study:

Dr. Kessie Govender, Dr. Francis Ting and Dr. James Kirby, Dr. Marien Boers and Dr. Raphael Mukaro for sharing their valuable data for this study. Without the data sets graciously provided by these gentlemen, this study would not have been possible.

Dr. Marcel Zijlema who graciously attended to my queries regarding SWASH.

Dr. Schoonees for his guidance and advice. Thank you for always having a paper and some advice available that can point me back to a path paved with sanity.

A hat-tip to the open source community. This study was produced with TeXstudio, SWASH and SciLab. SWASH source code was compiled on CAE Linux.

My father for all his support on my road to get to this point. I did not always take the quickest or easiest route. Your patience is appreciated. I am forever indebted for all you have done.

To my wife for your patience and help in getting all these words, pictures and numbers to type. To my son for constantly reminding me about the important things in life.

To my Lord and Saviour Jesus Christ for His gift of grace and mercy in my life.

Dedications

This thesis is dedicated to my family.

Contents

List of Figures

List of Tables

Nomenclature

Abbreviations

2DV	2-Dimensional including Vertical
BDF	Backward Differencing Scheme
BDS	Backward Upwind Differencing Scheme
CDS	Central Differencing Scheme
CFL	Courant Friedrichs Lewy
CSIR	Council for Scientific and Industrial Research
FIR	First Order Upwind
HFA	Hydrostatic Front Approximation
LDA	Laser Doppler Anemometry
LDV	Laser Doppler Velocimetry
PIV	Particle Image Velocimetry
RMSE	Root-Mean-Squared Error
SWASH	Simulating Waves Till Shore
SWL	Still Water Level
TKE	Turbulent Kinetic Energy

Chapter 1

Introduction

1.1 General

The surf zone is an extremely dynamic area of the ocean. The science and dynamics of the surf zone have been studied for several decades (i.e. Longuet-Higgins and Cokelet (1976)) and many attempts have been made to mathematically describe these dynamic interactive processes that occur in the surf zone. These include the dynamic interaction of the surf zone with the land (shoreline) in the form of sediment transport, solitary wave breaking, the formation of rip currents, longshore wave-driven currents and much more. The accurate prediction of these dynamic and often chaotic processes enables the coastal engineer to make more accurate assumptions in terms of his design parameters which, in turn, result in safer, more cost-effective designs. In order to test a range of nearshore design parameters, the engineer will simulate the offshore and nearshore processes with physical and/or numerical models. In most cases, numerical models are used.

Many types of numerical models exist that are suited to a particular application; e.g. Delft3D-FLOW (WL|Delft Hydraulics, 2014), which is a hydrodynamic model and specifically excludes waves. However, numerical models normally need some form of calibration in order to make reliable predictions. The calibration process mainly involves the specifying and tuning of mathematical constants to make the numerical model results fit the recorded physical data under similar input parameters.

Calibration becomes even more difficult in the surf zone where the unpredictability of depth-induced wave-breaking processes dominates (Zijlema (2014), Chang and Liu (1999) and Christensen *et al.* (2002)). Although not impossible, accurately describing the surf zone in terms of depth-limited wave breaking without any calibration data is very difficult.

In recent years, non-hydrostatic wave models have been developed which have been released for general use (e.g. SWASH (Zijlema *et al.* (2011)) and NHWave which is based on the work of Ma *et al.* (2012)). In theory, these mod-

els are robust in nature and numerically resolve depth-induced wave breaking without external parameters having to be specified (Smit, 2014).

However, more work is needed to quantify this statement. This thesis proposes to investigate the robustness of the non-hydrostatic wave model SWASH in simulating wave shoaling and breaking in the surf zone, which is one of the driving forces of sediment transport and pollution advection, dissipation and transport in the nearshore zone.

1.2 Problem setting

To enable coastal engineers to design solutions for given engineering problems sufficiently and economically, a list of physical variables needs to be quantified and used as input into the design. In a significant number of engineering applications, the interaction of the surf zone with the land is of importance. This implies that the evolution of the waves in the surf zone, from deep water to shoaling to breaking to the dissipation in the swash zone, is important to understand and quantify in a way that can be useful in engineering design. In addition, deep water wave data is more readily available than nearshore data. It is thus up to the design engineer to transform the offshore, deep water waves to the nearshore to determine the nearshore wave characteristics that are needed as input design parameters.

Tools for simulating nearshore depth-induced wave-breaking within the realm of coastal engineering/science include physical scaled models (e.g. flume or 3D basin tests), various wave theories (e.g. Stokes, Cnoidal, Solitary, Snell's law etc.) and numerical models. Although physical modelling is a brilliant method to study wave behaviour in a controlled environment, the time it takes to build the models and the high cost involved makes this solution unattractive, especially at concept and preliminary design stages. Hughes (1993), however, argues that physical models are cost effective given the scale of coastal engineering projects, but in the same breath also concedes that numerical tools are the first choice when the numerical results can be trusted with engineering accuracy.

The Coastal Engineering Manual (USACE, 2002) provides analytical techniques and methods for the design, formulation and expected performance outcomes of a broad range of environmental, structural and coastal processes for coastal engineering projects. Many wave-breaking theories (McCowan (1891), Goda (1970), Weggel (1972), Komar and Gaughan (1973) and Smith and Kraus (1991)) are presented, along with their limitations and applications to practical problems in coastal engineering science.

First and foremost, a sufficient understanding of the physical coastal processes is required. All research conducted in the field and in the laboratory contributes to the translation of the dynamic interaction of these processes into the mathematics that forms the back end of numerical models.

Numerical models in coastal engineering have benefited from many advances in understanding and incorporating the numerous physical processes and phenomena that occur in the surf zone. Cavaleri *et al.* (2007) divide the advancement of numerical modelling into two time frames: a period of great and rapid advancement at the beginning of a science (i.e. developing a numerical model) and a period where the focus falls on the application of the newly developed tools resulting from the "new" science.

This study falls into the former category of the two postulated by Cavaleri *et al.* (2007). Although the Navier-Stokes equations for shallow water flow have been around since the 1800s, the numerical tools needed to solve these equations efficiently only came with time. The advancement of numerical models is also a function of the advancement of technology and in particular the increase in computing speed and power. As computers become faster and more powerful, the relative sizes of the models increase (e.g. smaller grid cells means an increase in the number of grid points and thus an increase in the number of computational points).

Numerical simulations of the coastal processes can greatly aid in the design process, provided their limits in terms of application and numerical formulation (i.e. the equations, solvers and numerical schemes) are well understood by the engineer. However, as stated previously, calibration data is essential to verify the validity and reliability of the numerical model.

Various numerical models exist that simulate wave breaking. The models of Schäffer *et al.* (1993), Battjes and Janssen (1978), Battjes and Stive (1985) and Battjes and Groenendijk (2000) are the most well known; for instance, the roller model of Schäffer *et al.* (1993) is used in the DHI Mike21 Boussinesq model. A common feature of these wave breaking models is the requirement that a range of parameters is needed to numerically induce wave breaking and simulate the wave breaking energy loss in the model. This implies that the roller model must be calibrated before reliable numerical results are obtained.

Obtaining calibration data in the surf zone is practically very difficult. In the last 20 years, laboratory techniques like Particle Image Velocimetry and Laser-Doppler Velocimetry have been developed that can measure the velocity and turbulence structures of waves in the surf zone in the laboratory. The engineer is now faced with the problem of obtaining surf zone parameters in the laboratory that can be used as calibration data for the numerical model and the way in which the laboratory measurements relate to the prototype design.

1.3 Objectives of this study

The developers of SWASH (The SWASH Team, 2016) claim that

> "On the one hand, it [SWASH] provides numerical stability and

> robustness, and on the other hand it gives accurate results in a reasonable turn-around time."

In addition, Smit (2014) claims that

> "...with a sufficiently high vertical resolution non-hydrostatic models can properly determine the dissipation of breaking waves without additional model assumptions."

It is the objective of this thesis to compare the physical process of wave evolution in the surf zone (shoaling, breaking and energy dissipation through the roller) measured in the laboratory to results obtained by the numerical simulation model SWASH (Zijlema *et al.*, 2011). SWASH model results will be compared with laboratory data from peer reviewed published sources for this study. The main objectives of this study can be summarised in the following points:

1. Investigate the applicability, correlation and shortcomings of the numerical model SWASH for coastal engineering applications in the nearshore (shoaling / surf zone / swash zone) by comparing SWASH to breaking wave laboratory measurements.

2. Compare and analyse calibrated and uncalibrated results calculated by the SWASH models in the context of wave processes (energy, velocity, breaking, water levels, etc.) in the nearshore, especially in the surf zone (pre- and post-wave breaking), with the aim to quantify the error between the uncalibrated and calibrated models.

1.4 Areas of investigation

The following specific processes are investigated and analysed in this study:

- Wave height evolution: the wave height is compared as it shoals from deep water to the point of breaking and through the roller formation;

- Wave breaking: the point of incipient breaking is analysed and the factors that influence it. The SWASH model is analysed for the difference in spilling and plunging breakers as the data allows;

- Wave velocity: the internal wave velocity (phase velocity, particle velocity and turbulence velocities/intensities are compared; and

- Wave turbulence: the turbulence modelled by SWASH are compared with the results obtained from the physical experiments.

1.5 Data sets used

Two data sets were analysed for this study with each data set containing two types of waves; plunging and spilling breakers. The experimental methods and outcomes are described in the corresponding papers listed in Table 1.1.

Table 1.1: Laboratory data used in this study and the main researchers and their corresponding publications

Main Researcher(s)	Publications	Type of publication
K. Govender	Govender (1999)	Ph.D Thesis
F. Ting and J. Kirby	Ting and Kirby (1994); Ting and Kirby (1995); Ting and Kirby (1996)	Peer reviewed research articles (*Coastal Engineering*)

1.6 Organisation of study

This thesis is organised as follows:

Chapter 1 sets the background, aim and expected outcomes of this study;

Chapter 2 contains a literature review of the relevant physical surf zone processes;

Chapter 3 is a literature review of the SWASH numerical model with focus on the mathematical equations and some of the numerical schemes employed that are relevant to the surf zone;

Chapter 4 describes various laboratory measurement techniques, the physical model setup, measurement data sets, the parameters tested and the reported outcomes of the physical model data used in this study;

Chapter 5 tests and describes the sensitivity of various calibration parameters of the SWASH model. The outcomes of these tests inform the model parameters that test the accuracy the SWASH model in Chapter 6;

Chapter 6 The SWASH model is tested for accuracy by investigating and quantifying the relative error between the physical model data and a "calibrated" model, an "uncalibrated" model (assuming default parameters) and a hydrostatic front approximated SWASH model.

Chapter 7 concludes this study and reflects on the objectives set here and the realisation of these objectives.

Chapter 2

Shallow Water Hydrodynamics

2.1 General

This chapter looks at the physical surf zone processes as the wave enters shallow water and the turbulence phenomena produced by solitary breaking waves.

2.2 Water-wave kinematics and hydrodynamics

The waves seen breaking in the nearshore by the casual observer is just one of many types of waves found in the ocean. In a very general way, ocean waves can be described as the vertical motions of the ocean surface (Holthuijsen, 2007).

This study concerns itself with waves found in the ocean and focusses on waves found in the nearshore breaker zone.

Various types of waves are found in the ocean and the main distinguishing factor between them is the wave period. The various types of waves are summarised by Holthuijsen (2007) as follows:

1. Tides: The typical wave period is between twelve and twenty four hours. The waves are generated by the interaction between the earth, the moon and the sun.

2. Surges: The typical wave period is slightly less than the tidal wave period. Waves are generated by large scale storm effects on the water level (e.g. barometric pressure variation and/or severe winds).

3. Tsunami: These waves have a typical wave period of minutes and are produced by sudden tectonic shifts or massive landslides into the nearshore which produces an immediate large disturbance or shock to the water.

4. Seiches: Seiches are resonances found mainly in closed basins (e.g harbour basin) where the wave frequency is equal to the resonance frequency of the basin.

5. Infra-gravity waves: These have wave periods in the order of minutes and form as a result of groups of wind waves. These waves can be bound to a group of surface gravity waves, or, free travelling. The periods of these waves are in the order of minutes.

6. Wind generated surface gravity waves: These waves have periods typically less than 30s. Two forms of wind-generated waves exist:

    - Wind waves (sea): these waves are local waves generated by the local wind (peak period between 8s and 5s). They are short crested and irregular in frequency; and
    - Sea swell: these are waves that were generated by winds far offshore and continuously propagate over large distances. These waves are more regular, occur in wave groups and have typical periods of between 12s and 30s.

The process of the wind-generated surface gravity waves, the concept of depth-limited breaking and dissipation of energy will be discussed in the next section.

2.3 Wave formation

Waves are generated off-shore in deep water through wind that blows over a distance (fetch) for an amount of time. The shear stress of the surface water, disturbed by the wind, transfers energy into the water in the form of waves. The longer the wind blows, the more energy is transferred into the waves until fully developed seas are formed, as schematised in Figure 2.1. These waves can travel enormous distances without significant loss of energy due to the absence of anything interfering with its energy propagation (Dean and Dalrymple, 2001).

"Waves of permanent form" are waves that propagate in a uniform depth without deformation (Isobe, 2013). These "permanent form" waves travel long distances until it eventually encounters obstacles (e.g. land mass) which will transform the wave in some manner.

2.4 Wave propagation and shoaling

When the travelling swell waves approach a land mass, the water depth becomes less as the sea bottom slopes towards the land boundary, the influence of the bottom geometry (bathymetry) becomes apparent and pronounced. As soon as a significant depth is reached by the particular wave, its form (wave height, period, velocity, etc.) starts to change due to the influence of the depth and friction with the sea bottom on the propagating wave energy. As the wave

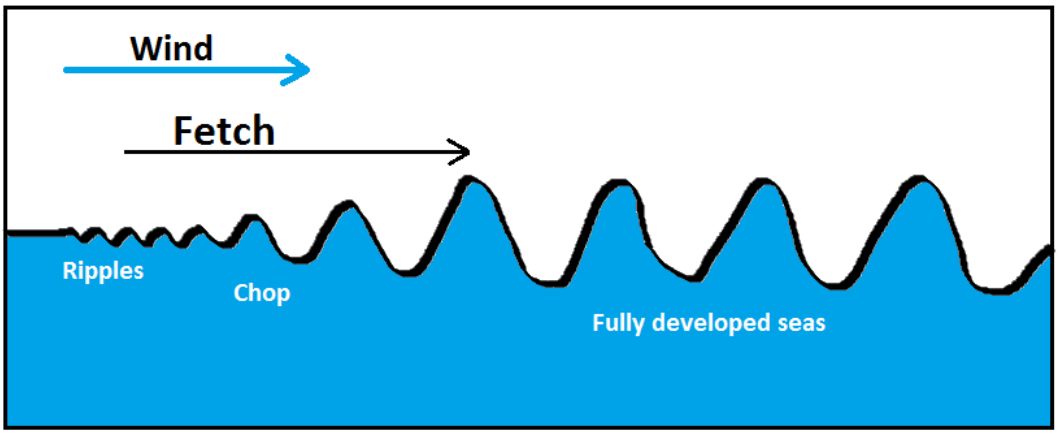

Figure 2.1: Schematic of the development of wind gravity waves in a wind fetch area

enters into shallower water, friction between the wave particle energy and the sea bottom causes the wave to slow down, the oscillatory motion of the wave particles become more asymmetric and the wave face becomes steeper (shoaling) and break due to the wave front becoming unstable (USACE, 2002). This process is illustrated in Figure 2.2.

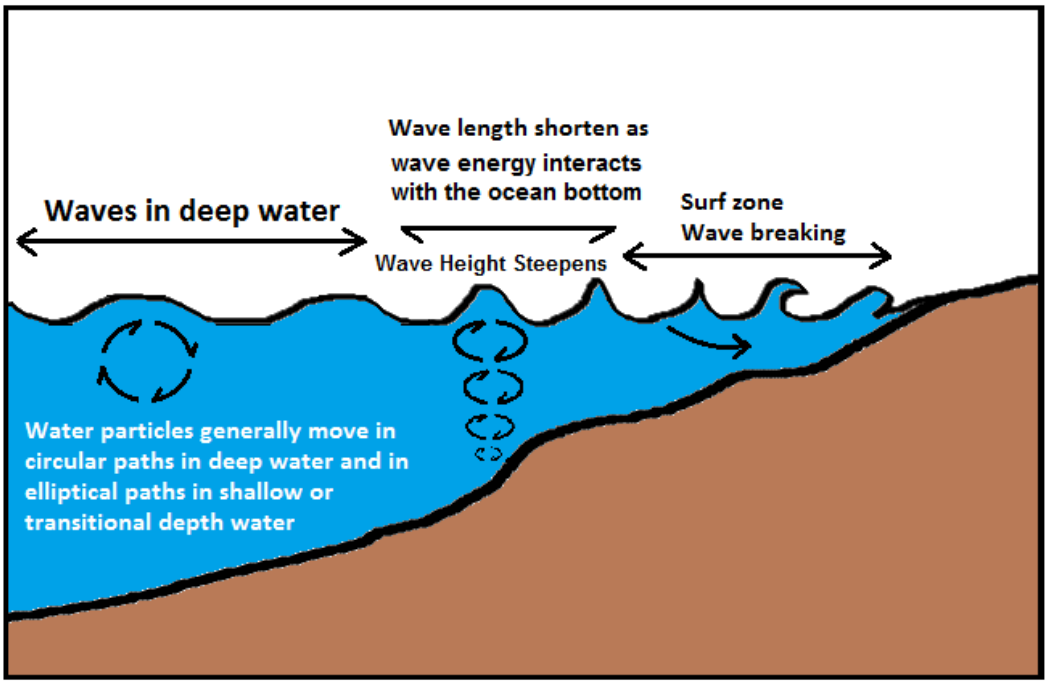

Figure 2.2: Schematic of the wave transformation process as the wave progresses from deep water into shallow water and eventual wave breaking

In most cases, the face of the shoaling wave becomes steep enough so that the momentum causes the crest of the wave to overtake the wave face and the wave pitches forward and breaks. This manifests itself in either an explosive overturning motion that impacts on the water surface in front of the face (plunging waves) or the wave crest rolls down the face of the wave, causing the wave to become turbulent (spilling waves). Figure 2.3 shows examples of a spilling wave and a plunging wave.

Figure 2.3: Photographs of a spilling wave (left panel) and a plunging wave (right panel)

The main variable responsible for the wave transformation from a particular shape offshore up to the point of breaking is the water depth. The wave height is both limited to the water depth (d) and the wavelength (L) of the propagating wave. Water waves are classified based on the relative depth criterion d/L (USACE, 2002):

1. Deep Water: $d/L \geq 0.5$
2. Intermediate depths: $0.5 < d/L \leq 0.05$
3. Shallow water: $d/L < 0.05$

It needs to be emphasised that "deep", "intermediate" and "shallow" must be interpreted in the context of water depth in conjunction with the wave length; i.e. "deep" water refers to water depths which are large relative to the wavelength.

2.5 Wave breaking

Basco (1985) characterises the wave-breaking process as water particles that move from irrotational to rotational and results in a turbulent bore consisting of various scales of turbulent flow.

For every wave travelling from deep water to shallow water, a limiting period and/or water depth exist where a wave will become unstable and break. The wave-breaking height is a function of the wave length in deep water and a function of both wave length and depth in shallow water (USACE, 2002).

Waves may break in the surf zone, continue through the surf zone as rollers and eventually dissipate in the swash zone.

In order to successfully evaluate a numerical model that models wave breaking, it is important to understand the onset of wave breaking and the factors that influence this process.

2.5.1 Process of wave breaking

The non-linear process of wave breaking in shallow water occurs when the wave steepness (H/L) reaches a limit that is dependent on the relative depth (d/L) and the beach slope. As a wave approaches an area where the bathymetry becomes shallower (either gradually or suddenly) relative to the wave length, the wave length (L) decreases due to bottom friction which increases the wave steepness. The wave height may also increase (shoaling) during this process (USACE, 2002). The face of the wave continues to steepen until it becomes steep enough for it to collapse in on itself or, according to Christensen *et al.* (2002), the wave crest velocity overtakes the wave phase velocity. Christensen *et al.* (2002) reports on experiments conducted by Chang and Liu (1999) who found that the fluid particle velocity at the tip of a plunging wave exceeded the phase velocity of the wave by a factor of 1.68. Measurements also indicated that the overturning wave face plunges into the water at an acceleration of 1.1 times to that of gravity.

2.5.2 Incipient Wave Breaking

The point at which the wave breaks is called the incipient breaking point. Various definitions for incipient wave breaking (H_b) exist:

i The point where the wave height is a maximum;

ii The point where the front face becomes vertical (for plunging breakers);

iii A moment before foam appears on the wave (for spilling breakers) USACE (2002); or

iv More formally proposed by Kamphuis (1991) :

> *Wave transformation is represented by a smooth curve beginning in deep water; [and] wave decay by a smooth curve beginning near the shoreline. The incipient breaking wave height, H_b, is defined as the maximum wave height; it occurs at the intersection of these two curves.*

See Figure 2.4 for a graphical representation of the criteria established by Kamphuis (1991) where the red points indicate the deep water smooth curve and the blue points the wave decay smooth curve.

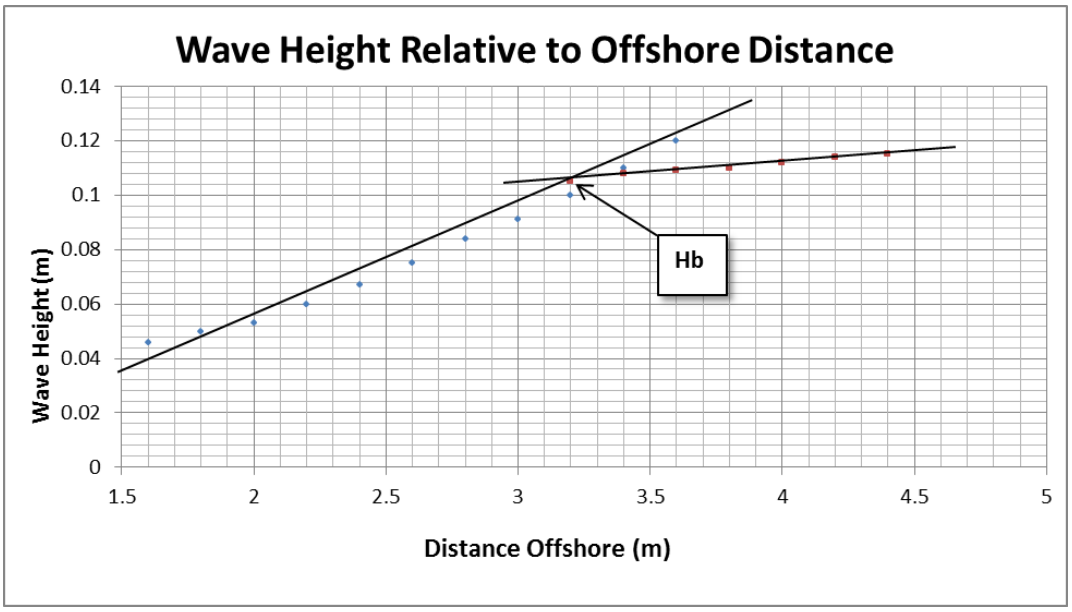

Figure 2.4: Determination of incipient breaking (from Kamphuis (1991))

It is quite possible that the application of the four definitions given above could result in a variation of the incipient breaking point in the cross shore direction for an arbitrary breaking wave. Due to the difficulty in measuring the incipient breaking point in the field, the choice of definition to determine this point is primarily governed by the practical considerations in measuring the incipient breaking point.

For this study it is assumed that the breaking point is at the instant where the wave height is a maximum. This is an assumption made due to the discreet water level sampling data available from physical models and the information available around the break point for these measurements.

2.5.3 Breaker index

In the field it is very difficult to identify the incipient breaking point, yet its importance is significant for the calculation of the breaker index. The breaker index is an important parameter in the design of structural elements in the surf zone where the worst condition is a wave slamming onto the structure. Two forms of this index exist:

- The breaker height index which provides a ratio of the breaking wave height (H_b) and the deep water wave height (H_0) as given in Equation 2.1; and
- The breaker depth index which provides a ratio of the breaking wave height (H_b) and the still water depth (d_b) at the point of wave breaking as given in Equation 2.2.

This study will concern itself with the breaker depth index as defined in Equation 2.2. Figure 2.5 illustrates the definition of the parameters used.

$$\Omega_b = \frac{H_b}{H_0} \tag{2.1}$$

$$\lambda_b = \frac{H_b}{d_b} \tag{2.2}$$

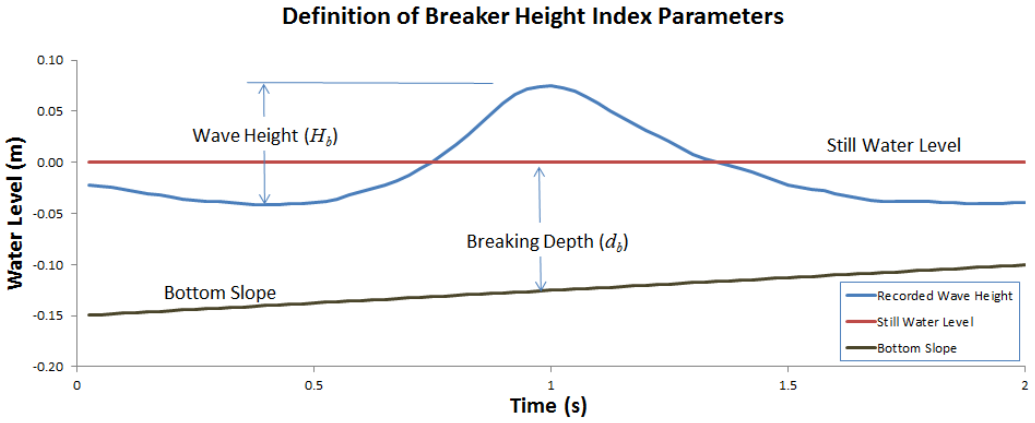

Figure 2.5: Definition of parameters used for calculating the breaker depth index

Battjes and Janssen (1978) found that a value of $\lambda_b = 0.78$ used as input into their surf zone dissipation model was in good agreement with the experimental data. Kaminsky and Kraus (1993) re-analysed a large number of data compiled from physical data and found λ_b values in the range of 0.60 to 1.59 with an average value of $\lambda_b = 0.78$. Battjes and Stive (1985) showed that the breaker index is dependent on various factors; i.e. bottom slope, incident wave steepness and even the wind.

The extreme variability of the breaking index parameter forces the engineer to pay closer attention to the wave-breaking mechanism. This is especially important when the safety of structures working in the surf zone (e.g. temporary jetties crossing the surf zone, near-shore drill platforms, etc.) are paramount.

2.6 Breaking wave zones

Christensen *et al.* (2002) divide the water column in which wave breaking occurs into three vertical zones; upper, middle and lower regions.

The upper region is characterised by the formation of the aerated foam above the trough level of the wave. Within spilling and plunging breakers, a sequence of "jet-splash" motions are observed. Vortex systems are generated from these jet-splash sequences. The vortices decrease in strength as wave energy is transferred to the turbulent motion in the air-bubble field. Eventually, the vortices collapse due to the flow under the trough of the wave. Vortex stretching also occurs due to to the interaction of the vortices, rising buoyant bubbles and the jet-splash (Lin and Hwung, 1992).

Christensen *et al.* (2002) report that research into the upper region of breaking waves has not gathered much attention mainly due to the complexity of the bubble/foam region.

The middle region (or transition zone) is the region of flow below the trough level but above the sea bed and has had a great deal more interest from researchers. This seems to be mainly due to the techniques that have been developed in the last 30 years. Imaging techniques like Particle Image Velocimetry (PIV) and Laser Doppler Velocimetry (LDV) can capture the particle velocity vectors in the non-aerated region fairly accurately. However, signal drop-out in the aerated regions is a major problem for PIV and LDV, especially in the upper breaking foam area and, in some cases, when bubbles are pushed down into the middle region (Christensen *et al.*, 2002).

Using PIV and LDV techniques, researchers identified:

1. The onshore flow of the mean velocity above trough level and the offshore mean flow below the trough level (Nadaoka and Kondoh, 1982);

2. Without the bottom influence, the turbulent length scale in the surf zone remains constant by approximately 0.2 to 0.3 times the water depth (Pedersen *et al.*, 1986);

3. Large-scale eddies can be correlated to the Reynolds stress (Nadaoka and Hino, 1989);

4. A plunging breaker turns the whole water column turbulent immediately after breaking, which has a direct influence on sediment transport in an onshore direction and particle diffusion in the surf zone (Ting and Kirby (1994) and Ting (2006)). This was also confirmed by Ting (2013) using PIV and LDV techniques in his laboratory study of plunging waves;

5. The turbulence level generated by spilling breakers is almost constant (Ting and Kirby, 1994);

The bottom region focuses on the interaction between the boundary layer flow and the sea bed. Cox *et al.* (1996) used LDV to investigate the bottom shear stress in the surf zone. The authors found that the horizontal velocities in the boundary layer could be fitted to a logarithmic profile over most of the phases in a wave period, both in the surf zone and seaward of the breaking point. As such, in the surf zone, the temporal variations in the shear stress can be estimated by using the measured horizontal velocities above the bed. Ting (2006) observed that large-scale turbulent structures were the sources of most of the turbulent kinetic energy (TKE) and shear stress near the bottom. In addition, the passage of these large-scale turbulent structures characterised the instantaneous velocity field near the sea bed.

Using PIV and LDV technology, Ting (2006) eloquently summarises the transport of turbulence during the wave breaking process as follows:

> *Organized flow structures transport turbulence energy and fluid momentum from the free surface to the bottom, where the presence of a solid boundary causes the turbulent fluid to spread out laterally.*

2.7 After breaking and dissipation in the swash zone

After the wave has broken, a roller forms that can be characterised as a moving bore. In this highly aerated region on the crest of the wave, most of the wave energy is transformed into turbulent kinetic energy. The aerated roller travels on the front face of the wave with a speed approximately equal to the wave celerity (Govender, 1999).

Zhang *et al.* (2014) studied the slope of the breaking wave roller. The authors demonstrated that the variation of the roller slope is an important process in surf zone modelling and by applying the measured roller slopes into conventional momentum and energy balance equations, the simulations of wave setup and roller length evolution are improved. The authors measured roller slope values of between 0.2 and 0.8. The roller slope values peaked at the break point (in the order of 0.8) and decrease with the dissipating wave energy as the roller propagated shoreward.

Carini *et al.* (2015) used thermal infrared (IR) imagery to study the length- and time scale variability of dissipation due to wave breaking in the surf zone. The authors developed an algorithm to identify breaking waves in the surf zone based upon the fact that active and residual foam have unique signatures in thermal IR imagery. The authors found good agreement between the experimental data and commonly used models (i.e. Duncan (1981) and Janssen and Battjes (2007)) nested within near-shore circulation models.

2.8 Bed friction

As a travelling wave moves over shallower depths and the wave starts to interact with the bed, it is believed that the roughness of the bed has a direct influence on the bottom drag experienced by the wave. Feddersen *et al.* (2003) conducted field experiments and tested the hypothesis that the bottom drag coefficient depends on bottom roughness. The authors found that the bottom roughness and the drag coefficient are smaller offshore of the breaker zone and larger within the surf zone. Further, their research suggests that breaking wave-generated turbulence increases the drag coefficient in the surf zone. In fact, the drag coefficient in the surf zone was consistently larger for a variation of roughness parameters compared to outside the surf zone.

2.9 The transformation of the wave velocity in travelling waves

The velocity of travelling waves can be described in three different ways (Holthuijsen, 2007):

1. Instantaneous velocity: The velocity vector of a water particle as it travels in time. The velocity of each particle will vary within the same wave phase. The path of the particle is in a circular or elliptical shape and is referred to as the "orbital velocity";

2. Phase velocity: The travelling speed of the whole phase of the wave, or, in other words, the forward speed of the wave $C = L/T$ (where C is the wave celerity, L the wave length and T the wave period); and

3. Group velocity: Ocean waves travel in groups made up of individual waves. The group of waves travel at its own velocity less or equal to the phase velocity of the member waves in that group ($C \geq C_g$).

Each of these velocity characteristics will behave differently in deep water compared to the nearshore zone where the water depth gets shallower. In shallow water, the orbital velocity will become more elliptic and the phase velocity will slow down as the wave shoals and transforms in the near shore (as discussed in Section 2.4).

2.10 Wave setup

The super elevation of the average water level due to wave action is called the wave setup. The lowering (setdown) and elevation of the still water level in the near shore by the wave action are due to the cross-shore radiation stress which is given as (USACE, 2002):

$$\frac{d\bar{\eta}}{dx} = -\frac{1}{\rho g d}\frac{dS_{xx}}{dx} \tag{2.3}$$

where $\bar{\eta}$ is the water elevation, x the cross-shore distance, d the water depth and $\frac{dS_{xx}}{dx}$ the cross-shore radiation stress. It is assumed that the maximum setdown occurs at (or near to) the wave breaking point.

Assuming linear wave theory, the wave setup at the still water level ($\bar{\eta}_s$) can be described as the setdown at the breakpoint plus a function of the breaker heigh index multiplied by the still water depth at the breakpoint. Note that this formulation is valid for plane beaches. The case for complex geometries needs more careful scrutiny (USACE, 2002).

Haller *et al.* (2002) performed laboratory experiments on a fixed barred beach and compared their measured results to those predicted by Equation 2.3. The authors found that the calculated error over the bar between η_{mean} and $\eta_{measured}$ is relatively small. However, Equation 2.3 tends to underpredict the setup at the shoreline.

Soomere *et al.* (2013) used numerical methods during their study of wave setup near complex geometries. The authors found that, during storms, wave setup can form up to a third of the total water level increase which significantly raises the risk of coastal flooding if not taken into account during the design stage of the coastal protection.

2.11 Turbulence

As noted in Section 2.2, turbulence is one of the processes that occurs in a breaking wave and readily in the surf zone. Turbulence can, in general, be described as unsteady random and chaotic behaviour of the water particles (Versteeg and Malalasekera, 2007). This means that the velocity fluctuations are in all directions and can, strictly speaking, only be described in three dimensions; i.e. the flow is intermittent, diffusive, three-dimensional and chaotic (Roberts and Webster, 2002).

Feddersen (2012) describes the surf zone turbulent kinetic energy as the balance between the dissipation of the turbulence induced by the breaking wave and the downward vertical turbulent diffusion of the turbulent source.

Instead of providing a definition, Tennekes and Lumley (1972) describe the characteristic features of turbulent flow as follows:

1. Irregularity: The flow is considered to be chaotic and in all directions and displays great randomness in terms of length and time scales. Predicting the velocity vectors in a subsequent time step based on the previous time step is not possible. Thus, it is necessary to describe the turbulent motion of the flow through statistical methods.

2. Large Reynolds numbers: Instability of the water particles happens at large Reynolds numbers. As the Reynolds number represents the ratio of the inertial force to the viscous force, an increase in Reynolds number indicates that the viscous forces are incapable of damping the velocity fluctuations occurring in the flow. The result is the increase in the number and frequency of the random velocity fluctuations when the flow transitions from laminar to turbulent.

3. Diffusivity: The most important practical feature of turbulent flow is the diffusivity. Rapid mixing, spread of velocity fluctuations and increased rates of mass, heat and momentum transfer are all features of turbulent flows. It is these characteristics that aid in the rapid mixture of particles (e.g. particulate species, sediment, pollutants, etc.) with the ambient waters.

4. Dissipation: The kinetic energy is dissipated through cascading turbulent scales. The (mean) flow transfers energy to the large scale eddies which in turn transfers energy to smaller scale eddies until the energy is dissipated into internal energy.

5. Three-dimensional fluctuations: Turbulent flows are always three dimensional and are characterised by high levels of fluctuating vorticity. In the description of turbulent flows, vorticity dynamics is an important characteristic.

As stated above, turbulence has an infinite number of scales (or degrees of freedom) which manifests in a cascading fashion (Tennekes and Lumley (1972) and Andersson *et al.* (2011)). There is a wide range of scales in turbulent flow that cascades from large scales (large eddies or vortices), which is in the order of the flow geometry, to the small scales, which are defined by the diffusive action of the molecular viscosity. In practise, this means that the breaking wave transfers the large scale turbulent kinetic energy in a cascading fashion to the smaller scales over time. A large eddy can also contain, within itself, smaller eddies; i.e. different length scales can co-exist within each other. Inside the turbulence of the flow, eddies stretch, rotate and breakup to form two or more smaller eddies. Note that this eddy stretching is absent from two-dimensional flow and is purely a feature of turbulent flow in three dimensions (Tennekes and Lumley, 1972).

This process continues through the evolution of the turbulent flow over time. At the smallest scale (Kolmogorov scale) the frictional forces become too large and the kinetic energy is dissipated. Viscosity plays a large role in determining these scales due to the fact that the kinetic energy is eventually destroyed by the viscous forces; i.e. the larger the viscosity, the larger the scales. Infinitely small eddies are prevented due to the viscous stresses. As a result, there must be a minimum scale of turbulence (Andersson *et al.*, 2011).

Roberts and Webster (2002) observe that the energy transfer rate from the large eddies cascaded downward is proportional to their energy multiplied by the rotational frequency. It is known that the eddies lose most of their energy after one or two overturns. With the kinetic energy proportional to the velocity squared and the rotational frequency proportional to the standard deviation of the velocity divided by the integral length scale, the energy dissipation can be given as (Roberts and Webster, 2002):

$$\epsilon \sim \frac{\tilde{u}^3}{l} \tag{2.4}$$

where ϵ is the energy dissipation, $\tilde{u}$ the mean velocity and l the integral length scale.

A breaking (plunging) wave can be seen as a large eddy (upon overturning and plunging into the water below) breaking up into smaller and smaller eddies (white water or "roller") until the wave energy is spent and dissipated on the beach. The reader can imagine the randomness of the forces contained in the breaking wave and the inherent difficulty in quantifying and predicting the random fluctuating velocity vectors in the breaking wave.

Andersson *et al.* (2011) define the length scale of the large eddies l_0 as

$$l_0 = \frac{k^{3/2}}{\epsilon}$$

Furthermore, the time scale τ to reduce the large scale eddy to the smallest scale eddy is given as

$$\tau = \frac{k}{\epsilon}$$

where k is defined as the mean kinetic energy per unit mass associated with the turbulent eddies and is termed the Turbulent Kinetic Energy (TKE). The TKE effectively measures the intensity of the velocity fluctuations in the different directions. The dissipation of the TKE is denoted by ϵ.

The large-scale eddies depend mostly on the large-scale structures like flow and the boundary conditions and have large time scales while the small-scale eddies exist with very short time scales and lengths. It is thus assumed that the short scale turbulence is statistically independent of the large-scale structures; i.e. the mean flow (Andersson *et al.*, 2011).

The universal equilibrium range is an assumption that the smaller eddies will always evolve much more rapidly relative to the large eddies and will adjust very quickly to changes in the external flow.

In light of this, some fundamental assumption need to be made with regards to the small-scale turbulent motions observed in highly turbulent flow (Reynolds numbers in the order of 10^5). Andersson *et al.* (2011) relate the Kolmogorov hypotheses as follows:

i During turbulent flow (i.e. high Reynolds numbers), directional information of the small scale eddies is lost in the chaotic scale-reduction process (cascading). In other words, the small-scale motions become statistically isotropic during turbulent flow and are thus statistically independent of the mean flow and large scale turbulence. This assumption is valid for length-scales where $l \ll l_0$.

ii Small-scale eddies contained within large-scale eddies can rapidly adapt to changes within the flow structure in order to maintain dynamic equilibrium due to the energy transfer rate from the large eddies. Within the universal equilibrium range, a range known as the "inertial range" exists where the kinetic energy dissipation (ϵ) is dominant and is independent of the viscosity. In this range, the turbulent statistics have a universal form uniquely defined by ϵ.

iii The viscosity of the fluid and the downward cascading energy transfer to the subsequent smaller scales are the dominant processes in the "dissipative range" of the turbulent flow. At these small scales, dissipation (ϵ) and viscosity (ν) are the main variables concerning the statistics of the turbulent flow. The dissipation and viscosity are known as the Kolmogorov scale (η) which describes the size of the smallest turbulence scales and occurs within the "dissipative range" and the Kolmogorov length-scale given as:

$$\eta = \left(\frac{\nu^3}{\epsilon}\right)^{1/4}$$

The Kolmogorov hypotheses are graphically presented in Figure 2.6.

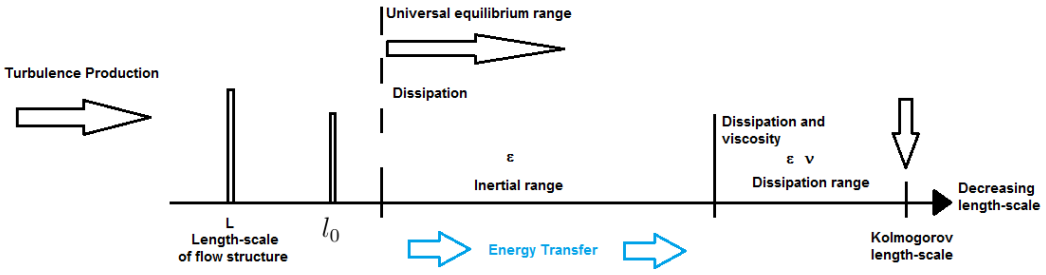

Figure 2.6: Turbulent energy dissipation and the dissipation ranges according to the Kolmogorov hypotheses (adapted from (Andersson *et al.*, 2011))

Ting and Kirby (1995) investigated the turbulence induced by a strong plunging breaker and report the following:

- The particular wave condition and the beach slope determines the dynamics of the surf zone turbulence; i.e. the turbulence in the inner surf zone vary for different deep water wave conditions.
- The turbulence intensities vary over a wave period. This is made apparent by the variation of turbulence intensities between spilling and plunging breakers.
- Turbulence levels are greatest under the wave crest but have a rapid decline as the wave crest passes.
- Large-scale structures of turbulence transport govern the surf zone turbulence dynamics. Turbulence generated from the breaking waves is transported towards the land by convection in such a way that the turbulent flow pattern moving shore-ward is dependant on its history.

The quantification of turbulence (velocity fluctuations, TKE, ϵ, etc.) is discussed in the next section.

2.12 Randomness of turbulence and mathematical methods

The infinite range of time scales and length scales that exist within turbulent flow makes a deterministic approach to mathematically resolving turbulence very difficult to nearly impossible (Andersson *et al.*, 2011). The velocity of a water particle for an observer at a stationary point will appear random, irregular and chaotic. For this reason, statistical methods are employed to describe the velocity of the water particles in turbulent flow.

In order to describe the instantaneous velocity, the particle velocity can be decomposed into three basic components. This process is generally known as Reynolds decomposition.

$$u(t) = \bar{u} + \tilde{u} + u'(t) \tag{2.5}$$

i Average velocity: $\bar{u}$ denotes the mean velocity over a period of time and is calculated as follows:

$$\bar{u} = \frac{1}{N} \sum_{t=0}^{T} u_t \tag{2.6}$$

where N is the number of velocity records between $t = 0$ and $t = T$ and u_t the sampled instantaneous velocity record.

ii Orbital velocity: $\tilde{u}$ denotes the orbital velocities that can easily be calculated from linear wave theory. For all practical calculation purposes,

the orbital velocity is considered to be included in the average velocity such that

$$u(t) = \bar{u} + u'(t) \tag{2.7}$$

iii Turbulent fluctuation: u' denotes the turbulent fluctuation component and is graphically illustrated in Figure 2.7. u' can be calculated by subtracting the average velocity from the instantaneous velocity; i.e. $u' = u - \bar{u}$. u' represents the relative fluctuation of the velocity from the mean for the observed time series.

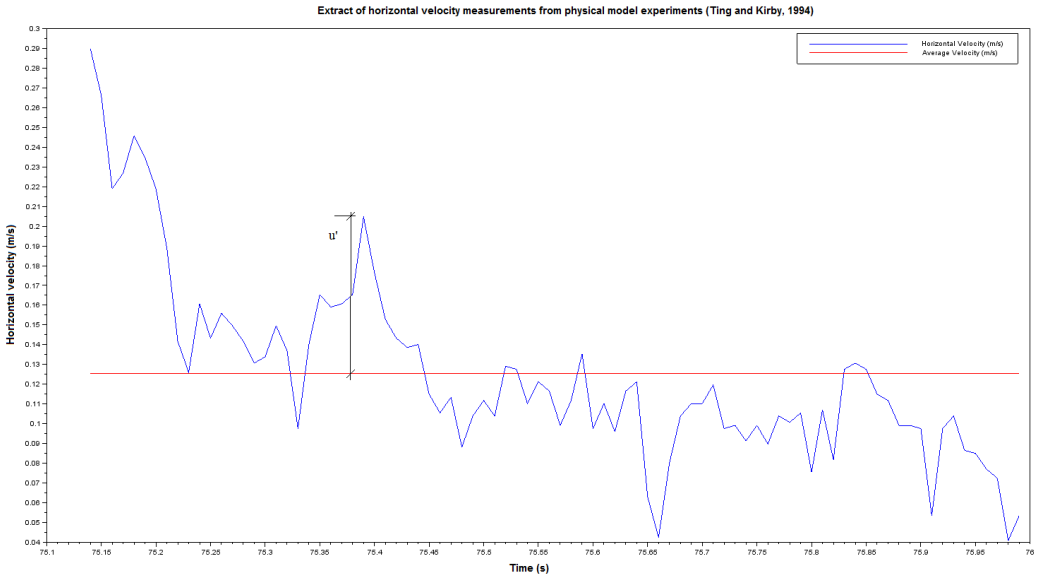

Figure 2.7: Sample from a measured horizontal velocity record - Ting and Kirby (1994). The average velocity for this time series is given by the red horizontal line

The variance of the fluctuations (u') is used to describe the magnitude of the velocity fluctuations

$$u' = \frac{1}{N}\sum_{t=0}^{T}(u_t - \bar{u})^2 \tag{2.8}$$

where $\bar{u}$ is the average between times $t = 0$ and $t = T$.

The standard deviation (root mean squared) is used to calculate the turbulence intensities (Equation 2.9).

$$u'_{rms} = \sqrt{u'} = \sqrt{\frac{1}{N}\sum_{t=0}^{T}(u_t - \bar{u})^2}$$

$$u'_{rms} = \sqrt{u'} = \sqrt{\frac{1}{N}\sum_{t=0}^{T}(u'_t)^2} \tag{2.9}$$

where N is the number of turbulent velocity fluctuation records between $t = 0$ and $t = T$ and u'_t the calculated turbulent velocity fluctuation (Equation 2.5).

The turbulent kinetic energy (k) is given by half of the sum of the turbulent fluctuations in all directions:

$$k = \frac{1}{2}(u'u') = \frac{1}{2}(u' + v' + w') = \frac{1}{2}((u'_{rms})^2 + (v'_{rms})^2 + (w'_{rms})^2) \tag{2.10}$$

Boers (2005) notes that the production and dissipation of kinetic energy near the surface of a breaking wave versus the kinetic energy near the bed (where friction is dominant) in the water column will differ from each position. A possible way to describe this behaviour mathematically might be to use a kinetic energy balance equation. A general form is given in Equation 2.11. Note that this equation only describes the vertical dissipation (the horizontal advective and diffusive turbulent kinetic energy terms are omitted).

$$\frac{\partial k}{\partial t} = \frac{\partial}{\partial z}\left(\frac{\nu_t}{\sigma_k}\frac{\partial k}{\partial z}\right) + \text{Prod.} + \text{Dissipation} \tag{2.11}$$

where σ_k is the Prandtl coefficient and ν_t the eddy viscosity. Equation 2.11 describes the variation in the turbulent kinetic energy (TKE) over time by considering the diffusive TKE in the vertical direction.

Launder and Spalding (1974) describe the mathematical evolution of the TKE (k) and the kinetic energy dissipation (ϵ) through the formulation of the $k - \epsilon$ turbulence model for high Reynolds numbers as follows:

$$\frac{\partial k}{\partial t} = \frac{1}{\rho}\frac{\partial}{\partial x_k}\left[\frac{\nu_t}{\sigma_k}\frac{\partial k}{\partial x_k}\right] + \frac{\nu_t}{\rho}\left(\frac{\partial U_i}{\partial x_k} + \frac{\partial U_k}{\partial x_i}\right)\frac{\partial U_i}{\partial x_k} - \epsilon \tag{2.12}$$

$$\frac{\partial \epsilon}{\partial t} = \frac{1}{\rho}\frac{\partial}{\partial x_k}\left[\frac{\nu_t}{\sigma_\epsilon}\frac{\partial \epsilon}{\partial x_k}\right] + \frac{C_1\nu_t}{\rho}\frac{\epsilon}{k}\left(\frac{\partial U_i}{\partial x_k} + \frac{\partial U_k}{\partial x_i}\right)\frac{\partial U_i}{\partial x_k} - C_2\frac{\epsilon^2}{k} \tag{2.13}$$

where ρ is the water density, x_i and x_k the directional coordinate in Cartesian space, U_i and U_k the mean directional velocity component and C_1 and C_2 constants. The constants proposed by Launder and Spalding (1974) are presented in Table 2.1.

The $k - \epsilon$ turbulence model is but one of many turbulence models used in numerical modelling today.

2.13 Some final thoughts

Much more have been published on the wave-breaking process with each author contributing a specialised part that forms the whole. This study cannot be

Table 2.1: Values of the constants proposed by Launder and Spalding (1974) for the $k-\epsilon$ model

C_1	C_2	σ_k	σ_ϵ
1.44	1.92	1.0	1.3

exhaustive enough to contain all the micro-nuances of the vast collection of research on this subject. Other external influences on wave breaking (e.g. the effect of wind and strong return currents) have not been considered. However, focusing on the major components of wave transformation, wave breaking and energy dissipation, will give the reader a sufficient overview of the processes one is expected to observe in a numerical model.

The physical processes described in this section are the major quantifiable processes normally needed in engineering design. If these processes are understood in the physical realm and can be simulated, with confidence, in the numerical space, then the numerical tools will enable the engineer to test an extended collection of climate and extreme conditions as part of his design.

The next section will explore the theoretical capabilities of the numerical model SWASH. The same processes will be described in terms of their mathematics contained in the model.

Chapter 3

Numerical Wave Transformation Model SWASH

3.1 Introduction

This chapter describes the numerical model SWASH (Simulating WAves till SHore - Zijlema *et al.* (2011)) used in this study to simulate the wave-breaking and surf-zone processes.

A general overview of the SWASH model and its capabilities are given. Thereafter, the SWASH model is described more specifically in terms of its ability to simulate wave breaking and the resulting turbulence in the surf zone. The mathematical capabilities and routines programmed in SWASH that attempt to simulate the processes described in Chapter 2 are discussed. The software version used in this thesis is SWASH version 3.14AB.

The focus of this section is placed on the features of SWASH that are relevant to wave breaking in shallow water.

3.2 Background

The numerical model SWASH was developed by Delft University of Technology and is also maintained by this institution. It was specifically developed for simulating non-hydrostatic, free surface, rotational flows in one and two dimensions. The intention of the code is to numerically predict the transformation of surface waves in coastal waters up to the extent of the wave reaching the shore - as such the name SWASH, an acronym for Simulating WAves till SHore (Zijlema *et al.*, 2011).

Compared to the classical Navier-Stokes equations, non-hydrostatic models can efficiently compute free-surface flows by describing the free-surface flow as a single valued function. This makes the non-hydrostatic model much less complex than a Boussinesq model and as a result, more robust (Rijnsdorp *et al.*, 2012).

The designers of the model aim to provide a robust and efficient model that can simulate a wide range of time and space scales for surface waves in complex environments. The code was developed over the last 13 years and is based on the work of Stelling and Zijlema (2003), Stelling and Duinmeijer (2003), Zijlema and Stelling (2005) and Zijlema and Stelling (2008).

The model is based on an explicit second-order finite difference numerical scheme whereby mass and momentum are strictly conserved at a discrete level. As such, the model is able to effectively track the point of incipient breaking without providing any additional parameters given a sufficient vertical resolution. As such, SWASH simulates the correct gradual change of form of the broken wave into a steady bore due to the momentum conservation, as detailed in Stelling and Duinmeijer (2003). Frequency dispersion is improved through the increase in the number of vertical layers (Zijlema *et al.*, 2011).

Studies conducted by previous researchers (Smit *et al.* (2013) and Smit (2014)) concluded that SWASH can resolve dissipation due to wave breaking in a short-crested wave field.

3.3 Governing equations

In order to describe the depth-averaged, non-hydrostatic, free-surface flows, SWASH employs the Non-linear Shallow Water Equations (NLSW) which can be derived directly from the incompressible Reynolds-averaged Navier-Stokes Equations (RANS). The NLSW includes vertical acceleration (Zijlema *et al.*, 2011).

Conserving mass and momentum of a free surface incompressible fluid with constant density, the NSWE are described by Smit *et al.* (2013) as follows for a 2DV formulation:

$$\frac{\partial u}{\partial t} + \frac{\partial uu}{\partial x} + \frac{\partial wu}{\partial z} = -\frac{1}{\rho}\frac{\partial (p_h + p_{nh})}{\partial x} + \frac{\partial \tau_{xz}}{\partial z} + \frac{\partial \tau_{xx}}{\partial x} \tag{3.1}$$

$$\frac{\partial w}{\partial t} + \frac{\partial uw}{\partial x} + \frac{\partial ww}{\partial z} = -\frac{1}{\rho}\frac{\partial p_{nh}}{\partial z} + \frac{\partial \tau_{zz}}{\partial z} + \frac{\partial \tau_{zx}}{\partial x} \tag{3.2}$$

$$\frac{\partial u}{\partial x} + \frac{\partial w}{\partial z} = 0 \tag{3.3}$$

where the variables are defined as follows:

t: time

x, z : describing the local coordinate system (z pointing upwards)

ρ : fluid density

p_h and p_{nh} : hydrostatic and non-hydrostatic pressures respectively

$u(x,z,t)$ and $w(x,z,t)$: horizontal and vertical velocities respectively in space and time

$\tau_{xx}, \tau_{xz}, \tau_{zx}, \tau_{zz}$: turbulent stress terms.

The hydrostatic pressure is expressed explicitly as a function of the free surface level, $\zeta(x,t)$, as $p_h = g\rho(\zeta - z)$ so that

$$\frac{\partial p_h}{\partial z} = -g\rho \text{ and } \frac{\partial p_h}{\partial x} = g\rho\frac{\partial \zeta}{\partial x}$$

where g is the gravitational acceleration.

Considering the mass balance for the whole water column, the time evolution of the surface elevation is given by

$$\frac{\partial \zeta}{\partial t} + \frac{\partial}{\partial x}\int_{-d}^{\zeta} u dz = 0 \tag{3.4}$$

The water column is vertically bounded by the surface elevation $\zeta(x,t)$ and the stationary bottom $d(x)$ relative to the still water level z_0.

The equations given are in Cartesian notation, although the most general framework that would be used is curved orthogonal. The extension to three dimensions is given in Zijlema and Stelling (2005) and Zijlema and Stelling (2008).

The kinematic boundary conditions imposed are that no particle shall leave the surface and no particle shall penetrate the fixed bed level $d(x)$. Equations (3.1) to (3.4) are solved by imposing

$$w = \frac{\partial \zeta}{\partial t} + u\frac{\partial \zeta}{\partial x} \qquad \text{at } z = \zeta(x,t) \tag{3.5}$$

$$w = -u\frac{\partial d}{\partial x} \qquad \text{at } z = -d(x) \tag{3.6}$$

In general, SWASH assumes closed horizontal domain bound by vertical planes where waves are generated by prescribing a horizontal velocity to the particles normal to the boundary over the vertical.

3.4 Wave breaking

When waves break in nature (where the wave transforms into a bore), momentum is conserved but not energy. SWASH employs numerical methods that successfully simulate these shock-capturing schemes[1]. However, for the purposes of this study it is important to note that if the momentum conservation

[1] A For a complete treatment of these numerical methods, see Stelling and Duinmeijer (2003).

is retained in the numerical scheme, the NLSW automatically results in the ability to be shock capturing (Zijlema, 2014).

Without needing to resolve complex processes, such as wave generated turbulence or overturning of the surface, the equations given thus far are capable of simulating the overall characteristics of a quasi-steady breaking bore in the surf zone. During wave breaking in nature, the entire front of the wave becomes turbulent (either overturning or spilling down the front face). However, the bore front is stabilised by the downward transport of momentum due to the turbulent stresses. The result is that a quasi-steady bore develops. In the SWASH model, these stabilising effects and the turbulent energy created in the breaking process are not accounted for. Instead, the steepness of the wave front will continue to increase until a jump-discontinuity (equal to the local wave height) develops. Across the discontinuity, momentum conservation is strictly enforced which results in an energy dissipation rate proportional to the local wave height cubed (H^3) (Smit, 2014).

Such a treatment of wave breaking has the advantage that it does not require any additional measures to account for the wave-breaking processes or to keep track of energy dissipation. It does, however, require a high horizontal and vertical resolution in the order of 10 - 20 vertical layers. A coarse vertical resolution (less than 5 layers) will result in the early onset of incipient breaking and an underestimation of the horizontal velocities at the crest of the wave; i.e. the non-hydrostatic pressure gradient is overestimated. The high resolutions are required because the characteristic vertical length scale at incipient breaking is the wave height (H) as opposed to the wave length (L) in deep or intermediate water (Smit, 2014).

However, note that the non-hydrostatic wave-flow model can be locally reduced to the NLSW equations by enforcing a hydrostatic pressure distribution at the front of the wave. Consequently, the wave will rapidly transform into the characteristic saw-tooth shape. Momentum is conserved and the dissipation is captured over the resulting discontinuity consistent with the high vertical resolution approach. Smit (2014) terms this approach the "HFA approach" (Hydrostatic Front Approximation). Essentially, the HFA regards the entire turbulent wave front as a sub-grid feature of the flow and can be compared with the disabling of the dispersive terms in the Boussinesq equation. HFA allows the enforcing of wave breaking at low vertical resolutions. This means that the non-hydrostatic pressure is set to zero once the model grid point is in front of the breaking wave and the vertical acceleration is no longer resolved in the grid point (Smit, 2014).

The wave breaking is enforced by tracking the rate of surface rise ($\partial\zeta/\partial t$) and enforcing the non-hydrostatic condition when the rate of surface rise exceeds a pre-set value (α). Thus, the grid-point is labelled for hydrostatic computation if $|\partial\zeta/\partial t| > c\alpha$ (with c the wave celerity). The point becomes non-hydrostatic again when the wave crest has passed. In addition, wave persistence (β) is modelled by reducing the local criterion from α to β in

a neighbouring grid-point. Thus, the neighbouring point is also labelled for hydrostatic computation if $|\partial\zeta/\partial t| > c\beta$ with $\beta < \alpha$. All other grid points not conforming to this criteria are labelled for non-hydrostatic computation. Reasonable results are achieved with $\alpha = 0.6$ and $\beta = 0.3$ (Smit, 2014).

Clearly, the α and β values become additional calibration parameters within the SWASH model. If wave-breaking calibration data exists for the numerical model, computational time can significantly be reduced by activating the HFA, tuning the α and β values in accordance with the measurements and reducing the vertical discretisation significantly.

3.5 Numerical Schemes

In general, a second order finite difference scheme that conserves momentum and mass (accurate in space and time) is employed in SWASH. The computational domain consists of columns of constant width in the x-and y-direction and equally spaced vertical layers between the fixed bottom and spatially varying free surface (The SWASH Team, 2016). This is illustrated in Figure 3.1 for a discretisation of 20 vertical layers.

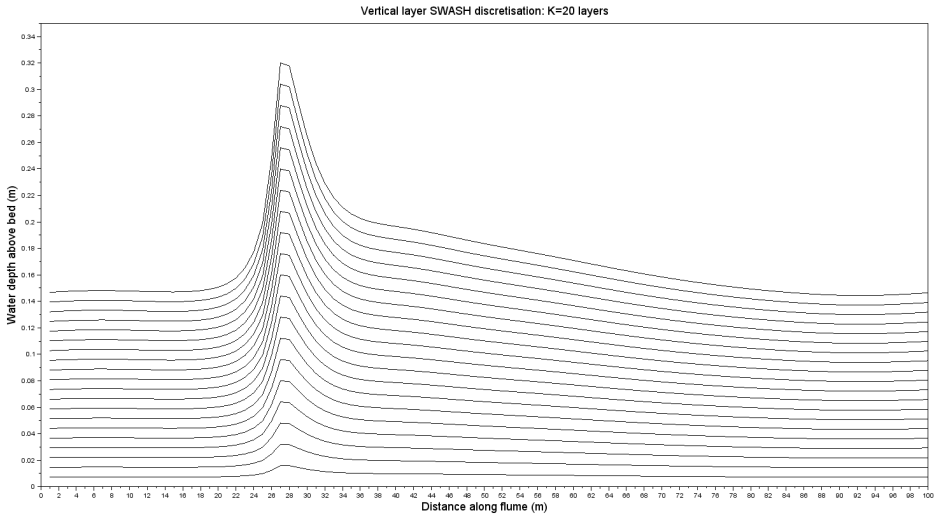

Figure 3.1: Illustration of the vertical layer discretisation employed in SWASH

The Keller-box scheme is used to approximate the pressure gradients in the vertical momentum equation for low (generally between 1 and 5 vertical layers) while a standard central differences approach is used for typically 15 or more layers. The standard scheme is preferred for a higher vertical resolution

because it is more robust and the dispersion characteristics are sufficiently accurate (Smit *et al.*, 2013).

The Hansen scheme (a second order leapfrog scheme) is adopted for integration of the horizontal momentum and continuity so that the wave amplitude will not be changed. To retain second-order accuracy in time for the horizontal advection and momentum terms, a MacCormack predictor-corrector scheme is applied. The vertical advection and viscosity terms are integrated in time using the semi-implicit θ-method. By solving the depth-averaged continuity equation for the solution of the water elevation, global mass is conserved (i.e. Equation 3.4) while local mass continuity is enforced by solving a Poisson equation for the pressure correction. Due to the additional computational cost of the iterations that is needed to solve for pressure correction, the efficient BiCGSTAB method is employed to solve the unsymmetric Poisson equation iterations (Zijlema, 2014).

3.6 Non-hydrostatic mode

The SWASH Team (2016) describes how SWASH can be used in a purely hydrostatic mode or the option to account for the non-hydrostatic pressure can be activated. The purely hydrostatic assumption (default if the latter option is not explicitly specified) can be made in the case of the simulation of long waves, i.e. tides, storm surges, etc., akin to a purely hydrodynamic model, e.g. Delft3D-FLOW.

The non-hydrostatic option must be activated when the vertical accelerations become dominant (e.g. the simulation of wave breaking or wave propagation over a steep slope). With non-hydrostatic mode activated, two numerical schemes are employed. The modeller can choose between a classic central differencing scheme and a Keller-Box scheme. The former is intended for applications where the vertical properties are important (e.g. flow over steep and varying bottom and wave breaking) and the latter for accurate short wave propagation (The SWASH Team, 2016).

As mentioned in Section 3.5, it is computationally expensive to iteratively solve the Poisson equation. In fact, most of the computational effort lies in inverting the Poisson pressure matrix. As such, two solvers for the Poisson equation are included; a Strongly Implicit Procedure (SIP) and BiCGSTAB (preconditioned with an incomplete LU factorisation) solver (The SWASH Team, 2016).

These options are given in order to fine tune the convergence of the iterative Poisson solution and can save computational time for large domain flows with multiple vertical layers. For instance, the rank of the Poisson pressure matrix can be reduced by assuming a constant pressure in, say, the bottom layer. For example, for a 2 layer simulation with the top layer occupying 85% of the water column, approximately 30% of the computational time can be saved by

assuming the pressure in the bottom layer as constant and thus reducing the rank of the pressure matrix by one (The SWASH Team, 2016).

3.7 Turbulence models

In order to close the Reynolds-averaged Navier-Stokes momentum equations, modelling of the turbulent fluxes and turbulent stresses needs to be employed. A turbulence model is employed in SWASH to approximate the dissipation and (turbulent) mixing due to the wave breaking.

In the surf zone, the horizontal transport mechanism is moderate while the vertical transport mechanism dominates. This implies that the horizontal length scales are relatively larger than the vertical ones (Zijlema, 2014).

The scale of the dissipation during wave breaking is given by the viscosity term which can describe the large scale turbulent motion in the surface roller, assuming that the turbulence is in local equilibrium. Vertical coupling, and additional numerical stability is introduced through a stress term based on a turbulent viscosity approximation (Zijlema *et al.*, 2011).

To allow for horizontal mixing SWASH employs three horizontal eddy viscosity models: Constant eddy viscosity, Prandtl mixing length and the Smagorinsky model. For this study, the Prandtl mixing length model is used and is defined as follows:

$$\nu_h = l_m^2 \sqrt{2\left(\frac{\partial u}{\partial x}\right)^2 + 2\left(\frac{\partial v}{\partial y}\right)^2 + \left(\frac{\partial u}{\partial x} + \frac{\partial v}{\partial y}\right)^2} \tag{3.7}$$

where ν_h is the horizontal eddy viscosity, l_m is the mixing length (which is estimated to be proportional to the typical wave height). Note that the Smagorinsky model is not enabled for one dimensional simulations.

Zijlema *et al.* (2011) further note that this type of mixing does not only represent the lateral mixing but also the longitudinal momentum exchange occurring at the travelling bore.

The $k-\epsilon$ model, as formulated by Launder and Spalding (1974), is employed by SWASH to compute the vertical viscosity. The vertical eddy viscosity (ν_v) inherent to the stress terms (e.g. $\tau_{zz} = \nu_v \partial w/\partial z$) is obtained from the $k-\epsilon$ closure model. The Reynolds stress is related to the mean rate of strain through the eddy viscosity as follows:

$$-\overline{u'w'} = \nu_v \frac{\partial u}{\partial z} \tag{3.8}$$

with the vertical eddy viscosity given as

$$\nu_v = c_\mu \frac{k^2}{\epsilon} \tag{3.9}$$

where k is the TKE and ϵ the dissipation rate of the TKE.

The empirical coefficients proposed by Launder and Spalding (1974) are used in the $k - \epsilon$ model (see Section 2.12). However, Zijlema (2014) notes that the constants are derived from experiments on isotropic turbulence and local equilibrium shear layer. This implies that the values of the constants remain unsure when applied to oscillatory wave-induced turbulent boundary layer. These constants cannot be changed by the user.

3.8 SWASH simulation of the cross-shore velocity moments

Liao (2015) investigated and validated the cross-shore velocity moments simulated by SWASH in the context of cross-shore sediment transport. Liao divided the velocity moments into three contributing components: undertow, wave asymmetric flow and wave-grouping long wave flow. She concluded that the velocity moments are relatively well simulated in SWASH. The three components listed above make up the total flow. The most dominant of these being the seaward undertow; the shoreward asymmetric component is of secondary importance while the long wave flow adds a relatively small contribution to the total flow. Liao (2015) concludes that SWASH is capable of simulating the vertical flow structure and wave decay reliably. However, the total flow is underestimated in SWASH when compared to the experimental data of Roelvink and Stive (1989).

3.9 Bound Waves

Rijnsdorp *et al.* (2012) demonstrated the capabilities of SWASH to simulate the transformation of infragravity waves propagating over a flat and plane slope induced by a bi-chromatic wave-group. The authors found that SWASH correctly generates and propagates bound infragravity waves at the inflow boundary and throughout the computational domain for a horizontal bottom simulation. For a plane slope, the authors concluded that SWASH is capable of simulating the cross-shore transformation of bound infragravity waves. However, for free outgoing infragravity waves, SWASH tends to overestimate the magnitude of the free infragravity waves.

For steeper slopes, SWASH showed an increase in the wave height of outgoing free infragravity waves. Rijnsdorp *et al.* (2012) report that this observation is consistent with what is observed in published literature and experimental data.

In SWASH, bound waves are incorporated by adding a second-order solution to the primary waves. Liao (2015) found that SWASH resolved the surface elevation correctly by adding bound long waves to the model when the

flume experiments conducted by Roelvink and Stive (1989) were modelled by SWASH.

3.10 Vertical Resolution

Smit (2014) reports that a coarse vertical resolution (e.g. 3 to 5 vertical layers) cannot be used when investigating the case of wave breaking in SWASH. The coarse resolution will underestimate the horizontal velocities near the crest of the wave and delay the onset of transition of the wave into the characteristic sawtooth shape during the roller phase. A sufficiently fine vertical resolution (e.g. 20 layers) ensures that the influence of the non-hydrostatic pressure gradient is not overestimated during wave breaking and it is thus not necessary to impose the hydrostatic pressure distribution (refer to Section 3.4).

It is imperative to note that a coarse resolution can indeed be used when the hydrostatic pressure distribution is imposed explicitly through the Hydrostatic Front Approximation (HFA) due to the fact that the HFA regards the turbulent front of the wave as a sub-grid feature of the flow (Smit, 2014). In the SWASH model, the HFA must be explicitly enabled and is defined by specifying two parameters: the steepness of the wave front (α) and a persistence parameter (β).

3.11 Bottom friction

Swash employs four bottom friction models: Constant friction (or a linear formulation), Chezy coefficient, Manning coefficient and Colebrook-White (which incorporates the Nikuradse roughness height). Note that these formulations (Chezy and Manning) are, in their defining theories, based on depth-averaged flows and were historically formulated for channel flow (see Chadwick *et al.* (2013) for more details). However, these formulations can be used in a vertical multi-layer mode.

The SWASH user manual also states that the Manning formulation provides a good representation for wave dynamics in the surf zone relative to the other formulations and that a Manning value of $n = 0.019$ is recommended for wave-breaking scenarios. The manual also recommends the use of the log-law formulation when modelling in multi-layer mode, especially in cases where the depth averaged velocity is equal to zero (The SWASH Team, 2016).

As noted in Section 2.8 the apparent roughness in the surf zone is not related to the physical bed roughness and that the apparent roughness in the surf zone can be substantially higher than in the non-breaking region. This is due to the influence of the wave-breaking turbulence on the horizontal momentum within the bottom boundary layer (Smit *et al.*, 2013). SWASH caters for a variation in the bottom roughness parameter across the surf zone

and a spatially varying parameter can be applied to the model. In essence, the friction parameter can be used as a calibration parameter.

3.12 Boundary conditions and the moving shoreline

Boundary types imposed in SWASH include: water level, velocity (normal to the boundary), Riemann, linearised Riemann, weakly reflective, Sommerfeld radiation and an outflow condition where the water depth is aligned to the bottom level for supercritical flow. Boundary conditions can be imposed at specific vertical layers (The SWASH Team, 2016).

At closed boundaries, a free-slip condition is imposed at parallel boundaries while the normal velocity is zero at closed boundaries. In addition, two types of onshore conditions are considered here: a moving shoreline and an absorbing boundary. The latter is implemented using Sommerfield's radiation condition which allows long waves to cross the boundary without reflections (see Stelling and Zijlema (2003) for details on the implementation).

The moving boundary (in cases where run-up and inundation are studied) is defined numerically in such a manner that the water depth is non-negative at every time step which means that flooding is never faster than one grid size (Δx) per time step. As such, drying and flooding does not need any special formulation as this is taken care of inherently in the numerical scheme (Zijlema *et al.*, 2011). The complete numerical implementation of this scheme is described in Stelling and Duinmeijer (2003) and is very efficient in large-scale inundations.

3.13 Initial boundary conditions

Numerical boundary information needs to be supplied to the model in order to solve the momentum and continuity equations. Normally a simulation will start with the "zero" boundary condition imposed, i.e. still water with no initial velocity or disturbance. With the zero boundary condition, the simulation time must be long enough to achieve a steady state. Obviously, with known boundary conditions (e.g. tidal forcing) the simulation must be long enough to satisfy the design parameters imposed by the modeller.

Various wave generating mechanisms are employed in SWASH and waves can be generated along one or two boundaries, e.g. wave spectrum or a specified time series at each point at the boundary. SWASH assumes that the local boundary depth is uniform or varies slowly and that the boundary is a sufficient distance away from the point(s) of interest in the model. SWASH has the capability to generate regular (through a time series or by specifying the wave height, period and direction) or irregular waves through a spectrum or a time

series. Spectral input can be from a file specifying the spectral parameters or from the known Jonswap, Pierson-Moskowitz or TMA spectral shapes (The SWASH Team, 2016).

Note that some evanescent modes might be included when specifying a spectrum at the boundary and will be removed by SWASH. The evanescent modes are an inherent property of the model equations and it is the dispersive properties of the model equations that determine the frequency at which these modes are generated. The cut-off frequency is the frequency at which the evanescent modes are generated and can be calculated by Equation 3.10

$$\omega_{cf} = 2K\sqrt{\frac{g}{d}} \tag{3.10}$$

where K is the number of vertical layers used in the model and d the depth at the wave boundary. Thus, the lowest wave period that can be considered in the SWASH wave model equals $T_{min} = 2\pi/\omega_{cf}$; for example, at a depth of $d = 25m$ and two vertical layers ($K = 2$) the minimum (or cut-off) frequency is calculated as $\omega_{cf} = 0.40Hz$. Note that the energy due to the evanescent modes are very small and thus negligible. However, SWASH will issue a warning to the modeller if more than 10% of the total wave components are the evanescent modes that are removed (The SWASH Team, 2016).

3.14 Discretisation

SWASH employs a finite differences/volume discretisation in a staggered grid setup to solve the governing equations (The SWASH Team, 2016)

Figure 3.2 shows the locations of the computational points employed by SWASH. The velocity components are computed at the centre of the cell faces (in 3DV mode) while the water level is computed at the centre of the cell (green square in Figure 3.2). As mentioned in Section 3.6, two schemes are used to compute the non-hydrostatic mode; the standard- and Keller-box scheme. The standard scheme computes the pressure at the cell centre (red circle in Figure 3.2) while the Keller-box scheme calculation point is at the top and centre of the grid cell (blue circle in Figure 3.2).

The SWASH Team (2016) reports that this computational scheme does not need any further discretisation at the free surface as it allows the simple implementation of the zero-pressure boundary condition at the free surface. Very few number of vertical grid points are needed with this discretisation in order to enhance the accuracy of the frequency dispersion of short crested waves (within numerical limits).

For breaking waves, careful attention needs to be paid to the discretisation of the advection terms in the momentum equation. SWASH considers the discretisation of the momentum equations separately; i.e. the u-momentum equa-

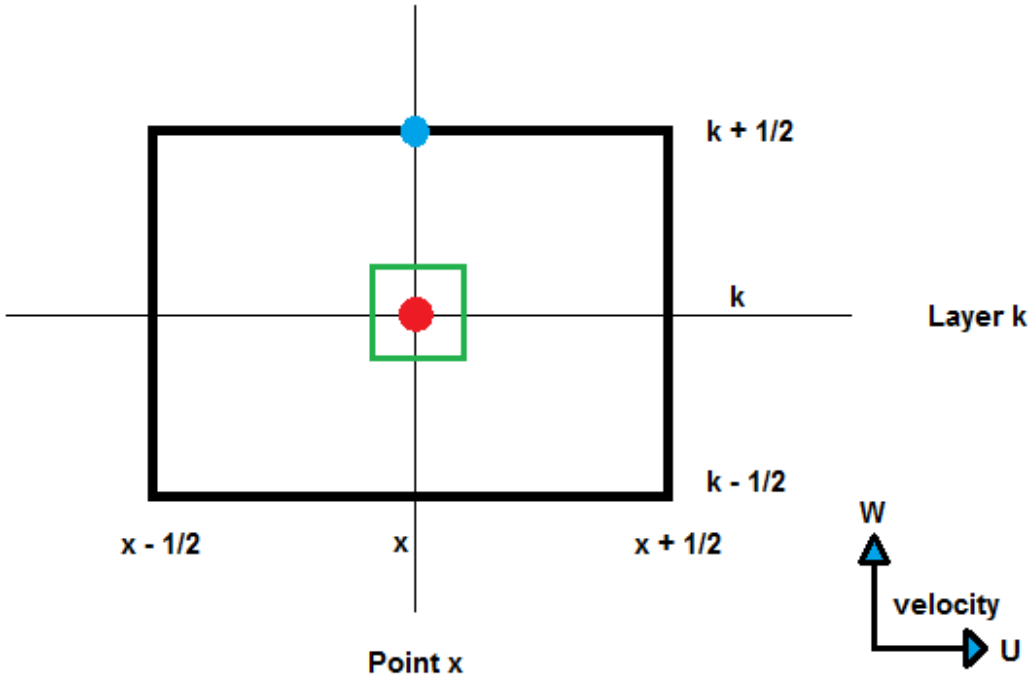

Figure 3.2: Locations of computation points for water level, velocity and non-hydrostatic pressure in a single 2DV grid in SWASH

tion: horizontal and vertical advection $\left(\frac{\partial uu}{\partial x} \text{ and } \frac{\partial uw}{\partial x}\right)$ and the w-momentum equation: horizontal and vertical advection $\left(\frac{\partial wu}{\partial z} \text{ and } \frac{\partial ww}{\partial z}\right)$.

The following guidelines and recommendations are made in the SWASH manual with regards to the discretisation of the various advection terms in the momentum equation (The SWASH Team, 2016):

- u-momentum equation: horizontal advection
  The default scheme employed by SWASH is the second order backward differencing scheme (BDF) and is recommended for most applications. In some cases where higher harmonics are involved (e.g. wave breaking), the central differencing scheme (CDF) is used. The fist order upwind scheme (FIR) is numerically diffusive for this term.

- u-momentum equation: vertical advection
  This term is only activated when multiple vertical layers are used. The default scheme employed is the first order upwind scheme (FIR) and is stable and preferred in most cases. Central differencing or higher order upwind can be employed in where the many vertical layers are used or higher order harmonics are present.

- w-momentum equation: horizontal advection
  These terms are negligibly small compared to the vertical pressure gradient and are normally ignored. However, the second order BDF scheme is employed when the non-hydrostatic component is activated or breaking is important. When higher harmonics are involved, the CDF might be used.

- w-momentum equation: vertical advection
  This term is only included when the standard layout for the non-hydrostatic pressure is activated. This term is by default discretised by the first order upwind scheme.

In summary, the following discretisation combinations in the context of wave breaking are possible and listed in Table 3.1.

Table 3.1: Summary of default and alternative schemes that can be used in the SWASH simulation of wave breaking

Option	u-momentum		w-momentum	
	Horizontal	Vertical	Horizontal	Vertical
Default	BDF	FIR	BDF	FIR
Alternatives	CDF	CDF / Higher order upwind	CDF	FIR

3.15 Momentum/Energy conservation

Within SWASH, the option exists to enforce the stipulation that the advection term must be strictly momentum conservative or the conservation of the energy head. This simply means that the variation of the total amount of momentum/energy within a given domain is equal to the balance of the net in- and out flow of the momentum/energy plus the contribution of other sources generating the momentum/energy within the domain. For rapid varied flows, e.g. wave breaking, conservation properties become crucial especially in the calculation of features like the propagation speed of a bore or incipient breaking.

SWASH will do intelligent switching between the conservation of energy head or the conservation of momentum. As the default, when the conservation of momentum or energy head is explicitly conserved, SWASH will apply the conservation of energy head in strong contracting flows while momentum conservation will be applied in other situations.

Chapter 4

Laboratory Analysis

4.1 General

This chapter describes the various laboratory techniques used to measure the transition, breaking and dissipation of waves in the nearshore. The physical setup, measurement equipment and analysis techniques for the laboratory data sets (Table 1.1) are detailed in this chapter.

4.2 Particle velocity and wave height measurements

In order to extract velocity information from the physical models, various measuring techniques are used. Here follows a cursory description of these techniques relevant to this study.

4.2.1 Particle Image Velocimetry

Particle Image Velocimetry (PIV) seeds the water in the flume with reflective, neutrally buoyant (or suspended) particles and tracks the displacement of these particles over time using digital image analysis techniques. A laser is focused at a given frequency on a particular area in the flume, digitally recording consecutive images of the seed-particles as they move in space and time due to the wave action. The velocity of the particle is then calculated by the change in distance of the particle $(x(t + \Delta t) - x(t))$ over the time interval of the consecutive images (Δt). Typically, these images are processed and velocity vectors from the observed seed particles calculated from consecutive images (Govender, 1999).

From these PIV measurements, assembled velocity vectors of the spilling and plunging waves were produced. Time- and phase-averaged velocity data from these measurements were made available for the use in this study.

4.2.2 Laser Doppler Velocimetry

Laser Doppler Velocimetry (LDV) measure vertical flow and horizontal velocities at one position at a time. The laser can be immersible or outside the flume. LDV is also sometimes referred to as laser-Doppler Anemometry (LDA).

The LDV technique scatters light from minute suspended particles in the flow that cross the point of two intersecting lasers. The Doppler shift in the frequency of the scattered light is detected and the particle velocities calculated. The Doppler shift, f_D, is calculated from the wavelength of the scattered light, the velocity vector of the particle motion and the angles (orientation) of the receiving equipment. No transfer function is necessary as the particle velocities are linearly related to the Doppler frequency which is, in turn, linearly related to the output voltage (DanTec Dynamics). Due to the sampling frequency of the measurement being very high and the measuring volume very small ($\sim 0.1mm^3$), small scale turbulence is easily and accurately measured. Calibration coefficients are inherent to the measurement instruments. Signal disturbance from air bubbles is relatively small due to the relatively short length of the laser beams (Boers, 2005).

4.2.3 Wave heights

Capacitance wave probes are normally used to record the instantaneous water level at a fixed location over time. Govender (1999) developed a wave height measurement technique called a "keogram." A keogram is obtained by digitally analysing black and white video recorded images of the flume at specific measuring points. The wave measurement is obtained at each position by assembling a vertical line of pixel intensity values for consecutive images. Stacked side by side, these lines of pixel intensities produce a new image called the "keogram." From this image, it is simple to measure the wave height and, in addition, identify the water-foam boundary. Figure 4.1 shows an example of a keogram, the digitised water levels of the keogram, the recorded wave gauge water levels and a comparison of the two measurements.

Note from Figure 4.1 that the keogram in the shallow water (where wave breaking has already taken place) reports "higher" wave heights than the wave gauge measurements. In the deep water section of the flume, no such discrepancy is observed. Govender (1999) reports that this is an expected result as the aerated areas of a broken wave (bubble entrainment) would have lower electrical conductivity and would, in essence, result in a wave probe measurement that is lower in wave height at the peaks and troughs.

4.2.4 Practical challenges

Govender (1999) points out practical challenges when measuring velocity and turbulence in the surf zone:

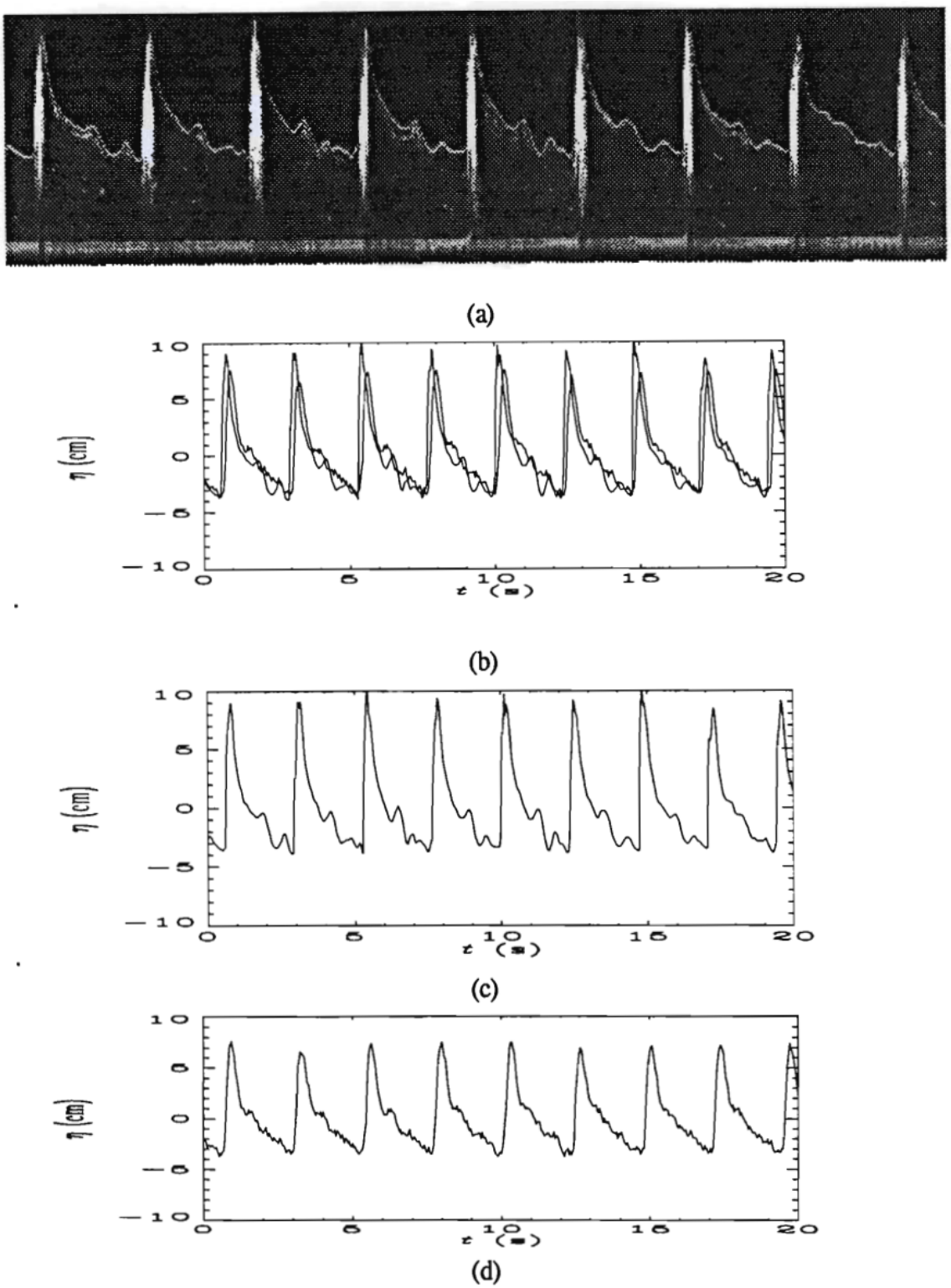

Figure 4.1: Time series of a plunging wave in the surf zone where (a) shows the assembled keogram; (b) a composite wave height plot of the wave gauge and digitised keogram; (c) the wave heights from the digitised keogram; and (d) wave heights as recorded by the probe (image appears in Govender (1999))

- Because of the highly turbulent nature of the surf zone, statistical techniques are needed to describe the turbulence measurements. This requires long sampling and recording times in order to extract meaningful statistical quantities.
- Simulation of the surf zone has surface flow moving in an onshore direction and offshore flow from the undertow. As such, the particle seeds do not stay in one place for long (i.e. some end up on the "beach" area and some accumulate at the breakpoint). The area under measurement needs to be perpetually supplied of particles in order to have meaningful measurements.
- The aerated region of wave breaking appears as white streaks on the PIV images which obscure the seeded particles.

4.3 Laboratory Experiment: Govender (1999)

4.3.1 Experimental setup

Govender (1999) conducted wave-breaking experiments in a glass-walled 2D flume at the Coastal Engineering Laboratory of the CSIR in Stellenbosch, South Africa.

The basic flume model setup used by Govender (1999) in the physical model is shown in Figure 4.2.

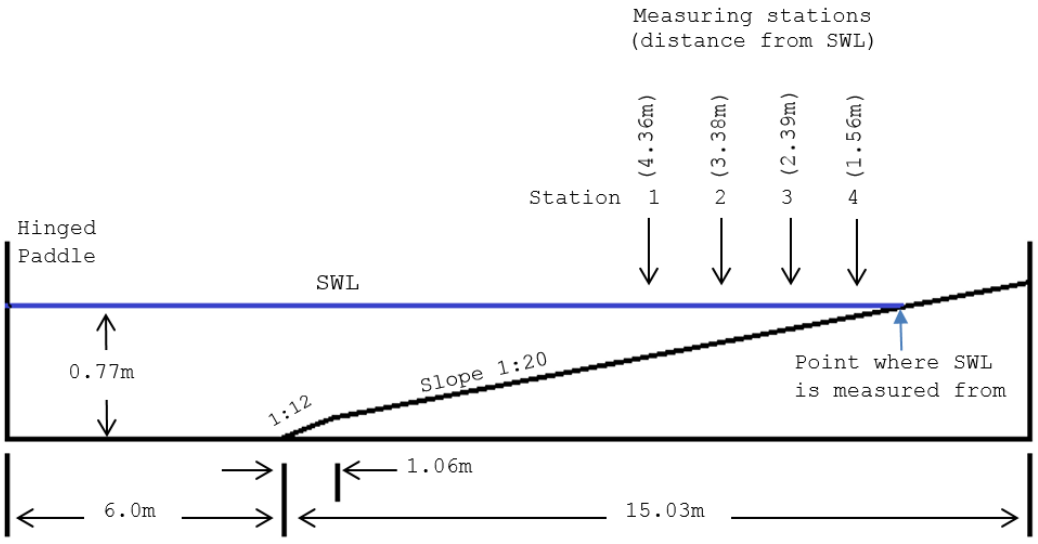

Figure 4.2: Schematic of the experimental flume setup as published in Govender (1999).

Two types of monochromatic waves were generated over a plane slope of 1:20 during the physical modelling: a spilling wave and a plunging wave. The modelled wave characteristics are given in Table 4.1 where H_o (m) is the deep water wave height; d_o (m) is the depth at the wave paddle; f (Hz) is the wave frequency; T (s) is the wave period; L_o (m) is the deep water wave length; H_b (m) is the observed wave height at the breakpoint and h_b (m) is the local still water depth at the breakpoint.

Table 4.1: Wave characteristics modelled by Govender (1999)

Wave Type	H_o (m)	d_o (m)	f (Hz)	T (s)	L_o (m)	H_b (m)	h_b (m)
Spilling	0.16	0.77	0.9	1.11	2.04	∼0.160	0.22
Plunging	0.11	0.77	0.4	2.50	6.87	∼0.175	0.16

4.3.2 Data measurements

The wave height data recorded is the keogram output for the spilling and plunging waves along the sloped section of the flume (spaced approximately 0.10m apart). The wave height data was recorded at approximately 24Hz for a total time interval of 40 seconds.

The PIV measurements calculated the instantaneous particle velocity at four separate locations. From these measurements, the phase averaged samples of instantaneous velocity, wave height and turbulence intensities over a full wave cycle were calculated. In addition, time-averaged velocity, turbulence intensities and calculated TKE from the experiments are given.

4.3.3 Aim of experiments and published outcomes

Spilling and plunging wave breaker experiments were conducted in order to record and analyse velocity and turbulent structures within the pre-breaking zone, breaker zone and subsequent energy dissipation.

The measured orbital velocity fields were compared with linear theory. Govender (1999) found that linear theory over-predicted the orbital velocities below the trough level and under-predicted the orbital velocities above the trough level. Orbital velocities calculated with linear theory showed over-predictions in the order of 100% in spilling wave and over a 100% in the plunging waves.

Investigation of the turbulent structures generated in the surf zone was conducted by the computation of the phase ensemble averaged turbulence intensities and vorticity from the PIV measurements. It was found that peak turbulence intensities were measured near the front face of the wave where wave breaking was taking place. Time-averaged turbulence intensities showed

an increase from the bed level to trough level and a decrease thereafter. The peak time averaged TKE occurred above trough level. The maximum TKE dissipation rate (ϵ) was shown by Govender (1999) to occur above trough level around the mean water level. Below the trough level, the dissipation rate decreased exponentially. Turbulent length scales were estimated from ϵ. From the bed to the trough level the length scales displayed mostly a decreasing trend.

Using video techniques, the roller geometry for the spilling and plunging breakers was quantified. Through the inner surf zone, the normalised roller geometry was shown to be nearly constant while increasing towards the middle of the surf zone.

4.3.4 Output locations

Wave heights were recorded at 65 locations for the plunging waves and at 67 locations for the spilling waves along the sloped section of the wave flume. PIV velocity measurements were conducted at three separate locations for the spilling and plunging conditions. As indicated in Figure 4.2, stations 1,3 and 4 were analysed for the plunging breaker case while stations 1, 2 and 3 were used for the spilling breaker condition. The breakpoint for the plunging breaker was located 3.25m from the SWL and 4.38m from the SWL for the spilling breaker (see Figure 4.2).

The plunging wave characteristics are given in Govender (1999) and reproduced in Table 4.2.

Table 4.2: Wave characteristics for the plunging wave case at the relevant measuring stations

Station number	Distance from Breakpoint (m)	Local Wave Height (m)	Still Water Depth (m)
1	-1.11	0.150	0.218
3	0.86	0.115	0.119
4	1.69	0.078	0.078

The spilling wave characteristics are given in Table 4.3.

4.4 Laboratory Experiment: Ting and Kirby (1994)

4.4.1 Experimental setup

Ting and Kirby (1994) performed their wave experiments in a glass-walled flume at the Ocean Engineering Laboratory, University of Delaware, U.S.A.

Table 4.3: Wave characteristics for the spilling wave case at the relevant measuring stations

Station number	Distance from Breakpoint (m)	Local Wave Height (m)	Still Water Depth (m)
1	0.02	0.150	0.218
2	1.22	0.110	0.169
3	2.21	0.065	0.119

The basic setup used by Ting and Kirby (1994) in the physical model is shown in Figure 4.3.

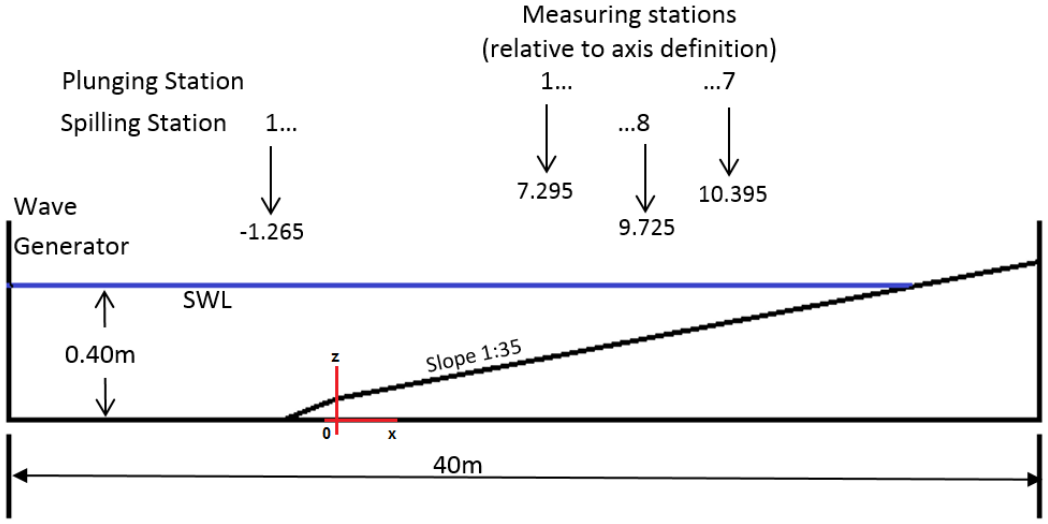

Figure 4.3: Schematic of the experimental flume setup as published in Ting and Kirby (1994)

Ting and Kirby (1994) performed physical model experiments on a 1:35 plane slope studying spilling and plunging waves. Monochromatic waves were generated to produce the spilling and plunging waves. The wave characteristics are given in Table 4.4 where H_o (m) is the deep water wave height; H_h (m) is the wave height in the horizontal region of the flume; T (s) is the wave period; x_b (m) is the x-coordinate of the breakpoint relative to the measuring axis; and d_b (m) is the local still water depth at the breaking point.

4.4.2 Aim of experiments and published outcomes

Ting and Kirby (1994) performed their physical model experiments to study the undertow and turbulence produced by spilling and plunging waves. The authors used a Laser-Doppler anemometer to record fluid velocities in various

Table 4.4: Wave characteristics modelled by Ting and Kirby (1994)

Wave Type	H_o (m)	H_h (m)	T (s)	H_0/L_o	x_b (m)	d_b (m)
Spilling	0.127	0.125	2.0	0.020	6.400	0.196
Plunging	0.089	0.128	5.0	0.002	7.795	0.156

points across the flume. Instantaneous wave heights and the average wave set-up were also measured. The main focus of the paper was to analyse and compare the turbulence levels induced by the breakers and the difference in transport mechanisms induced by the waves.

The authors found that the turbulence levels are much higher for the plunging breaker than for the spilling breaker while the turbulence intensities and vertical variation in the undertow velocity across the water column are much higher for the plunging breaker than the spilling breaker. In addition, the turbulent kinetic energy advection direction differs significantly due to the mean flow for each type of breaker; the plunging breaker directs the TKE landward while the TKE is directed seaward for the spilling breaker.

Two more publications followed from this experiment where the characteristics of the plunging wave (Ting and Kirby, 1995) and the spilling wave were investigated (Ting and Kirby, 1996) individually.

The analysis of the plunging wave showed that the distribution of turbulence under a plunging wave is a function of the diffusive and advective transport of the turbulence. The production and dissipation of turbulence are of the same order of magnitude but not necessarily in equilibrium. It was further shown that only a small amount of energy is lost below trough level due to turbulence production and viscous dissipation (Ting and Kirby, 1995).

The analysis of the spilling breaker showed that the diffusive transport is the primary mechanism of turbulence transport while advection is important near the surface. Similar to the plunging breaker, wave energy loss is small below the trough level of the wave (Ting and Kirby, 1996).

4.4.3 Output locations and data measurement

Fluid velocities due to the wave action were recorded and analysed in various points across the flume. The fluid velocities were sampled at 100Hz and wave velocities recorded for just over 4 minutes. The locations of the velocity measuring points and the local still water depth for the plunging and spilling breakers are given in Table 4.5. Seven velocity measuring stations were set up for the plunging wave. Note that the reference point in the flume is located at the start of the plane slope.

The data measured at these points are the instantaneous horizontal and vertical velocities and the water level.

Table 4.5: Locations of the velocity measuring stations for both the plunging and spilling breakers in the Ting and Kirby (1994) experiments

Station	Plunging Wave		Spilling wave	
No.	x(m)	d(m)	x(m)	d(m)
1	7,295	0.169	-1.295	0.400
2	7.795	0.156	5.945	0.208
3	8.345	0.142	6.665	0.185
4	8.795	0.128	7.275	0.169
5	9.295	0.113	7.885	0.152
6	9.795	0.096	8.495	0.137
7	10.395	0.079	9.110	0.119
8			9.725	0.097

Capacitance wave gauges were used to measure wave heights and wave setup across the flume with a sampling frequency of 50Hz. Measurements were made approximately every 0.5m from x=-1.50m to x=11.0m. Water level measurements were recorded for around 200 seconds and the wave set-up calculated for this period using meaningful data.

Calculated turbulence intensities and TKE for each measurement point were supplied by the authors. It was verified that the instantaneous velocity measurements supplied corresponds to the published turbulence intensity values when using Equation 2.9.

Chapter 5

Sensitivity Analysis and Calibration of the SWASH Model

5.1 General

Numerical models are reliable only when the resultant calculations are shown to reasonably agree with the observed processes for the same scenarios. This chapter tests the effect of varying certain numerical parameters in SWASH and the influence they have on the modelled wave height, incipient breaking point and velocities. The calculated results are compared to the measured data of Govender (1999) for plunging and spilling breakers and conclusions drawn from the sensitivity analysis.

The main aim of this chapter is to highlight and report on the relative sensitivity of the numerical parameters that exist within SWASH which can be adjusted in order to calibrate a wave breaking numerical model with measured data.

5.2 Numerical model parameters

The numerical sensitivity of the SWASH model is conducted in the context of the surf zone processes of wave shoaling, wave breaking, particle velocities and turbulence.

The SWASH model results are compared to the experimental data described in Chapter 4. The numerical parameters that are varied in this study are as follows:

- Number of vertical layers: The number of vertical discretisation are varied between 5, 15, 20, 30 and 35 vertical layers (see Section 3.10). The SWASH modelled results are compared to the measured data in terms of the incipient breaking point;

- Friction coefficient: The Manning friction coefficient is varied between $n = 0.010$, $n = 0.030$ and $n = 0.050$ (see Section 3.11). The friction coefficient is kept constant across the SWASH model domain for each of these Manning values;

- The interpolation of the water depth in the velocity points through the use of numerical limiters: The calculation of the water depth in the velocity points is subjected to four higher order interpolation schemes with flux limiter: First order upwind, Superbee, QUICK and the MinMod scheme[1];

- Momentum conservation: The effect of explicit momentum conservation is varied. For all simulations the effect of enforcing momentum conservation everywhere compared to the default SWASH setting is tested, i.e. specifying the command DISCREET UPW MOM or leaving it out of the setup so that the default is activated (see Section 3.15); and

- The discretisation of the horizontal and vertical advective terms of the u- and w-momentum equations are tested. The varied combinations are given in Table 5.1 (also see Section 3.14).

Table 5.1: Summary of the discretisation schemes used for the u- and w-momentum equations in the SWASH calibration

Option	u-momentum		w-momentum	
	Horizontal	Vertical	Horizontal	Vertical
Default	BDF	FIR	BDF	FIR
AdvTerm 1	BDF	CDF	BDF	FIR
AdvTerm 2	BDF	FIR	CDF	FIR

During the setup of the numerical model, some inherent assumptions are made and are listed as follows:

i The physical model geometry is reproduced in SWASH as accurately as possible. The horizontal discretisation (Δx) and time step are chosen for numerical stability and convergence in accordance with the well known Courant number and CFL condition

$$Cr = \frac{\Delta t(\sqrt{gd} + |u|)}{\Delta x} \leq 1 \tag{5.1}$$

[1] A detailed description of the numerical schemes employed by SWASH (i.e. First order upwind, Superbee, QUICK and the MinMod schemes) is beyond the scope of this study. The reader is referred to Versteeg and Malalasekera (2007) for a detailed analysis of the equations behind the numerical schemes available in SWASH.

ii The packaged SWASH wave maker functions are used where possible. However, for the experiments of Ting and Kirby (1994), a cnoidal wave signal is used, which is not available in SWASH. A cnoidal wave height signal was produced externally and used in SWASH as a direct input time series. The water level measurements from the SWASH model and the experimental outputs were verified and found to be in agreement.

iii Some "default" numerical parameters assumed in SWASH include the following:

- Wave breaking is not explicitly stipulated; i.e the HFA is not activated;
- The number of vertical layers modelled for all sensitivity tests are kept at 20 apart from the specific layer sensitivity test conducted.
- The horizontal and vertical eddy viscosity are calculated using the Prandtl and $k - \epsilon$ formulations;
- The non-hydrostatic option "STANDARD" is activated; and
- Initial water level, horizontal and vertical velocities are all set to zero.

5.2.1 Comparison of results

The SWASH numerical results are compared with the measured Govender (1999) data in terms of:

- Maximum water level measurements at positions cross-shore in the flume. The water level measurements are given relative to the still water level. The measurements begin at a point close to the start of the sloped section and continue up to where the still water level (SWL) meets the sloped bottom. The measurements are spaced approximately 0.10m apart. The maximum water level over the whole time series recorded for a range of measuring points is used to determine the incipient breaking point. Note that the x-axis values are given in distance from the point where the SWL meets the sloping bottom. As such, the wave direction indicated in the water level plots will appear to be from right to left for the Govender (1999) data;

- Phase averaged water levels are reported at four locations in the flume. The first point is located at the furthest point offshore of the breaking point (in "deeper" water); the second, during shoaling just before wave breaking; the third, right after wave breaking; and the fourth in shallow water where the steady bore has already developed. The details of the locations are given in Table 5.2; and

- Phase averaged velocities: Modelled SWASH phase averaged horizontal (u)- and vertical (w) instantaneous velocities are compared to recorded PIV results. This is done at four locations in the water column and at two cross-shore points in the flume: a point just before breaking (Point 1) and a point after breaking (Point 3 for plunging breaker and Point 2 for the spilling breaker). Refer to Figure 4.2 for the graphical layout of these points).

Table 5.2: Output locations, distance from the SWL and the still water depth at the output locations for the SWASH simulation results

	Water levels	Distance from SWL (m)	Depth at SWL (m)
Plunging Wave	PWP1	8.35	0.420
	PWP2	3.40	0.170
	PWP3	3.20	0.160
	PWP4	0.90	0.045
Spilling Wave	SWP1	8.35	0.42
	SWP2	4.61	0.23
	SWP3	4.31	0.21
	SWP4	1.00	0.05

5.2.2 Other significant parameters

The calculated turbulence (TKE) and wave set-up in the surf zone are direct results of the calibration parameters for the specific models. Although these parameters are important results, they are not considered to be calibration parameters in the same way as water level and velocity are. Instead, it is expected that turbulence and wave set-up will correspond to the measured data if the water level and velocity of the modelled waves are calibrated relative to the physical measurements.

Turbulence: The turbulence intensities from the physical models are calculated from the statistical methods explained in Chapter 2.12. From these equations (Equation 2.5 to Equation 2.10) it follows that the turbulence intensities and TKE in the physical models are calculated directly from the fluctuations of the instantaneous measured horizontal and vertical velocities.

SWASH employs numerical models to model the turbulence (i.e. Prandtl and the $k-\epsilon$ model) and thus different results between calculated and modelled results are naturally expected. For instance, the velocity fluctuations of the eddies recorded in the physical models will not be seen in the instantaneous particle velocities calculated by SWASH.

The calculated TKE from the physical models (Equation 2.10) is compared with the modelled TKE produced by SWASH. This is discussed in Chapter 6.6.

Wave setup / setdown: Ting and Kirby (1994) measured wave setup and setdown at measuring points across the flume. Their results are compared to the setup/setdown calculated by the SWASH model. Due to the fact that wave setup is primarily a function of the wave height, it is assumed that a numerical model that is calibrated in terms of wave height will reflect a good comparison to the measured results in terms of wave setup.

5.2.3 Interpolation of the modelled grid to the experimental grid

In order to compare the measured data with the SWASH model, it is pertinent to note the interpolation between the SWASH output grid and the measured data output grid. The measured output considers a static frame of reference at a point in the flume and calculates the particle velocity vectors in time on a fixed regular grid over time; i.e. at an arbitrary point x,y in the frame of reference, there exists either a water point (with a velocity value) or air (no velocity). Figure 5.1 shows a simplified schematisation of the measured flume reference grid and the SWASH reference grid.

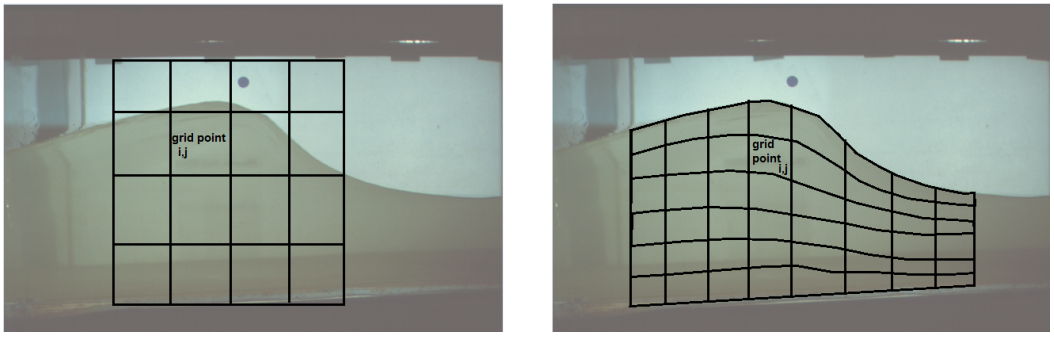

Figure 5.1: Schematisation of the measured flume reference grid and the SWASH grid. Left panel is the flume reference grid and right panel the SWASH schematised grid

In essence, the SWASH vertical layers adapt percentage wise with time relative to the water level (refer to Figure 3.1). Note that fixed vertical water level can also be specified in SWASH; however, one layer must be enabled to adjust dynamically with the changing water level.

To compare the measured data to the modelled data, the SWASH modelled output must be interpolated onto the flume static reference grid. This interpolation is done using a cubic spline interpolation.

5.3 Plunging waves

This section describes the sensitivity of the SWASH model relative to the variation in friction coefficients, discretisation of the horizontal and vertical advection terms and the water depth at the velocity points interpolation method. The calculated SWASH results are compared to the plunging wave measurements of Govender (1999). The aim is to:

1. Find the best numerical approximation that will correspond to the physical measurements; and

2. Demonstrate the sensitivity of the numerical parameters of the calculated SWASH model results in terms of the incipient breaking point, wave height and velocities in the horizontal and vertical directions.

5.3.1 Vertical resolution

Smit (2014) and The SWASH Team (2016) state that a high vertical resolution of between 10 and 20 layers will be adequate to account for wave breaking processes and to keep track of the incipient breaking point. By implication, a vertical resolution that is too low to account for the vertical flow structures will cause an early onset of wave breaking. Liao (2015) found that a vertical resolution of between 20 and 30 layers proved to be sufficiently fine in modelling the undertow. This section only considers the influence of the number of vertical layers on the incipient breaking point.

Although the guideline of "10 to 20 layers" has been shown by Smit (2014) to be a valid assumption, the influence on the incipient breaking point is tested by varying the vertical resolution in SWASH with 15, 20, 30 and 35 vertical layers and comparing it to the measured Govender (1999) plunging wave data. The vertical resolution values are chosen as a range based on the work of Smit (2014) and Liao (2015). The calculated SWASH results are given in Figure A.1. The momentum is explicitly conserved in the left panel but not so in the panel on the right. Note that the wave direction in the plot is from right to left on the x-axis.

Two main observations can be made from Figure A.1:

- The momentum conservation has the most influence on the position of the incipient breaking point. The significant variation in results seen in Figure A.1 between the left and the right panels are solely as a result of varying the strict momentum conservation requirement. The 35 layer model and 15 layer models appear to be the most consistent between the two figures while the 20 and 30 layer models show the most variation between the two modes.

  The momentum conservation increases the maximum wave height at the breaking point with approximately 10mm for 20 vertical layers but re-

duces the maximum wave height by the same amount for a SWASH model with 30 vertical layers. With this increase and decrease, the breaking point also moves onshore or offshore accordingly; and

- The increase in the number of vertical layers from 15 to 35 does not improve the accuracy of the location of the incipient breaking point.

A further attempt at defining the influence that a number of vertical layers have on the incipient breaking point is shown in Figure A.2 where the maximum water level for vertical layers of 5, 15 and 35 layers are given.

It seems as if the effect of momentum conservation is dampened when the maximum water level results presented on the right and left panel of Figure A.2 are compared. It is clear from the results that a variation in the vertical resolution has an influence on the location of the breaking point. Contrary to what Smit (2014) reports, a reduction in the vertical resolution seems to move the incipient breaking point further offshore.

From these results, it can be concluded that the vertical resolution and the explicit conservation of momentum have an influence on the cross-shore location of the breaking point. Figure A.2 suggests that this point is resolved further onshore with an increase in the vertical resolution.

For a high (35) or low (5 or 15) amount of vertical layers, the incipient breaking point remains constant regardless of the momentum conservation applied. For vertical layers of 15 or 20 layers, the momentum seems to have a pronounced influence on the modelled results, much more so than the influence of the number of vertical layers on the incipient breaking point.

5.3.2 Friction parameters

As reported in Section 3.11, the Manning friction formulation is suggested by The SWASH Team (2016) when modelling surf zone processes. It is worth stating here that Liao (2015) tested the influence of varying the bottom friction using the Nikuradse formulation. Note that this work was conducted within the context of horizontal velocity 5cm above the flume bed. The author concluded that the bottom friction is not a major contribution in the SWASH calculation of the vertical velocity, nor in the wave decay.

Using the experimental setup of Govender (1999) for plunging breakers, the Manning value in the SWASH models was varied between $n = 0.010$, which is equivalent to plywood and $n = 0.050$, which is the value for natural channels in a poor condition (see Chadwick *et al.* (2004) for an exposition of the Manning coefficient).

The results of the model are shown in Figure A.3 where the maximum wave heights in the time recorded series are plotted for each measurement point along the flume. Note that the wave direction in the plot is from right to left.

From Figure A.3 it can be seen that an increase in the friction parameter has a significant impact on the incipient breaking point when momentum is conserved. A relatively small increase in wave height at the breaking point is observed when momentum is conserved compared to no explicit conservation of momentum for friction coefficients of $n = 0.03$ and $n = 0.05$.

Figure A.4 and Figure A.5 plot the phase averaged water level at given points in the flume. It can be seen from both of these figures that a lower friction value ($n = 0.010$) fits the data very well before wave breaking. After breaking, the higher friction values fit the data well. An over-prediction of the average wave height is seen for higher friction values around the breakpoint. This is expected given the results reported earlier with regards to the maximum wave height.

When momentum is conserved, the phase-averaged wave height is marginally higher than in the case of non-explicit conservation of momentum.

A significant result is seen in the phase-averaged wave height well after breaking (bottom right panels of Figure A.4 and Figure A.5) where the conserved momentum model for higher Manning values shows a good fit to the measured data.

This result bears further investigation. A SWASH model with variable bottom friction in the model domain is run. The Manning friction value of $n = 0.010$ is used for all bottom points before wave breaking and a value of $n = 0.050$ for all values after the point of wave breaking. This is compared to constant friction values of $n = 0.010$ and $n = 0.050$. The result of this analysis is shown in Figure A.6.

It can be seen from Figure A.6 that the modelled variable friction field shows the same result as that for a constant friction value of $n = 0.010$ - the friction value before the breaking point. The influence of the higher friction value specified after wave breaking is not reflected in the results. As reported in Section 2.8 and Section 3.11, the apparent roughness in the breaking zone differs from the non-breaking zone. From this SWASH result it can be seen that the friction parameter has a greater influence on the non-breaking region than on the turbulent breaking region.

Considering the phase averaged water level results, it can be concluded that higher Manning friction values with momentum conserved show the best agreement with the measured results, especially where the water levels after wave breaking are important. Before wave breaking, the average wave heights are overestimated by approximately 25mm. A variable friction field adds no additional value to the accuracy of the SWASH results as the bottom friction seems to have the most influence on the wave energy prior to wave breaking.

The influence of the friction parameters and momentum conservation on the horizontal velocity for measuring station P1 (before wave breaking) are illustrated in Figure A.7 and Figure A.8.

From both Figure A.7 and Figure A.8 it is clear that a higher Manning friction value fits the measured horizontal velocity results well in terms of

phase averaged shape and peak horizontal velocity at all points throughout the water column. Note that near the bed (top right panel), the SWASH model overestimates the peak horizontal velocity by approximately 0.1m/s.

Comparing the case where momentum is conserved with the case where momentum is not explicitly conserved, it is clear that the latter option shows excellent results across the water column for Manning values of $n = 0.030$ and $n = 0.050$.

The influence of the friction parameter and momentum conservation on the vertical velocity for measuring station P1 (before wave breaking) are illustrated in Figure A.9 and Figure A.10.

The vertical velocities compare in much the same way as the horizontal velocities considering Figure A.9 and Figure A.10. The SWASH calculations fit well with the measured results for higher manning values and for the case where momentum is not explicitly conserved.

It can be concluded that a Manning value of $n = 0.030$ and not explicitly conserving momentum result in the best fit for the SWASH calculations when compared with the measured horizontal and vertical velocities for measuring Station 1.

The influence of the friction parameter and the momentum conservation on the horizontal velocity for measuring station P3 (after wave breaking) is illustrated in Figure A.11 to Figure A.12.

After wave breaking (Station P3) it is clear that the friction parameter plays a greater role in determining the horizontal velocity of the propagating bore. The SWASH results show a good fit for a Manning value of $n = 0.030$ in the lower part of the water column (panels top left and top right) while the peak horizontal velocity is severely under predicted near the water surface (bottom left and right panels). Note the difference in scale for the bottom right panels in Figure A.11 and Figure A.12. The Govender (1999) data shows peak horizontal phase averaged velocities of approximately 2.2m/s which is deemed as unnaturally high as opposed to the maximum horizontal velocity calculated by SWASH in the order of 0.5m/s. It is assumed that an undocumented measurement error might have been reported by Govender (1999) in the measured data. The shape of the phase-averaged SWASH horizontal calculations is in a good agreement with the measurements despite the lower calculated velocities.

The lower Manning value tends to under-predict the horizontal velocity throughout the water column. In contrast, the higher Manning value over-predicts the peak horizontal velocity in the bottom half of the water column and under-predicts the same in the upper water column.

The explicit conservation of momentum does not seem to have a major influence on the variation of the modelled SWASH results.

The influence of the friction parameter and the momentum conservation on the vertical velocity for measuring station P3 (after wave breaking) is illustrated in Figure A.13 and Figure A.14.

The vertical velocities measured by Govender (1999) and calculated by SWASH are relatively low after breaking. It can be seen in Figure A.13 and Figure A.14 that the peak vertical velocity is well represented by SWASH even though the physical measurements show some random individual points. It is clear that the choice of friction parameter or the conservation of momentum has little influence on the vertical velocities after breaking.

Considering the visual output presented here (Figure A.11 to Figure A.14), it can be concluded that, after wave breaking, a Manning value of $n = 0.030$ results in the best fit for the SWASH calculations when compared with the measured horizontal and vertical velocities for measuring Station 3. However, a clear conclusion cannot be reached for horizontal velocities near the surface as the measured data produces exceptionally high values. The conservation of momentum after wave breaking does not have a significant influence on the SWASH modelled results.

Note that from this point onwards, all other sensitivity tests are performed with a constant Manning friction value of $n = 0.030$.

A summary of the friction parameter sensitivity findings is given in Table 5.3.

Table 5.3: Summary of the friction parameter sensitivity in SWASH for a plunging wave when compared to the Govender (1999) measured data

Parameter	**Number of vertical layers**
Incipient breaking	Significant influence when momentum is conserved for 20 to 30 layers. Incipient breaking point moves offshore with lower number of layers.
Parameter	**Friction**
Incipient breaking	Significant influence when momentum is conserved
Maximum wave height	Higher Manning values result in better fit.
	Before breaking / **After breaking**
Phase averaged wave height	Lower friction values. Momentum insignificant / Higher friction values produce better fit Momentum insignificant
Phase averaged horizontal velocity	Higher friction values better fit Momentum not conserved better fit to measurements / Friction plays a significant role Insensitive to momentum conservation
Phase averaged vertical velocity	Higher friction values Momentum not conserved / Insensitive to friction value Insensitive to momentum conservation

5.3.3 Horizontal and vertical advection terms of the momentum equation

Liao (2015) investigated the sensitivity of the SWASH results with a variation in the discretisation of the horizontal and vertical advection terms. The author varied combinations of the horizontal advection terms ($\frac{\partial uu}{\partial x}$ and $\frac{\partial uw}{\partial x}$) with combinations of second order backward upwind differencing (BDF) and standard central differencing (CDF). This was done in conjunction with a variation in the vertical advection terms ($\frac{\partial wu}{\partial z}$ and $\frac{\partial ww}{\partial z}$) with combinations of first order upwind differencing (FIR) and standard central differencing.

Liao (2015) found that wave decay was not sensitive to variations in the horizontal advection term $\frac{\partial uw}{\partial x}$. However, relative to the horizontal advection term, wave decay was observed to be more significant with a change in the vertical advection term $\frac{\partial wu}{\partial z}$ discretisation. The author found that the combination of second order backward upwind differencing for the horizontal advection terms and first order upwind differencing scheme used for the vertical advection terms proved to be the most accurate schemes for simulating wave height transformation and wave setup across the surf zone.

In order to test the influence of various discretisation schemes on the water level and velocity calculations in SWASH, a combination of discretisation methods, as detailed in Section 5.2 and given in Table 5.1, was compared to the measured Govender (1999) plunging wave data (refer also to Section 3.14).

Figure A.15 shows the influence of the discretisation schemes on the maximum wave height calculated at points across the flume. The SWASH results are compared to the measurements made by Govender (1999).

The variation in discretisation schemes has a negligibly small influence on the incipient breaking point. The only influence on the results can be seen with the variation in the momentum conservation. In Figure A.15 (left panel) it can be seen that the incipient breaking point shifts shoreward when momentum is conserved explicitly. The variation in the discretisation schemes shows almost no difference between them when momentum is not explicitly conserved (right panel). Only the SWASH default discretisation scheme is influenced by the conservation of momentum when comparing the maximum water levels across the flume.

Figure A.16 and Figure A.17 plot the phase averaged water level at four given points in the flume.

The phase-averaged water level plots clearly show that the default and AdvTerm2 schemes compare well with the measured flume data. Peak wave heights before breaking are higher when compared to the measured data than after breaking where they compare very well to the measured data. The AdvTerm1 scheme does not compare well to the measured data post wave breaking as it under-predicts the peak wave heights.

In addition, the conservation of momentum has more of an influence on the shape of the wave height over the normalised wave phase than the wave

height; i.e. the conservation of momentum steepens the wave face more than the alternative option. However, the peak wave heights follow the same pattern displayed by the momentum explicitly conserved option for pre- and post breaking in the flume. However, the nearshore wave phase average heights (PWP4) are better represented by the default advection scheme when momentum is conserved (compare bottom right panels of Figure A.16 and Figure A.17).

Considering purely the wave height, it can be concluded that the default discretisation scheme of the advection terms with momentum conserved explicitly shows the best fit to the measured data.

Next, the influence of the various schemes on the horizontal and vertical velocity is investigated. The influence of the discretisation schemes and the momentum conservation on the horizontal velocity for measuring station P1 (before wave breaking) is illustrated in Figure A.18 and Figure A.19.

Note the discrepancy between the measured and modelled data at a distance of 18.8cm above the bed (bottom left panel of Figure A.18) for $0.65 < t/T < 0.9$: this is a quirk of the interpolation between the measured data grid (regular static grid) and the swash dynamic grid in order to be able to compare the data sets (see Section 5.2.3 for the discussion on the interpolation).

From both Figure A.18 and Figure A.19 it can be seen that the AdvTerm 1 and AdvTerm2 schemes fit the measured horizontal velocity results well in terms of phase averaged shape and peak horizontal velocity at all points throughout the water column.

The default advection scheme has the most variation in terms of phase-averaged velocity shape when comparing the case where momentum is conserved with the case where momentum was not explicitly conserved. In both momentum cases, the AdvTerm 1 and AdvTerm2 schemes show the best fit while the default scheme shows a good fit where momentum was not explicitly conserved. The same observations are valid for the vertical phase averaged velocities which are shown in Figure A.20 and Figure A.21.

The vertical velocities compare in much the same way as the horizontal velocities considering Figure A.20 and Figure A.21. The SWASH calculations fit well with the measured results for the schemes AdvTerm 1 and AdvTerm 2. Momentum conservation does not seem to play a significant role in the discretisation schemes except in a minor manner for the AdvTerm Default scheme.

It can be concluded that the AdvTerm 1 and AdvTerm 2 schemes, regardless of the option of momentum conservation, result in the best fit for the SWASH calculations with the measured horizontal and vertical velocities for measuring Station 1.

The influence of the various advection schemes and the momentum conservation on the horizontal velocity for measuring station P3 (after wave breaking) is illustrated in Figure A.22 to Figure A.23.

The SWASH results show a good fit for the default advection scheme near the bed (top panels) to near surface part (bottom left panel) of the water column while the peak horizontal velocity is severely underpredicted at the water surface (bottom right panel) due to the very high horizontal velocities measured by Govender (1999) near the water surface. Note the difference in scale for the bottom right panels in Figure A.22 and Figure A.23. The default scheme shows good results in both of the tested momentum cases. The other advection schemes (AdvTerm 1 and 2) show good results for the case where momentum is not explicitly conserved.

The influence of the advection schemes and the momentum conservation on the vertical velocity for measuring station P3 (after wave breaking) is illustrated in Figure A.24 and Figure A.25.

The vertical velocities measured by Govender (1999) and calculated by SWASH are relatively low after breaking. It can be seen in Figure A.24 and Figure A.25 that the peak vertical velocity is well represented by SWASH even though the physical measurements show some random individual points. It is clear from the results that neither the choice of advection schemes nor the conservation of momentum have any significant influence on the vertical velocities after breaking.

It can be concluded that the default scheme, regardless of momentum option, showed the best fit to the measured results for horizontal and vertical velocities after wave breaking. However, this result is inconclusive regarding the horizontal velocities near the water surface.

A summary of the type of advection discretisation scheme sensitivity findings is given in Table 5.4.

Table 5.4: Summary of the type of advection discretisation schemes sensitivity in SWASH for a plunging wave when compared to the Govender (1999) measured data

Parameter	Advection Schemes	
Incipient breaking	Influence on default scheme when momentum is conserved	
Maximum wave height	No significant difference between schemes. Higher wave height for default sheme with momentum	
	Before breaking	**After breaking**
Phase averaged wave height	Default and AdvTerm 2 scheme best fit Momentum conservation alters wave shape	Default and AdvTerm 2 scheme best fit
Phase averaged horizontal velocity	AdvTerm 1 and AdvTerm 2 scheme best fit Insensitive to momentum conservation	Default sheme insensitive to momentum conservation; Other schemes good fit where momentum not conserved.
Phase averaged vertical velocity	AdvTerm 1 and AdvTerm 2 scheme best fit Insensitive to momentum conservation	Insensitive to advection scheme Insensitive to momentum conservation

5.3.4 Water depth in velocity points

The water depth in the velocity points is not uniquely defined due to the staggered mesh used by SWASH (see Figure 3.2). As such, the distance between the calculation point for the water depth and the velocity point must be interpolated in some way. Standard interpolation would entail taking the arithmetic mean over the distance in the cell (Tan, 1992). However, SWASH uses first order upwinding instead of the usual interpolation techniques. Various higher order accuracy schemes with flux limiters are included in SWASH to obtain second-order accuracy in space (The SWASH Team, 2016).

By default, SWASH approximates the depth in velocity points by the MUSCL limiter. Versteeg and Malalasekera (2007) describe the mathematics of these higher order schemes and their area of application in detail.

In order to test the sensitivity of higher order schemes in the interpolation of the water depth in velocity points, various higher order interpolation schemes with flux limiter (First Order Upwind, Superbee, Quick and MinMod) are compared with each other and with the measured data from Govender (1999). In addition, explicit momentum conservation is also varied.

Figure A.26 shows the influence of the higher order schemes on the maximum wave height calculated at points across the flume. The SWASH results are compared to the measurements made by Govender (1999).

Comparing the left panel with the right panel of Figure A.26, it can be seen that there is very little difference in the numerical results when momentum is conserved explicitly compared to when momentum is not conserved explicitly.

The incipient breaking point appears to be the same for all the interpolation schemes conducted regardless of the momentum mode.

The variation in the interpolation limiter schemes shows a significant variation in the calculated maximum wave height across the flume. The MinMod scheme has the best fit in terms of maximum wave height to the measured results. The first order scheme under-predicts the maximum wave height (by a little over 10mm) while the Superbee and QUICK limiter schemes over-predict the wave heights by the same margin at the peak maximum wave height. The QUICK and Superbee limiter schemes show to have very similar calculated results.

Figure A.27 and Figure A.28 plot the phase averaged water level at four given points in the flume.

As expected, there is no significant difference in the phase-averaged wave heights when momentum is conserved explicitly compared to when momentum is not conserved explicitly. Again, a difference in calculated wave height prior to wave breaking is observed (top panels) when compared to post wave breaking (bottom panels). The first order upwind limiter shows excellent results prior to breaking, especially at the point before breaking (top right panel), while the other schemes over predict the phase-averaged wave height - the MinMod limiter by approximately 10mm and the others by a higher margin of

15mm. Post-wave breaking the first order upwind scheme under predicts the wave height (by a fraction less than 30mm) while the other schemes show well calculated results, albeit slightly less than the measured data. In all cases, the trough of the wave is not well represented by the schemes.

Considering the water level analysis, it can be concluded that a variation in the interpolation limiter schemes has an influence mainly on the calculated water levels but has no significant influence on the incipient breaking point. The MinMod scheme shows the best fit to the measured data with regards to maximum water level while the first order upwind scheme shows excellent correlation to the measured data pre-wave breaking. Post-wave breaking, the remainder of the schemes correlate fairly well with the measured data. On average, the MinMod scheme shows to be the best fit in terms of the measured data.

The influence of the higher order interpolation schemes and the momentum conservation on the horizontal velocity for measuring station P1 (before wave breaking) is illustrated in Figure A.29 and Figure A.30.

The explicit conservation of momentum does not seem to have any significant influence on the results when comparing Figure A.29 and Figure A.30 with each other.

The first order scheme fits the measured horizontal velocity results very well in terms of phase averaged shape and peak horizontal velocity at all points throughout the water column. The MinMod and Superbee schemes also show very good agreement with the measured results with the QUICK limiter having the most variation.

The same observations is valid for the vertical phase averaged velocities which are shown in Figure A.31 and Figure A.32.

Negligibly minor variations in phase averaged vertical velocity at the peak is observed between the lower- and upper half of the water column. Regardless, the calculated results compare very well to the measured results for all limiters tested.

It can be concluded that the first order upwind scheme shows the best fit with the measured results throughout the water column when considering Figure A.31 and Figure A.32. The other schemes also perform acceptably well with the exception of the QUICK scheme that overestimates the horizontal and peak velocities throughout the water column.

The influence of the various higher order interpolation limiter schemes and the momentum conservation on the horizontal velocity for measuring station P3 (after wave breaking) is illustrated in Figure A.33 to Figure A.34.

The SWASH results show a good fit for the all the schemes in the bottom part (panels top left and top right) of the water column while the peak horizontal velocity is severely underpredicted in the upper half of the water column (bottom left and right panel) due to the extremely high peak horizontal velocity recorded by Govender (1999) near the surface. Note the difference in scale for the bottom right panels in Figure A.33 and Figure A.34. The QUICK

scheme shows a minimal variation in shape compared to the other schemes. This would imply that the maximum phase-averaged velocity in the QUICK scheme is extended slightly in time, i.e. some type of lag occurs.

The influence of the advection schemes and the momentum conservation on the vertical velocity for measuring station P3 (after wave breaking) is illustrated in Figure A.35 and Figure A.36.

The vertical velocities measured by Govender (1999) and calculated by SWASH are relatively low after breaking. It can be seen in Figure A.35 and Figure A.36 that the peak vertical velocity is well represented by SWASH despite the physical measurements showing some random individual points. The choice of interpolation schemes or the conservation of momentum has little influence on the horizontal and vertical velocities after breaking.

It can be concluded that the MinMod scheme shows the best-calculated result when the maximum wave height is considered while the first order upwind scheme shows the best results for the phase averaged horizontal velocity calculations across the whole water column. In addition to the first order upwind scheme, the other schemes also show good agreement with the measured results for measuring Station 1 while all schemes show a good fit for the data from measuring Station 3.

A summary of the water depth to velocity point interpolation scheme sensitivity findings is given in Table 5.5.

Table 5.5: Summary of the water depth to velocity point interpolation schemes sensitivity in SWASH for a plunging wave when compared to the Govender (1999) measured data

Parameter	Water depth in velocity points	
	Before breaking	**After breaking**
Incipient breaking	Insensitive to momentum conservation	
Maximum wave height	Insensitive to scheme used	
	MinMod scheme shows best fit.	
	Other schemes over/under predict wave height	
Phase averaged wave height	MinMod scheme shows best fit. Insensitive to momentum conservation	QUICK and Superbee good fit Insensitive to momentum conservation
Phase averaged horizontal velocity	FIR shows best fit	FIR shows best fit
	Other schemes also good fit Insensitive to momentum conservation	Other schemes also good fit Insensitive to momentum conservation
Phase averaged vertical velocity	All schemes show good fit	All schemes show adequate fit to the data
	QUICK scheme has slight lag in wave shape Insensitive to momentum conservation	Insensitive to momentum conservation

5.4 Spilling wave calibration

This section describes the sensitivity of the SWASH model relative to the variation in vertical resolution, friction coefficients, discretisation of the horizontal and vertical advection terms and the interpolation method for the calculation of the water depth at the velocity points. The calculated SWASH results are compared to the spilling wave measurements of Govender (1999). The same methodology employed for the plunging waves is followed in the next section for the spilling waves.

5.4.1 Vertical resolution

The influence on the incipient breaking point of the spilling waves is tested by varying the vertical resolution in SWASH and comparing it to the measured Govender (1999) wave data. This section only considers the influence of the number of vertical layers on the incipient breaking point.

The calculated SWASH results for models with 15, 20, 30 and 35 vertical layers are given in Figure A.37. The momentum is explicitly conserved in the left panel but not so in the panel on the right. Note that the wave direction in the plot is from right to left on the x-axis.

The momentum conservation does not have any significant influence on the incipient breaking point and neither does the amount vertical layers shown in Figure A.37. All the calculated results are shown to be over-predicting the incipient breaking point by approximately 1.0m shoreward.

A further attempt at defining the influence that a number of vertical layers have on the incipient breaking point is shown in Figure A.38 where the maximum water level for vertical layers of 5, 15 and 35 layers is compared to the measured data.

It is clear from the results that a variation in the vertical resolution has an influence on the location of the breaking point. The same result is observed here than what was reported for the plunging breaker; i.e. a reduction in the vertical resolution seems to move the incipient breaking point further offshore by a significant margin of 1m compared to the results of models with a higher number of vertical layers.

From these results, it can be concluded that the vertical resolution has an influence on the cross-shore location of the breaking point. Figure A.38 confirms that this point is resolved further onshore with an increase in the vertical resolution.

5.4.2 Friction parameters

Using the experimental setup of Govender (1999) for spilling breakers (see Section 4.3 for the details) the Manning value was varied between $n = 0.010$ and $n = 0.050$. The results of the model are shown in Figure A.39 where

the maximum wave heights in the time recorded series are plotted for each measurement point along the flume. Note that the wave direction in the plot is from right to left.

No observable difference is discernible between the incipient breaking point nor the maximum wave heights for the variation in the momentum parameter. There is a slight difference in the incipient breaking point when the friction factor is increased; i.e. an increase in the friction parameter causes the breaking point to shift in an offshore direction. In addition, no significant difference in maximum wave height is seen between the calculated SWASH results.

Figure A.40 and Figure A.41 plot the phase averaged water level at given points in the flume. It can be seen from both the figures that the peak wave heights are underpredicted in the shoaling wave while the troughs are overestimated by approximately the same margin. The peak wave heights fit very well with the recorded measurements around the breakpoint with the lower friction values ($n = 0.010$ and $n = 0.030$) showing a better fit in terms of shape. Note that, again, the phase averaged shape of the SWASH results are slightly overestimating the measured values.

In terms of wave heights, it can be concluded that a variation in the friction parameter does not seem to have a significant influence on altering the maximum wave heights nor the phase-averaged wave heights. The variation in the conservation of the momentum parameter does not make a significant difference in the results.

The influence of the friction parameter and the momentum conservation on the horizontal velocity for measuring station P1 (before wave breaking) is illustrated in Figure A.42 and Figure A.43.

From both Figure A.42 and Figure A.43 it is clear that the Manning friction value has a significant influence on the phase averaged horizontal velocities prior to the wave breaking; a variation of up to 0.2m/s is seen near the bed between Manning values of $n = 0.010$ and $n = 0.050$ (top left panel). Higher Manning friction values $n = 0.050$ increase the horizontal velocity in the near bottom part of the wave. This situation is gradually reversed towards the water surface; i.e. lower Manning values ($n = 0.010$) increase the horizontal velocity (bottom right panel). A Manning value of $n = 0.030$ seems to fit the data well across the water column. Again, the variation in the momentum conservation criteria proved to have no significant influence on the published results.

The influence of the friction parameter and the momentum conservation on the vertical velocity for measuring station P1 (before wave breaking) is illustrated in Figure A.44 and Figure A.45.

A variation in the friction parameter does not have great influence in the calculated results for the vertical phase averaged results across the water column. The calculated results seem to fit the measured data very well across the water column for all friction parameters tested. The variation in the mo-

mentum conservation criteria proved to have no significant influence on the published results.

It can be concluded that the friction parameter only has a significant influence when considering the horizontal instantaneous velocity and that higher friction values tend to overestimate the velocities and vice versa.

The influence of the friction parameter and the momentum conservation on the horizontal velocity for spilling waves at measuring station P2 (after wave breaking) is illustrated in Figure A.46 to Figure A.47.

Higher Manning friction values $n = 0.050$ increase the horizontal velocity in the near bottom part of the wave (top left panel). This situation is gradually reversed towards the water surface; i.e. lower Manning values ($n = 0.010$) increase the horizontal velocity (bottom right panel). A Manning value of $n = 0.030$ seems to be the best fit to the measured data in the lower half of the water column while the value of $n = 0.010$ is an adequate fit for the upper half of the water column. Note the high horizontal velocities measured by Govender (1999) near the water surface (bottom right panel). The SWASH models under-predict these measurements by at least 0.6m/s. The magnitude of the phase-averaged velocities is in good agreement with the measured results across the water column. The variation in the momentum conservation criteria proved to have no significant influence on the published results.

The influence of the friction parameter and the momentum conservation on the vertical velocity for measuring station P2 (after wave breaking) is illustrated in Figure A.48 and Figure A.49.

A variation in the friction parameter does not have great influence in the calculated results for the vertical phase averaged results across the water column. The calculated results seem to fit the measured data very well or the lower half of the water column (top panels) and to some degree the top half of the water column (bottom left panel). However, the near surface calculated results do not seem to fit the measured data very well (bottom right panel).

It can be concluded that a Manning value of $n = 0.03$ results in the best fit for the SWASH calculations with the measured horizontal and vertical velocities for measuring Station 2. However, the calculated near surface velocities (bottom right panel) differ from the measured results in shape and peak horizontal and vertical velocities. The calculated results are insensitive to the explicit conservation of momentum.

A summary of the friction parameter sensitivity findings is given in Table 5.6.

Table 5.6: Summary of the friction parameter sensitivity in SWASH for a spilling wave when compared to the Govender (1999) measured data

Parameter	**Friction**
Incipient breaking	Slight variation with increase in friction value.
Maximum wave height	Insensitive to momentum Insensitive to Manning value variation Insensitive to momentum
	Before breaking	**After breaking**
Phase Averaged wave height	Lower friction values better fit Momentum insignificant	Lower friction values better fit Momentum insignificant
Phase averaged horizontal velocity	Variation in velocity trend across water column for variation in friction value. n=0.030 best fit. Momentum insignificant	Variation in velocity trend across water column for variation in friction value. n=0.030 best fit. Momentum insignificant
Phase averaged vertical velocity	Insensitive to Manning value variation Insensitive to momentum	Insensitive to friction value Insensitive to momentum conservation

5.4.3 Horizontal and vertical advection terms of the momentum equation

In order to test the influence of various discretisation schemes on the water level and velocity calculations in SWASH a combination of discretisation methods, as detailed in Chapter 5.2 and given in Table 5.1, were compared to the measured Govender (1999) spilling wave data sets.

Figure A.50 shows the influence of the discretisation schemes on the maximum wave height calculated at points across the flume. The SWASH results are compared to the measurements made by Govender (1999).

Figure A.50 shows a significant difference in the calculated values when comparing AdvTerm 2 and the SWASH default with the AdvTerm1 discretisation scheme. The AdvTerm 1 scheme shows a good fit to the measured data in terms of maximum wave shape across the offshore part of the flume. AdvTerm 2 and the SWASH default schemes have variations in maximum wave height shape post wave breaking and further offshore. Quite a pronounced concentration of maximum wave heights is observed between x=6m and x=8m. All calculated results show an overestimation in the maximum wave height. A variation in momentum does not have any significant influence on the results.

Figure A.51 and Figure A.52 plot the phase averaged water level at four given points in the flume.

The phase-averaged water levels plots show very little difference in average water calculation between the various schemes before and after breaking. Contrary to the maximum water levels, the calculated SWASH results fit the measured data well. No significant variation in the schemes is observed when momentum is explicitly conserved.

Considering purely the wave height, it can be concluded that the advection terms have very little influence on the Water level calculations. The AdvTerm 1 scheme shows some correlation to the maximum water level measurements but needs to be interpreted correctly. Momentum does not have an influence on the calculated results.

Next, the influence of the various schemes on the horizontal and vertical velocity is investigated. The influence of the discretisation schemes and the momentum conservation on the horizontal velocity for measuring station P1 (before wave breaking) is illustrated in Figure A.53 and Figure A.54.

From both Figure A.53 and Figure A.54 it can be seen that there is not a lot of variation between the various advection scheme calculated SWASH results. All the advection schemes tested show a good comparison to the measured data for the spilling breaker case before wave breaking. On average, the SWASH AdvTerm 1 scheme shows the best fit to the measured data. The explicit conservation of momentum does not have an influence on the calculated results.

The same observations are valid for the vertical phase averaged velocities which are shown in Figure A.55 and Figure A.56.

The vertical velocities compare in much the same way as the horizontal velocities considering Figure A.55 and Figure A.56. The SWASH calculations fit well with the measured results for all the schemes tested. Momentum conservation does not play any significant role in the discretisation schemes.

It can be concluded that the AdvTerm 1 scheme, regardless of the option of momentum conservation results, has the best fit when compared with the measured horizontal and vertical velocities for measuring Station 1.

The influence of the various advection schemes and the momentum conservation on the horizontal velocity for measuring station P2 (after wave breaking) is illustrated in Figure A.57 to Figure A.58.

The SWASH results show a significant variation in horizontal velocity near the bottom (top left panel) for the various schemes. The default scheme has the best fit to the measured data in the lower half of the water column. AdvTerm 1 under-predicts while AdvTerm 3 over-predicts the horizontal velocities at this point. This scenario changes towards the water surface where the AdvTerm 1 scheme shows a better fit with the measured data and the default theme the least. All the schemes severely underestimate the horizontal velocity near the surface. Explicitly enforcing momentum does not have any significant bearing on the modelled results.

The influence of the advection schemes and the momentum conservation on the vertical velocity for measuring station P2 (after wave breaking) is illustrated in Figure A.59 and Figure A.60.

A variation in the advection schemes does not have great influence in the calculated results for the vertical phase averaged results across the water column. The calculated results seem to fit the measured data well for the lower half of the water column (top panels) and to some degree the top half of the water column (bottom left panel). Some variation is seen for the AdvTerm 2 scheme. However, the near surface calculated results do not seem to fit the measured data very well (bottom right panel). The best fit seems to be the AdvTerm 1 scheme.

It can be concluded that the SWASH default scheme shows the most consistent fit to the measured data as no scheme really stands out as being consistent throughout all the modelled variations. On the other hand, the largest errors between measured and modelled are relatively small in the areas away from the surface or bed. Momentum has no influence on the calculated results.

A summary of the friction parameter sensitivity findings is given in Table 5.7.

Table 5.7: Summary of the discretisation scheme for the advection term sensitivity in SWASH for a spilling wave when compared to the Govender (1999) measured data

Parameter	Advection Schemes	
Incipient breaking	No significant influence on incipient breaking point	
Maximum wave height	Insensitive to momentum conservation	
	AdvTerm 1 scheme shows best fit relative to wave shape	
	Insensitive to momentum conservation	
	Before breaking	**After breaking**
Phase averaged wave height	Insensitive to schemes	Insensitive to schemes
	Fits data well	Fits data well
	Insensitive to momentum	Insensitive to momentum
Phase averaged horizontal velocity	All schemes show good fit	Variation in velocity trend across water column for variation in advection schemes
	AdvTerm 1 shows best fit in general	
	Insensitive to momentum	Insensitive to momentum
Phase averaged vertical velocity	All schemes show good fit	Insensitive to advection scheme
	AdvTerm 1 shows best fit in general	Insensitive to momentum conservation
	Insensitive to momentum	

5.4.4 Water depth in velocity points

In order to test the sensitivity of higher order schemes in the interpolation of the water depth in velocity points, various higher order interpolation schemes with flux limiter (First Order Upwind, Superbee, Quick and MinMod) are compared with each other and with the measured data from Govender (1999). In addition, explicit momentum conservation is also varied.

Figure A.61 shows the influence of the higher order schemes on the maximum wave height calculated at points across the flume. The SWASH results are compared to the measurements made by Govender (1999).

Comparing the left panel with the right panel of Figure A.61, a significant difference in the maximum wave height can be seen for the first order upwind scheme. The other schemes show good agreement with the measured data with the MinMod scheme displaying the best fit. The first order upwind scheme under predicts the maximum wave elevation across the flume by approximately 30mm while the Quick and Superbee slightly over predicts the maximum wave height by approximately 10mm. The variation in momentum has no significant influence on the calculated results.

Figure A.62 and Figure A.63 plot the phase averaged water level at four given points in the flume.

As expected, the first order upwind scheme under-predicts the phase-averaged wave height while the other schemes show very good agreement around the breaking point and further offshore. The trough of the wave before breaking (top right panel) is slightly over-predicted by all the schemes. However, a very good fit is obtained at the point after breaking. Again, momentum has no significant influence on the results.

In terms of water levels, the first order upwind scheme severely under-predicts the maximum and phase-averaged wave heights. All other schemes fit the measured data equally well. The momentum mode has no significant influence on the results.

The influence of the higher order interpolation schemes and the momentum conservation on the horizontal velocity for measuring station P1 (before wave breaking) is illustrated in Figure A.64 and Figure A.65.

In step with the phase-averaged wave heights, the phase-averaged velocities show good agreement for the various schemes apart from the first order upwind scheme. The first order upwind scheme under-predict the horizontal wave velocities at the peaks while over predicting the return flow velocities across the whole water column. All the other schemes show a good fit with the measurements. In a minor way, the MinMod scheme shows the best overall fit to the measured data upon visual inspection. Momentum has no significant influence on the results.

The vertical velocities compare in much the same way as the horizontal velocities; all the schemes, apart from the first order upwind scheme, show good agreement with the measured results. The greatest variation in the calculated

results is seen in the near-surface layer of the water column (bottom right panel). The MinMod scheme shows the best general fit to the measured results. The momentum conservation criteria do not make a significant difference in the calculated results.

It can be concluded that the MinMod scheme shows the best-calculated result when the maximum wave height, along with the phase averaged horizontal and vertical velocity calculations across the whole water column, are compared to the measured data. The first order upwind scheme shows the worst fit across the whole water column.

The influence of the various higher order interpolation limiter schemes and the momentum conservation on the horizontal velocity for measuring station P2 (after wave breaking) is illustrated in Figure A.68 to Figure A.69.

After wave breaking, more variation between the calculated results is observed. Again, the first order upwind scheme is the worst performer when compared to the measured data. The Superbee limiter shows the best fit to the measured results in the lower half of the water column. All schemes over predict the horizontal velocities in the lower water column (top panels). In the upper water column, the calculated velocities underestimate the measured data by up to 0.8m/s near the water surface (lower right panel). Momentum conservation does not have an effect on the results.

The influence of the advection schemes and the momentum conservation on the vertical velocity for measuring station P2 (after wave breaking) is illustrated in Figure A.70 and Figure A.71.

The vertical velocities for the broken wave measured at Station 2 show the same general pattern as the horizontal velocities where the first order upwind does not compare well to the measured results relative to the other schemes tested. The MinMod and Superbee schemes show a satisfactory fit to the measured data. Near the water surface, return flow velocities are underestimated by the SWASH models while the near-surface velocities shoreward flow velocities are overestimated.

It can be concluded from the post-breaking velocity analysis that the first order upwind scheme does not compare well to the measured data while the other schemes all show satisfactory correlation. The SWASH calculated order of magnitude correlates well with the measured data. The momentum mode has no influence on the results.

A summary of the friction parameter sensitivity findings is given in Table 5.8.

Table 5.8: Summary of the water depth to velocity points interpolation schemes sensitivity in SWASH for a spilling wave when compared to the Govender (1999) measured data

Parameter	**Water depth in velocity points**	
Incipient breaking	Insensitive to momentum conservation	
Maximum wave height	Insensitive to scheme used MinMod scheme shows best fit. First order not good fit. Other schemes over predict wave height	
	Before breaking	**After breaking**
Phase averaged wave height	MinMod scheme shows best fit. Insensitive to momentum conservation	QUICK and Superbee good fit Insensitive to momentum conservation
Phase averaged horizontal velocity	FIR shows worst fit Other schemes good fit Insensitive to momentum conservation	FIR shows worst fit Other schemes good fit Insensitive to momentum conservation
Phase averaged vertical velocity	FIR shows worst fit Other schemes good fit MinMod best fit in general Insensitive to momentum conservation	FIR shows worst fit Other schemes good fit MinMod and Superbee best fit in general Insensitive to momentum

5.5 Summary of the calibration parameters used in the SWASH analysis

The outcome of the numerical sensitivity exercise for the plunging and spilling wave cases, as reported by Govender (1999), are summarised in Table 5.9.

Table 5.9: Calibration parameters used in the analysis of the SWASH model

	Plunging wave	**Spilling wave**
Friction	Manning $n = 0.030$	Manning $n = 0.030$
Advection Schemes	Adv Scheme 2 CDF for the horizontal velocity w-momentum term	Adv Scheme 1 CDF for the vertical velocity u-momentum term
Water depth in velocity points	MinMod limiter	MinMod limiter
Momentum	Momentum conserved	Momentum conserved

Chapter 6

Systematic Analysis of the SWASH Model

6.1 Introduction

This chapter compares measured wave breaking data (from Govender (1999) and Ting and Kirby (1994)) with SWASH model results. Three modes of the SWASH model are run and compared with the measured data. These modes are: a calibrated model, an uncalibrated model, and a model assuming the hydrostatic front approximation (HFA). The Root Mean Square Error is calculated between the SWASH models and the measured data and the results reported on.

The aim of this exercise is to show the relative error between measured data and a "calibrated" and an "uncalibrated", or, HFA SWASH model. This comparison is limited to the study at hand; i.e. 2DV and for a plunging and breaking wave on plane slopes of 1:20 and 1:35.

Modelled turbulence values are compared to calculated turbulence values and discussed. SWASH calculated wave set-up is compared to measured data and analysed.

The outcome of this chapter is to determine a general confidence level in the SWASH model given the study parameters.

6.2 Methodology

The measured data from Govender (1999) and Ting and Kirby (1994) are compared to SWASH modelled output of three different modes of a SWASH model. The three modes are defined as follows:

1. "Calibrated" SWASH model: The input parameters for this numerical model follows from the sensitivity exercise conducted in Chapter 5. Refer to Table 5.9 for these parameters.

2. "Un-calibrated" SWASH model: The input parameters for this model assumes the default parameters assumed by SWASH along with some recommended values; i.e. the SWASH manual recommended Manning friction value of $n = 0.019$.

3. The HFA condition - where wave breaking parameters are specified (see Section 3.4) - SWASH modelling is conducted. This type of model is on par with the uncalibrated SWASH model in that default recommended SWASH values are assumed as far as possible. The HFA SWASH model assumes the following:

   - Number of vertical layers: 5.
   - Non-hydrostatic "standard" scheme is employed as opposed to the recommended Keller-box scheme. This is done in order to maintain parameter integrity between the models and make them directly comparable.
   - The default α and β breaking criterion values are assumed.

The root-mean-squared error between the models is calculated to provide an index for the relative error between the compared models.

$$RMSE = \sqrt{\frac{1}{N}\sum_{i=1}^{N}\left(f_{i,measured} - f_{i,modelled}\right)^2}$$

where N is the number of samples for a given quantity; $f_{i,measured}$ is the laboratory measured quantity; and $f_{i,modelled}$ is the SWASH modelled quantity.

In addition, the maximum time series values (water levels and velocities) of the flume measurements are calculated for the given wave condition and a percentage RMSE, is determined by calculating the RMSE as a percentage of the maximum time series value. This is a relative indication of the deviation from the maximum value for the property investigated.

$$\%RMSE = \frac{RMSE}{\text{Max(phase averaged time series)}} \times 100\%$$

The percentage RMSE gives a relative value of the error between the measured and modelled data at the maximum point in the time series. In general, the maximum value (e.g. the maximum wave height or maximum horizontal value at the wave crest) is normally the area of interest for the design engineer. Thus, with the percentage RMSE, a relative index is determined that must be read in conjunction with the data (e.g. the phase averaged water level) from which it is calculated.

The calculated turbulence (TKE) from the measured results is calculated and compared to the modelled SWASH results.

6.3 Standard SWASH input parameters

Some of the general SWASH model input parameters are described as follows:

- Horizontal discretisation: $\Delta x = 0.04$
- Time step: $\Delta t = 0.001$ with an automatic time step adjustment for a stability range of $0.1 < Cr < 0.4$.
- Un-calibrated friction Manning value of 0.019
- Twenty vertical layers are specified for the calibrated and uncalibrated models while five vertical layers are specified for the HFA condition model.
- Simulation time of 6 min was allowed with 40 seconds of results used in the data comparison for the Govender (1999) data and 120 seconds for the Ting and Kirby (1994) data. These times are linked to the amount of data that was made available by the researchers.
- Average wave statistics were calculated over the trailing 5 minutes of the 6 minute simulation; e.g. wave setup, $H_{1/3}$, average velocity, etc.

6.4 Simulation results: Water levels

The recorded water levels are compared with the three SWASH model scenarios in terms of the maximum water level, phase-averaged water level and wave set-up at specific points in the flume. The breaker depth index is also analysed. The wave measured vs. modelled comparisons are reported for the data sets by Govender (1999) and Ting and Kirby (1994).

The incipient breaking point, maximum and minimum water levels, particularly at the breaking point, are important design parameters in calculating the breaker depth index (refer to Section 2.5.3).

6.4.1 Water level output points

Numerical results are compared to the measured data in terms of the maximum recorded water level across the flume and phase-averaged water level data at specific points for plunging and spilling waves. Note that the Govender (1999) data is measured as distances from an onshore point (Refer to Figure 4.2) where the still water level (SWL) meets the plane slope. This means that the maximum measurements across the flume are referenced from right to left when considering the plotted output while the Ting and Kirby (1994) data is referenced from an offshore point and the results will appear as if the wave is travelling from left to right.

The location of the phase-averaged water level output points are given in Table 6.1. In general, the first output point is taken offshore of the breaking point (shoaling wave), the second point as close to pre-breaking as the measurements allow, the third point is measured immediately after wave breaking and point four a distance after breaking (propagating bore).

Table 6.1: Output locations, distance from the SWL and the still water depth at the output locations for the SWASH simulation results

		Govender Data		Ting and Kirby Data	
	Water levels	Distance from shore (m)	SWL Depth (m)	Distance from reference (m)	SWL Depth (m)
Plunging Wave	PWP1	8.35	0.420	2.00	0.326
	PWP2	3.40	0.170	7.80	0.155
	PWP3	3.20	0.160	8.00	0.150
	PWP4	0.90	0.045	9.50	0.106
Spilling Wave	SWP1	8.35	0.420	1.50	0.338
	SWP2	4.61	0.230	6.40	0.196
	SWP3	4.31	0.210	6.50	0.193
	SWP4	1.00	0.050	9.00	0.123

6.4.2 Incipient breaking point

The maximum recorded water levels across the flume for the plunging and spilling waves are shown in Figure B.1 and Figure B.2.

The incipient breaking point in the Govender (1999) plunging wave (Figure B.1 left panel) is shown to be a distance of approximately 0.8m from the recorded data incipient breaking point for both the SWASH calibrated and uncalibrated models. The SWASH models also display higher maximum water levels across the flume when compared to the measured data. The SWASH HFA model resolves the incipient breaking point at approximately the same point as the measured data but at much higher maximum water levels (approximately 20mm at the breaking point).

The spilling wave (Figure B.1 right panel) follows the trend of the plunging breaker as described above. The only difference is that the HFA condition shows lower maximum wave heights compared to the measured data.

The same trend is observed in the Ting and Kirby (1994) plunging data as shown in Figure B.2 (left panel). The SWASH calibrated and uncalibrated plunging model breaking point is shown to break earlier in the flume compared to the recorded data by approximately 0.8m. The SWASH HFA plunging

model is a very good fit to the measured data in terms of breaking point and maximum wave heights.

The spilling wave comparison shows good agreement with the measured data for all three SWASH models tested. The measured data shows a significantly lower water level measurement in the shoaling part of the wave.

6.4.3 Breaker depth Index

The breaker depth index for each of the SWASH modelled wave scenarios is calculated and compared to the breaker depth index calculated for the measured data. Figure B.3 shows the time normalised plot of a single wave at the respective incipient breaking points for each model compared to the measured data from which the H_{max} at the incipient breaking point can be read.

Table 6.2 details a typical breaker depth index calculation using the Govender (1999) plunging wave. The same calculation exercise was conducted for the Ting and Kirby (1994) data but is omitted. The results of the Ting and Kirby (1994) calculation is given in Table 6.3.

Table 6.2: Breaker depth index comparison for the plunging wave between the Govender (1999) data and the SWASH modelled data

	Govender Flume data	SWASH Calibrated	SWASH Un-calibrated	SWASH HFA
Breaking point distance from SWL (m)	3.20	4.00	4.00	3.40
Still Water Depth (m) (d_b) (m)	0.16	0.201	0.201	0.17
Max water level (m)	0.135	0.140	0.148	0.138
Min water level (m)	-0.043	-0.037	-0.034	-0.036
H_b (m)	0.179	0.178	0.182	0.174
Breaker depth index (H_b/d_b)	1.12	0.88	0.91	1.02

Table 6.3 shows the breaker depth index for both the Govender (1999) and Ting and Kirby (1994) data sets compared to the SWASH modelled values for both plunging and spilling breakers.

It can be seen from Table 6.3 that the SWASH modelled breaker depth index varies between 0.88 and 1.02 in comparison to the calculated index of 1.12 for the Govender (1999) plunging wave measured data. This represents an under prediction of between 10% and 27%. The spilling wave also under predicts the measurement by approximately 33% for the calibrated and un-calibrated SWASH models. In contrast, the SWASH HFA model shows very good agreement with the measured data.

Table 6.3: Calculated breaker depth index for both measured data sets and both plunging and spilling breakers compared to the SWASH modelled data

Govender (1999) Breaker Depth Index	Measured flume data	SWASH Calibrated	SWASH Un-calibrated	SWASH HFA
Plunging	1.12	0.88	0.91	1.02
Spilling	0.60	0.41	0.41	0.59

Ting and Kirby (1994) Breaker Depth Index	Measured flume data	SWASH Calibrated	SWASH Un-calibrated	SWASH HFA
Plunging	1.23	1.06	1.09	1.23
Spilling	0.81	0.80	0.76	0.80

The SWASH calibrated and uncalibrated models under-predict the plunging wave Ting and Kirby (1994) data by approximately 15% while the HFA, again, shows a very good correlation to the measured data. The spilling wave models compare very well with the measured data for all the numerical models conducted.

The SWASH HFA model predicts the breaker height very well while the other models do not seem to adequately resolve the incipient breaking point which, in turn, leads to an underestimation of the breaker depth index.

6.4.4 Phase averaged water levels

6.4.4.1 Plunging Waves

The phase-averaged water level comparison between the measured data sets of Govender (1999) and Ting and Kirby (1994) and the SWASH models for plunging waves are given in Figure B.4 and Figure B.5 respectively.

The phase-averaged models all compare very well to the measured data for both plunging wave data sets. Notable exceptions are the troughs that are not well resolved in all of the Govender simulations; i.e. the troughs overestimate the wave height by a small margin. In contrast, the SWASH models all show good agreement with the Ting and Kirby data. The SWASH HFA model has the least fit across all points for both data sets with the exception of the offshore point in Figure B.4 (Govender data set - bottom right panel) where it fits the measured data exceptionally well.

The RMSE for both data sets is given in Table 6.4 for the plunging waves along with the maximum water level at each measuring point and the percentage RMSE relative to the maximum water level. The colour codes are relative to the lowest number in the table and show an increase in RMS error from a deeper shade of green (smaller RMSE) to yellow (higher RMSE). In addition, the measured water levels vs. SWASH modelled water levels are given in Fig-

ures B.6 and B.7. These figures illustrate the relative errors reported in the RMSE tables.

Table 6.4: Root mean squared water level error (m) for the Govender (1999) and Ting and Kirby (1994) data relative to the SWASH models for plunging waves, maximum measured phase averaged water level and percentage RMSE error relative to the maximum water level

Plunging Waves	RMSE (m) Govender	SWASH Calibrated	SWASH Un-calibrated	SWASH HFA	Maximum Water Level (m)	% RMSE Calibrated	% RMSE Un-calibrated	% RMSE HFA
	PWP1	0.006	0.007	0.007	0.075	8%	9%	9%
	PWP2	0.007	0.007	0.015	0.113	6%	6%	14%
	PWP3	0.009	0.013	0.019	0.133	7%	10%	14%
	PWP4	0.008	0.009	0.005	0.047	16%	20%	10%
	RMSE (m) Ting and Kirby	SWASH Calibrated	SWASH Un-calibrated	SWASH HFA	Maximum Water Level (m)	% RMSE Calibrated	% RMSE Un-calibrated	% RMSE HFA
	PWP1	0.005	0.005	0.007	0.117	4%	4%	6%
	PWP2	0.010	0.011	0.016	0.158	7%	7%	10%
	PWP3	0.012	0.013	0.015	0.152	8%	8%	10%
	PWP4	0.016	0.016	0.019	0.108	15%	15%	17%

Table 6.4 reports a RMSE for the Govender (1999) data of less than 1.0cm (maximum 0.88cm) for the calibrated model and a maximum error after breaking of 1.3cm for the uncalibrated SWASH model. The HFA model reports the largest errors around the breaking point (1.5cm and 1.9cm). The Ting and Kirby (1994) data set shows slightly higher discrepancies (RMSE between 0.5cm to 1.6cm) but is very consistent with the Govender data set. Again, the calibrated and uncalibrated models perform very well while the SWASH HFA model's performance is less so. A consistent increase in RMSE at the breaking and propagating areas of the wave for all the SWASH models can be seen.

The percentage error is less than 10% for the calibrated and uncalibrated models for the shoaling waves and waves before and after the breakpoint. The propagating bore shows a higher percentage RMSE ranging between 10% and 20%. Although the HFA model reports relatively higher error percentages compared to the uncalibrated model, it can be seen that, overall, the SWASH HFA model %RMSE is only slightly higher.

6.4.4.2 Spilling Waves

The phase-averaged water level comparison between the measured data sets of Govender (1999) and Ting and Kirby (1994) and the SWASH models for spilling waves are given in Figure B.8 and Figure B.9 respectively.

The phase-averaged SWASH models all compare very well to the measured data for both spilling wave data sets. Note that the peak in the shoaling wave for the Govender (1999) data is under-predicted by approximately 1.5cm while the same is over-predicted by approximately 1.5cm for the Ting and Kirby (1994) data. The breakpoints (SWP2 and SWP3) are very well matched to the measured data for the calibrated and uncalibrated SWASH models for

both data sets. An exception is the propagating bore (SWP4 in Figure B.9 - bottom right panel). The SWASH models resolve the peak wave height but have some significant discrepancies in the shape of the spilling wave; i.e. the troughs of the Govender (1999) data are slightly over predicted.

The SWASH HFA model shows the least fit across all points for both data sets in terms of wave shape. However, the peaks wave heights are well resolved for the SWASH HFA model.

The RMSE, maximum measured water levels and percentage RMSE (relative to the maximum water level) are given in Table 6.5 for the spilling waves. The relative colour codes show an increase in RMS error from a deeper shade of green (smaller RMSE) to yellow (higher RMSE). The measured water levels vs. SWASH modelled water levels are given in Figures B.10 and B.11. These figures illustrate the relative errors reported in the RMSE tables.

Table 6.5: Root mean squared water level error (m) for the Govender (1999) and Ting and Kirby (1994) relative to the SWASH models for spilling waves, maximum phase averaged water level and percentage RMSE error relative to the maximum water level

	RMSE Govender	SWASH Calibrated	SWASH Un-calibrated	SWASH HFA	Maximum Water Level (m)	% RMSE Calibrated	% RMSE Un-calibrated	% RMSE HFA
Spilling Waves	SWP1	0.008	0.010	0.012	0.090	9%	11%	13%
	SWP2	0.009	0.011	0.010	0.094	9%	12%	11%
	SWP3	0.009	0.008	0.009	0.091	9%	9%	9%
	SWP4	0.004	0.003	0.007	0.034	12%	9%	20%
	RMSE Ting and Kirby	SWASH Calibrated	SWASH Un-calibrated	SWASH HFA	Maximum Water Level (m)	% RMSE Calibrated	% RMSE Un-calibrated	% RMSE HFA
	SWP1	0.009	0.010	0.007	0.075	12%	13%	10%
	SWP2	0.006	0.006	0.021	0.134	5%	5%	16%
	SWP3	0.005	0.006	0.014	0.134	4%	5%	11%
	SWP4	0.020	0.019	0.025	0.058	34%	32%	44%

Table 6.5 reports a RMSE of less than a 1cm (maximum 0.9cm) for the calibrated model and a maximum error just before breaking of 1.1cm for the uncalibrated SWASH model for the Govender (1999) data. The HFA model reports a maximum error of 1.2cm and 1.0cm for the shoaling wave at the point just before breaking. When considering the %RMSE, it can be seen that the SWASH calibrated and uncalibrated models fit the measured data very well (%RMSE between 9% and 12%). In general, the SWASH HFA model also fits the measured data well apart from a 20% relative error in the propagating bore.

The RMSE for the Ting and Kirby (1994) data shows a relatively larger error across the board ranging between 0.9cm and 2.0cm for the calibrated model, between 1.0cm and 1.9cm for the uncalibrated model and between 0.7cm and 2.5cm for the SWASH HFA model. The largest error margins are calculated after wave breaking (propagating bore) for the calibrated and uncalibrated models. The SWASH HFA model shows its largest errors in the breaking and propagating part of the wave. The largest discrepancy between

the measured and modelled data is in the propagating bore (between 32% and 44%). The shoaling and breaking part of the wave is well resolved by the models, especially around the breaking point (%RMSE of 5%). The SWASH HFA model shows the largest comparative percentage error.

6.4.5 Wave Setup and Setdown

Figure B.12 shows the modelled wave set-up and measured wave set-up and set-down for the Ting and Kirby (1994) plunging and spilling wave data. Note that wave set-up/set-down data was not supplied for the Govender (1999) data.

From Figure B.12 it can be seen that the SWASH model generally over predicts the wave set-up for all models tested by an insignificant margin of between 5mm (plunging waves) and 10mm (SWASH HFA model for the spilling wave). The SWASH models for plunging waves are for all practical purposes the same while a more pronounced sensitivity is seen in the SWASH spilling wave models.

6.5 Simulation results: Velocity

6.5.1 Velocity output points

The phase-averaged particle velocity comparison between the measured data sets of Govender (1999) and Ting and Kirby (1994) and the SWASH models are reported at two cross shore points in the flume: before wave breaking and after wave breaking. Table 6.6 gives the cross-shore locations for the two data sets where the phase-averaged velocity is calculated.

The output at each cross-shore point is given at four points within the water column: near the flume bed, in the lower half of the water column, in the upper half of the water column and near the water surface but, as far as possible, below the trough level.

6.5.2 Phase averaged plunging wave comparison

6.5.2.1 Horizontal velocity before plunging breaking

The phase-averaged horizontal particle velocity comparison between the measured data sets of Govender (1999) and Ting and Kirby (1994) and the SWASH models for plunging waves at the cross-shore point before wave breaking are given in Figure B.13 and Figure B.14 respectively.

The calibrated and uncalibrated horizontal velocity modelled data show an excellent fit to the measured Govender (1999) data across the whole of the water column. Note that the SWASH HFA model does not compare well in most cases, especially with regards to the shape of the data. The velocities

Table 6.6: Particle velocity measurement points in the flume for the plunging and spilling wave data for the Govender (1999) and Ting and Kirby (1994) data sets

	Govender data			
	Before wave breaking		After wave breaking	
	Distance from SWL	Depth to SWL	Distance from SWL	Depth to SWL
Plunging wave	4.360m	0.218m	3.38m	0.119m
Spilling wave	4.360m	0.218m	2.39m	0.169m
	Ting and Kirby Data			
	Before wave breaking		After wave breaking	
	Distance from reference	Depth to SWL	Distance from reference	Depth to SWL
Plunging wave	7.295m	0.169m	7.795m	0.156m
Spilling wave	5.945m	0.208m	6.665m	0.185m

near the bottom are underestimated by the SWASH HFA model and slightly overestimated in the remainder of the water column.

The calibrated and uncalibrated SWASH models compared with the Ting and Kirby (1994) measured data over predicts the peak horizontal velocity in the lower half of the water column by 0.2m/s near the bed and by 0.1m/s in the lower third of the water column. The SWASH HFA model shows good agreement with the peak velocity but has discrepancies compared to the shape of the measured data. In general, The SWASH models fit the Ting and Kirby (1994) data relatively well with due cognisance of the discrepancies seen in the peak values in the lower half of the water column.

The RMSE and %RMSE for the horizontal plunging wave particle velocity are given in Table 6.7. In addition, the phase averaged measured horizontal velocities vs. SWASH modelled horizontal velocities are given in Figures B.15 and B.16. These figures illustrate the relative errors reported in the RMSE tables.

Table 6.7 reports an average error of approximately 10% across the water column for the Govender (1999) calibrated and uncalibrated models (note that the interpolation error between SWASH model grid and the physical measurements is ignored in the RMSE calculations). The relative %RMSE between the calibrated and uncalibrated models is for all practical reasons identical. The SWASH HFA data shows a larger discrepancy across the water column compared to the other SWASH models (up to RMSE $\approx$ 0.13m/s for the HFA compared to RMSE $\approx$ 0.05m/s at the same location for the calibrated model).

Despite the peak velocity discrepancy in the lower half of the water column for the Ting and Kirby (1994) data, the overall phased average RMSE error

Table 6.7: Root mean squared horizontal velocity error (m/s) before wave breaking for the Govender (1999) and Ting and Kirby (1994) relative to the SWASH models for plunging waves, maximum phase averaged horizontal velocity and percentage RMSE error relative to the maximum horizontal velocity

	Before wave breaking							
Plunging Waves: U-Velocity	RMSE (m/s) Govender	SWASH Calibrated	SWASH Un-calibrated	SWASH HFA	Max Vel (m/s)	% RMSE Calibrated	% RMSE Un-calibrated	% RMSE HFA
	Bottom	0.044	0.029	0.124	0.51	9%	6%	25%
	Mid water	0.036	0.042	0.066	0.51	7%	8%	13%
	Mid water	0.047	0.036	0.135	0.55	9%	7%	25%
	Top	0.063	0.057	0.120	0.61	10%	9%	20%
	RMSE (m/s) Ting and Kirby	SWASH Calibrated	SWASH Un-calibrated	SWASH HFA	Max Vel (m/s)	% RMSE Calibrated	% RMSE Un-calibrated	% RMSE HFA
	Bottom	0.066	0.064	0.102	0.61	11%	11%	17%
	Mid water	0.063	0.056	0.114	0.61	10%	9%	19%
	Mid water	0.069	0.066	0.112	0.64	11%	10%	18%
	Top	0.067	0.074	0.125	0.69	10%	11%	18%

averages around 11% for the SWASH calibrated and uncalibrated models. This is comparable to the Govender (1999) data. Again, the SWASH HFA model shows higher error percentages compared to the other SWASH models.

6.5.2.2 Vertical velocity before plunging breaking

The phase-averaged vertical particle velocity comparison between the measured data sets of Govender (1999) and Ting and Kirby (1994) and the SWASH models for plunging waves are given in Figure B.17 and Figure B.18 respectively.

Both the calibrated and uncalibrated SWASH models show a very good fit to the measured Govender (1999) and Ting and Kirby (1994) data. A large percentage of the measured vertical velocity points are fitted by the SWASH model results.

The SWASH HFA model has some discrepancies in the modelled shape of the wave phase. Regardless, the peak positive velocities are well resolved, more so for the Govender data than for the Ting and Kirby data.

The RMSE and %RMSE for the vertical plunging wave velocities are given in Table 6.8. The measured vertical phase averaged velocities vs. SWASH modelled vertical velocities are given in Figures B.19 and B.20. These figures illustrate the relative errors reported in the RMSE tables.

The relative error for the Govender data is between 10% and 19% and between 5% and 10% for the Ting and Kirby data. Both the data sets show very good correlation with the measured data. The RMSE of the vertical velocities falls mainly well below 0.05m/s. The HFA data have consistently larger percentage RMSE than the calibrated and calibrated models.

The Govender data show a high percentage error near the wave surface. From Figure B.17 it can be seen that the percentage error reported near the surface is inflated by a few modelled points that do not fit the measurements.

Table 6.8: Root mean squared vertical velocity error (m/s) before wave breaking for the Govender (1999) and Ting and Kirby (1994) data relative to the SWASH models for plunging waves, maximum phase averaged vertical velocity and percentage RMSE error relative to the maximum vertical velocity

	Before wave breaking							
Plunging Waves: Z-Velocity	RMSE (m/s) Govender	SWASH Calibrated	SWASH Un-calibrated	SWASH HFA	Max Vel (m/s)	% RMSE Calibrated	% RMSE Un-calibrated	% RMSE HFA
	Bottom	0.013	0.012	0.025	0.09	15%	14%	28%
	Mid water	0.014	0.013	0.038	0.17	8%	7%	23%
	Mid water	0.033	0.032	0.057	0.33	10%	9%	17%
	Top	0.076	0.075	0.082	0.39	19%	19%	21%
	RMSE (m/s) Ting and Kirby	SWASH Calibrated	SWASH Un-calibrated	SWASH HFA	Max Vel (m/s)	% RMSE Calibrated	% RMSE Un-calibrated	% RMSE HFA
	Bottom	0.006	0.007	0.010	0.06	10%	11%	15%
	Mid water	0.009	0.010	0.021	0.13	7%	8%	16%
	Mid water	0.010	0.012	0.033	0.23	4%	5%	14%
	Top	0.017	0.019	0.050	0.35	5%	6%	14%

These can be mainly attributed to the interpolation between the grids (e.g. the interpolation between the grids produces a modelled velocity of 0m/s compared to -0.18m/s at $t/T = 0.35$).

In general, the vertical velocities are very well represented by the calibrated and uncalibrated SWASH models and in a lesser way by the SWASH HFA model. The modelled horizontal and vertical plunging breaker velocities are compared to the measured data for positions in the flume after wave breaking. Note that the Govender data set recorded the velocity a distance of 0.86m after the plunging breaking point while Ting and Kirby recorded their data at the break point. In order to consistently compare the post-breaking velocities, an additional point located 0.55m past the breaking point was analysed for the Ting and Kirby (1994) data.

6.5.2.3 Horizontal velocity after plunging breaking

The phase-averaged horizontal particle velocity comparison between the measured data sets of Govender (1999) and Ting and Kirby (1994) and the SWASH models for plunging waves after breaking are given in Figure B.21 and Figure B.22 respectively.

None of the SWASH models represents the measured Govender data very well at any positions in the water column. This result was expected considering the same result was observed during the sensitivity testing in Chapter 5.

The SWASH models maintain a constant velocity "shape" throughout the water column. The calibrated, uncalibrated and HFA models all differ in resolving the peak horizontal velocity. Throughout the water column, the SWASH calibrated model seems to resolve the peak wave velocity in the lower third of the water column, with the most notable exception the velocities measured towards the wave surface (bottom right panel). However, as pointed out

before, the Govender data show high-velocity measurements near the surface. Note the difference in the vertical scale used in the bottom right panel.

The SWASH modelled data fit the Ting and Kirby measured data very well. The peak wave velocity is under-predicted by 0.2m/s close to the flume bed and over predicted by all SWASH models by the same margin a little higher up in the water column. Very good agreement is seen between the measured and modelled data in the top half of the water column. The HFA SWASH model under predicts the peak velocities at the bed and over predicts the peak velocities in the rest of the water column.

The RMSE and %RMSE for the horizontal plunging wave velocities are given in Table 6.9. The measured horizontal phase averaged velocities vs. SWASH modelled horizontal velocities are given in Figures B.23 and B.24. These figures illustrate the relative errors reported in the RMSE tables.

Table 6.9: Root mean squared horizontal velocity error (m/s) after wave breaking for the Govender (1999) and Ting and Kirby (1994) data relative to the SWASH models for plunging waves, maximum phase averaged vertical velocity and percentage RMSE error relative to the maximum horizontal velocity measurements

	After wave breaking							
Plunging Waves: U-Velocity	RMSE (m/s) Govender	SWASH Calibrated	SWASH Un-calibrated	SWASH HFA	Max Vel (m/s)	% RMSE Calibrated	% RMSE Un-calibrated	% RMSE HFA
	Bottom	0.085	0.150	0.103	0.17	51%	90%	61%
	Mid water	0.095	0.128	0.127	0.15	63%	85%	84%
	Mid water	0.241	0.227	0.260	0.41	58%	55%	63%
	Top	0.740	0.789	0.715	2.18	34%	36%	33%
	RMSE (m/s) Ting and Kirby	SWASH Calibrated	SWASH Un-calibrated	SWASH HFA	Max Vel (m/s)	% RMSE Calibrated	% RMSE Un-calibrated	% RMSE HFA
	Bottom	0.057	0.059	0.082	0.62	9%	9%	13%
	Mid water	0.063	0.057	0.124	0.61	10%	9%	20%
	Mid water	0.072	0.066	0.119	0.63	11%	10%	19%
	Top	0.093	0.094	0.146	0.67	14%	14%	22%

The analysis presented above is confirmed by the RMSE calculations; the Govender data show up to a 90% RMSE discrepancy with the measured data. Note the maximum velocity near the water surface of 2.18m/s which is exceptionally high. The Ting and Kirby data show errors in the order of 10% while the SWASH HFA model have %RMSE in the order of 20%.

It is very likely that the measured Govender (1999) data contains a lot of turbulent velocity data (large-scale random fluctuations) as the measuring point is 0.86m from the plunging break point. The question to be answered is whether it is beyond the ability of SWASH to accurately simulate the roller post wave breaking or whether the model results are accurate but the measurements are not. To investigate this we turn to the Ting and Kirby (1994) data.

Note that the Ting and Kirby (1994) data analysed in Figure B.22 is measured at the break point. In order to make a fair comparison relative to the

Govender (1999) data, the same horizontal breaking analysis is performed for a measuring point approximately 0.55m from the breakpoint for the Ting and Kirby (1994) data (refer to Station 3 in Table 4.5). The resultant phase-averaged velocity plot for the modelled SWASH data and Ting and Kirby (1994) measurements are shown in Figure B.25.

From Figure B.25 it can be seen that the SWASH models show a very good fit to the Ting and Kirby (1994) data when compared with the SWASH modelled and measured data shown in Figure B.21 for the Govender (1999) data.

It can be seen in Figure B.25 that the peak horizontal velocity is overestimated by the SWASH calibrated and uncalibrated models near the bed. The SWASH uncalibrated model shows the best fit to the data in the remainder of the water column while the calibrated model under predicts the peaks velocities. The HFA model severely over predicts the peak velocities but the remainder of the wave phase is well represented throughout the water column.

The RMSE and %RMSE for the horizontal plunging wave velocities are given in Table 6.10 for the Ting and Kirby (1994) plunging data at a point approximately 0.55m after the wave breakpoint. The error statistics for the Govender (1999) data is repeated in Table 6.10 in order to compare the results directly. The measured horizontal phase averaged velocities vs. SWASH modelled horizontal velocities (at a distance of 0.55m from break point) are given in Figure B.26. This figure illustrates the relative errors reported in the RMSE tables for the Ting and Kirby (1994) data only.

Table 6.10: Root mean squared horizontal velocity error (m/s) after wave breaking for the Govender (1999) and Ting and Kirby (1994) data relative to the SWASH models for plunging waves, maximum phase averaged vertical velocity and percentage RMSE error relative to the maximum horizontal velocity measurements

	After wave breaking							
Plunging Waves: U-Velocity	RMSE (m/s) Govender	SWASH Calibrated	SWASH Un-calibrated	SWASH HFA	Max Vel (m/s)	% RMSE Calibrated	% RMSE Un-calibrated	% RMSE HFA
	Bottom	0.085	0.150	0.103	0.17	51%	90%	61%
	Mid water	0.095	0.128	0.127	0.15	63%	85%	84%
	Mid water	0.241	0.227	0.260	0.41	58%	55%	63%
	Top	0.740	0.789	0.715	2.18	34%	36%	33%
	RMSE (m/s) Ting and Kirby	SWASH Calibrated	SWASH Un-calibrated	SWASH HFA	Max Vel (m/s)	% RMSE Calibrated	% RMSE Un-calibrated	% RMSE HFA
	Bottom	0.060	0.063	0.118	0.48	13%	13%	25%
	Mid water	0.062	0.063	0.130	0.46	14%	14%	29%
	Mid water	0.074	0.063	0.125	0.47	16%	13%	27%
	Top	0.067	0.051	0.112	0.54	12%	9%	20%

The RMSE analysis shows the Ting and Kirby (1994) data having %RMSE in the order of 15% for the calibrated and uncalibrated models while the HFA model shows %RMSE in the order of 25%. Compared to the Govender (1999) data for the same post wave-breaking condition, it can be clearly seen that the

SWASH models are able to model the wave horizontal velocities after wave breaking.

6.5.2.4 Vertical velocity after plunging breaking

The phase-averaged vertical particle velocity comparison between the measured data sets of Govender (1999) and Ting and Kirby (1994) and the SWASH models for plunging waves after breaking are given in Figure B.27 and Figure B.28 respectively.

The modelled SWASH results resolve the peak vertical velocities very well for the calibrated and uncalibrated across the water column when compared to the measured Govender (1999) vertical velocity data. Note that the modelled phase-averaged wave shape does not conform to the measured data points very well. However, it is suspected that the measured vertical PIV data might contain a number of large-scale turbulence in this post-breaking zone. For instance, there is a sudden transition in the Govender (1999) data near the wave surface (bottom right panel of Figure B.27) at $t/T = 0.6$ from a vertical velocity of $0.2m/s$ to a velocity of $-0.3m/s$.

On the other hand, the calibrated and uncalibrated SWASH models show an excellent fit to the Ting and Kirby (1994) data in terms of peak vertical velocity and phase-averaged wave shape. The SWASH HFA model does not fit the measured data in the upper water column well.

The RMSE and %RMSE for the vertical plunging wave velocities are given in Table 6.11. In addition, the measured vertical phase averaged velocities vs. SWASH modelled vertical velocities are given in Figures B.29 and B.30. These figures illustrate the relative errors reported in the RMSE tables.

Table 6.11: Root mean squared vertical velocity error (m/s) after wave breaking for the Govender (1999) and Ting and Kirby (1994) data relative to the SWASH models for plunging waves, maximum phase averaged vertical velocity and percentage RMSE error relative to the maximum vertical velocity measurements

	After wave breaking							
Plunging Waves: Z-Velocity	RMSE (m/s) Govender	SWASH Calibrated	SWASH Un-calibrated	SWASH HFA	Max Vel (m/s)	% RMSE Calibrated	% RMSE Un-calibrated	% RMSE HFA
	Bottom	0.0063	0.0070	0.0067	0.03	49%	57%	49%
	Mid water	0.0071	0.0073	0.0152	0.06	46%	50%	49%
	Mid water	0.0088	0.0135	0.0188	0.16	37%	36%	43%
	Top	0.0078	0.0095	0.0045	0.18	49%	49%	57%
	RMSE (m/s) Ting and Kirby	SWASH Calibrated	SWASH Un-calibrated	SWASH HFA	Max Vel (m/s)	% RMSE Calibrated	% RMSE Un-calibrated	% RMSE HFA
	Bottom	0.004	0.004	0.006	0.05	8%	8%	12%
	Mid water	0.006	0.007	0.018	0.12	5%	6%	15%
	Mid water	0.008	0.008	0.032	0.23	4%	4%	14%
	Top	0.015	0.013	0.056	0.36	4%	4%	15%

The large percentage error in the Govender / SWASH model comparison is expected considering Figure B.27. %RMSE of around 50% is observed across

the water column for all SWASH models. The lowest percentage model error calculated is 36%. In contrast, all the SWASH models show a very good fit to the Ting and Kirby (1994) data. %RMSE in the order of 5% to 8% for the calibrated and uncalibrated models are calculated. The SWASH HFA model shows errors in order of 15% when compared to the Ting and Kirby (1994) data.

The same additional analysis is performed for the vertical modelled velocities considering a point approximately 0.55m after wave breaking for the Ting and Kirby (1994) data as for the horizontal velocities. The phase-averaged vertical velocity is shown in Figure B.31.

From Figure B.31 it can be seen that large velocity gradients exist in the measured data and the data displays a distinct double peak in the maximum vertical velocity. The SWASH models (calibrated and uncalibrated) do not account for the double peak but adequately resolve the magnitude of the peak vertical velocity and modes a single peak relative to the measured data.

The RMSE and %RMSE for the vertical plunging wave velocities are given in Table 6.11. The Govender (1999) data statistical analysis is repeated here for the sake of convenience. The measured vertical phase averaged velocities vs. SWASH modelled vertical velocities (at a distance of 0.55m from break point) are given in Figure B.32. This figure illustrates the relative errors reported in the RMSE tables for the Ting and Kirby (1994) data only.

Table 6.12: Root mean squared vertical velocity error (m/s) after wave breaking for the Govender (1999) data (0.86m from breakpoint) and Ting and Kirby (1994) data (0.55m from breakpoint) relative to the SWASH models for plunging waves, maximum phase averaged vertical velocity and percentage RMSE error relative to the maximum vertical velocity measurements

	After wave breaking							
Plunging Waves: Z-Velocity	RMSE (m/s) Govender	SWASH Calibrated	SWASH Un-calibrated	SWASH HFA	Max Vel (m/s)	% RMSE Calibrated	% RMSE Un-calibrated	% RMSE HFA
	Bottom	0.0063	0.0070	0.0067	0.03	49%	57%	49%
	Mid water	0.0071	0.0073	0.0152	0.06	46%	50%	49%
	Mid water	0.0088	0.0135	0.0188	0.16	37%	36%	43%
	Top	0.0078	0.0095	0.0045	0.18	49%	49%	57%
	RMSE (m/s) Ting and Kirby	SWASH Calibrated	SWASH Un-calibrated	SWASH HFA	Max Vel (m/s)	% RMSE Calibrated	% RMSE Un-calibrated	% RMSE HFA
	Bottom	0.007	0.006	0.010	0.06	11%	10%	16%
	Mid water	0.011	0.011	0.021	0.15	7%	8%	14%
	Mid water	0.017	0.016	0.030	0.21	8%	8%	15%
	Top	0.032	0.028	0.042	0.28	11%	10%	15%

The %RMSE calculated for the Ting and Kirby (1994) data shows a percentage error in the order of 10% for the calibrated and uncalibrated models while the SWASH HFA model indicates an error in the order of 15%. This is again a significant improvement on the error margins calculated for the Govender data.

6.5.3 Phase averaged spilling wave comparison

6.5.3.1 Horizontal velocity before spilling breaking

The phase-averaged horizontal particle velocity comparison between the measured data sets of Govender (1999) and Ting and Kirby (1994) and the SWASH models for spilling waves at the cross-shore point before wave breaking are given in Figure B.33 and Figure B.34 respectively.

All the SWASH models fit the measured Govender (1999) data very well across the whole water column. Some discrepancies near the water surface (bottom right panel) are observed. There is a slight but marked difference between the results presented by the SWASH calibrated and uncalibrated models where it seems as if the calibrated model has the best fit overall and the uncalibrated model overestimates the horizontal velocity slightly. The HFA model follows the results of the uncalibrated model in general but underpredicts the peak velocities at the water surface.

Both the SWASH calibrated and uncalibrated results show an overestimation of approximately 0.1m/s in the lower half of the water column at the peak velocities for the measured Ting and Kirby (1994) data. A very good fit to the measured data for both these models is obtained in the upper half of the water column. Both the SWASH models under-predict the lower end of the horizontal velocities throughout the water column. The SWASH HFA model does not perform well when compared to the measured data anywhere in the water column relative to the phase averaged shape. However, the peak velocities are represented by the SWASH HFA model.

The RMSE and %RMSE for the horizontal spilling wave particle velocity are given in Table 6.13. In addition, the measured horizontal phase averaged velocities vs. SWASH modelled horizontal velocities are given in Figures B.35 and B.36. These figures illustrate the relative errors reported in the RMSE tables.

Table 6.13: Root mean squared horizontal velocity error (m/s) before wave breaking for the Govender (1999) and Ting and Kirby (1994) relative to the SWASH models for spilling waves, maximum phase averaged horizontal velocity and percentage RMSE error relative to the maximum horizontal velocity

Before wave breaking								
Spilling Waves: U-Velocity	RMSE (m/s) Govender	SWASH Calibrated	SWASH Un-calibrated	SWASH HFA	Max Vel (m/s)	% RMSE Calibrated	% RMSE Un-calibrated	% RMSE HFA
	Bottom	0.046	0.058	0.071	0.27	17%	22%	26%
	Mid water	0.051	0.068	0.084	0.30	17%	23%	28%
	Mid water	0.063	0.087	0.104	0.36	17%	24%	29%
	Top	0.101	0.154	0.132	0.51	20%	31%	26%
	RMSE (m/s) Ting and Kirby	SWASH Calibrated	SWASH Un-calibrated	SWASH HFA	Max Vel (m/s)	% RMSE Calibrated	% RMSE Un-calibrated	% RMSE HFA
	Bottom	0.060	0.064	0.166	0.41	15%	16%	41%
	Mid water	0.065	0.069	0.148	0.41	16%	17%	36%
	Mid water	0.060	0.058	0.124	0.44	14%	13%	28%
	Top	0.048	0.057	0.147	0.48	10%	12%	31%

From Table 6.13 it can be seen that the calibrated models fit the measured data the best with error margins in the order of 15% to 20% while large error margins (in the order of 30% to 40%) are seen for the HFA model. The uncalibrated model shows a small margin of additional error compared to the calibrated model for the Govender (1999) data but have the same error margins when comparing the models based on the Ting and Kirby (1994) data.

6.5.3.2 Vertical velocity before spilling breaking

The phase-averaged vertical particle velocity comparison between the measured data sets of Govender (1999) and Ting and Kirby (1994) and the SWASH models for spilling waves at the cross-shore point before wave breaking are given in Figure B.37 and Figure B.38 respectively.

All the SWASH models fit the measured data well for the Govender (1999) data across the whole water column. Some discrepancy is observed near the water surface where the downward (negative) velocities are slightly out of phase. However, the shape of all the SWASH models is a sufficient fit to the measured data.

The calibrated and uncalibrated SWASH models are an excellent fit to the observed Ting and Kirby (1994) data throughout the water column. However, the SWASH HFA model does not fit the measured data very well. In most cases, the HFA model resolves the peak velocities across the water column but does not fit the measured data shape very well.

The RMSE and %RMSE for the vertical spilling wave particle velocity are given in Table 6.14. The measured vertical phase averaged velocities vs. SWASH modelled vertical velocities are given in Figures B.39 and B.40. These figures illustrate the relative errors reported in the RMSE tables.

Table 6.14: Root mean squared vertical velocity error (m/s) before wave breaking for the Govender (1999) and Ting and Kirby (1994) relative to the SWASH models for spilling waves, maximum phase averaged vertical velocity and percentage RMSE error relative to the maximum vertical velocity

Before wave breaking								
Spilling Waves: Z-Velocity	RMSE (m/s) Govender	SWASH Calibrated	SWASH Un-calibrated	SWASH HFA	Max Vel (m/s)	% RMSE Calibrated	% RMSE Un-calibrated	% RMSE HFA
	Bottom	0.010	0.013	0.018	0.09	11%	14%	20%
	Mid water	0.020	0.031	0.046	0.24	8%	13%	20%
	Mid water	0.028	0.049	0.071	0.32	9%	15%	22%
	Top	0.088	0.224	0.250	0.50	18%	45%	50%
	RMSE (m/s) Ting and Kirby	SWASH Calibrated	SWASH Un-calibrated	SWASH HFA	Max Vel (m/s)	% RMSE Calibrated	% RMSE Un-calibrated	% RMSE HFA
	Bottom	0.008	0.006	0.016	0.07	11%	8%	21%
	Mid water	0.011	0.009	0.032	0.14	8%	7%	23%
	Mid water	0.018	0.017	0.043	0.20	9%	9%	22%
	Top	0.022	0.022	0.052	0.27	8%	8%	19%

The %RMSE for the calibrated models for both data sets is in the order of 10%. The uncalibrated model has a marginally higher %RSME than the calibrated model considering the Govender data set. The percentage error reported for the discrepancy discussed (Govender data in the upper water column) is 18%. The HFA model shows a percentage error of 20%.

The percentage RMSE error for the Ting and Kirby data is in the order of 10% for the calibrated and uncalibrated SWASH models and is practically identical in results. The SWASH HFA model has a larger RMSE in the order of 20% which was expected given the analysis above.

The modelled horizontal and vertical spilling breaker velocities are compared to the measured data for positions in the flume after wave breaking. Note that the Govender data set recorded the velocity a distance of 1.22m from the spilling breaking point while Ting and Kirby recorded their data a distance of 0.27m past the breaking point.

6.5.3.3 Horizontal velocity after spilling breaking

The phase-averaged horizontal particle velocity comparison between the measured data sets of Govender (1999) and Ting and Kirby (1994) and the SWASH models for spilling waves at the cross-shore point after wave breaking are given in Figure B.41 and Figure B.42 respectively.

The Govender (1999) data is relatively well represented by all the SWASH models in the lower half of the water column while the maximum measured horizontal velocities in the upper half of the water column are not resolved by the SWASH models. Maximum velocities of 1.39m/s and 1.66m/s are reported by the Govender (1999) data. It is suspected that large scale turbulence measured could be responsible for the high velocities reported by the author. The SWASH HFA model follows the trend of the calibrated model but over-predict the peak velocities in the lower half of the water column.

The SWASH uncalibrated model shows the best fit to the Ting and Kirby (1994) peak velocity data throughout the water column whereas the calibrated model shows the best fit to the peak return flow velocities. The reverse flow velocities are overestimated by up to 0.1m/s for the uncalibrated model. The calibrated model over predicts the peak horizontal velocities by approximately 0.2m/s. the SWASH HFA model does not fit the measured data very well. In most cases, the HFA model resolves the peak velocities across the water column but does not fit the measured data shape very well.

The RMSE and %RMSE for the horizontal spilling wave particle velocity are given in Table 6.15. The measured horizontal phase averaged velocities vs. SWASH modelled horizontal velocities after spilling wave breaking are given in Figures B.43 and B.44. These figures illustrate the relative errors reported in the RMSE tables.

Relatively large %RMSE is reported for the Govender (1999) data in the order of 40% up to 60% for all the SWASH models. In contrast, the calibrated

Table 6.15: Root mean squared horizontal velocity error (m/s) after wave breaking for the Govender (1999) and Ting and Kirby (1994) relative to the SWASH models for spilling waves, maximum phase averaged horizontal velocity and percentage RMSE error relative to the maximum horizontal velocity

After wave breaking								
Spilling Waves: U-Velocity	RMSE (m/s) Govender	SWASH Calibrated	SWASH Un-calibrated	SWASH HFA	Max Vel (m/s)	% RMSE Calibrated	% RMSE Un-calibrated	% RMSE HFA
	Bottom	0.062	0.080	0.058	0.18	35%	45%	32%
	Mid water	0.099	0.117	0.089	0.22	46%	54%	41%
	Mid water	0.472	0.457	0.488	1.39	34%	33%	35%
	Top	1.021	0.682	0.868	1.66	62%	41%	52%
	RMSE (m/s) Ting and Kirby	SWASH Calibrated	SWASH Un-calibrated	SWASH HFA	Max Vel (m/s)	% RMSE Calibrated	% RMSE Un-calibrated	% RMSE HFA
	Bottom	0.089	0.115	0.156	0.42	21%	28%	38%
	Mid water	0.073	0.074	0.144	0.41	18%	18%	35%
	Mid water	0.073	0.047	0.128	0.44	17%	11%	29%
	Top	0.032	0.060	0.139	0.49	7%	12%	28%

and uncalibrated models have relative RMSE errors in the order of 10% to 20% when compared to the Ting and Kirby (1994) data. From B.42 it can be seen that most of the relative error is contained in the negative (return) flow model data.

6.5.3.4 Vertical velocity after spilling breaking

The phase-averaged vertical particle velocity comparison between the measured data sets of Govender (1999) and Ting and Kirby (1994) and the SWASH models for spilling waves at the cross-shore point after wave breaking are given in Figure B.45 and Figure B.46 respectively.

The SWASH calibrated and uncalibrated models show a relatively good fit to the measured data in the lower third of the water column in terms of phase velocity shape. The peak velocities are slightly under-predicted by the models. Near the surface of the wave, large negative (reverse directional flow) values are reported by the data that do not get resolved by the SWASH models. Both the calibrated and uncalibrated models resolve the peak positive flows fairly well. The SWASH HFA model under predicts the vertical velocities throughout the water column and is not a very good fit to the measured data.

The calibrated and uncalibrated SWASH models show excellent fit to the observed Ting and Kirby (1994) data throughout the water column in terms of the peak velocities and phase shape. However, the SWASH HFA model does not fit the measured data very well. In most cases, the HFA model resolves the peak velocities across the water column but does not fit the measured data shape very well.

The RMSE and %RMSE for the vertical spilling wave particle velocity are given in Table 6.16. The measured vertical phase averaged velocities vs. SWASH modelled vertical velocities after spilling wave breaking are given in Figures B.47 and B.48. These figures illustrate the relative errors reported in

the RMSE tables.

Table 6.16: Root mean squared vertical velocity error (m/s) after wave breaking for the Govender (1999) and Ting and Kirby (1994) relative to the SWASH models for spilling waves, maximum phase averaged vertical velocity and percentage RMSE error relative to the maximum vertical velocity

After wave breaking								
Spilling Waves: Z-Velocity	RMSE (m/s) Govender	SWASH Calibrated	SWASH Un-calibrated	SWASH HFA	Max Vel (m/s)	% RMSE Calibrated	% RMSE Un-calibrated	% RMSE HFA
	Bottom	0.029	0.031	0.039	0.10	28%	31%	39%
	Mid water	0.041	0.059	0.100	0.26	16%	23%	39%
	Mid water	0.127	0.206	0.205	0.32	40%	64%	64%
	Top	0.159	0.263	0.225	0.18	87%	144%	124%
	RMSE (m/s) Ting and Kirby	SWASH Calibrated	SWASH Un-calibrated	SWASH HFA	Max Vel (m/s)	% RMSE Calibrated	% RMSE Un-calibrated	% RMSE HFA
	Bottom	0.006	0.004	0.012	0.05	12%	8%	26%
	Mid water	0.010	0.008	0.030	0.12	8%	7%	25%
	Mid water	0.015	0.014	0.045	0.19	8%	7%	24%
	Top	0.014	0.015	0.062	0.28	5%	5%	22%

Table 6.16 reports very large error percentages (up to 144%) for the Govender (1999) data near the water surface. The lower third of the water column reports a wide range of %RMSE between 16% and 64% for the Govender data. On the other hand, the Ting and Kirby (1994) show small error margins to the modelled calibrated and uncalibrated models (in the order of 8%) while the SWASH HFA reports %RMSE in the order of 25%.

6.6 Turbulence results

Both Govender (1999) and Ting and Kirby (1994) calculated the velocity fluctuations, turbulence intensities and TKE from the instantaneous velocity measurements. However, upon further analysis, it was found that the Govender (1999) turbulent intensity and turbulence data supplied proved to have errors in the raw data due to data corruption. The raw velocity data were not supplied by the author and thus, the turbulence intensity calculations could not be calculated from the velocity data. A such, the performance of the SWASH models with regards to turbulence will be compared only to the Ting and Kirby (1994) data.

6.6.1 Turbulent fluctuations

An example of the instantaneous variance in the horizontal velocity fluctuation of the measured Ting and Kirby (1994) data is shown in the top panel of Figure B.49 (also refer to Section 2.12). The sampling rate of the measured data is 100Hz and one single wave phase is shown. On the same plot, the modelled SWASH calibrated model result for the same wave phase is shown. This

particular wave phase is for a point approximately 0.55m after the breaking point and 4cm above the bed (mid-water column relative to the recorded wave trough level).

The bottom panel of Figure B.49 demonstrates the calculated variance of the measured (blue line) and modelled velocity (broken red line) measurement ($(u_t - \bar{u})^2$). Note that the SWASH modelled results (red broken line) are increased with a factor of 10000 in order to be able to discern it on the plot.

What is clearly demonstrated in Figure B.49 (top panel) is the ability of the laboratory techniques (PIV or, in this case, LDA) to record the turbulent fluctuations in the water column. The variance is an important measure of the turbulent fluctuations in the water column due to the wave breaking.

The absence of the same type of observed fluctuations in the SWASH model is expected as the SWASH model does not simulate the instantaneous velocity fluctuations. For the purpose of determining the turbulence in the model, SWASH employs various turbulence models to simulate the statistical turbulence in the model. As such, the modelled velocity cannot be used to determine the turbulence intensities. The reader is referred to Section 3.7.

6.6.2 Turbulent kinetic energy

Turbulent fluctuation measurements from the Ting and Kirby (1994) experiments were supplied by the authors from the flume bottom up to a level below the wave trough height, the crest and roller turbulence velocity detail (above trough height) are not available for analysis. Regardless, the data that was made available is used to calculate the theoretical TKE from the phase averaged turbulent velocity data. Note that only two dimensions were measured by the researchers; i.e. horizontal and vertical. In order to account for only two dimensions, the approximation proposed by Svendsen *et al.* (1978) is used as follows:

$$k = 1.33\frac{1}{2}(u'^2 + w'^2) \tag{6.1}$$

where u' represents the horizontal turbulence intensity component and w' represents the vertical turbulence intensity component.

The SWASH modelled TKE (for the calibrated SWASH model) is compared to the calculated TKE (Equation 6.1) in Figure B.50 and Figure B.52 where the phase averaged TKE contours are plotted relative to the water level. The SWASH modelled results are shown in the upper panel while the Ting and Kirby (1994) measurements are shown in the lower panel. Note the broken red line indicates the phase averaged water level. In addition, photographic images are shown that correspond to the approximate points where the TKE analysis for the measured data and SWASH model is discussed.

The measured contour data (lower panel of Figure B.50) shows good agreement with the turbulence observed in the still image, i.e. the downward tur-

bulent injection of turbulent aerated water in front of the wave crest. The turbulence is seen to extend to approximately the bed level. The SWASH modelled TKE only shows an increase in TKE in the crest of the wave and around the breaking wave face. The downward injection of turbulence is not seen in the SWASH model. However, some TKE is reported near the bed in the same order of magnitude than is observed at the wave trough level.

The calculated Ting and Kirby (1994) TKE and the modelled TKE are in the same order of magnitude.

Photographic images of the spilling wave breaking are given in Figure B.53. Note that a still image of the point under analysis (approximately 0.26m from the breaking point) is not available; thus two images before and after this point are shown in Figure B.53.

It is difficult to see the areas of turbulence in Figure B.53 in the same manner as the plunging wave due to the more gentle overturning of the spilling wave compared to the violent plunging wavefront of Figure B.51. From Figure B.52 it can be seen that there are some TKE cascading in front of the wave face below trough level for the measured data. In addition, some higher TKE values are observed at the surface level around $t/T = 0.025$ and $t/T = 0.30$, possibly from larger eddies left behind by the spilling wave face.

The SWASH model shows most of its TKE concentrated around the wave crest and at the bed directly below the wave crest in the same manner as the plunging wave case.

Time-averaged TKE, calculated from the Ting and Kirby (1994) instantaneous velocity data, and SWASH modelled TKE throughout the water column for various points across the flume for the plunging wave are given in Figure B.54.

The SWASH modelled and calculated TKE from the measured data computes to within the same order of magnitude.The vertical distribution of the TKE is modelled fairly well by the SWASH model. Although far from perfect, it can be concluded that the SWASH model is a reasonable representation of the measured data. It is not expected that the data must have a good fit with the measured data as the Prandtl and $k - \epsilon$ are merely models of the closure problem.

The same time averaged TKE, calculated from the measured instantaneous velocity data, and SWASH modelled TKE throughout the water column for various points across the flume for the spilling wave are given in Figure B.55.

Before and after wave breaking (top left and right panels) show the least fit to the measured data. The SWASH modelled results for the other cross-shore points in the flume, further away from the breaking point, show a good fit in terms of shape to the measured data. The SWASH model over predicts the TKE but remains in the same order of magnitude to the measured data.

Chapter 7

Conclusions and Recommendations

7.1 Background

This chapter concludes this study by considering the research conducted and providing a summary of the reported results.

Most commercial numerical wave models (e.g. SWAN (TU Delft) and Mike21 Boussinesq / Spectral Wave (DHI)) require the engineer to activate a wave breaking formulation in the software if wave breaking is to be taken into account in the calculations. This requires the modeller to specify a set of wave breaking parameters within the wave breaking formulation. This implies that, in order for the numerical model to be accurate, the wave breaking parameters need to at least be obtained through the process of a calibration exercise where, naturally, experimental data are required.

The challenge posed by the SWASH Team was inherent in their claim that with an adequate vertical resolution, SWASH can reliably resolve the dissipation processes of wave breaking without additional model assumptions and the need to specify wave breaking parameters (Smit, 2014). The aim of this study was to investigate this claim of Smit (2014) as the validity of such a claim will assist the coastal engineer during the preliminary design stage.

The objectives are briefly summarised as follows:

- Analyse the sensitivity of some numerical parameters of the SWASH model and compare it to measured data;
- Calibrate the numerical models with the measured data and compare the calibrated model with an uncalibrated model and with the SWASH HFA (lower vertical resolution but explicit enforcing of wave breaking);
- Determine the relative error margin between the three models; and
- Make a final conclusion with regards to the applicability of SWASH.

7.2 Conclusions from literature

Chapters 2 and 3 considered the physical processes encountered in the surf zone and the numerical capabilities of SWASH. This study compared the observed physical surf zone phenomena that need to be quantified as input parameters into design formulas with the capability of the numerical model to simulate these processes and produce sufficiently accurate output that can be reliably used as design input. It was found that the important parameters (incipient breaking, water levels, particle velocities and turbulence) can be numerically simulated in SWASH for plunging and spilling breaking waves.

7.3 Sensitivity analysis

From the sensitivity tests the following can be concluded:

- When the hydrostatic front approximation is not used, the number of vertical layers do make a difference in the SWASH model's ability to calculate the correct incipient breaking point. Smit (2014) recommends between 10 and 20 layers as a guideline. The context of the simulation must also be considered; i.e. if wave breaking is studied, then the vertical resolution has to be adequate in order to resolve the vertical flow structures. A lower number of vertical layers will save on computational time but might not resolve the velocities at the critical parts of the wave. On the other hand, if the maximum wave heights and breaking point are the focus of the study, then a lower number of vertical layers might suffice (see Section 5.3.1 and Section 5.4.1).

- The conservation of momentum has a large influence on the results of the plunging waves in terms of wave heights.

- The spilling waves are insensitive to the explicit conservation of momentum.

- The horizontal and vertical velocities before and after wave breaking are also insensitive to the mode of momentum conservation.

- Manning friction values for the plunging waves seem to have a variable influence pre- and post-wave breaking where lower numerical values produced good results before wave breaking and higher Manning values post breaking. The spilling breakers showed good correlation for lower Manning values pre- and post breaking (see Section 5.3.2 and Section 5.4.2).

- Limited options exist to vary the horizontal and vertical advection term discretisation. The options available might have more use as stability

parameters than of calibration parameters (see Section 5.3.3 and Section 5.4.3).

The plunging waves showed good results with the Advection Scheme 2 (which equates to using the central differencing scheme for the horizontal w-momentum term) while the spilling waves mostly showed favourable results using Advection Scheme 1 (central differencing scheme for the vertical u-momentum term).

- The water depth in velocity points showed good correlation with the measured plunging wave results in some way or another with all the schemes tested. However, the spilling waves did not agree with any results when using the First Order Upwind scheme. The MinMod scheme was found to be a good option for the spilling waves (see Section 5.3.4 and Section 5.4.4).

Accurate simulation of waves involving two very different wave states (irrotational flow pre-breaking and chaotic rotational flow post breaking) is in itself a difficult requirement for any numerical model. As demonstrated here, accurately representing the pre-breaking state through calibration might mean sacrificing accuracy in the post-breaking model results and vice versa.

It is up to the engineer to decide which aspect of the design is most important and to calibrate the SWASH model accordingly.

7.4 Model comparison and relative error

7.4.1 Water levels

The calculated water levels of the three SWASH models are compared to the measured data sets of Govender (1999) and Ting and Kirby (1994) for plunging and spilling breakers. The water levels were analysed in terms of incipient breaking point, breaker depth index, phase averaged water level and wave setup.

In general, the following was found:

Incipient breaking point and breaker depth index The calibrated and uncalibrated SWASH models for plunging waves resolve the incipient breaking point earlier than the measured data. The implication is that the water depth at an earlier point in the flume is deeper which will result in a lower breaker depth index. The spilling waves show a better agreement to the Govender (1999) data while an excellent agreement is seen with the Ting and Kirby (1994) data.

The SWASH HFA model proves a very good fit to the measured data in terms of the incipient breaking point and has the least discrepancy when compared with the calculated breaker depth index for the measured data.

The calibrated and uncalibrated models calculate lower breaker depth indices.

It can be concluded that the SWASH HFA model is a very good method for resolving the incipient breaking point and shows very good agreement with breaker depth index measurements.

Phase averaged water levels The calibrated and uncalibrated SWASH models show very good agreement with measured data for both spilling and plunging breakers. Relative errors between the measured data and the calibrated modelled data range in the order of 8% to 12%. The uncalibrated model only shows slightly higher RMSE percentages (in the range of 3% to 5%) compared to the calibrated model results.

The HFA model shows the largest error margin relative to the other models but not higher than a 10% difference compared to the calibrated and uncalibrated SWASH models.

The offshore point (PWP4 and SWP4) for all models are well represented in terms of peak wave height but not well represented in terms of wave shape.

It can be concluded that the SWASH model with an adequate vertical resolution (HFA not enabled) shows good agreement to the laboratory measured results for plunging and spilling breakers with a RMSE in the order of 10% to 12%.

Wave setup The wave setup is generally slightly overpredicted by SWASH for plane slopes by very small margins of between 5mm and 10mm. The SWASH modelled wave calculated setup can be considered as a conservative estimate.

7.4.2 Plunging wave velocities

Considering the plunging waves for the Govender (1999) and Ting and Kirby (1994) data, the horizontal and vertical velocities pre- and post breaking were analysed and the statistical errors between the predictions and measurements calculated.

In general, it was found that:

Pre wave breaking The calibrated and uncalibrated SWASH models all showed very good comparisons to the measured data for both data sets. In particular, the calibrated and uncalibrated models' %RMSE is in the order of 10% to 15%.

The calibrated and uncalibrated models show very similar results in terms of calculated %RMSE for both the data sets.

The horizontal and vertical phase averaged velocities are well represented by the SWASH models in terms of resolving the peak velocities. In many cases, the averaged shape is not very well represented.

The SWASH HFA model does not represent the horizontal or vertical velocities very well for any of the measurements. The %RMSE is consistently in the order of 20% to 25%.

Post wave breaking The calibrated and uncalibrated SWASH models all showed very good comparisons to the measured data for both data sets. In particular, the calibrated and uncalibrated models' %RMSE hovers around the 10% mark.

The calibrated and uncalibrated models show very similar results in terms of calculated %RMSE for both the data sets.

The SWASH HFA model does not represent the horizontal or vertical velocities very well for any of the measurements. The %RMSE is consistently in the order of 15% to 25%.

The horizontal and vertical phase averaged velocities are well represented by the SWASH models in terms of resolving the peak velocities but not necessarily in terms of shape over the wave phase. The relative error between the measured and modelled data is larger post-breaking than pre-breaking.

7.4.3 Spilling wave velocities

Reflecting on the spilling waves analysed for the Govender (1999) and Ting and Kirby (1994) data, the horizontal and vertical velocities pre- and post breaking were analysed and the statistical errors between the models and measurements calculated.

In general, it was found that:

Pre wave breaking The calibrated and uncalibrated SWASH models all showed very good comparisons to the measured data for both data sets.

The vertical velocities are better represented by the SWASH model compared to the horizontal velocities. %RMSE margins of between 15% and 20% are calculated for the horizontal velocities while the vertical velocities show calculated %RMSE margins in the order of 10%.

The calibrated and uncalibrated models show very similar results in terms of calculated %RMSE for the Ting and Kirby (1994) data. The uncalibrated model shows a slightly higher error percentage compared to the calibrated model for the Govender (1999) data.

The SWASH HFA model does not represent the horizontal or vertical velocities very well for any of the measurements. The %RMSE is consistently in the order of 20% to 30%.

Post wave breaking The calibrated and uncalibrated SWASH models all showed very good comparisons to the measured data for the Ting and Kirby (1994) data but not for the Govender (1999) data. The latter data set showed good correlation with the lower half of the water column but not near the surface, hence the large %RMSE margins reported.

Considering the results from the Ting and Kirby data set, vertical velocities are better represented by the SWASH model compared to the horizontal velocities. %RMSE margins of between 15% and 20% are calculated for the horizontal velocities while the vertical velocities show calculated %RMSE margins of the order of 10%.

The SWASH HFA model does not represent the horizontal or vertical velocities very well for any of the measurements and consistently reports %RMSE in the order of 25% to 40%.

The post-wave breaking data reports an overall larger error margin than the pre-wave breaking calculated errors.

7.4.4 Turbulence modelling

The modelled turbulent kinetic energy was calculated in SWASH using the Prandtl and the two equation $k-\epsilon$ models. The TKE modelled was compared to the measured TKE by looking at a phase-averaged contour plot and the time averaged energy over the water column for various points in the flume.

In general, it was found that the modelled results agree in order of magnitude to the measured results. and that the time averaged turbulence models over-predict the measured TKE but remain in the same order of magnitude. The time averaged turbulence modelled in the developed bore post wave breaking shows the same shape over the water column as the measured data.

It is recognised that turbulence models are approximate solutions to the closure problem of the Reynolds Averages Navier-Stokes equations and that the modeller cannot expect to see an exact representation of the measured chaotic instantaneous flow observed in breaking waves. A turbulence model's usefulness to the coastal engineer lies in its ability to predict the advection and diffusion of particles (e.g. suspended sediment) in the turbulent zone. This is an area that needs separate focused analysis.

7.5 Recommendations

The following recommendations are made:

- It is recommended that this research be extended to include waves breaking over steeper slopes and irregular slopes (e.g. wave breaking over an offshore bar). Only waves breaking on plane slopes were considered here.

- Quantifying and deriving wave statistics for random waves need to be investigated further. This study only considered regular waves. Thus, it is recommended that the capabilities of SWASH be investigated for random waves.

- This study was conducted in one dimension with vertical discretisation (2DV). The main driver is the fact that 2DV laboratory data are readily available to compare the model calculations to the measured data. In contrast, the surf zone is highly dynamic and complex when considering the interaction of the processes in the surf zone. It is recommended that this type of study be extended to three dimensions and processes such as the influence of rip currents, directional spreading, etc.

- The turbulence models included in SWASH are models that have been proven to produce reliable turbulence approximations. The inclusion of additional turbulence models must be considered (e.g. $k-\omega$). The possibility to extend the model for Large Eddy Simulations (LES) is also possible and must be considered. It is recognised that the computational effort for LES in a multi-layer environment will be computationally expensive.

- It is recommended that the effect of the wind on the wave energy in the surf zone be investigated further.

7.6 Some final thoughts

This study shows that the SWASH model is capable of numerically representing surf zone processes that can assist the engineer in his designs. In addition, it is shown that the model performs very well in most areas when an "uncalibrated" SWASH model is employed with accuracy limited to that of preliminary design stage, bearing in mind the context of 2DV and a controlled environment.

The SWASH model offers a vivid array of numerical schemes and parameters that can be utilised for calibration purposes. However, this does not overshadow the robustness and simplicity with which the model can be set up. Regardless, the model does live up to its claim of robustness and accuracy without specifying external parameters to a preliminary design level. Beyond this design level, proper calibration of the model is necessary before the model results can be utilised in detailed design.

List of References

Andersson, B., Andersson, R., Håkansson, L., Mortensen, M., Sudiyo, R. and van Wachem, B. (2011). *Computational Fluid Dynamics for Engineers*. Cambridge University Press.

Basco, D.R. (1985). A qualitative description of wave breaking. *Journal of Waterway, Port, Coastal, and Ocean Engineering*, vol. 111, no. 2, pp. 171–188.

Battjes, J. and Groenendijk, H. (2000). Wave height distributions on shallow foreshores. *Coastal Engineering*, vol. 40, no. 3, pp. 161–182.

Battjes, J. and Janssen, J. (1978). Energy loss and set-up due to breaking of random waves. *Coastal Engineering Proceedings*, vol. 1, no. 16.

Battjes, J.A. and Stive, M.J.F. (1985). Calibration and verification of a dissipation model for random breaking waves. *J. Geophys. Res.*, vol. 90, no. C5, pp. 9159–9167.

Boers, M. (2005). *Surf Zone Turbulence*. PhD, Delft University of Technology.

Carini, R.J., Chickadel, C.C., Jessup, A.T. and Thomson, J. (2015). Estimating wave energy dissipation in the surf zone using thermal infrared imagery. *Journal of Geophysical Research: Oceans*, vol. 120, no. 6, pp. 3937 – 3957.

Cavaleri, L., Alves, J.-H., Ardhuin, F., Babanin, A., Banner, M., Belibassakis, K., Benoit, M., Donelan, M., Groeneweg, J., Herbers, T., Hwang, P., Janssen, P., Janssen, T., Lavrenov, I., Magne, R., Monbaliu, J., Onorato, M., Polnikov, V., Resio, D., Rogers, W., Sheremet, A., Smith, J.M., Tolman, H., van Vledder, G., Wolf, J. and Young, I. (2007). Wave modelling - the state of the art. *Progress in Oceanography*, vol. 75, no. 4, pp. 603 – 674.

Chadwick, A., john Morfett and Borthwick, M. (2004). *Hydraulics in Civil and Environmental Engineering, Fourth Edition*. 4th edn. SPON Press, Taylor and Francis Group.

Chadwick, A., Morfett, J. and Borthwick, M. (2013). *Hydraulics in Civil and Environmental Engineering, Fifth Edition*. CRC Press.

Chang, K.-A. and Liu, P.-F. (1999). Experimental investigation of turbulence generated by breaking waves in water of intermediate depth. *Phys. Fluids*, vol. 11, no. 11, pp. 3390 – 3400.

Christensen, E., Walstra, D.-J. and Emerat, N. (2002). Vertical variation of the flow across the surf zone. *Coastal Engineering*, vol. 45, pp. 169–198.

Cox, D.T., Kobayashi, N. and Okayasu, A. (1996 6). Bottom shear stress in the surf zone. *Journal of Geophysical Research: Oceans (1978?2012)*, vol. 101, no. C6, pp. 14337–14348.

DanTec Dynamics (). Measurement principles of lda. Manufacturing of LDA electronics.
Available at: `http://www.dantecdynamics.com/measurement-principles-of-lda`

Dean, R.G. and Dalrymple, R.A. (2001). *Coastal processes with engineering applications*. Cambridge University Press.

Duncan, J. (1981). An experimental investigation of breaking waves produced by a towed hydrofoil. *Proc. R. Soc. London*, vol. 337, no. 1770, pp. 331–348.

Feddersen, F. (2012). Scaling surf zone turbulence. *Geophysical Research Letters*, vol. 39, no. 18. L18613.

Feddersen, F., Gallagher, E., Guza, R. and Elgar, S. (2003). The drag coefficient, bottom roughness, and wave-breaking in the nearshore. *Coastal Engineering*, vol. 48, pp. 189–195.

Goda, Y. (1970). A synthesis of breaker indices. *Transactions of the Japan Society of Civil Engineers*, vol. Vol 2, Part 2, pp. 227–230.

Govender, K. (1999). *Velocity, vorticity and turbulence measurements in the surf zone*. PhD, University of Natal, Durban.

Haller, M., Dalrymple, R.A. and Svendsen, I.A. (2002). Experimental study of nearshore dynamics on a barred beach with rip channels. *Journal of Geophysical Research*, vol. 107, no. C6.

Holthuijsen, L. (2007). *Waves in Oceanic and Coastal Waters*. Cambridge University Press.

Isobe, M. (2013). Evolution of basic equations for nearshore wave field. *Proc. Jpn. Acad., Ser. B*, vol. 89, pp. 34–50.

Janssen, T. and Battjes, J. (2007). A note on wave energy dissipation over steep beaches. *Journal of Coastal Engineering*, vol. 54, no. 9, pp. 711–716.

Kaminsky, G. and Kraus, N. (1993). Evaluation of depth-limited wave breaking criteria. *Proceedings of 2nd International Symposium on Ocean Wave Measurement and Analysis*, , no. Waves 93, pp. 180–193.

Kamphuis, J. (1991). Incipient wave breaking. *Coastal Engineering*, vol. 15, pp. 185–203.

Komar, P. and Gaughan, M.K. (1973). Airy wave theory and breaker height prediction. In: *Proceedings of the 13th Coastal Engineering Conference, American Society of Civil Engineers*, pp. 405–418.

Launder, B. and Spalding, D. (1974). The numerical computation of turbulent flows. *Computer Methods in Applied Mechanics and Engineering*, vol. 3, no. 2, pp. 269 – 289.

Liao, X. (2015). *Cross-shore velocity moments on the nearshore: Validating SWASH*. MSc, Delft University of Technology, Delft, the Netherlands.

Lin, C. and Hwung, H. (1992). External and internal flow fields of plunging breakers. *Exp. Fluids*, , no. 12, pp. 229 – 237.

Longuet-Higgins, M.S. and Cokelet, E.D. (1976). The deformation of steep surface waves on water. i. a numerical method of computation. *Proceedings of the Royal Society of London. Series A, Mathematical and Physical Sciences*, vol. 350, no. 1660, pp. 1–26.

McCowan, J. (1891). On the solitary wave. *Philosophical Magazine*, vol. 5th Series, Vol 36, pp. 430–437.

Nadaoka, K. and Hino, M.and Koyano, Y. (1989). Structure of the turbulent flow field under breaking waves in the surf zone. *J. Fluid Mech.*, , no. 204, pp. 359 – 387.

Nadaoka, K. and Kondoh, T. (1982). Laboratory measurements of velocity field structure in the surf zone by ldv. *Coastal Eng. Jpn.*, , no. 25, pp. 125 – 146.

Pedersen, C., Deigaard, R. and Sutherland, J. (1986). Turbulence measurements under broken waves. *Prog. Rep.*, , no. 74, pp. 125 – 146.

Rijnsdorp, D., Smit, P.B. and Zijlema, M. (2012). Non-hydrostatic modelling of infragravity waves using swash. In: *ICCE 2012: Proceedings of the 33rd International Conference on Coastal Engineering, Santander, Spain, 1-6 July 2012.*

Roberts, P.J.W. and Webster, D.R. (2002). Turbulent diffusion. In: Shen, H., Cheng, A., Wang, K., Teng, M. and Liu, C. (eds.), *Environmental Fluid Mechanics - Theories and Applications*, chap. 2, pp. 7–46. American Society of Civil Engineers, Reston, Va.

Roelvink, J. and Stive, M. (1989). Bar-generating cross-shore flow mechanisms on a beach. *Journal of Geophysical Research: Oceans*, vol. 94, no. C4, pp. 4785–4800.

Schäffer, H.A., Madsen, P.A. and Deigaard, R. (1993). A boussinesq model for waves breaking in shallow water. *Coastal Engineering*, vol. 20, no. 3, pp. 185 – 202.

Smit, Pieter, B. (2014). *Deterministic and Stochastic Modelling of Ocean Surface Waves*. PhD, Delft University of Technology, Delft, the Netherlands.

Smit, P., Zijlema, M. and Stelling, G. (2013). Depth-induced wave breaking in a non-hydrostatic, near-shore wave model. *Coastal Engineering*, vol. 76, pp. 1 – 16.

Smith, E.R. and Kraus, N. (1991). Laboratory study of wave-breaking over bars and artificial reefs. *Journal of Waterway, Port, Coastal, and Ocean Engineering*, vol. Vol 117, No. 4, pp. 307–325.

Soomere, T., Pindsoo, K., Bishop, S.R., Käärd, A. and Valdmann, A. (2013). Mapping wave set-up near a complex geometric urban coastline. *Nat. Hazards Earth Syst. Sci.*, vol. 13, pp. 3049–3061.

Stelling, G. and Zijlema, M. (2003). An accurate and efficient finite-difference algorithm for non-hydrostatic free-surface flow with application to wave propagation. *International Journal for Numerical Methods in Fluids*, vol. 43, no. 1, pp. 1 – 23.

Stelling, G.S. and Duinmeijer, S.P.A. (2003). A staggered conservative scheme for every froude number in rapidly varied shallow water flows. *International Journal for Numerical Methods in Fluids*, vol. 43, no. 12, pp. 1329–1354.

Svendsen, I., Madsen, P. and Hansen, J.B. (1978). Wave characteristics in the surf zone. In: *Proc. 16th Int Coastal Engineering Conference*, pp. 520 – 539.

Tan, W.Y. (1992). *Shallow water hydrodynamics: Mathematical theory and numerical solution for a two-dimensional system of shallow water equations.* Water and Power Press. Beijing. China,.

Tennekes, H. and Lumley, J.L. (1972). *A first course in turbulence.* Cambridge, Mass. : MIT Press.

The SWASH Team (2016). *SWASH User Manual: Software version 3.14AB.* Delft University of Technology.

Ting, F.C. (2006). Large-scale turbulence under a solitary wave. *Coastal Engineering*, vol. 53, no. 5?6, pp. 441 – 462.

Ting, F.C. (2013). Laboratory measurements of large-scale near-bed turbulent flow structures under plunging regular waves. *Coastal Engineering*, vol. 77, pp. 120 – 139.

Ting, F.C. and Kirby, J.T. (1994). Observation of undertow and turbulence in a laboratory surf zone. *Coastal Engineering*, vol. 24, no. 1, pp. 51–80.

Ting, F.C. and Kirby, J.T. (1995). Dynamics of surf-zone turbulence in a strong plunging breaker. *Coastal Engineering*, vol. 24, pp. 177–204.

Ting, F.C. and Kirby, J.T. (1996). Dynamics of surf-zone turbulence in a spilling breaker. *Coastal Engineering*, vol. 27, pp. 131–160.

USACE (2002). *Coastal Engineering Manual.* U.S. Army Corps of Engineers. Washington, D.C., 1110th edn.
Available at: `http://chl.erdc.usace.army.mil/chl.aspx?p=s&a=PUBLICATIONS;8`

Versteeg, H.K. and Malalasekera, W. (2007). *An introduction to computational fluid dynamics : the finite volume method*. 2nd edn. Harlow, England ; New York : Pearson Education Ltd. ISBN 9780131274983.

Weggel, J. (1972). Maximum breaker height. *Journal of the Waterways, Harbors and Coastal Engineering*, vol. Vol 98, No. WW4, pp. 529–548.

WL|Delft Hydraulics (2014). *Delft3D-FLOW: Simulation of multi-dimensional hydrodynamic flows and transport phenomena, including sediments: Software version 3.15.34158*. Delft Hydraulics.

Zhang, C., Chen, Y., Zheng, J. and Demirbilek, Z. (2014). Variation of wave roller slope in the surf zone. *Coastal Engineering Proceedings*, vol. 1, no. 34, p. 12.

Zijlema, M. (2014). Modelling vertical variation of turbulent flow across a surf zone using swash. *Coastal Engineering Proceedings*, vol. 1, no. 34.

Zijlema, M. and Stelling, G. (2008). Efficient computation of surf zone waves using the nonlinear shallow water equations with non-hydrostatic pressure. *Coastal Engineering*, vol. 55, no. 10, pp. 780 – 790.

Zijlema, M., Stelling, G. and Smit, P. (2011). Swash: An operational public domain code for simulating wave fields and rapidly varied flows in coastal waters. *Coastal Engineering*, vol. 58, no. 10, pp. 992 – 1012.

Zijlema, M. and Stelling, G.S. (2005). Further experiences with computing non-hydrostatic free-surface flows involving water waves. *International Journal for Numerical Methods in Fluids*, vol. 48, no. 2, pp. 169–197.

Appendices

Appendix A

Figures: Chapter 5

A.1 Output figures: Plunging Waves

A.1.1 Vertical layers

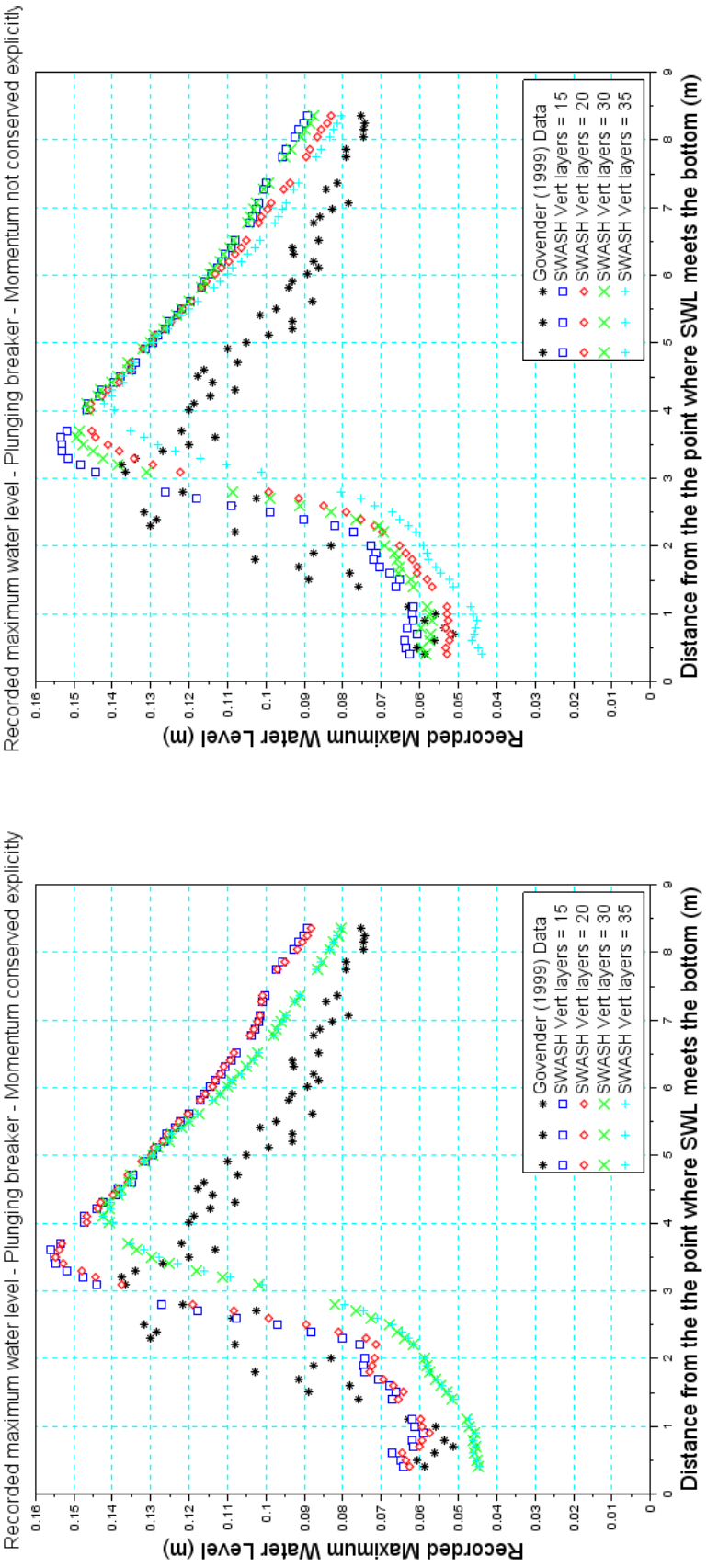

Figure A.1: Maximum water level in the recorded Govender (1999) and SWASH modelled time series for a variety of vertical layer resolutions measured in points cross-shore of the flume. Left panel shows wave heights with momentum conserved while the right panel shows wave heights without momentum conserved explicitly.

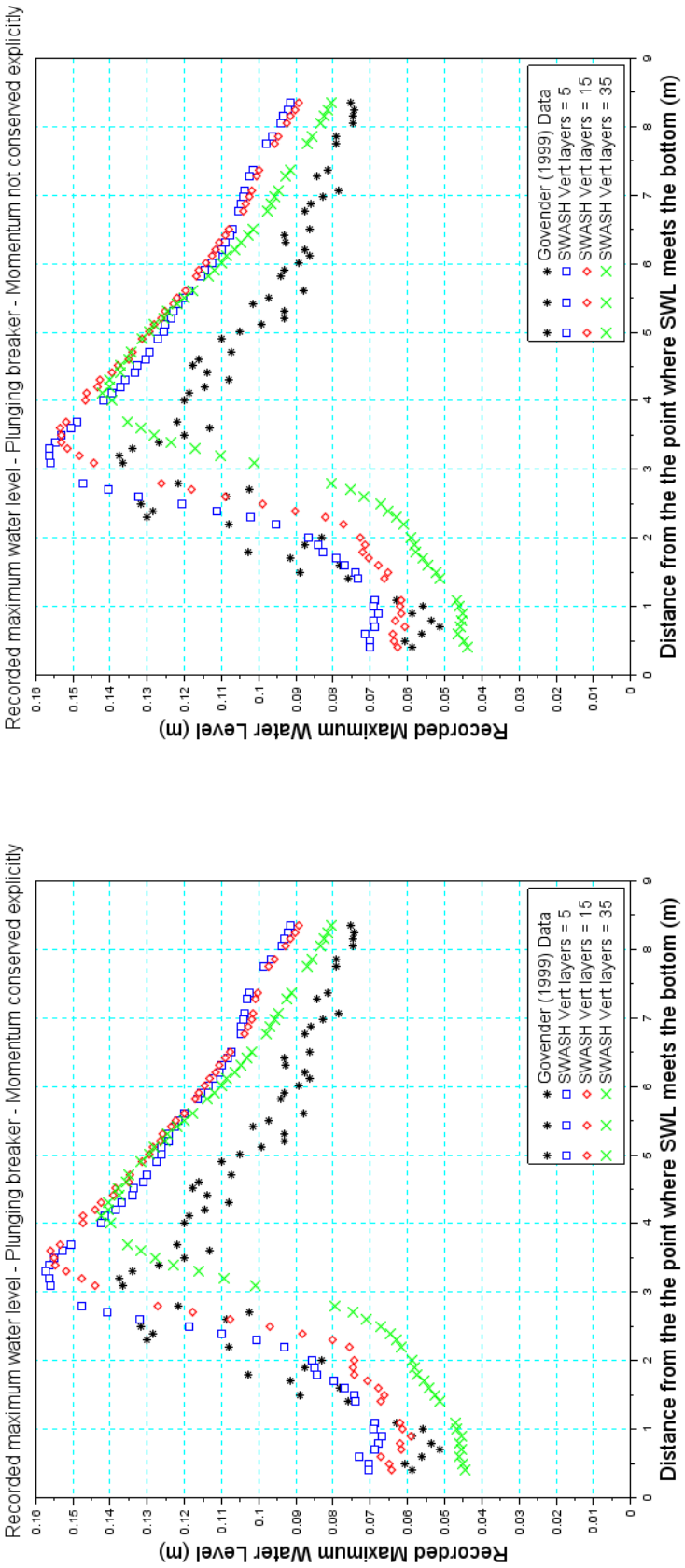

Figure A.2: Maximum wave heights in the recorded Govender (1999) and SWASH modelled time series for a variety of vertical layer resolutions measured in points cross-shore of the flume. Left panel shows wave heights with momentum conserved while the right panel shows wave heights without momentum conserved explicitly.

A.1.2 Bottom friction

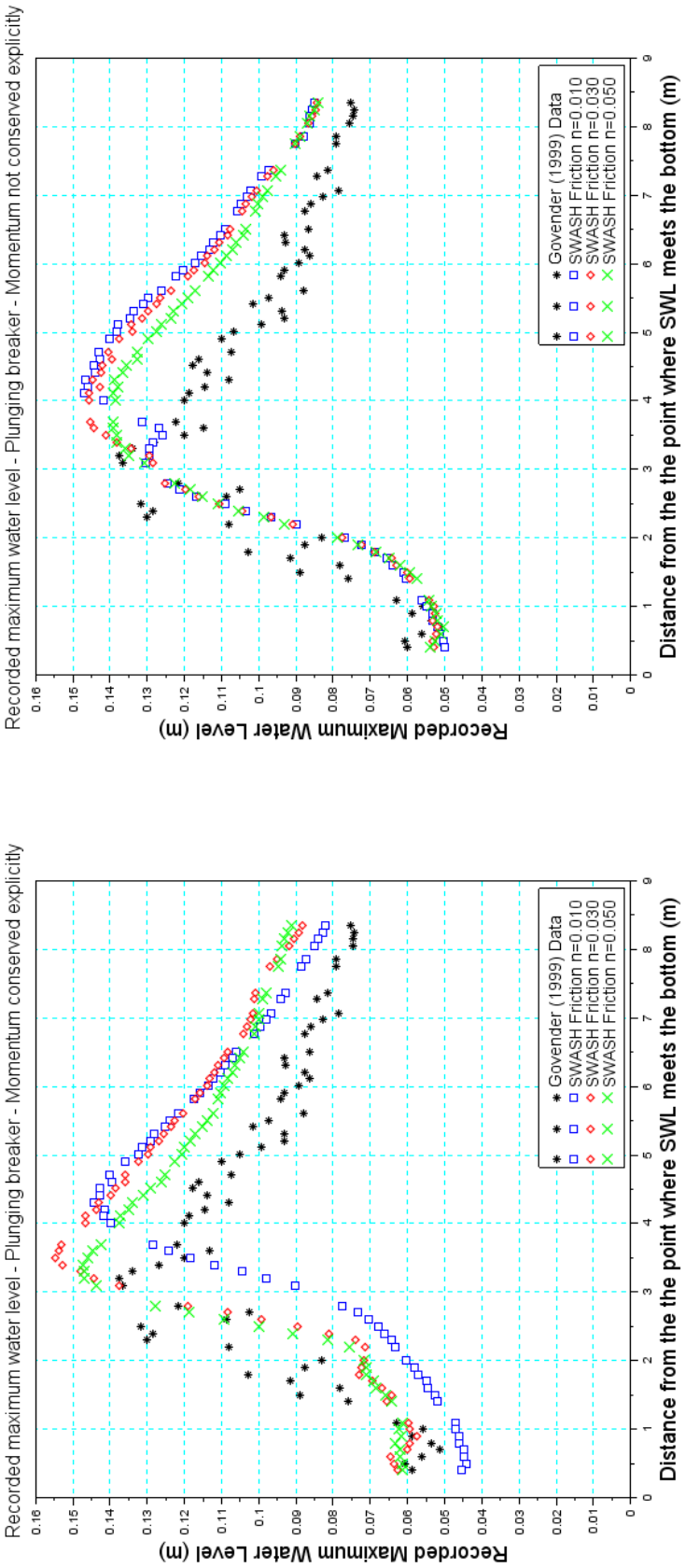

Figure A.3: Maximum wave heights in the recorded Govender (1999) and SWASH modelled time series for various Manning friction values measured in points cross-shore of the flume. Left panel shows wave heights with momentum conserved while the right panel shows wave heights without momentum conserved explicitly.

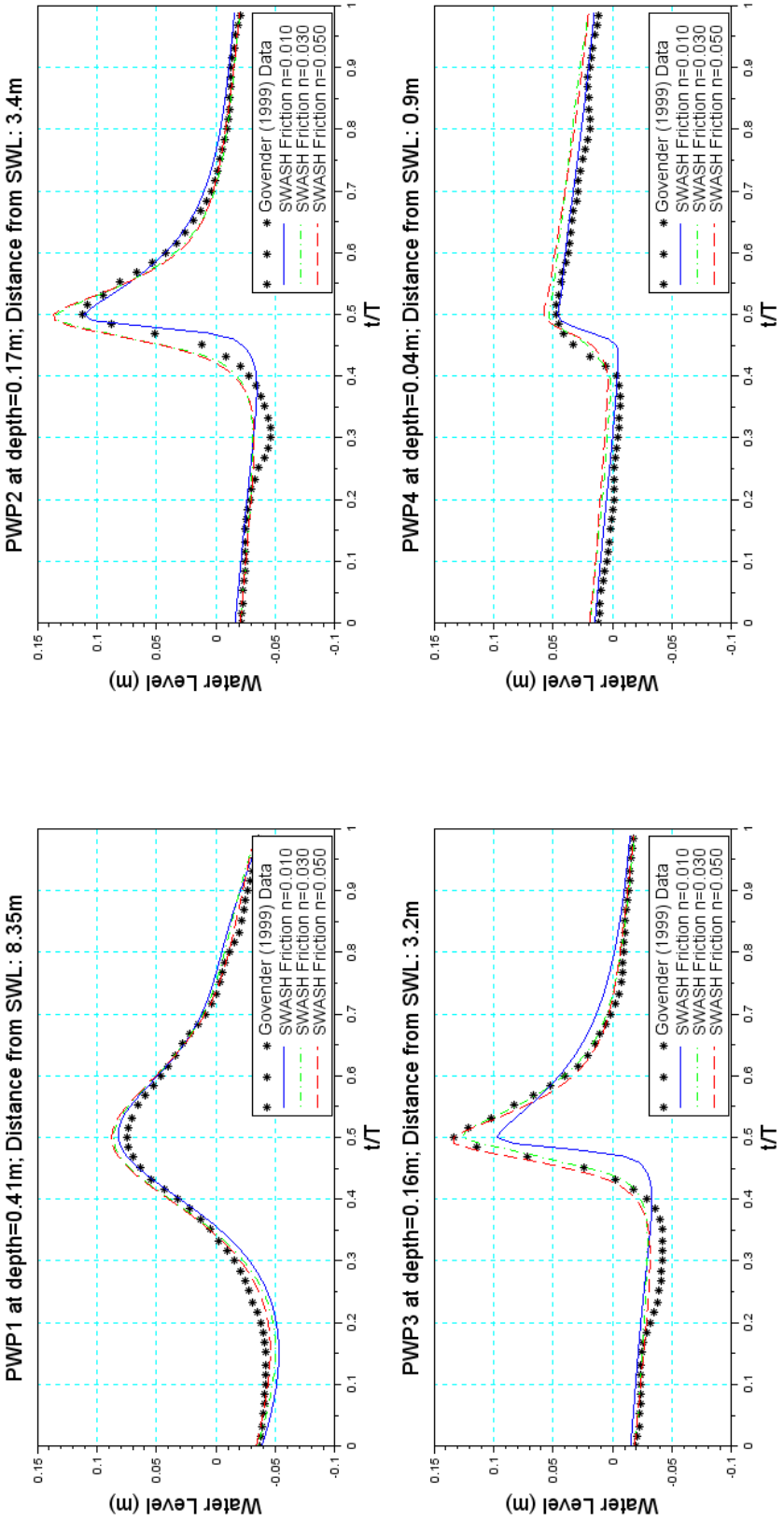

Figure A.4: Phase averaged wave heights in the recorded Govender (1999) and SWASH modelled time series for various Manning friction values at four measuring points in the flume - Momentum explicitly conserved

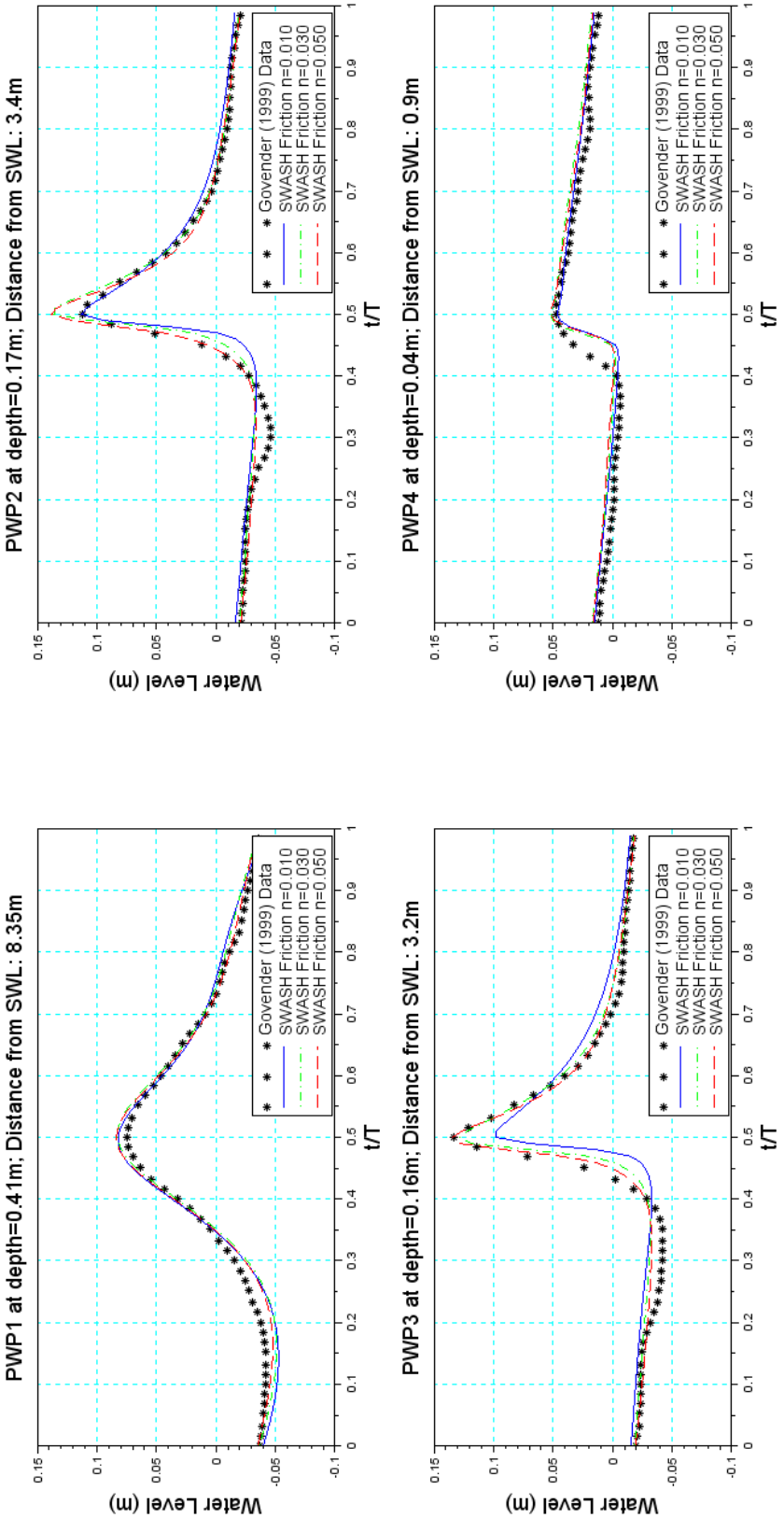

Figure A.5: Phase averaged wave heights in the recorded Govender (1999) and SWASH modelled time series for various Manning friction values at four measuring points in the flume - Momentum not explicitly conserved

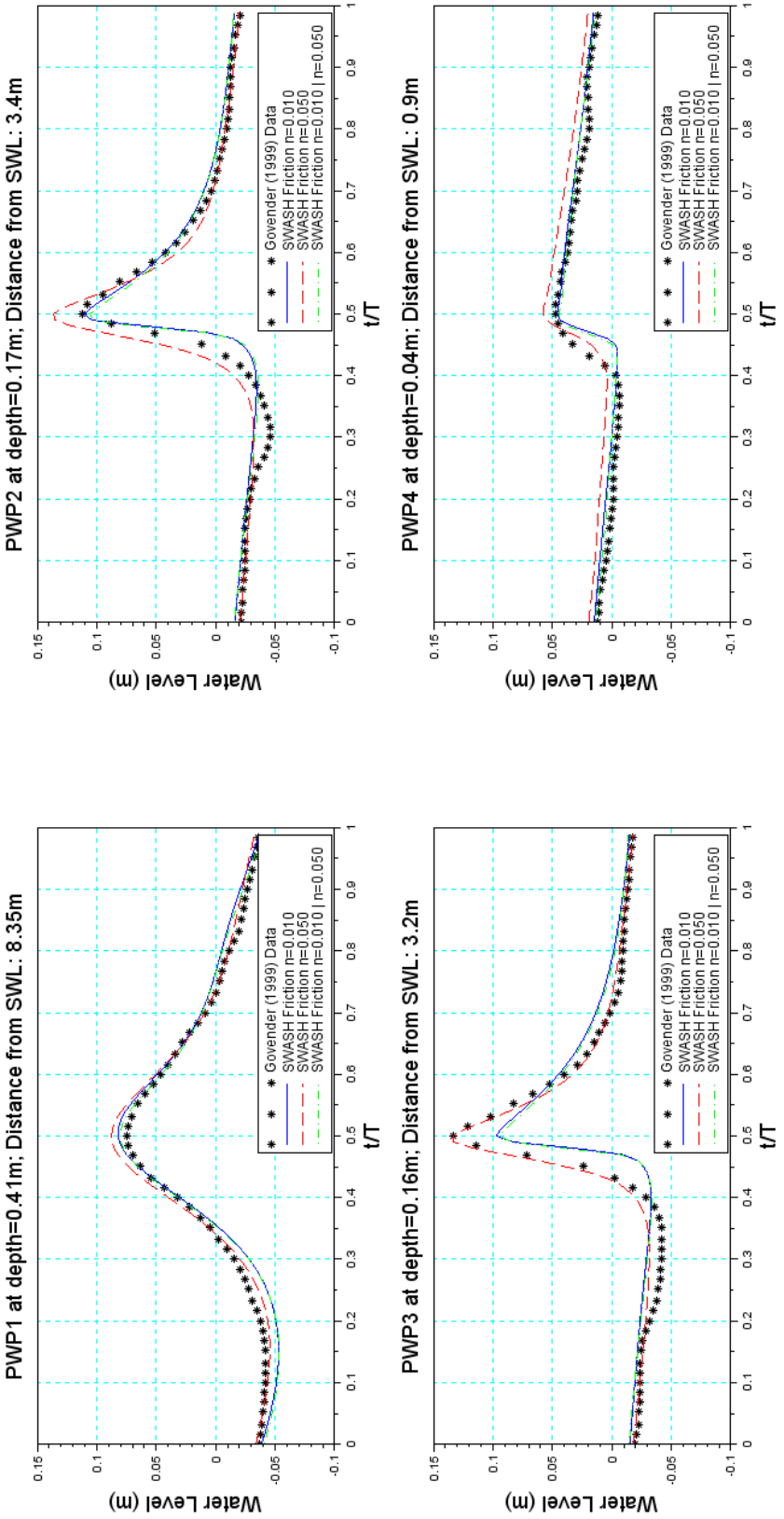

Figure A.6: Phase averaged wave heights for a variable friction scenario in the recorded Govender (1999) and SWASH modelled time series for various Manning friction values at four measuring points in the flume - Momentum explicitly conserved

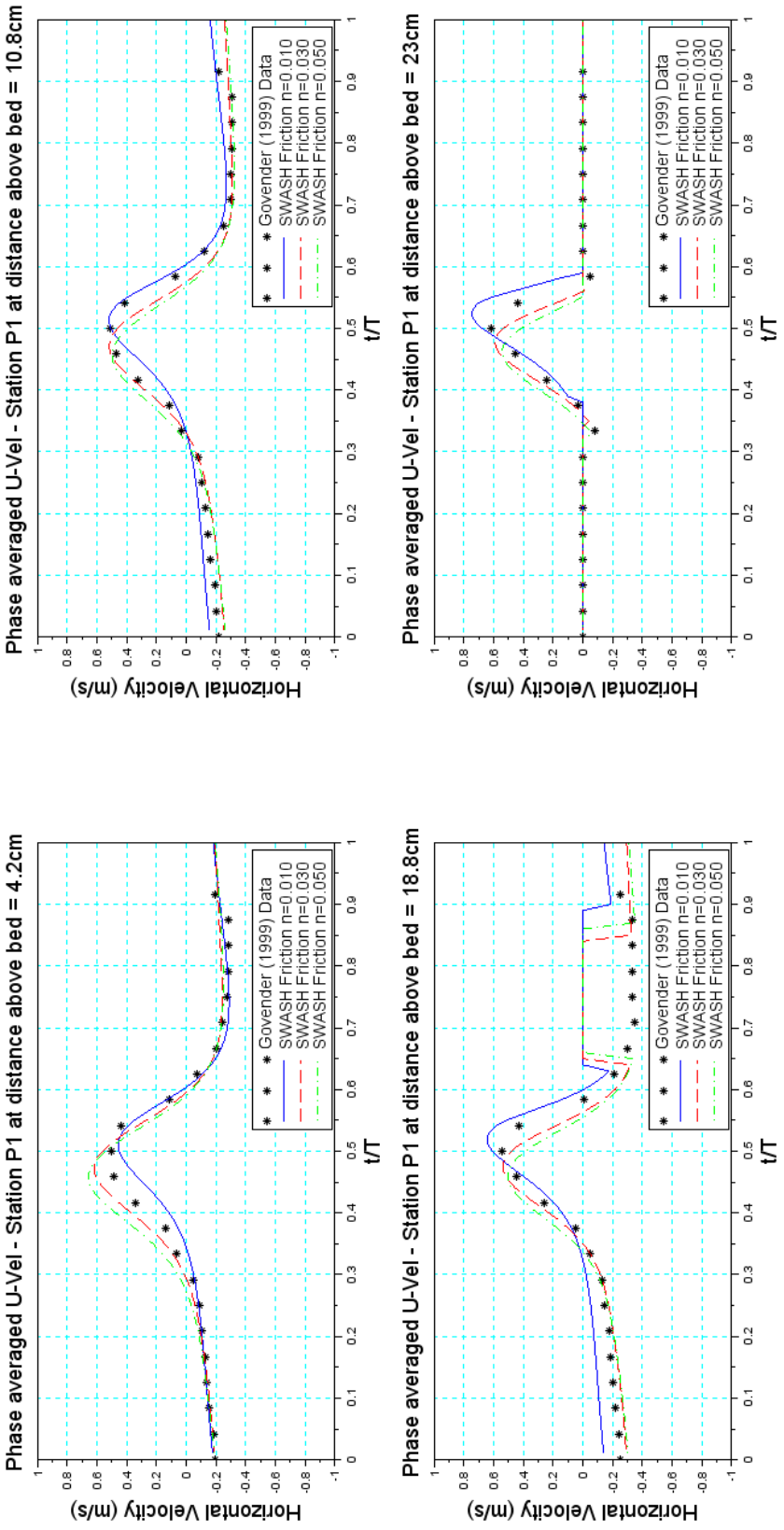

Figure A.7: Phase averaged horizontal velocity in the recorded Govender (1999) and SWASH modelled time series for various Manning friction values at measuring Station P1 - Momentum conserved

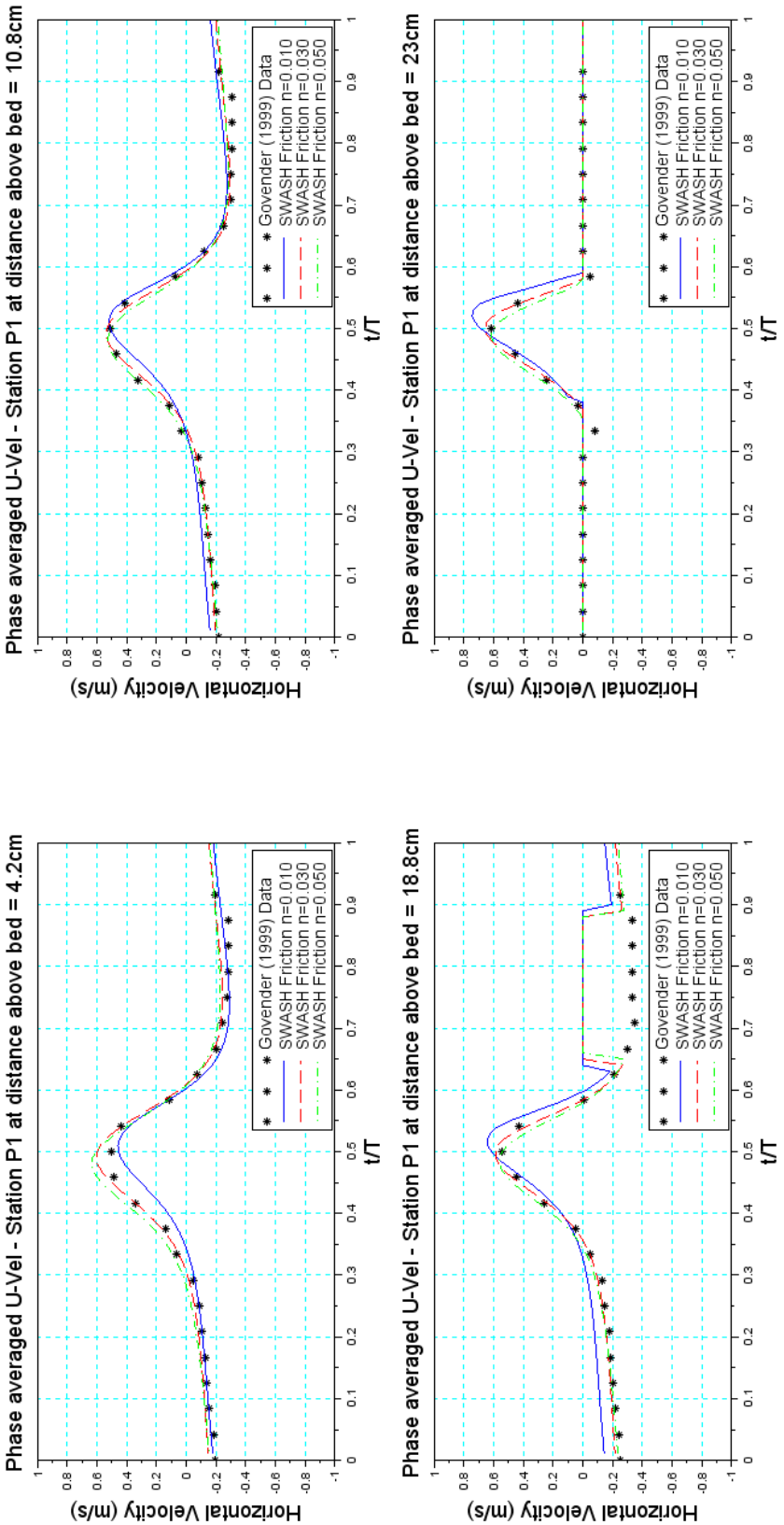

Figure A.8: Phase averaged horizontal velocity in the recorded Govender (1999) and SWASH modelled time series for various Manning friction values at measuring Station P1 - Momentum not explicitly conserved

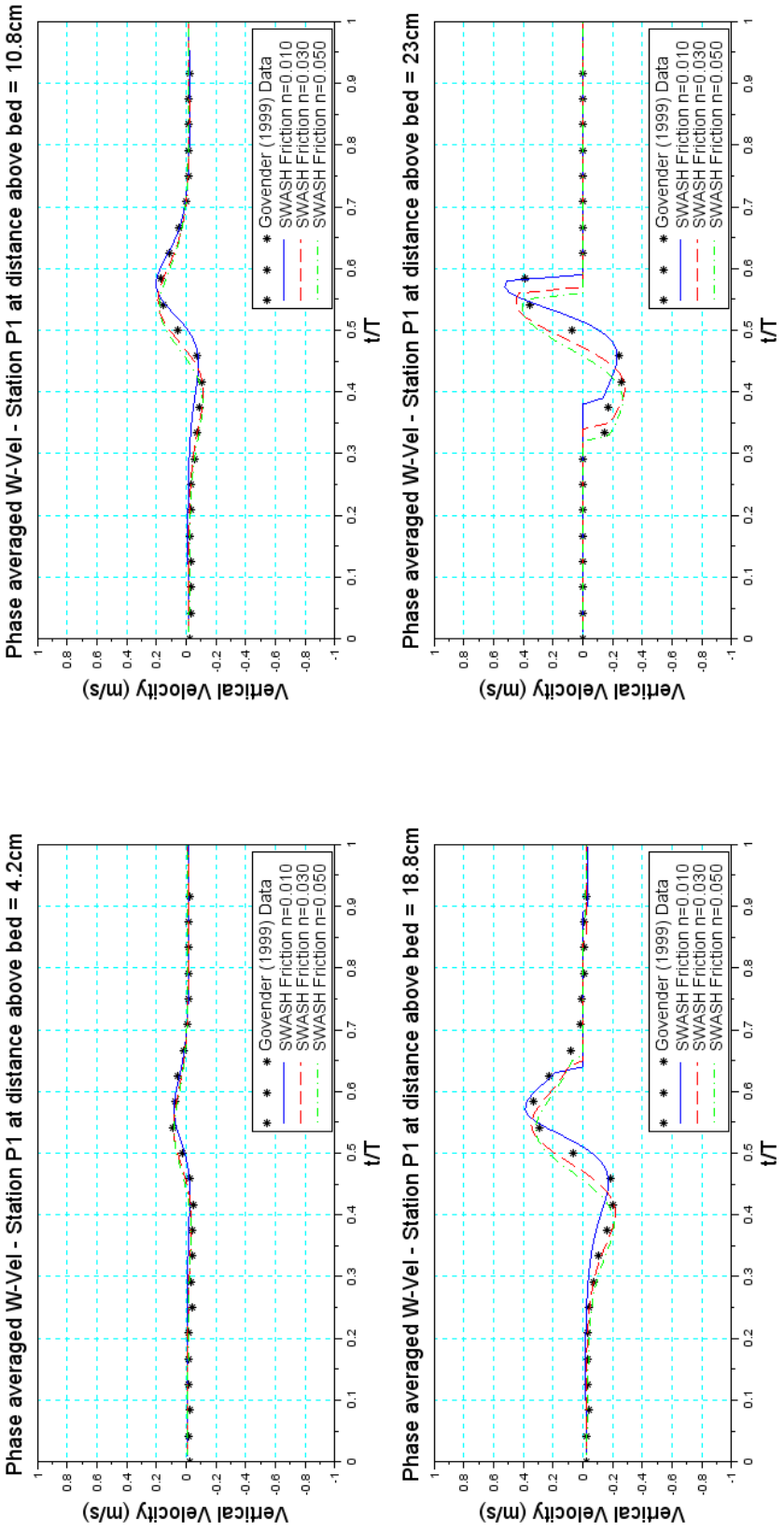

Figure A.9: Phase averaged vertical velocity in the recorded Govender (1999) and SWASH modelled time series for various Manning friction values at measuring Station P1 - Momentum conserved

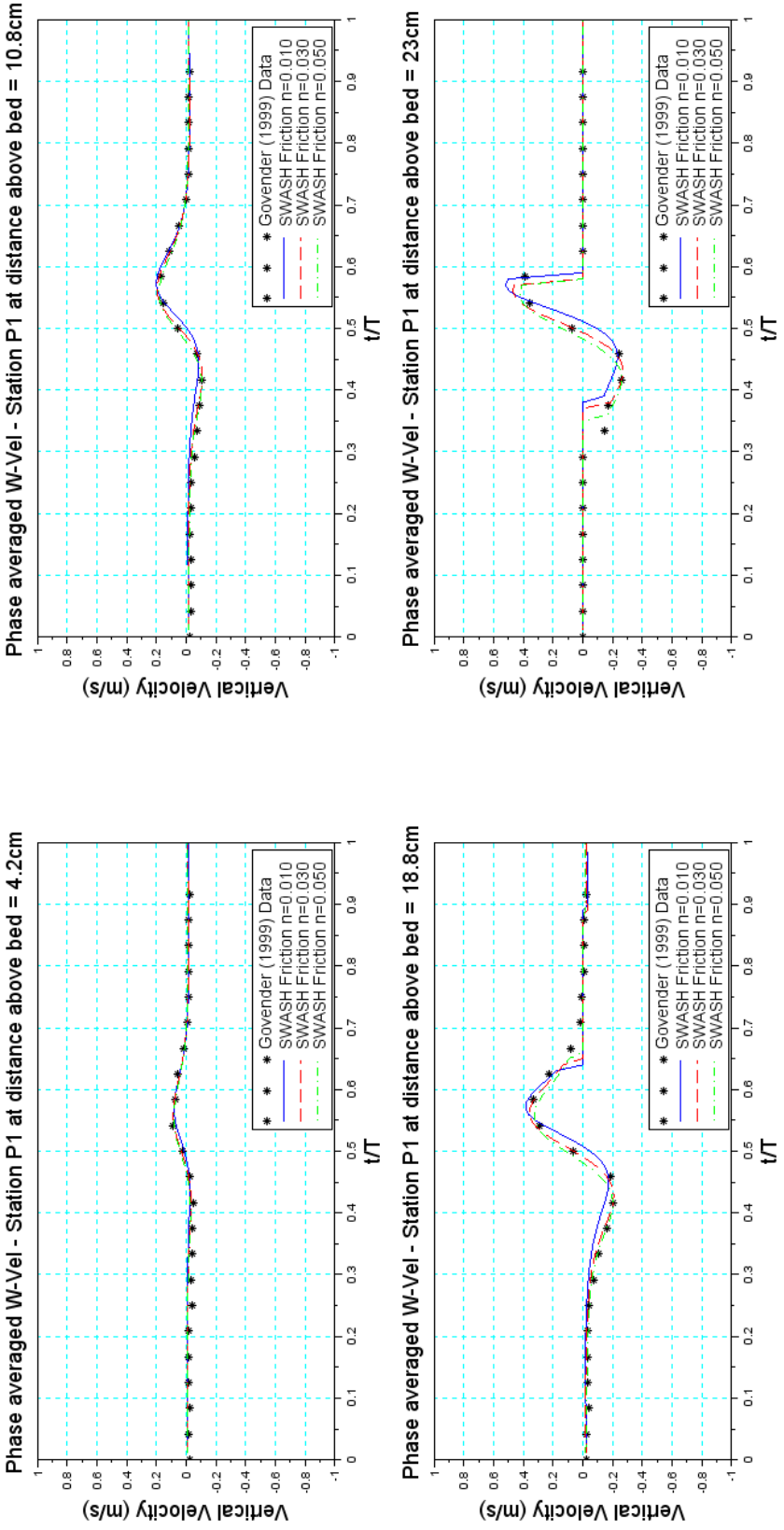

Figure A.10: Phase averaged vertical velocity in the recorded Govender (1999) and SWASH modelled time series for various Manning friction values at measuring Station P1 - Momentum not explicitly conserved

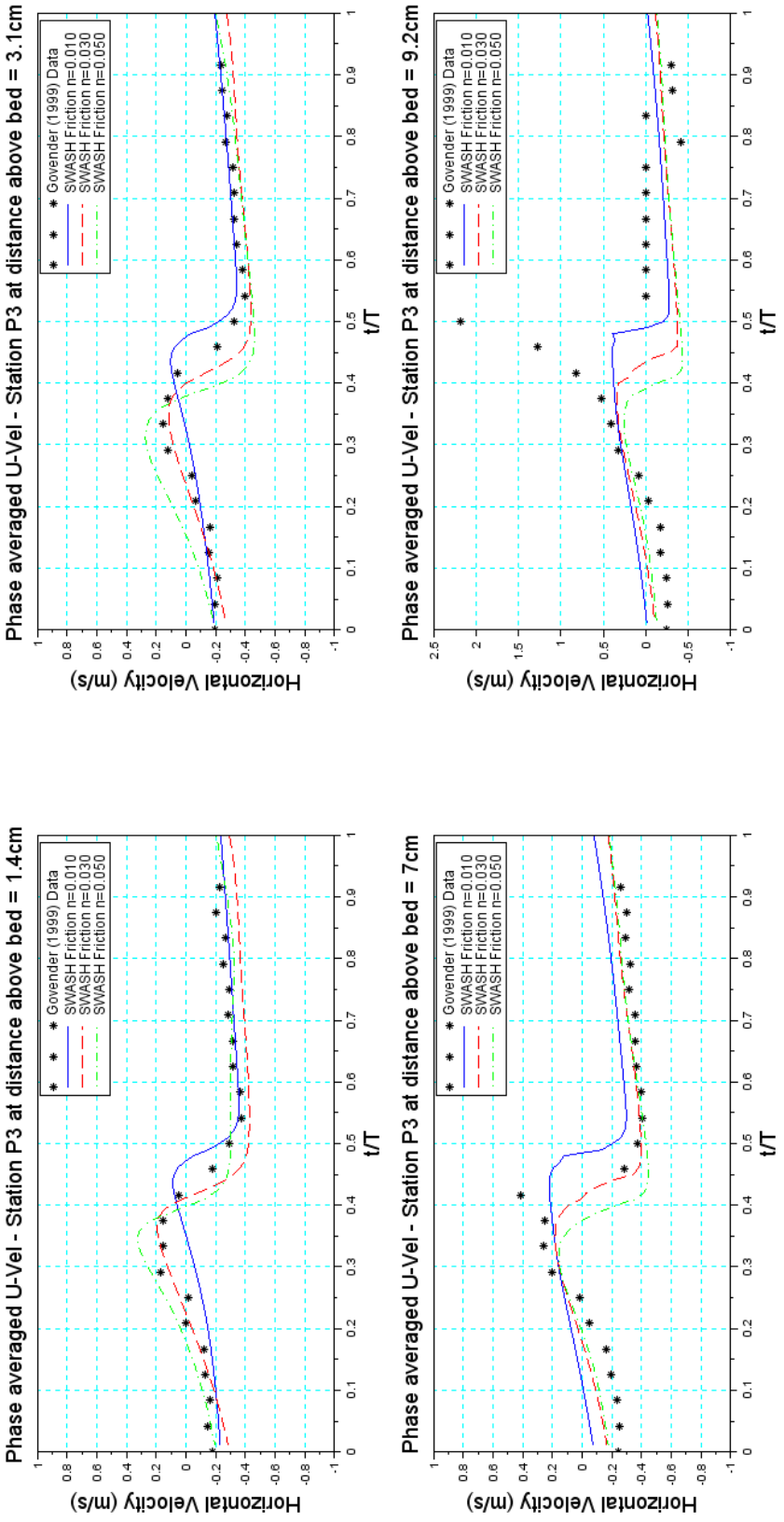

Figure A.11: Phase averaged horizontal velocity in the recorded Govender (1999) and SWASH modelled time series for various Manning friction values at measuring Station P3 - Momentum conserved

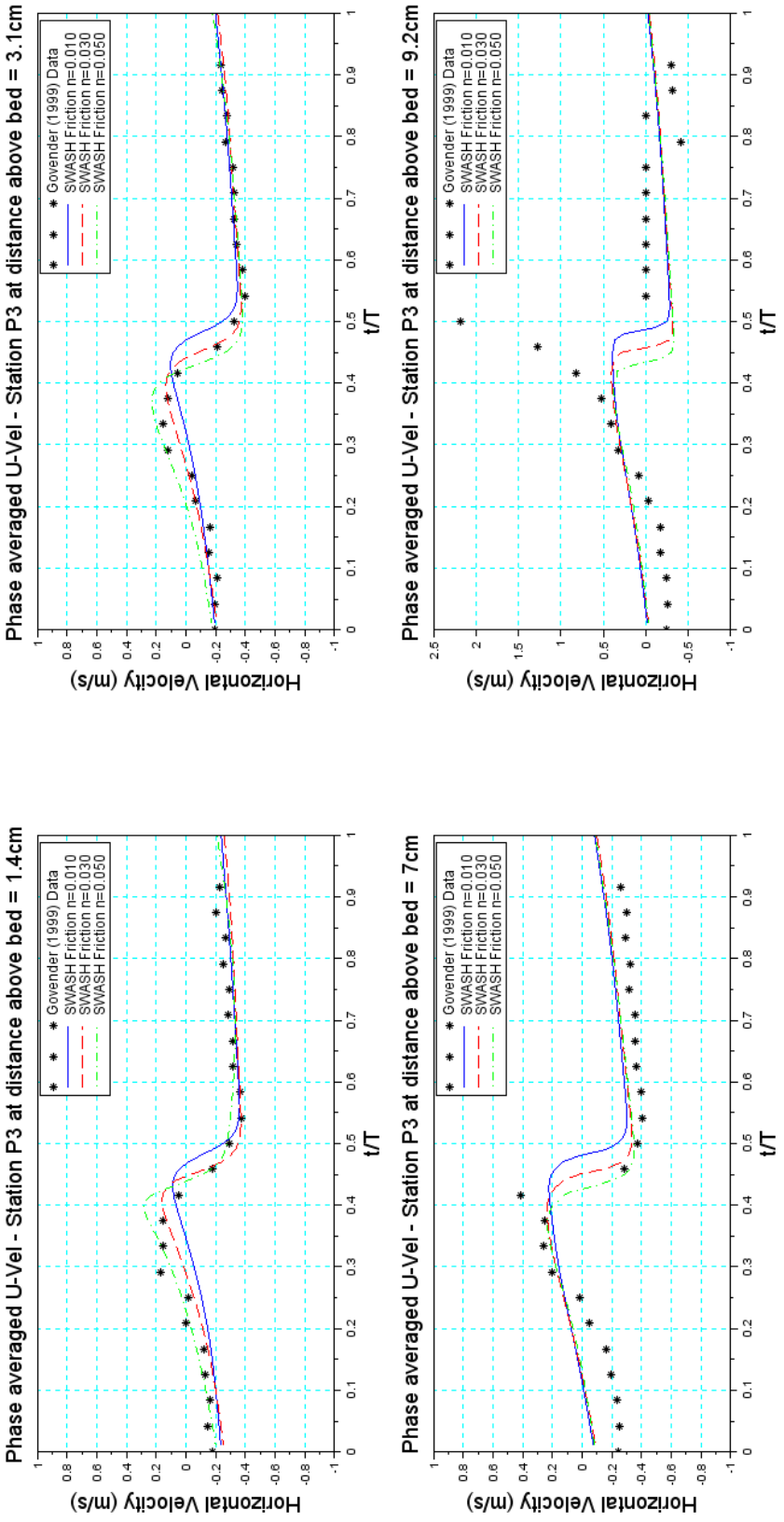

Figure A.12: Phase averaged horizontal velocity in the recorded Govender (1999) and SWASH modelled time series for various Manning friction values at measuring Station P3 - Momentum not explicitly conserved

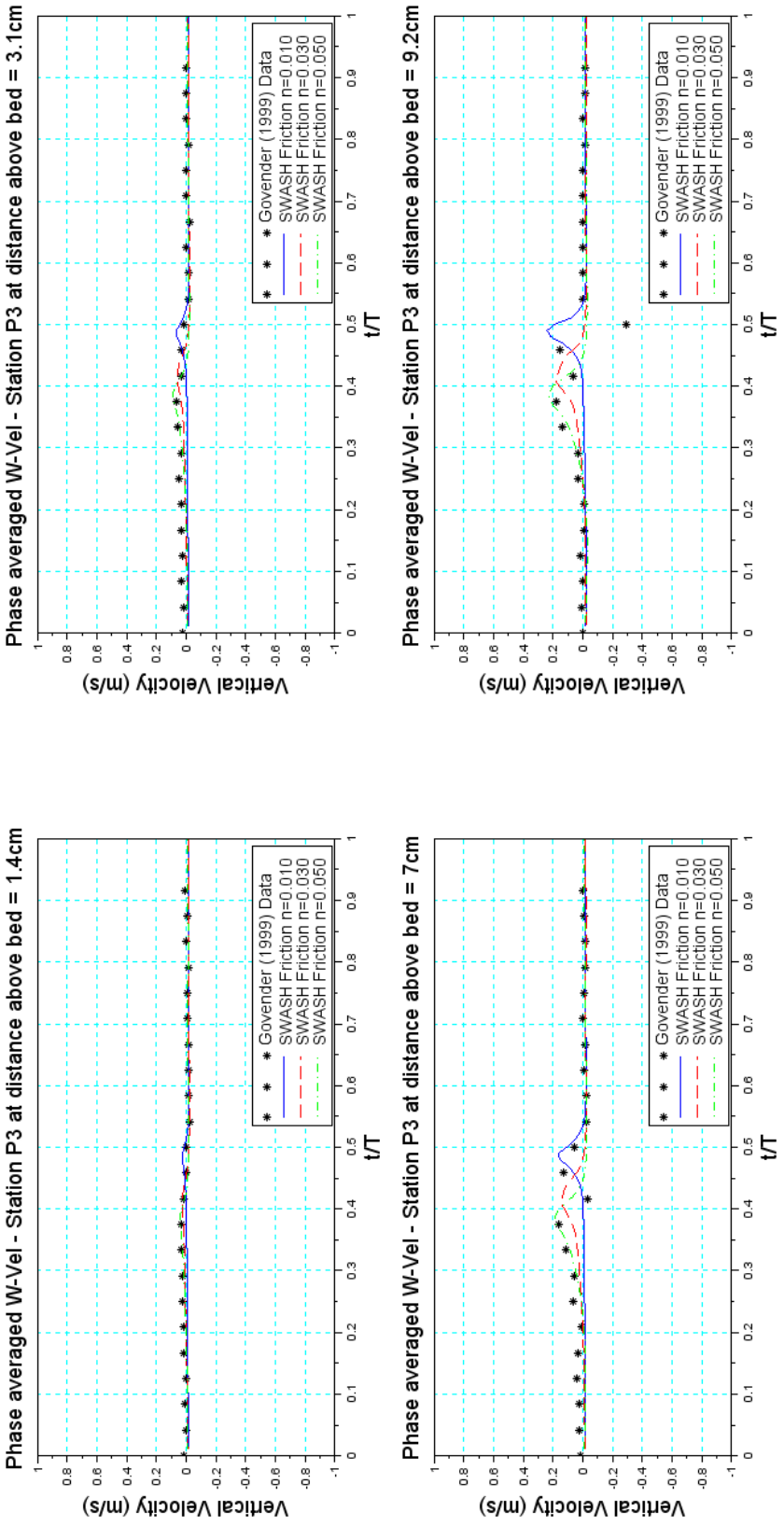

Figure A.13: Phase averaged vertical velocity in the recorded Govender (1999) and SWASH modelled time series for various Manning friction values at measuring Station P3 - Momentum conserved

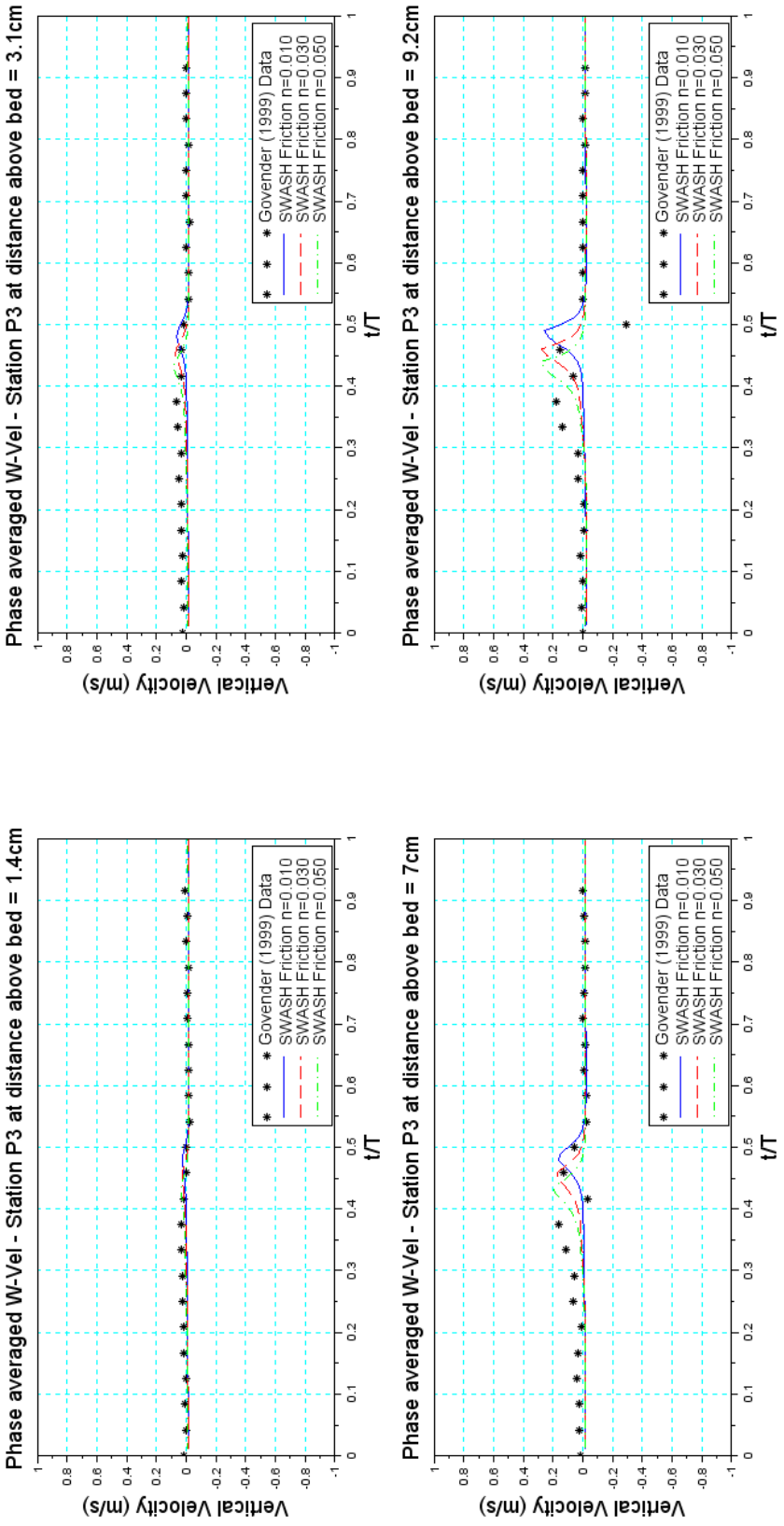

Figure A.14: Phase averaged vertical velocity in the recorded Govender (1999) and SWASH modelled time series for various Manning friction values at measuring Station P3 - Momentum not explicitly conserved

A.1.3 Horizontal and vertical advection terms of the momentum equation

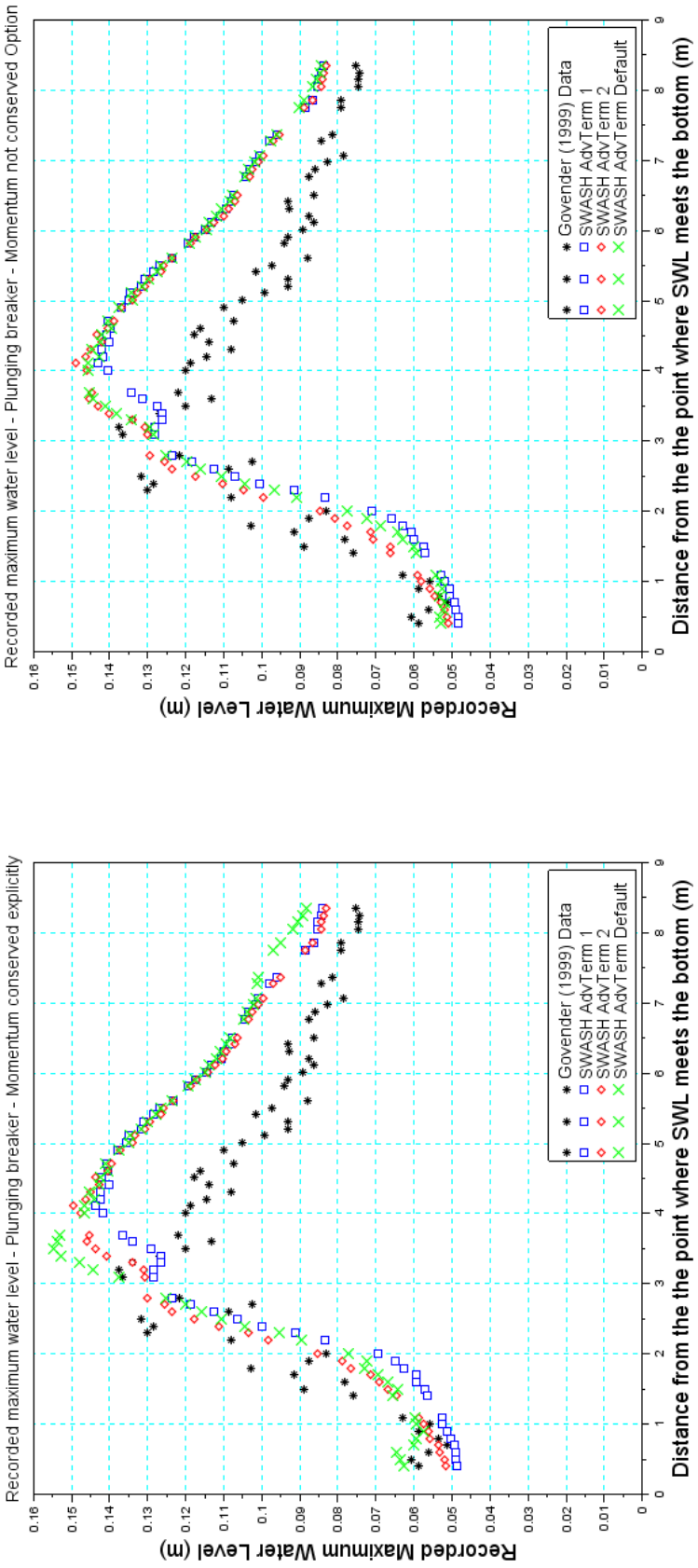

Figure A.15: Maximum wave heights in the recorded Govender (1999) and SWASH modelled time series for various advection term discretisation schemes measured in points cross-shore of the flume. Left panel shows wave heights with momentum conserved while the right panel shows wave heights without momentum conserved explicitly.

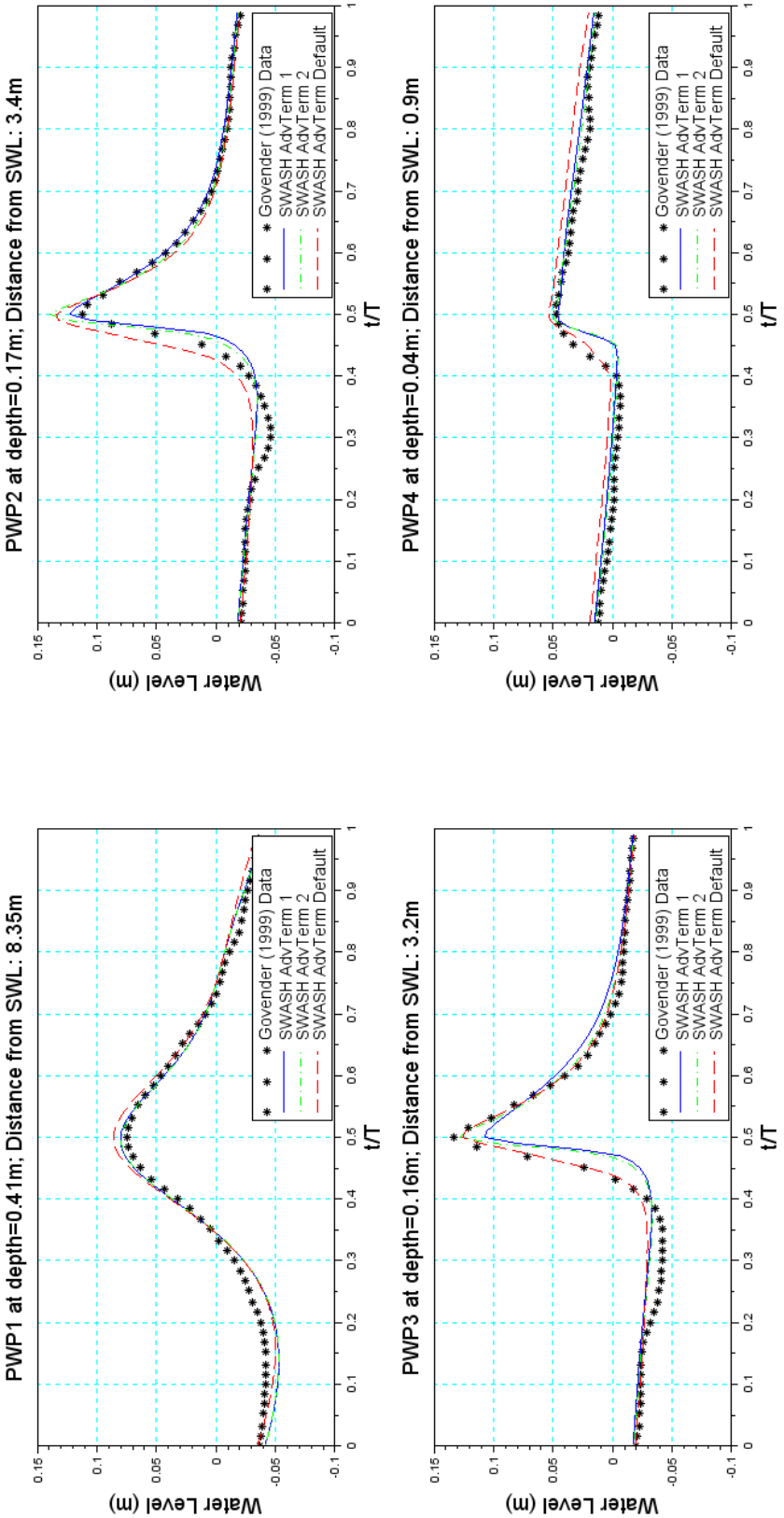

Figure A.16: Phase averaged wave heights in the recorded Govender (1999) and SWASH modelled time series for various discretisation schemes at four measuring points in the flume - Momentum conserved

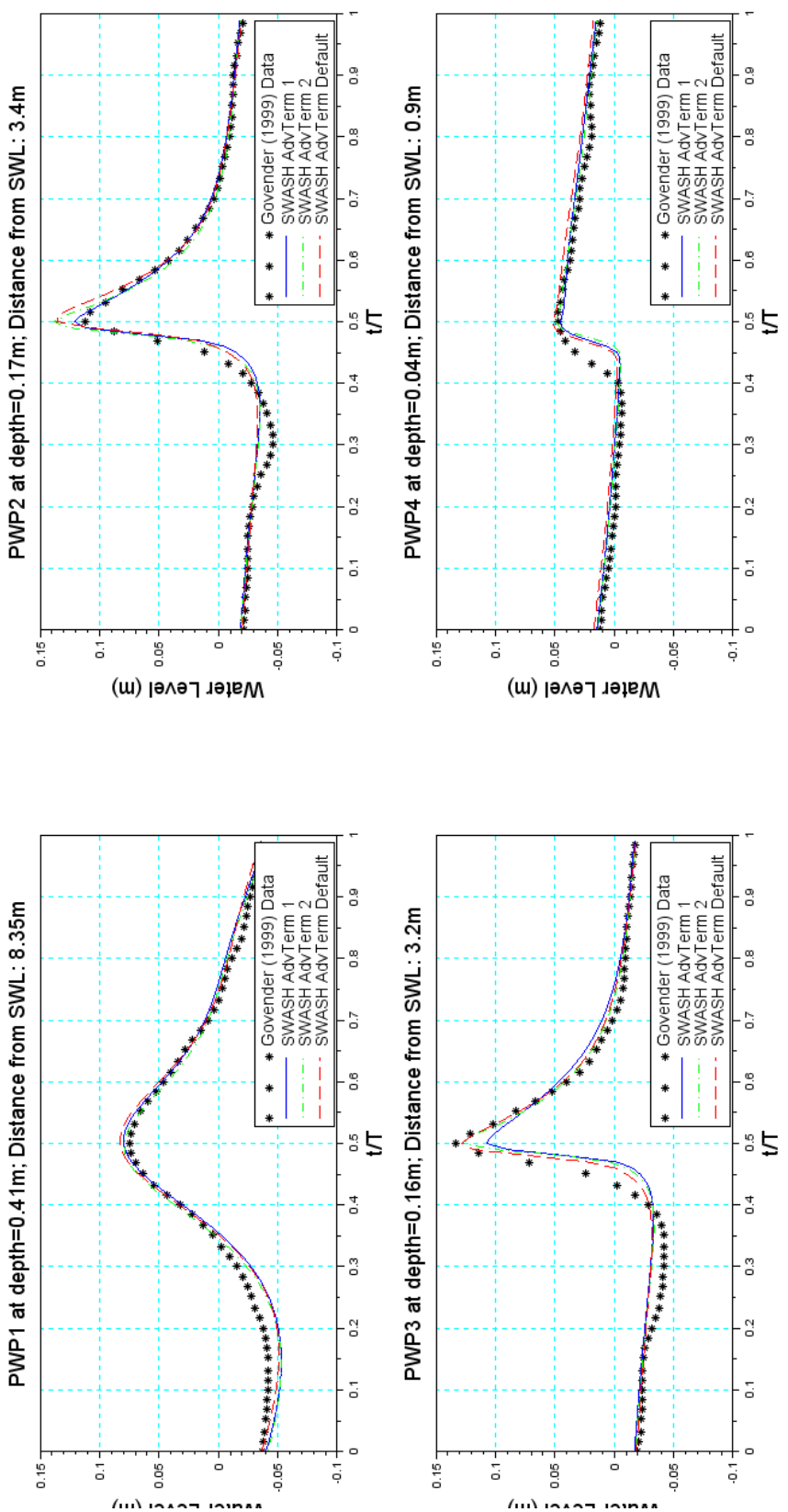

Figure A.17: Phase averaged wave heights in the recorded Govender (1999) and SWASH modelled time series for various discretisation schemes at four measuring points in the flume - Momentum not explicitly conserved

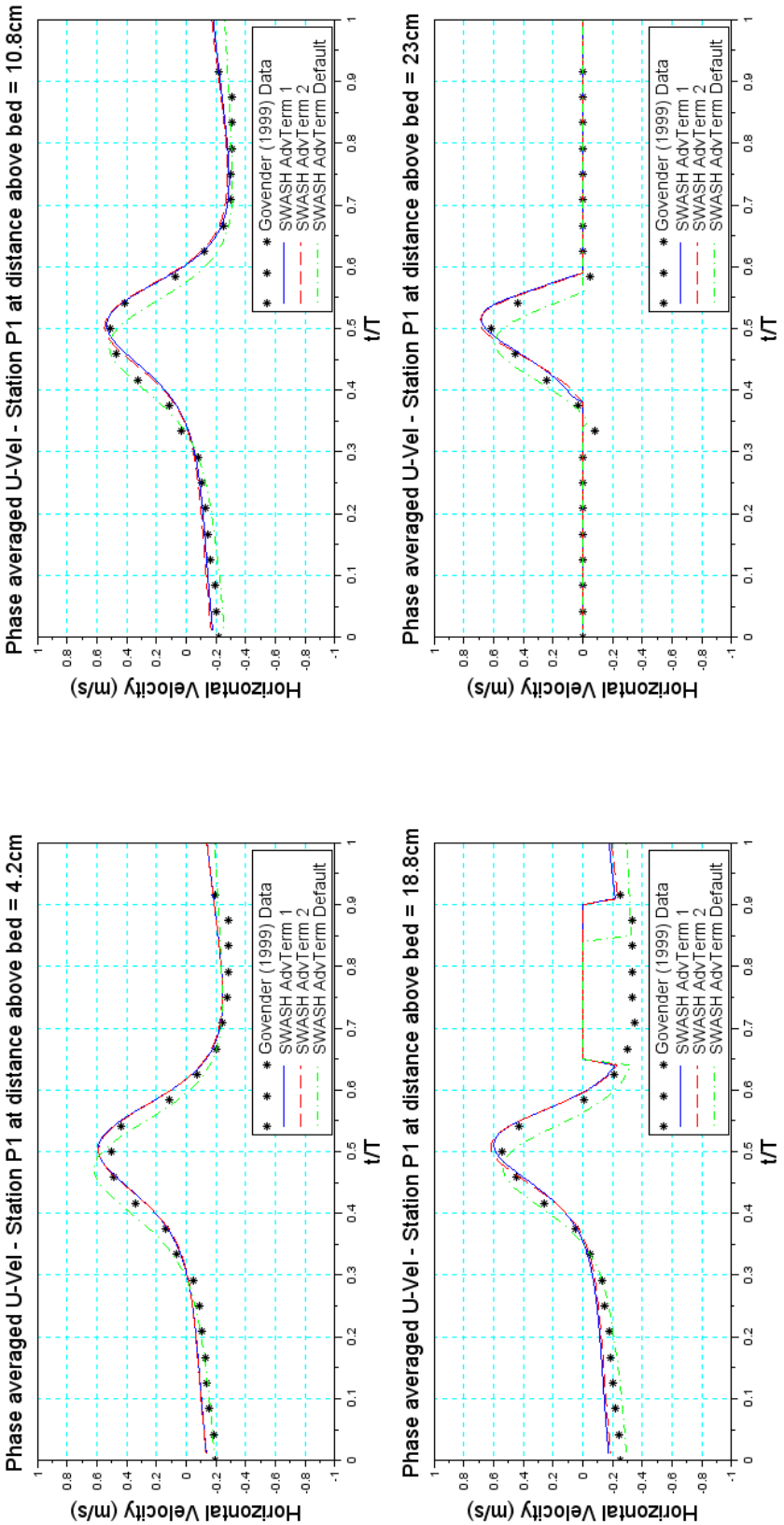

Figure A.18: Phase averaged horizontal velocity in the recorded Govender (1999) and SWASH modelled time series for various discretisation schemes at measuring Station P1 - Momentum conserved

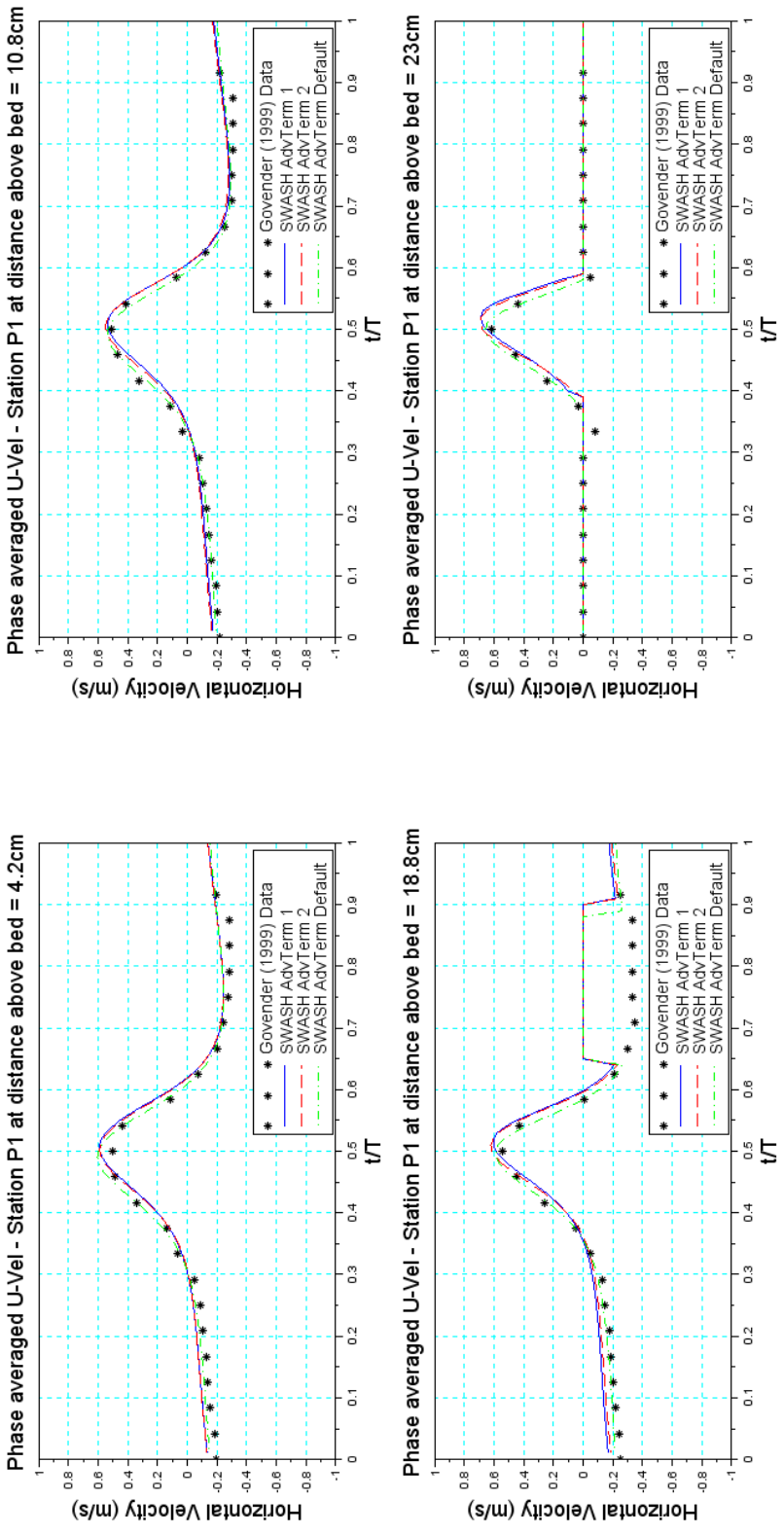

Figure A.19: Phase averaged horizontal velocity in the recorded Govender (1999) and SWASH modelled time series for various discretisation schemes at measuring Station P1 - Momentum not explicitly conserved

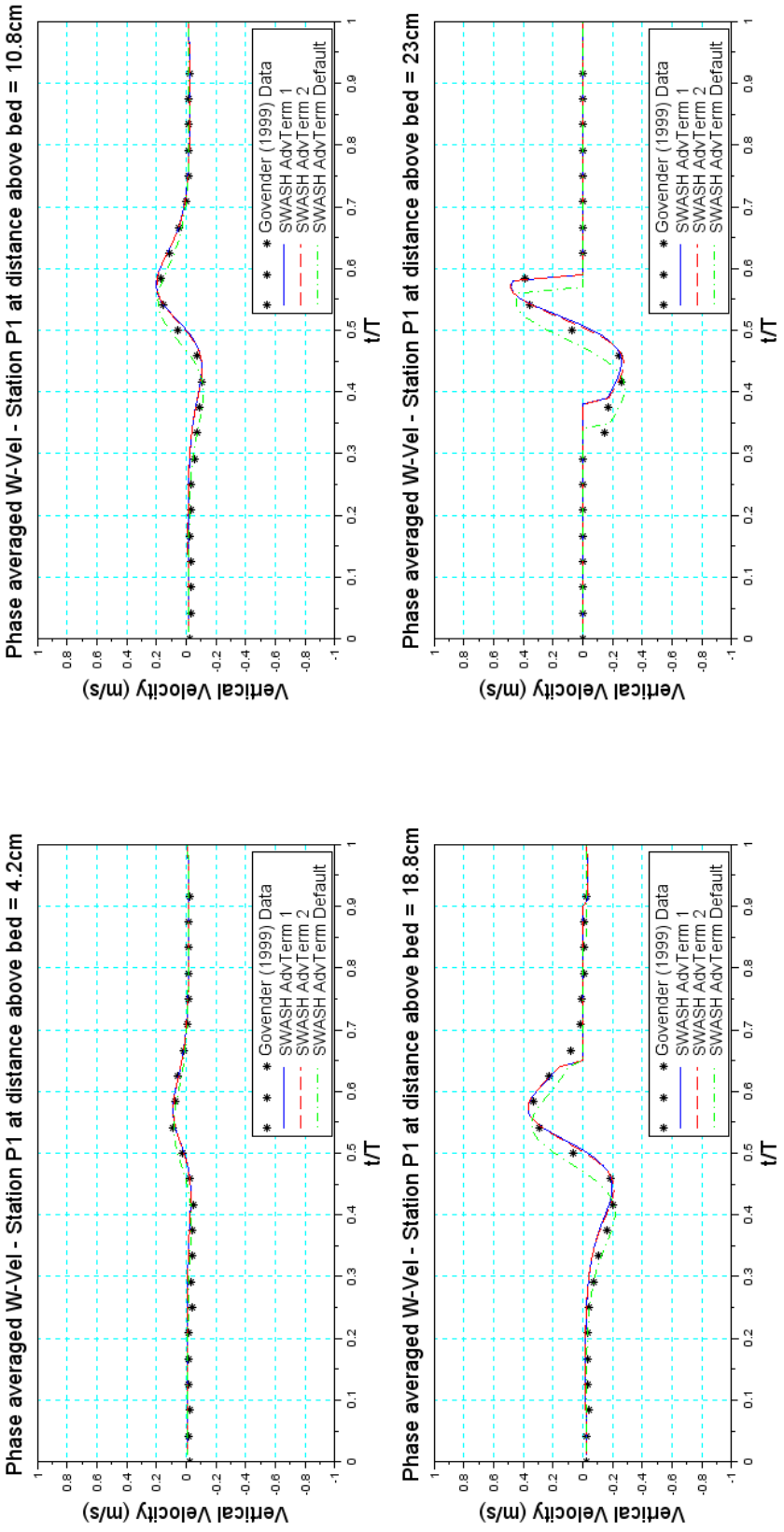

Figure A.20: Phase averaged vertical velocity in the recorded Govender (1999) and SWASH modelled time series for various discretisation schemes at measuring Station P1 - Momentum conserved

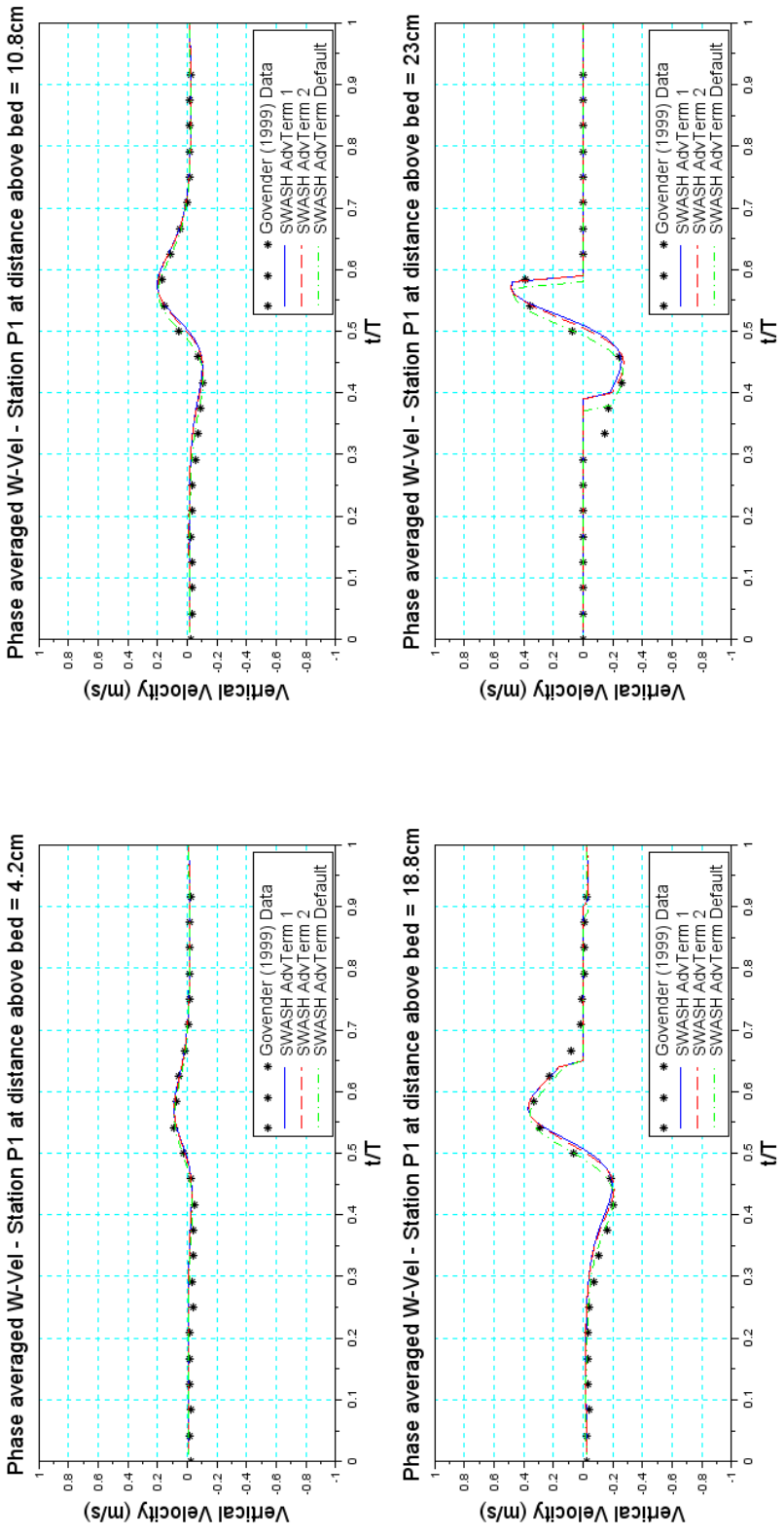

Figure A.21: Phase averaged vertical velocity in the recorded Govender (1999) and SWASH modelled time series for various discretisation schemes at measuring Station P1 - Momentum not explicitly conserved

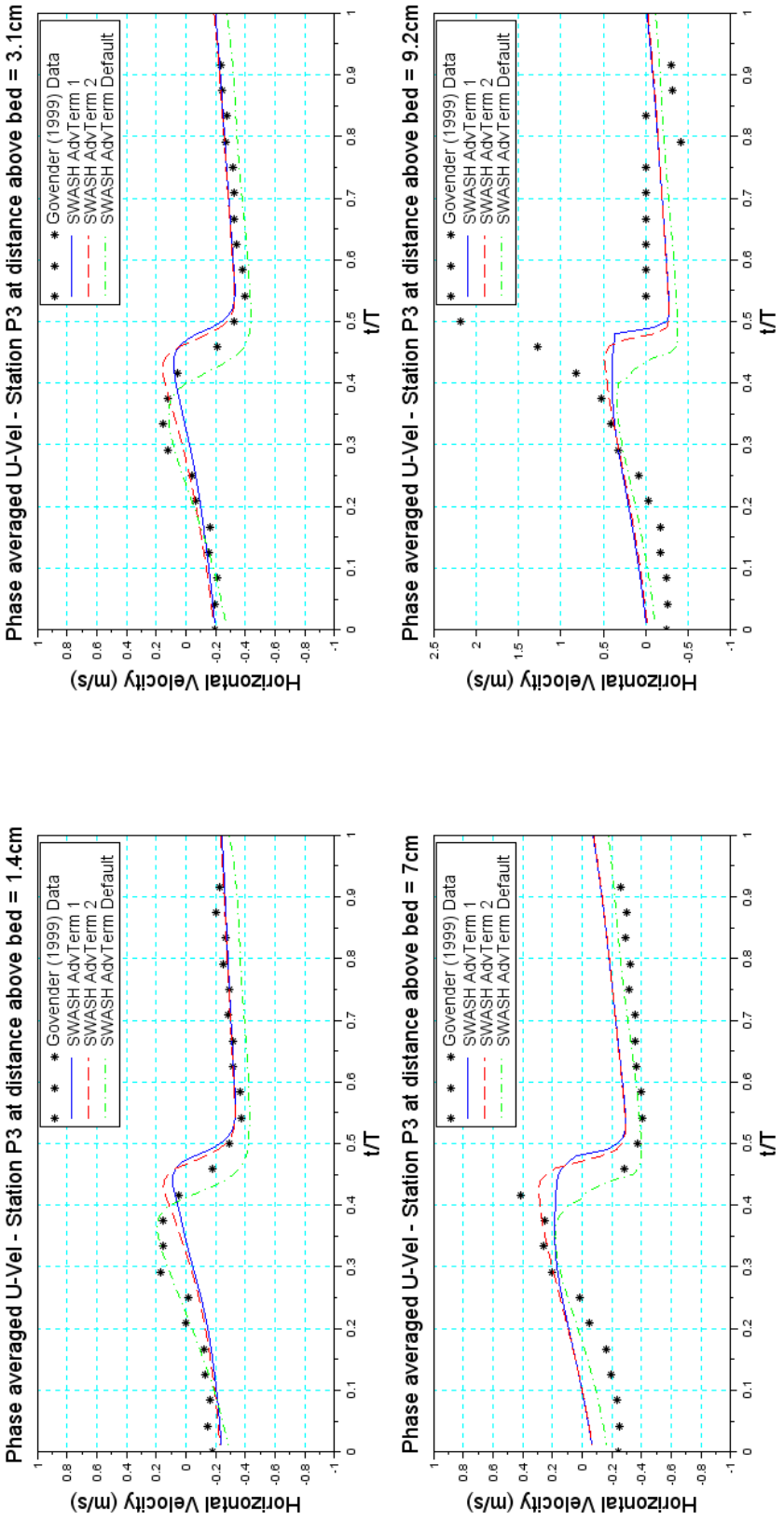

Figure A.22: Phase averaged horizontal velocity in the recorded Govender (1999) and SWASH modelled time series for various discretisation schemes at measuring Station P3 - Momentum conserved

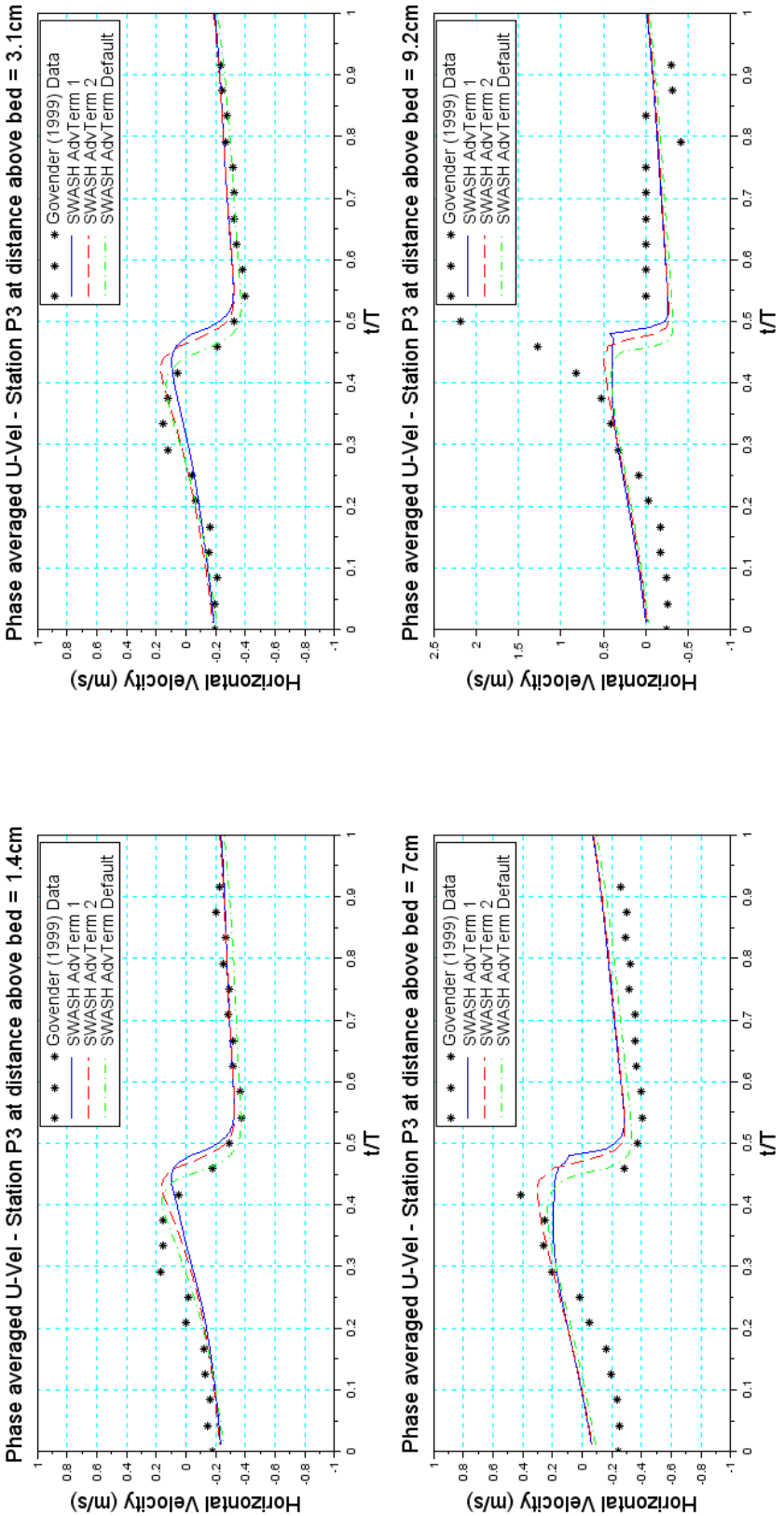

Figure A.23: Phase averaged horizontal velocity in the recorded Govender (1999) and SWASH modelled time series for various discretisation schemes at measuring Station P3 - Momentum not explicitly conserved

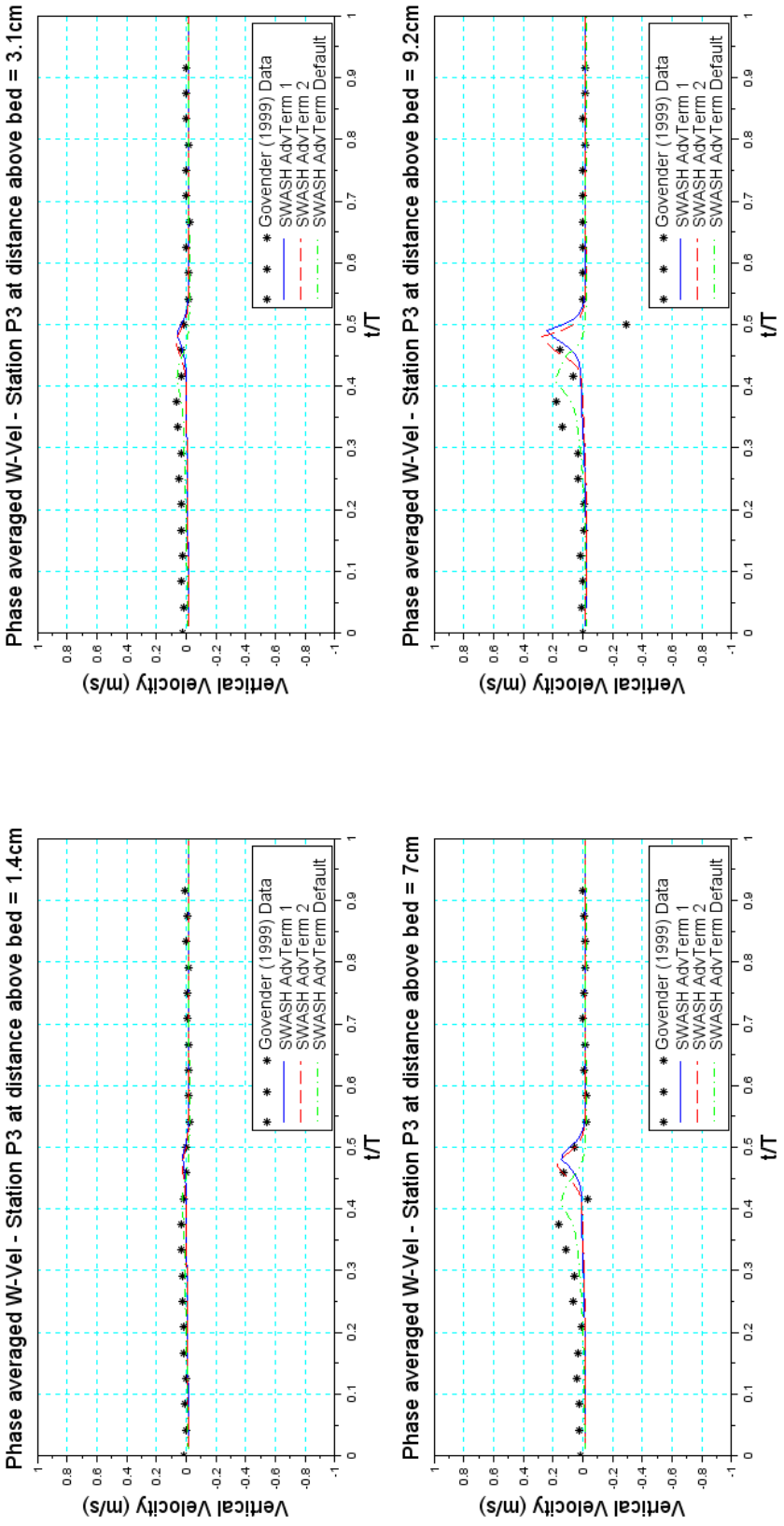

Figure A.24: Phase averaged vertical velocity in the recorded Govender (1999) and SWASH modelled time series for various discretisation schemes at measuring Station P3 - Momentum conserved

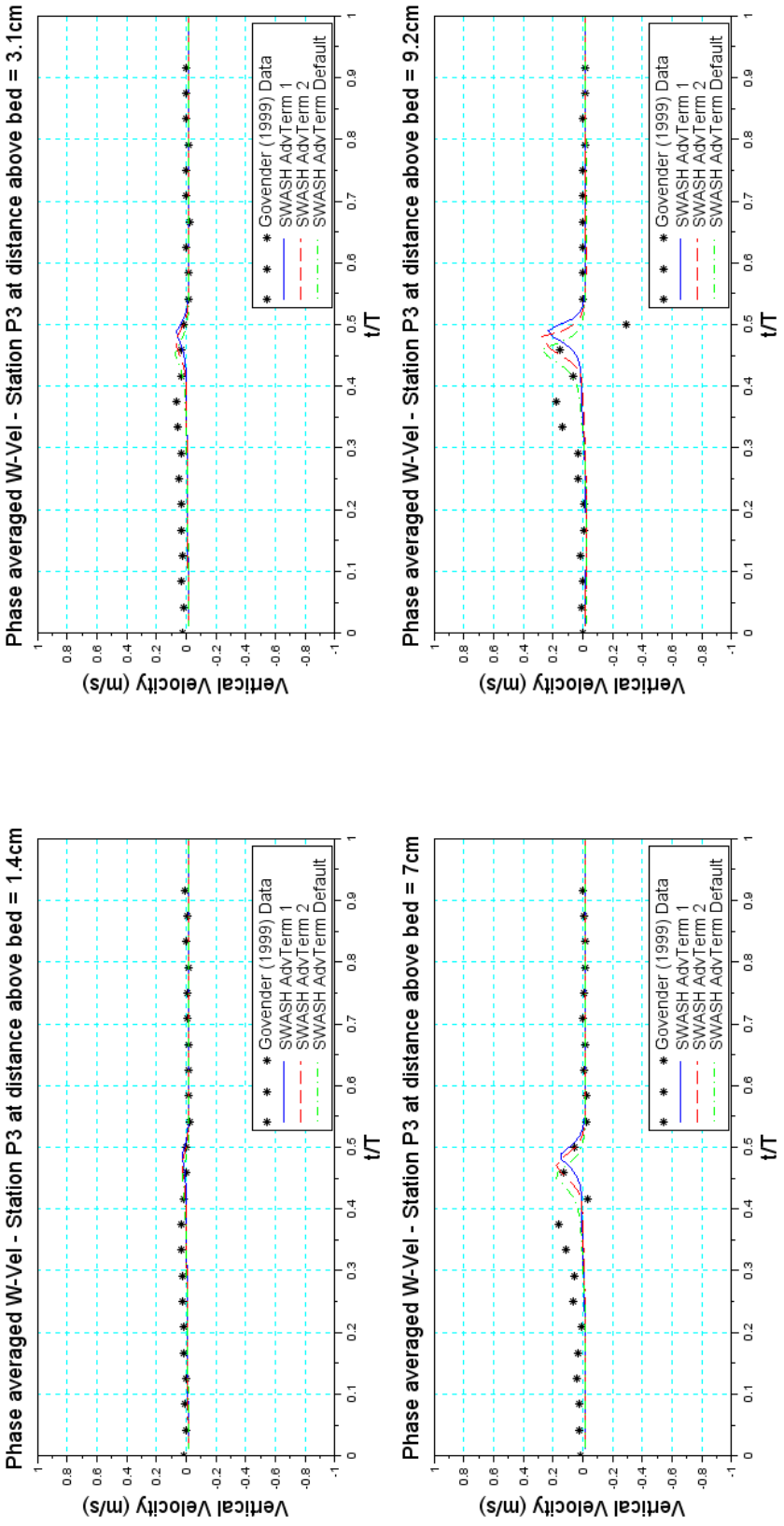

Figure A.25: Phase averaged vertical velocity in the recorded Govender (1999) and SWASH modelled time series for various discretisation schemes at measuring Station P3 - Momentum not explicitly conserved

A.1.4 Water depth in velocity points

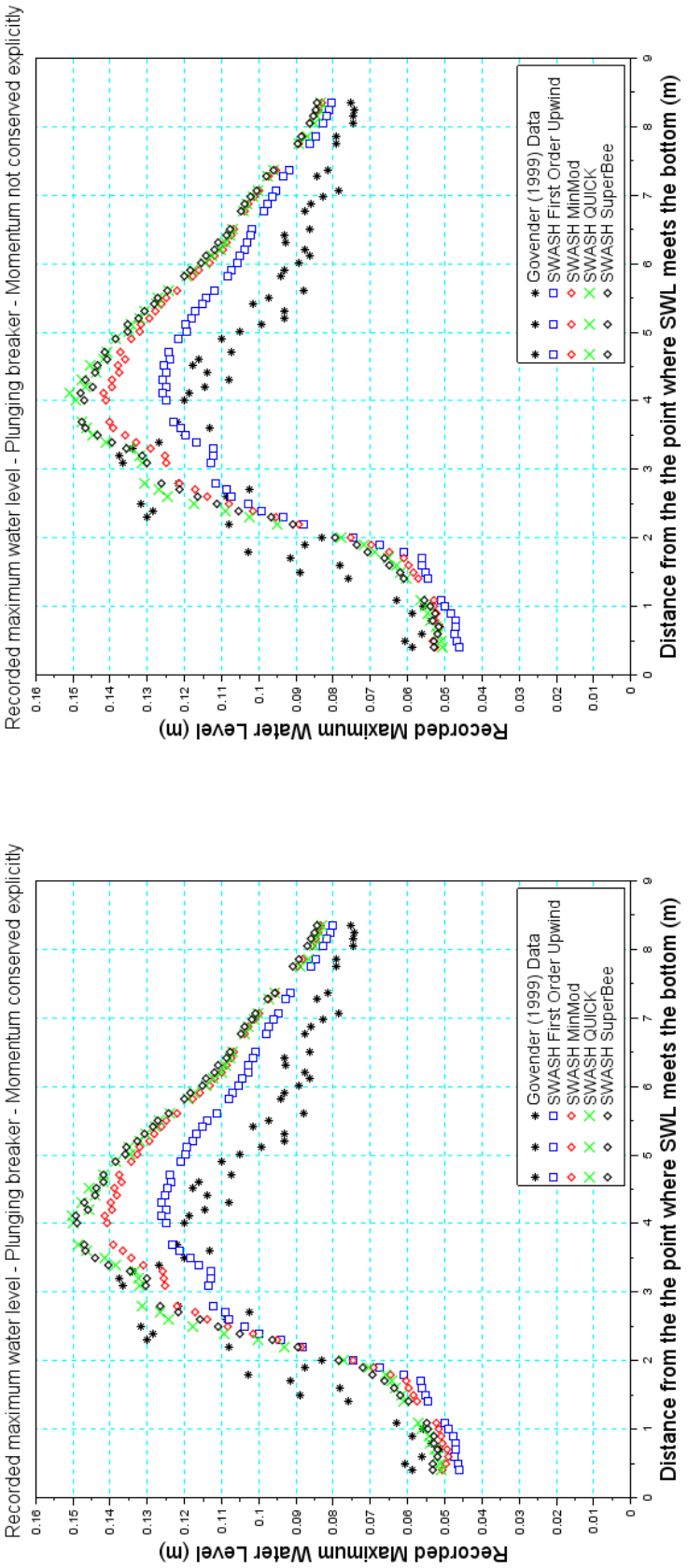

Figure A.26: Maximum wave heights in the recorded Govender (1999) and SWASH modelled time series for various higher order interpolation schemes measured in points cross-shore of the flume. Left panel shows wave heights with momentum conserved while the right panel shows wave heights without momentum conserved explicitly.

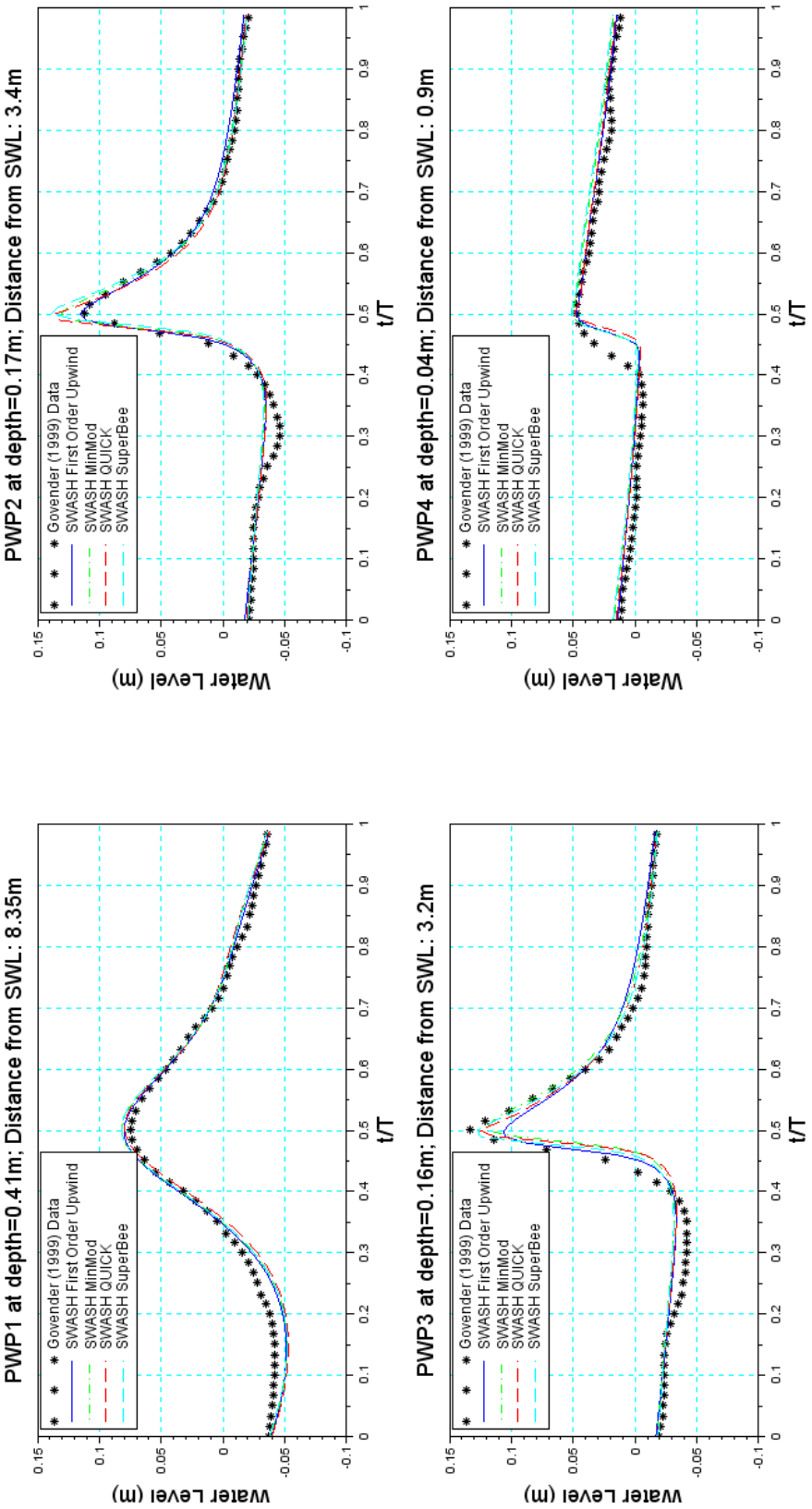

Figure A.27: Phase averaged wave heights in the recorded Govender (1999) and SWASH modelled time series for various higher order interpolation limiter schemes at four measuring points in the flume - Momentum conserved

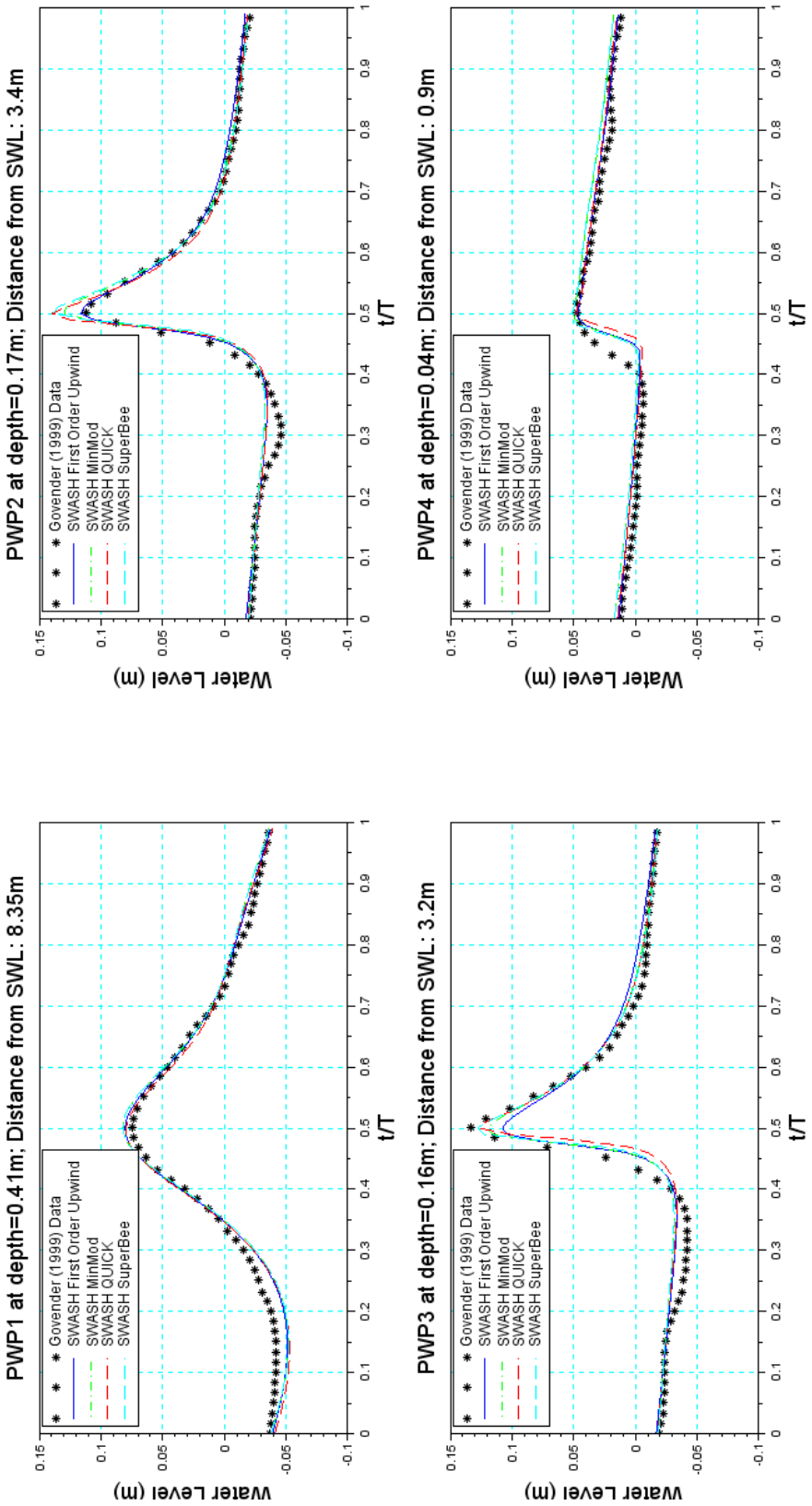

Figure A.28: Phase averaged wave heights in the recorded Govender (1999) and SWASH modelled time series for various higher order interpolation limiter schemes at four measuring points in the flume - Momentum not explicitly conserved

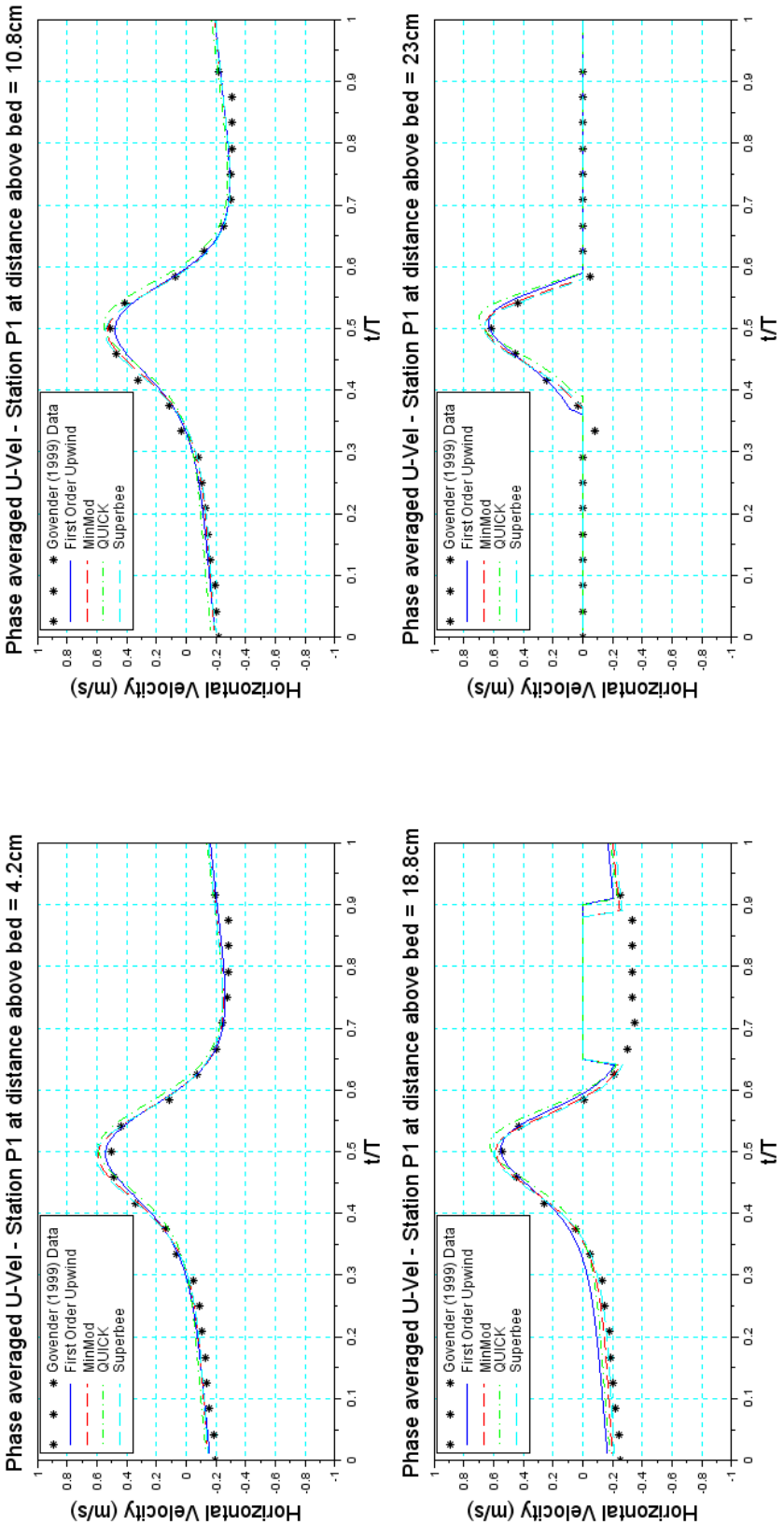

Figure A.29: Phase averaged horizontal velocity in the recorded Govender (1999) and SWASH modelled time series for various higher order interpolation limiter schemes at measuring Station P1 - Momentum conserved

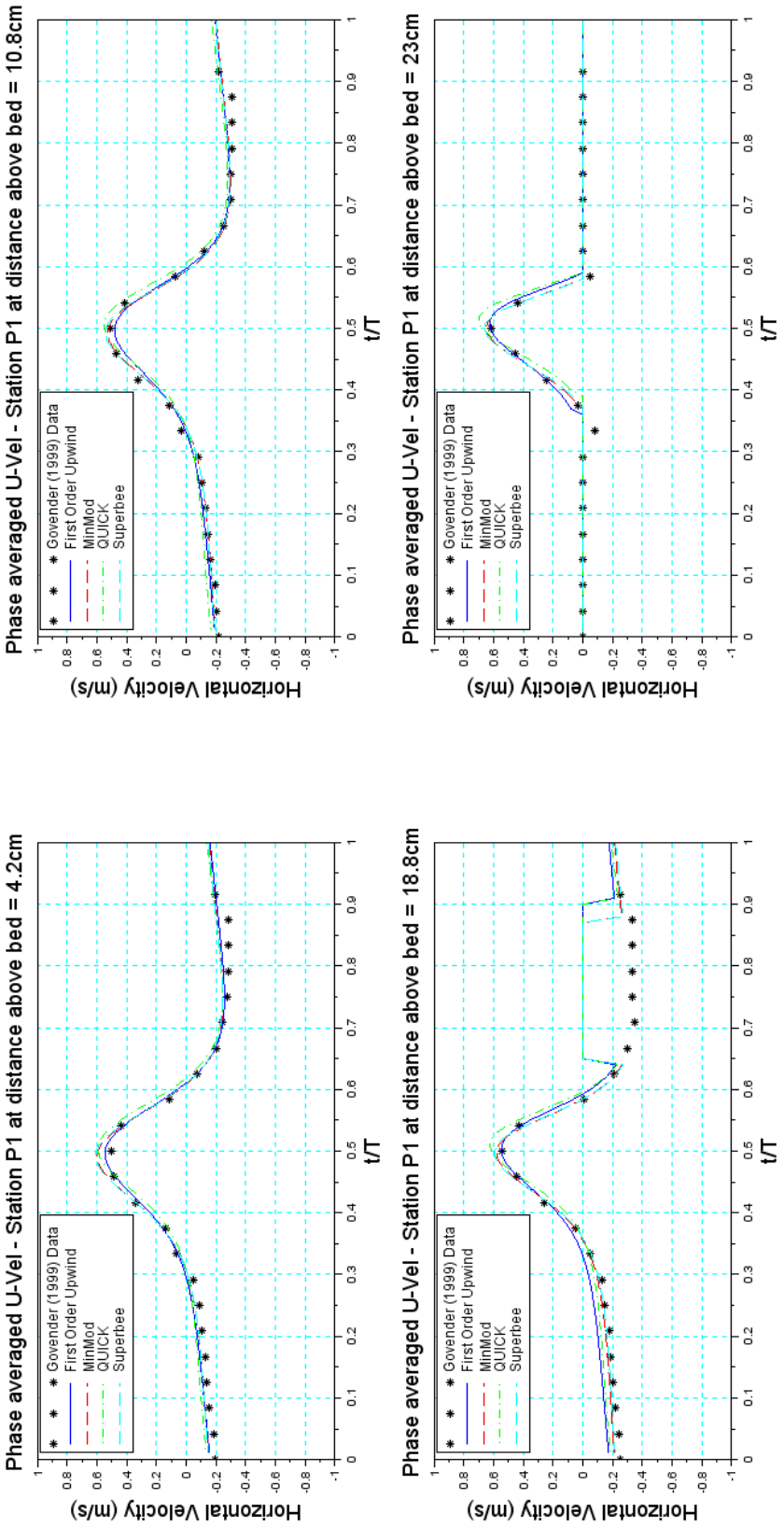

Figure A.30: Phase averaged horizontal velocity in the recorded Govender (1999) and SWASH modelled time series for various higher order interpolation limiter schemes at measuring Station P1 - Momentum not explicitly conserved

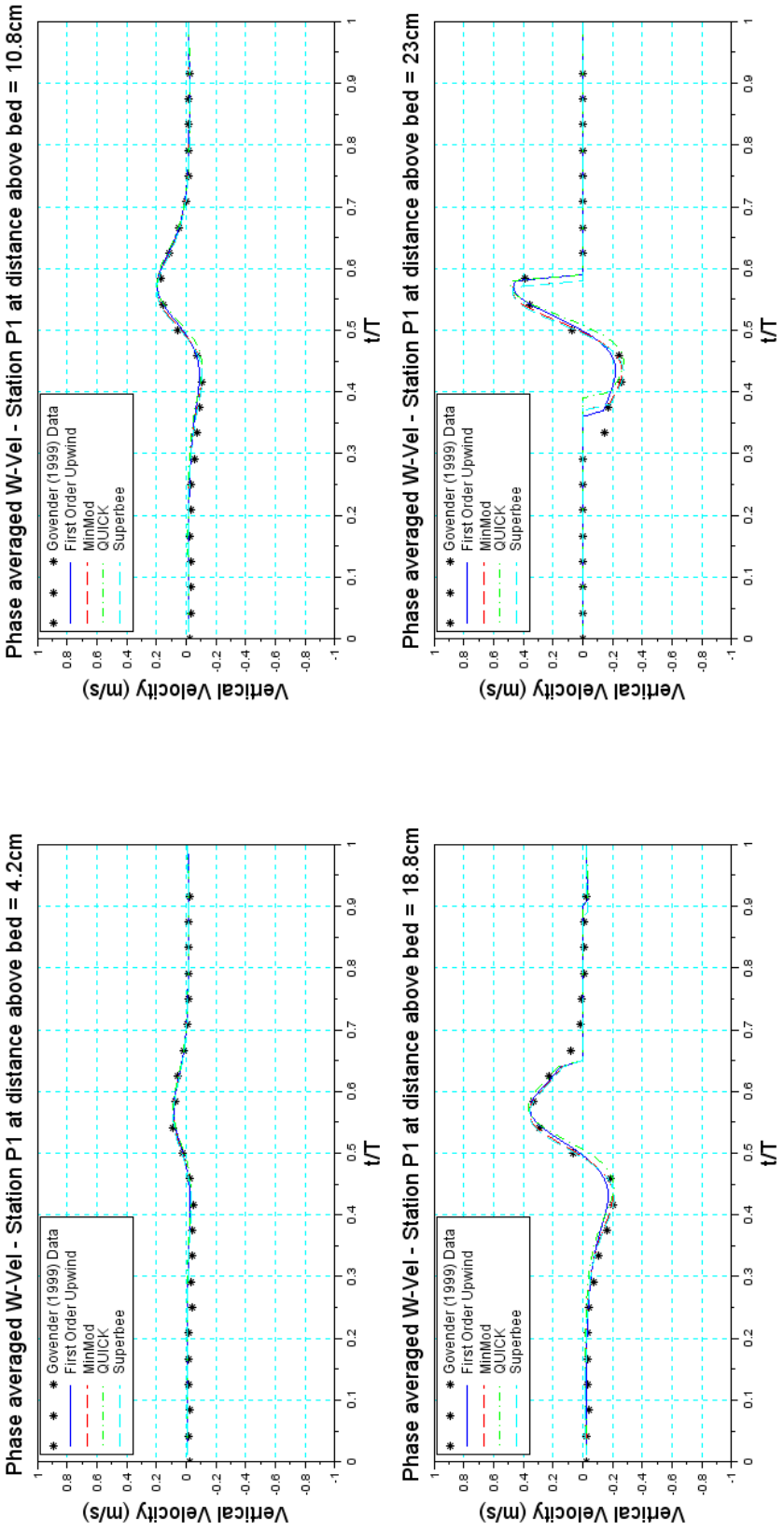

Figure A.31: Phase averaged vertical velocity in the recorded Govender (1999) and SWASH modelled time series for various higher order interpolation limiter schemes at measuring Station P1 - Momentum conserved

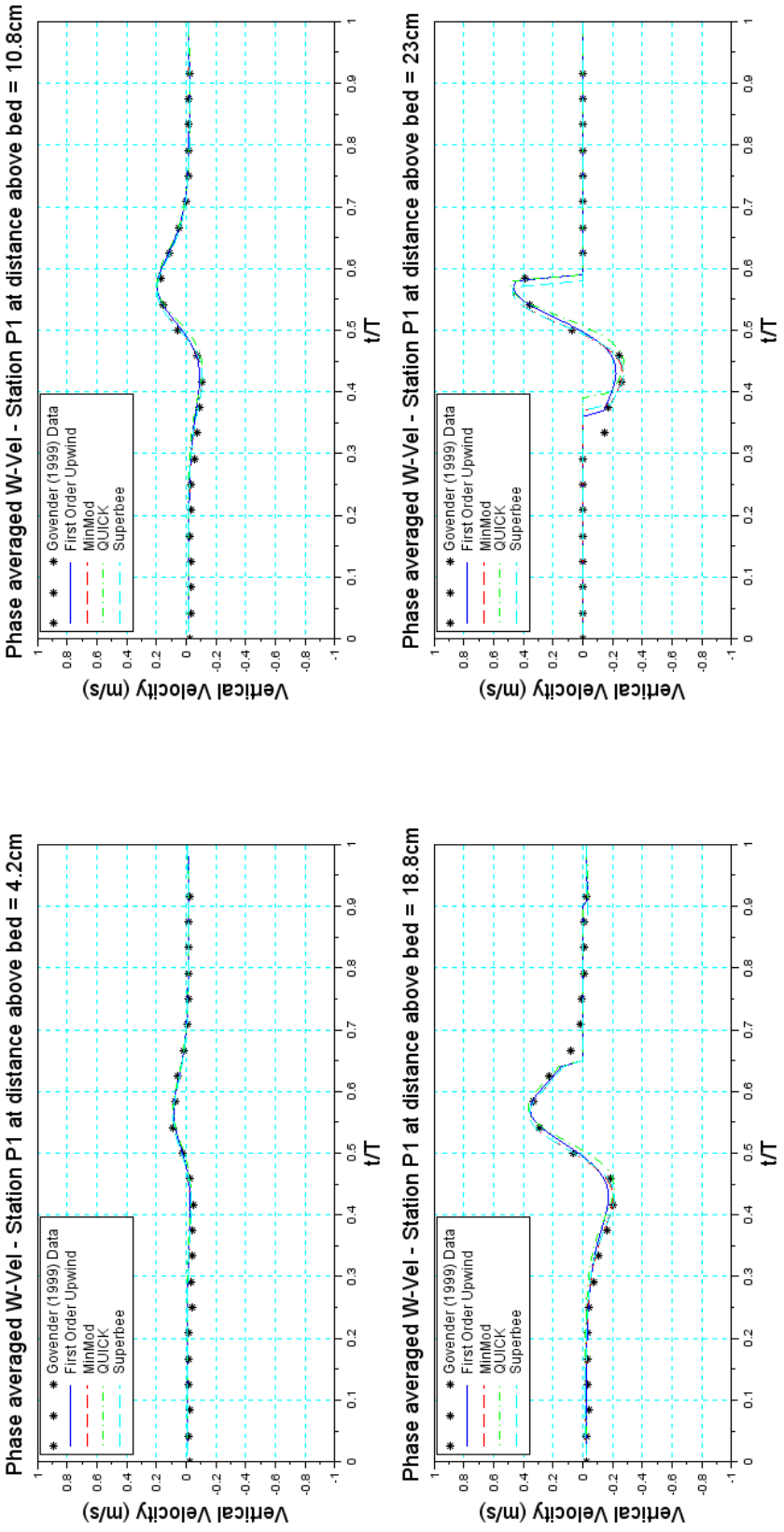

Figure A.32: Phase averaged vertical velocity in the recorded Govender (1999) and SWASH modelled time series for various higher order interpolation limiter schemes at measuring Station P1 - Momentum not explicitly conserved

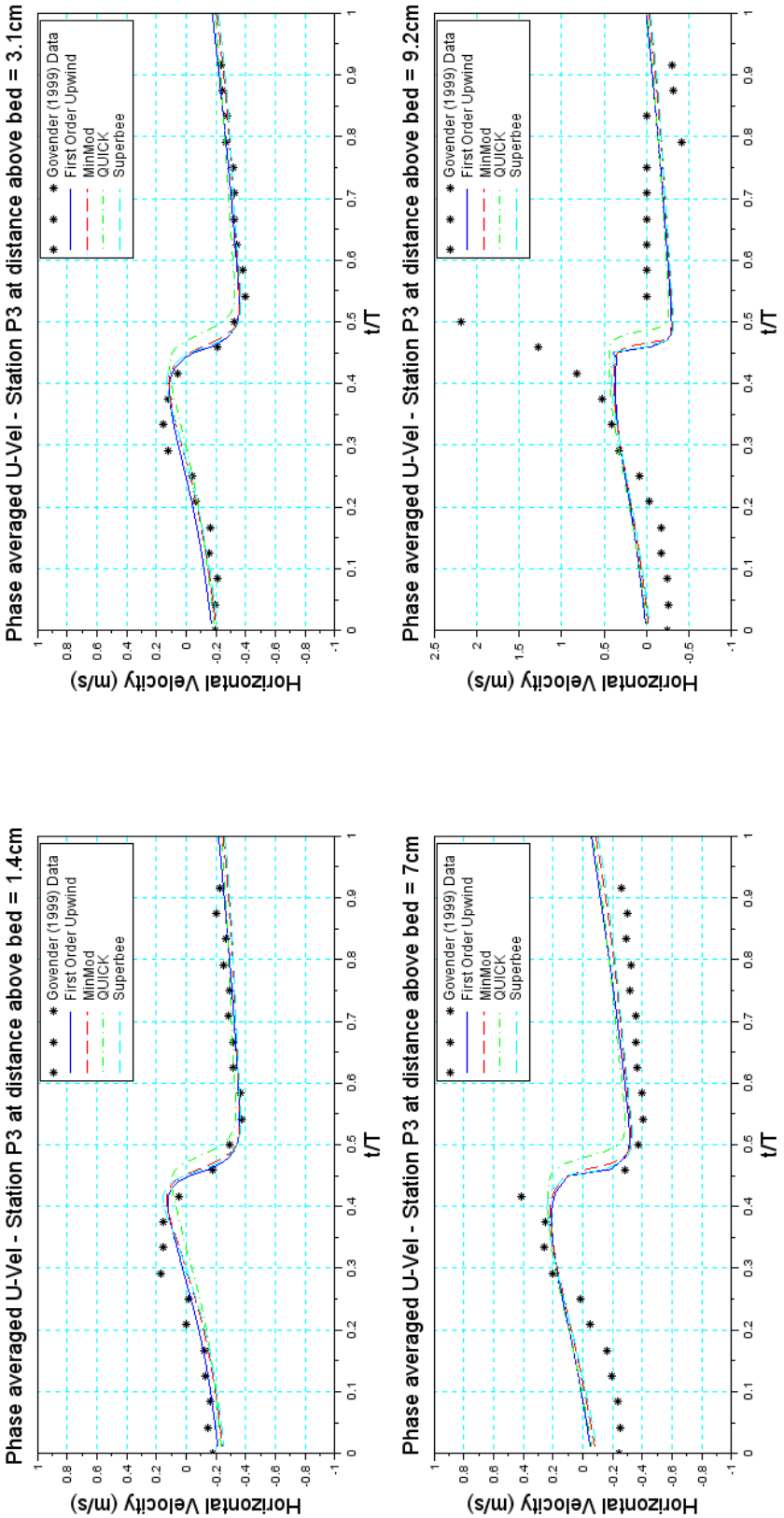

Figure A.33: Phase averaged horizontal velocity in the recorded Govender (1999) and SWASH modelled time series for various higher order interpolation limiter schemes at measuring Station P3 - Momentum conserved

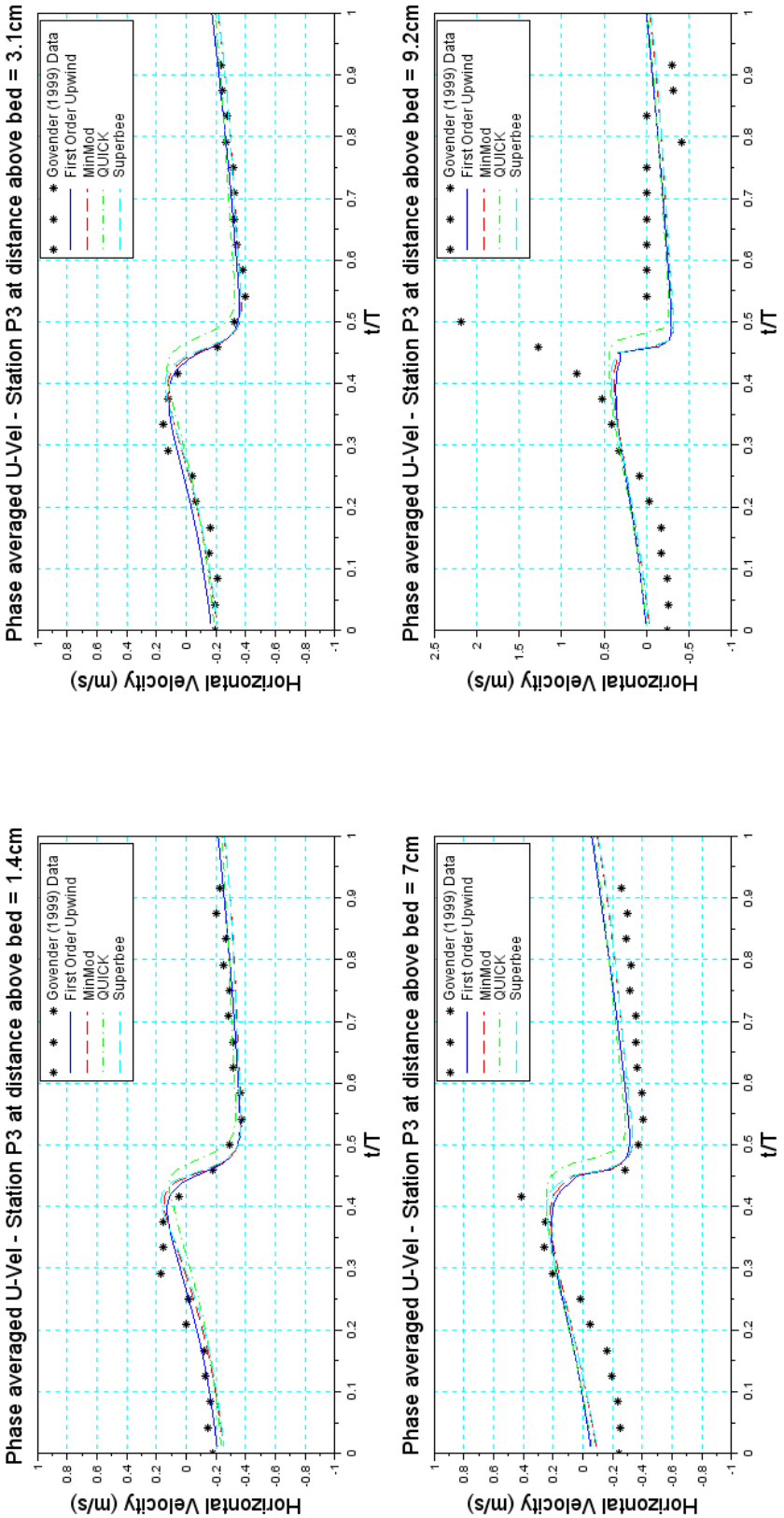

Figure A.34: Phase averaged horizontal velocity in the recorded Govender (1999) and SWASH modelled time series for various higher order interpolation limiter schemes at measuring Station P3 - Momentum not explicitly conserved

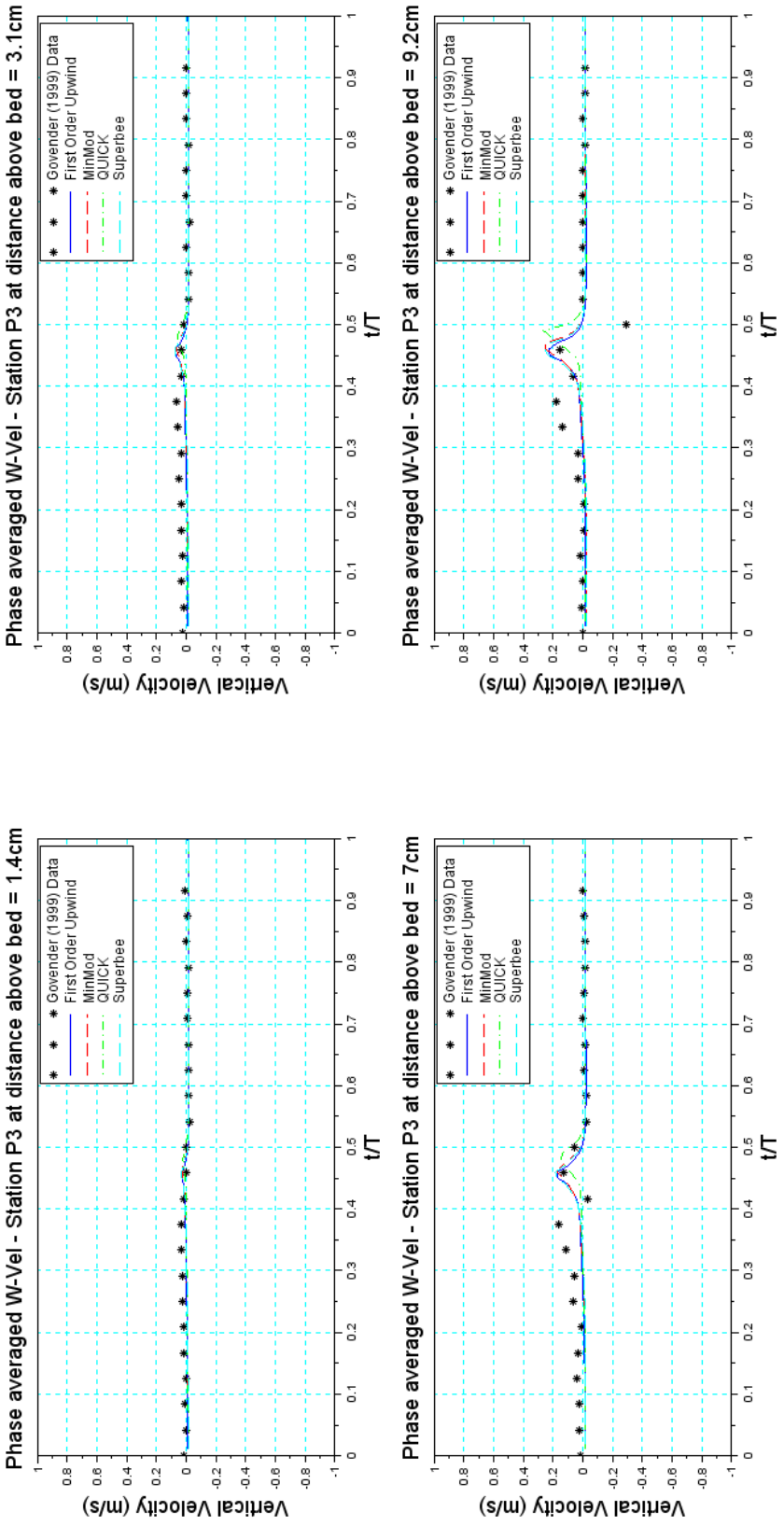

Figure A.35: Phase averaged vertical velocity in the recorded Govender (1999) and SWASH modelled time series for various higher order interpolation limiter schemes at measuring Station P3 - Momentum conserved

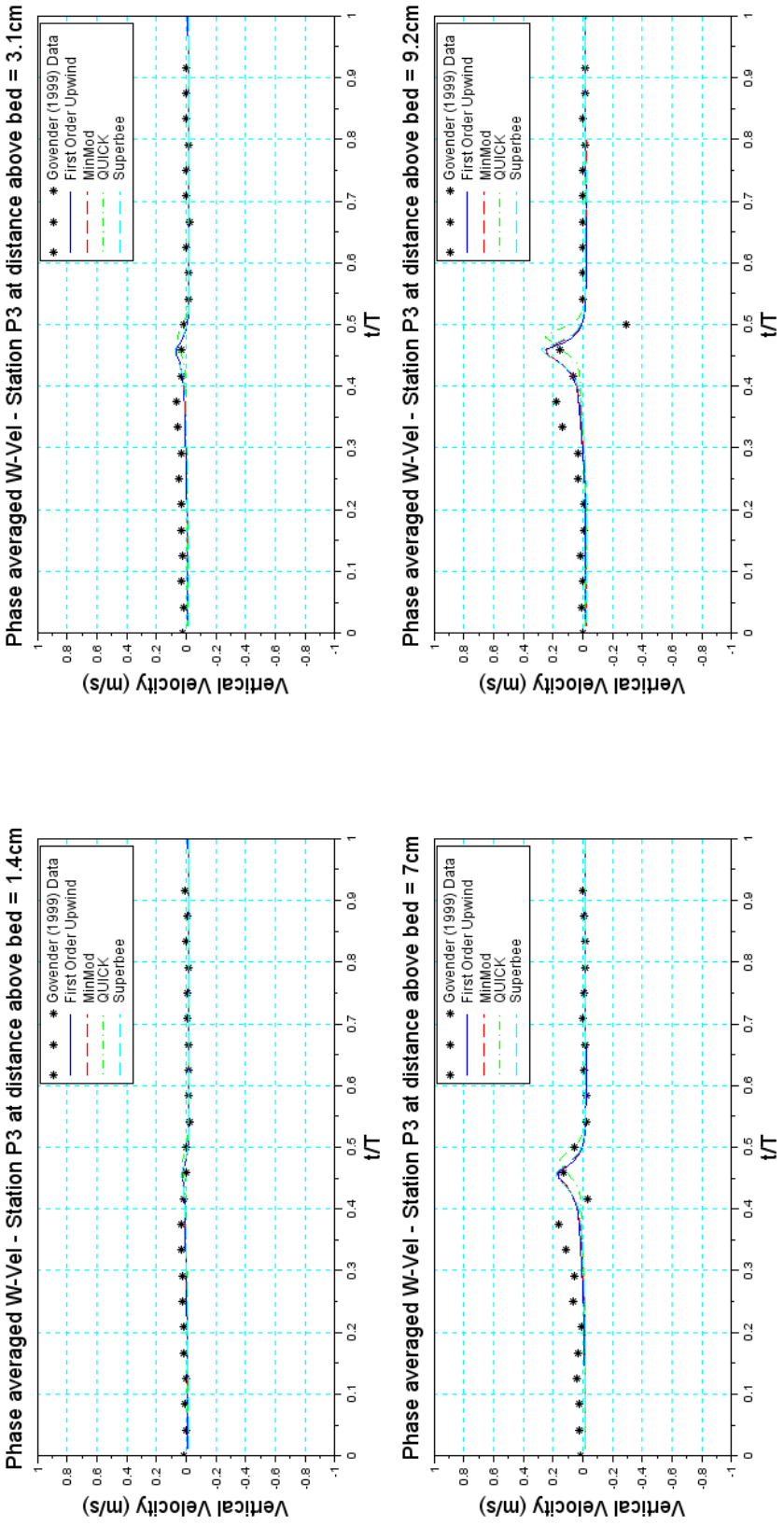

Figure A.36: Phase averaged vertical velocity in the recorded Govender (1999) and SWASH modelled time series for various higher order interpolation limiter schemes at measuring Station P3 - Momentum not explicitly conserved

A.2 Spilling wave calibration

A.2.1 Vertical resolution

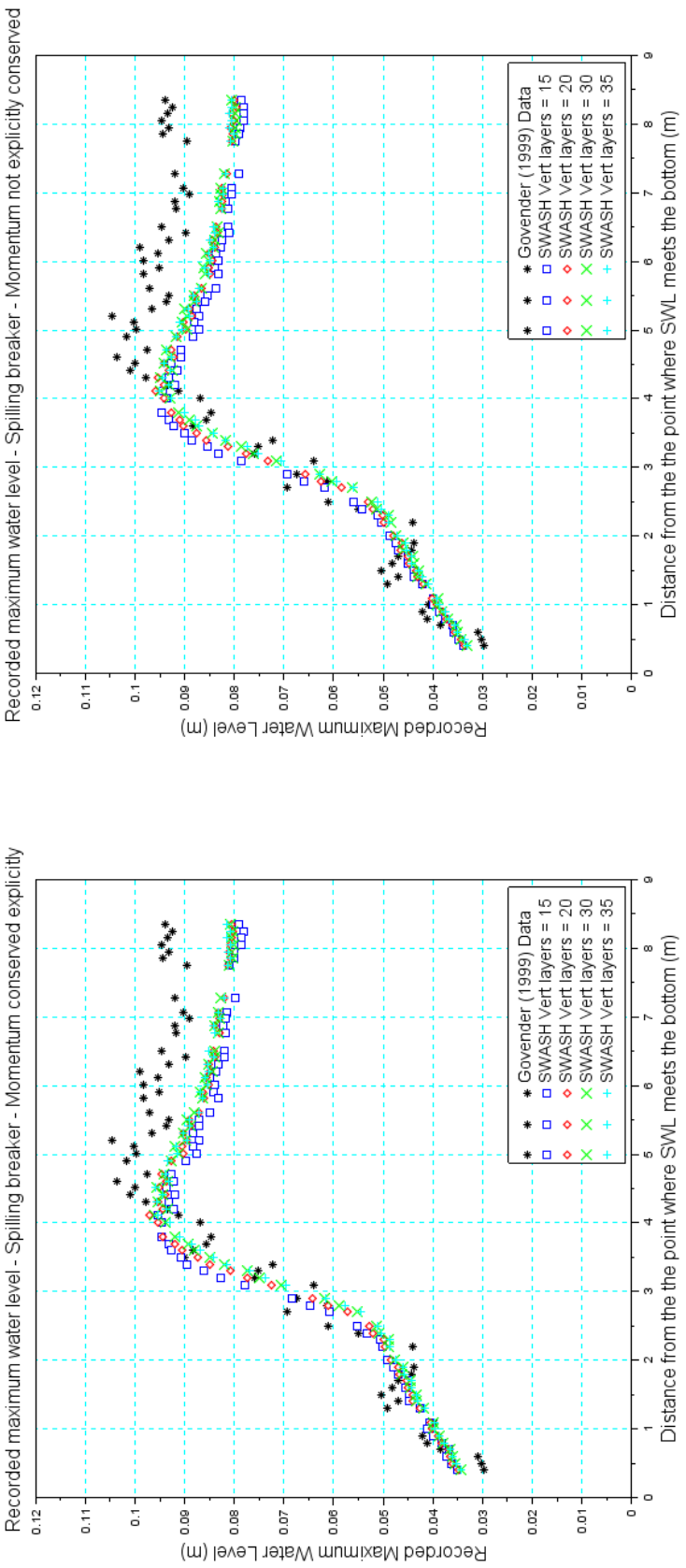

Figure A.37: Maximum water level in the recorded Govender (1999) and SWASH modelled time series (spilling wave) for a variety of vertical layer resolutions measured in points cross-shore of the flume. Left panel shows wave heights with momentum conserved while the right panel shows wave heights without momentum conserved explicitly.

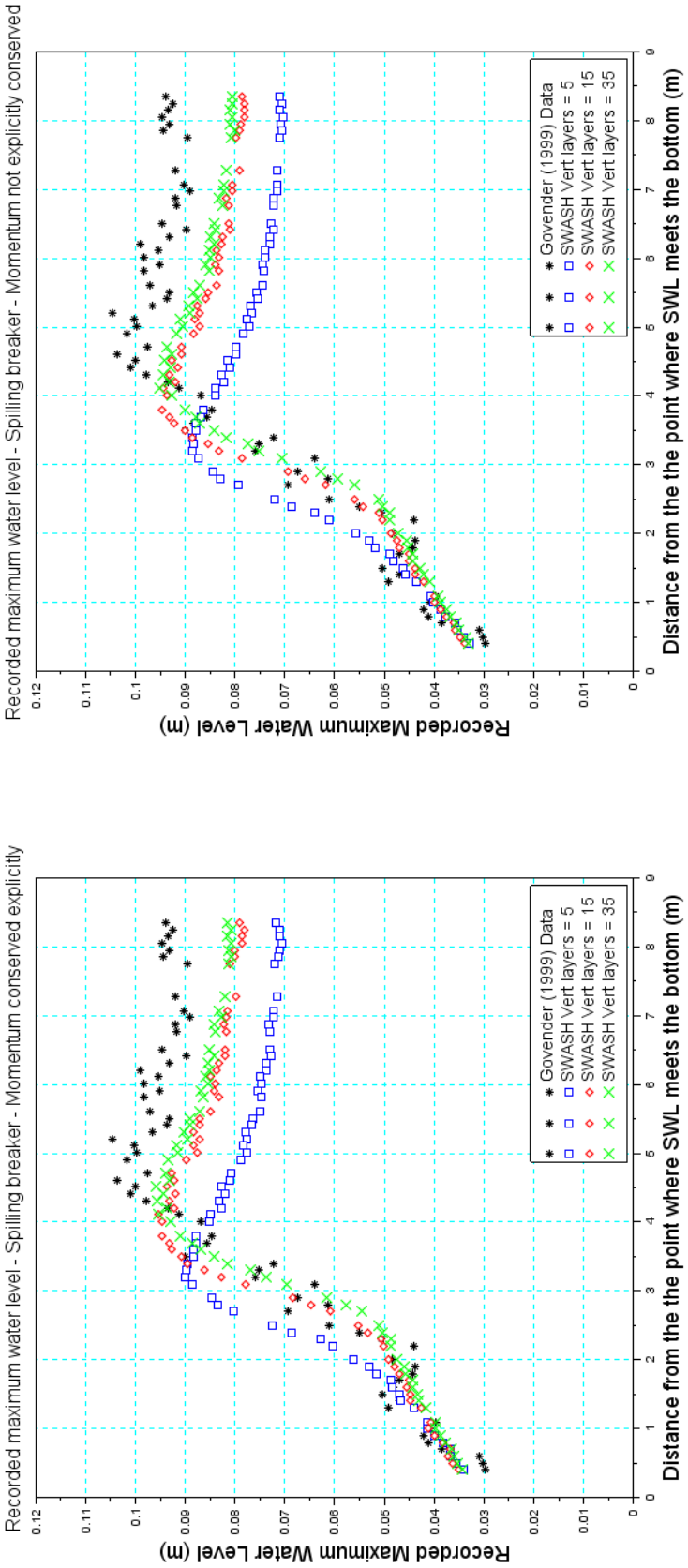

Figure A.38: Maximum wave heights in the recorded Govender (1999) and SWASH modelled time series (spilling wave) for a variety of vertical layer resolutions measured in points cross-shore of the flume. Left panel shows wave heights with momentum conserved while the right panel shows wave heights without momentum conserved explicitly.

A.2.2 Friction parameters

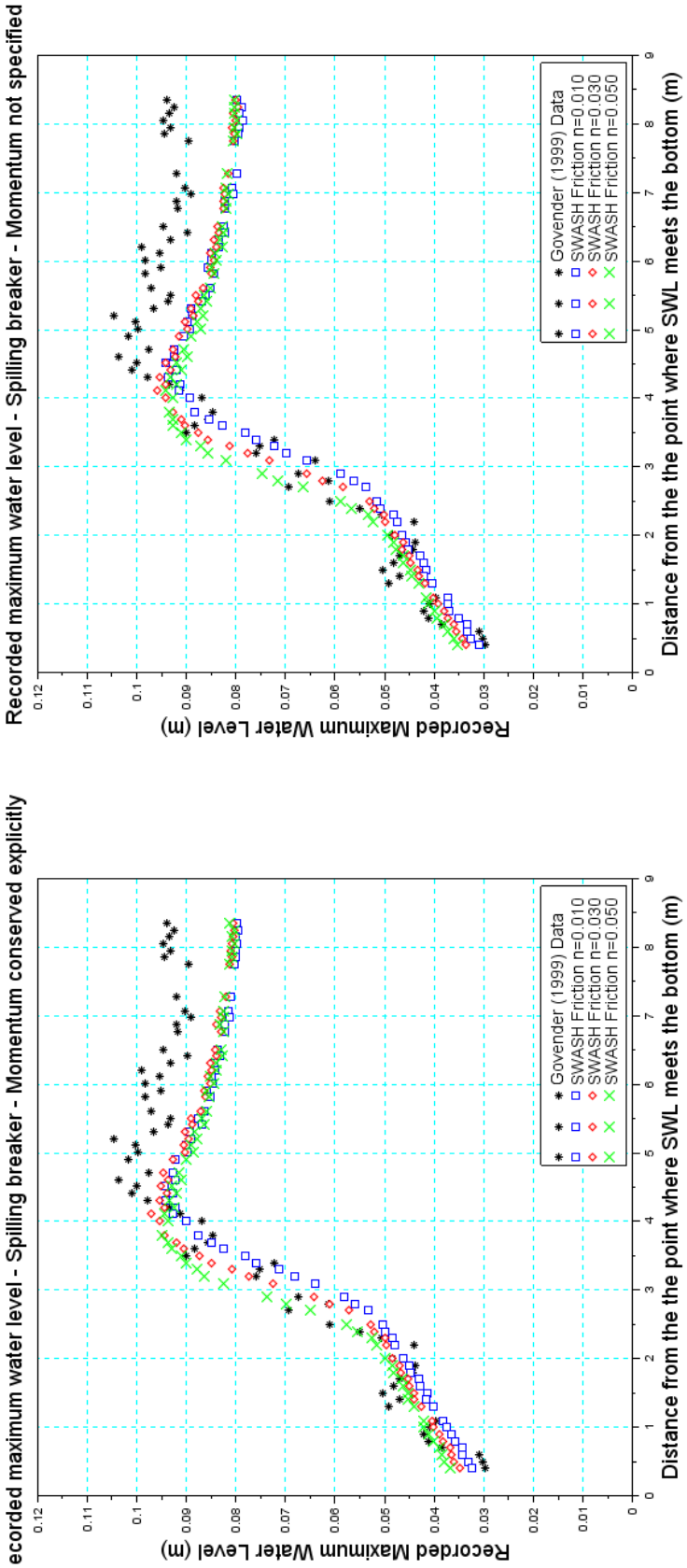

Figure A.39: Maximum wave heights for the spilling breaker in the recorded Govender (1999) and SWASH modelled time series for various Manning friction values measured in points cross-shore of the flume. Left panel shows wave heights with momentum conserved while the right panel shows wave heights without momentum conserved explicitly.

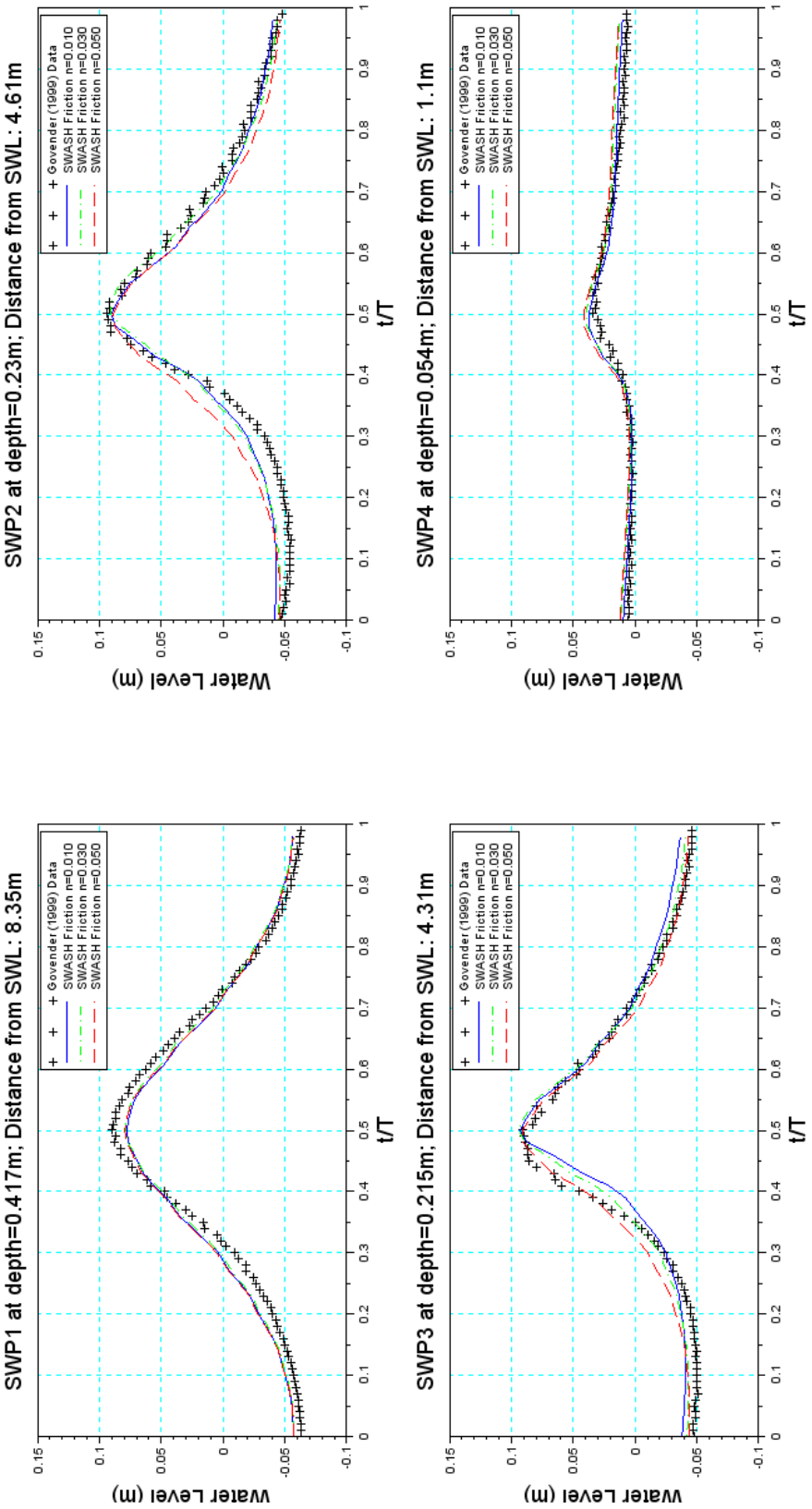

Figure A.40: Phase averaged wave heights in the recorded Govender (1999) and SWASH modelled time series for various Manning friction values at four measuring points in the flume - Spilling Breaker - Momentum conserved

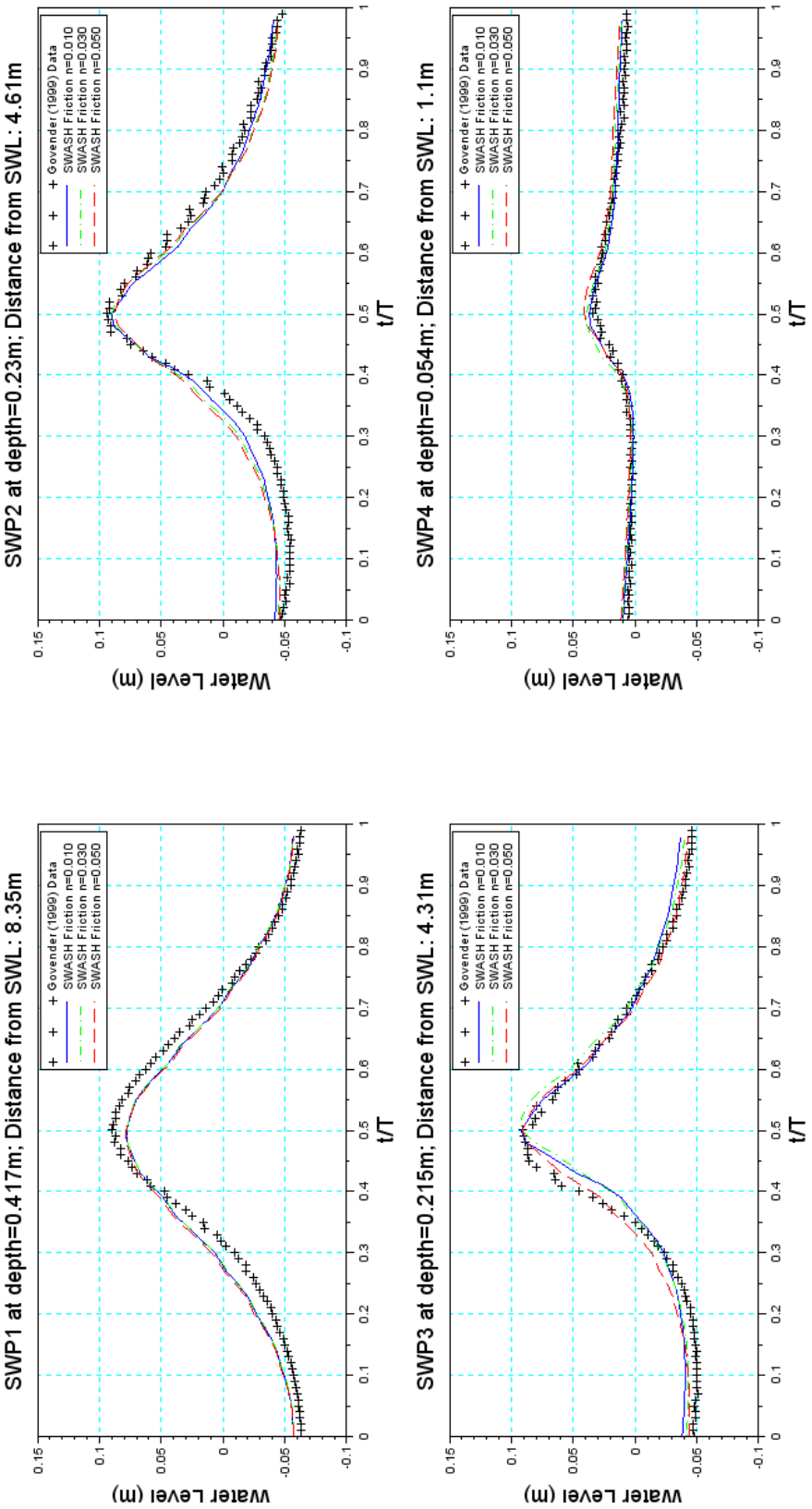

Figure A.41: Phase averaged wave heights in the recorded Govender (1999) and SWASH modelled time series for various Manning friction values at four measuring points in the flume - Spilling Breaker - Momentum not explicitly conserved

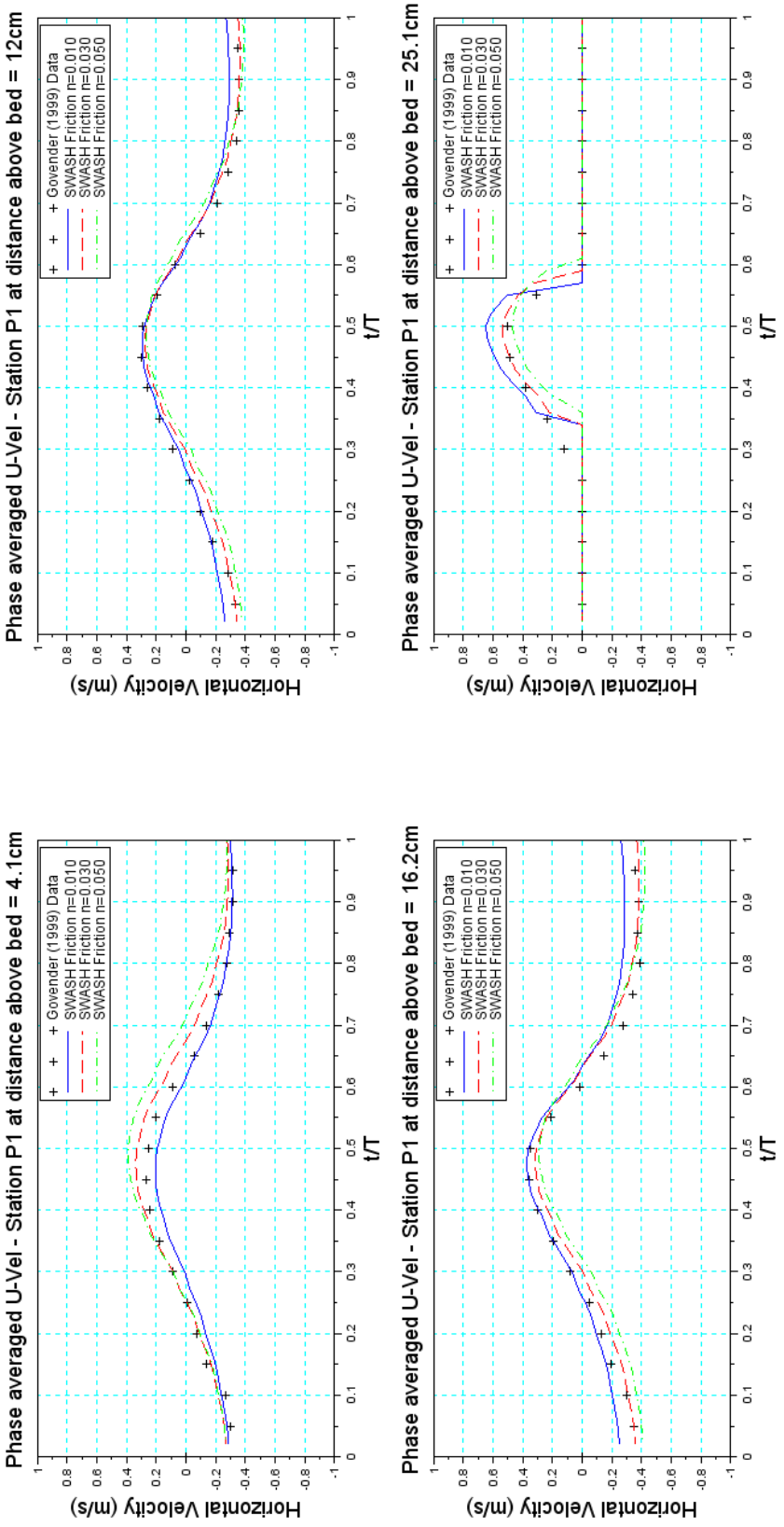

Figure A.42: Phase averaged horizontal velocity in the recorded Govender (1999) and SWASH modelled time series for various Manning friction values at measuring Station P1 - Momentum conserved

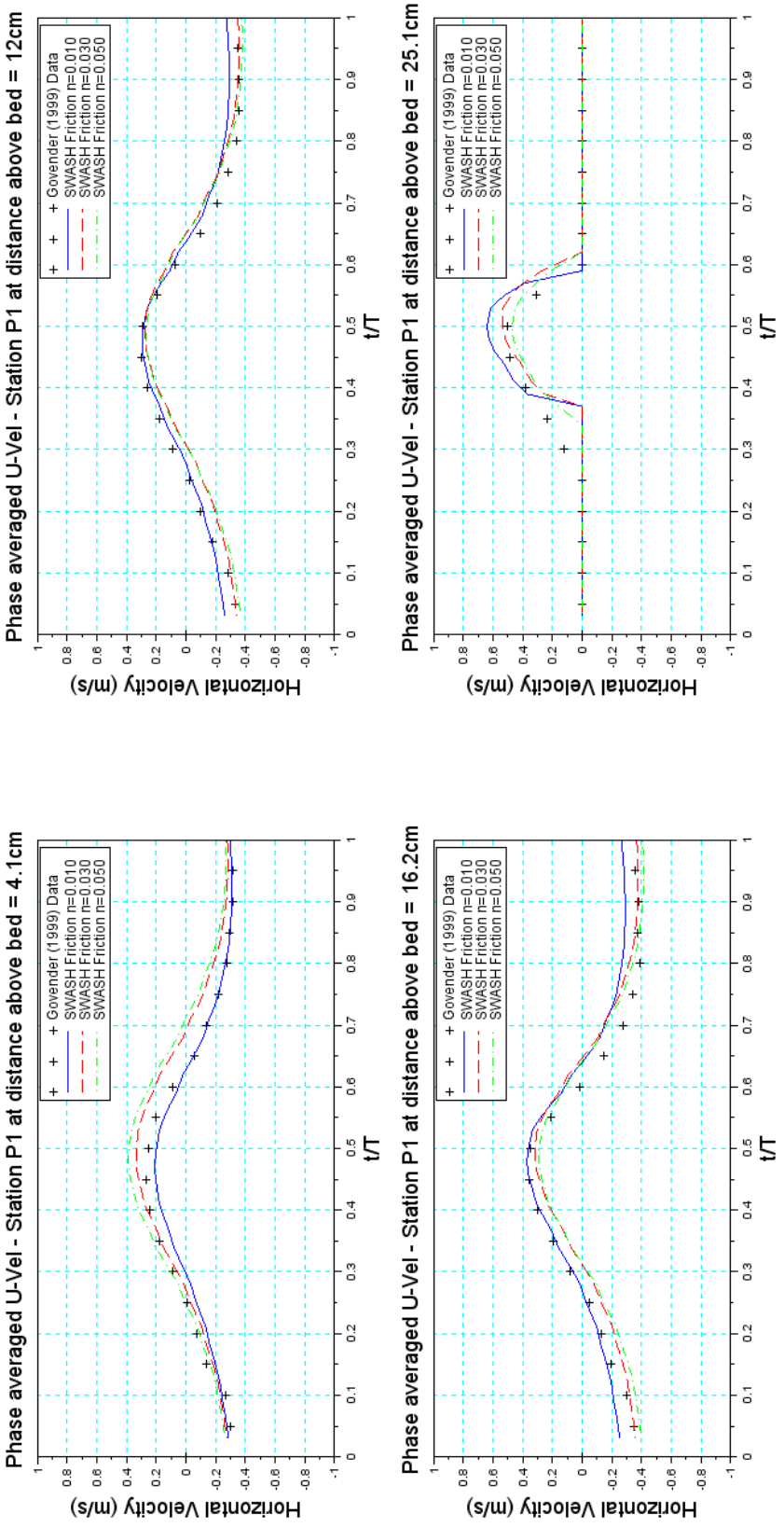

Figure A.43: Phase averaged horizontal velocity in the recorded Govender (1999) and SWASH modelled time series for various Manning friction values at measuring Station P1 - Momentum not explicitly conserved

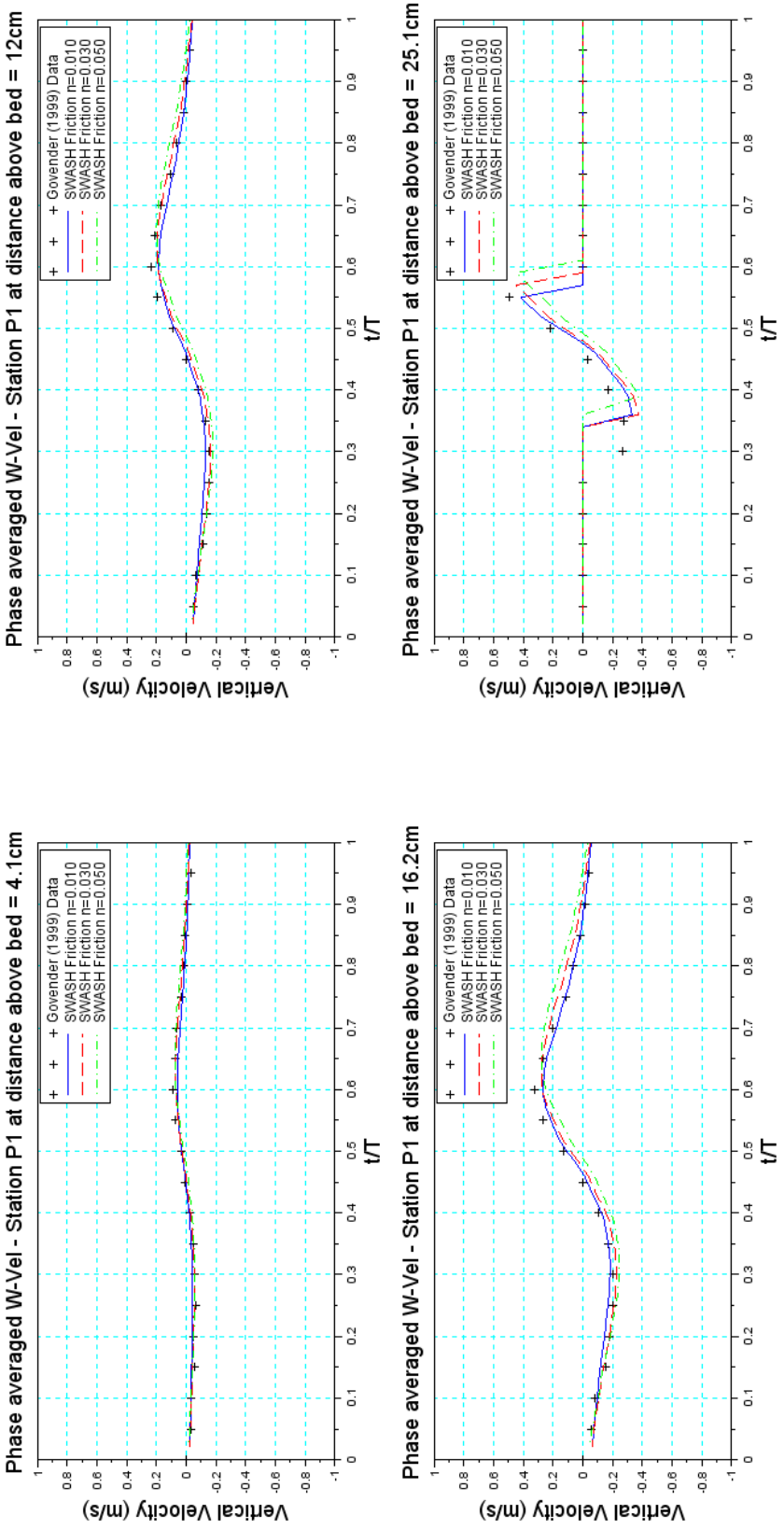

Figure A.44: Phase averaged vertical velocity in the recorded Govender (1999) and SWASH modelled time series for various Manning friction values at measuring Station P1 - Momentum conserved

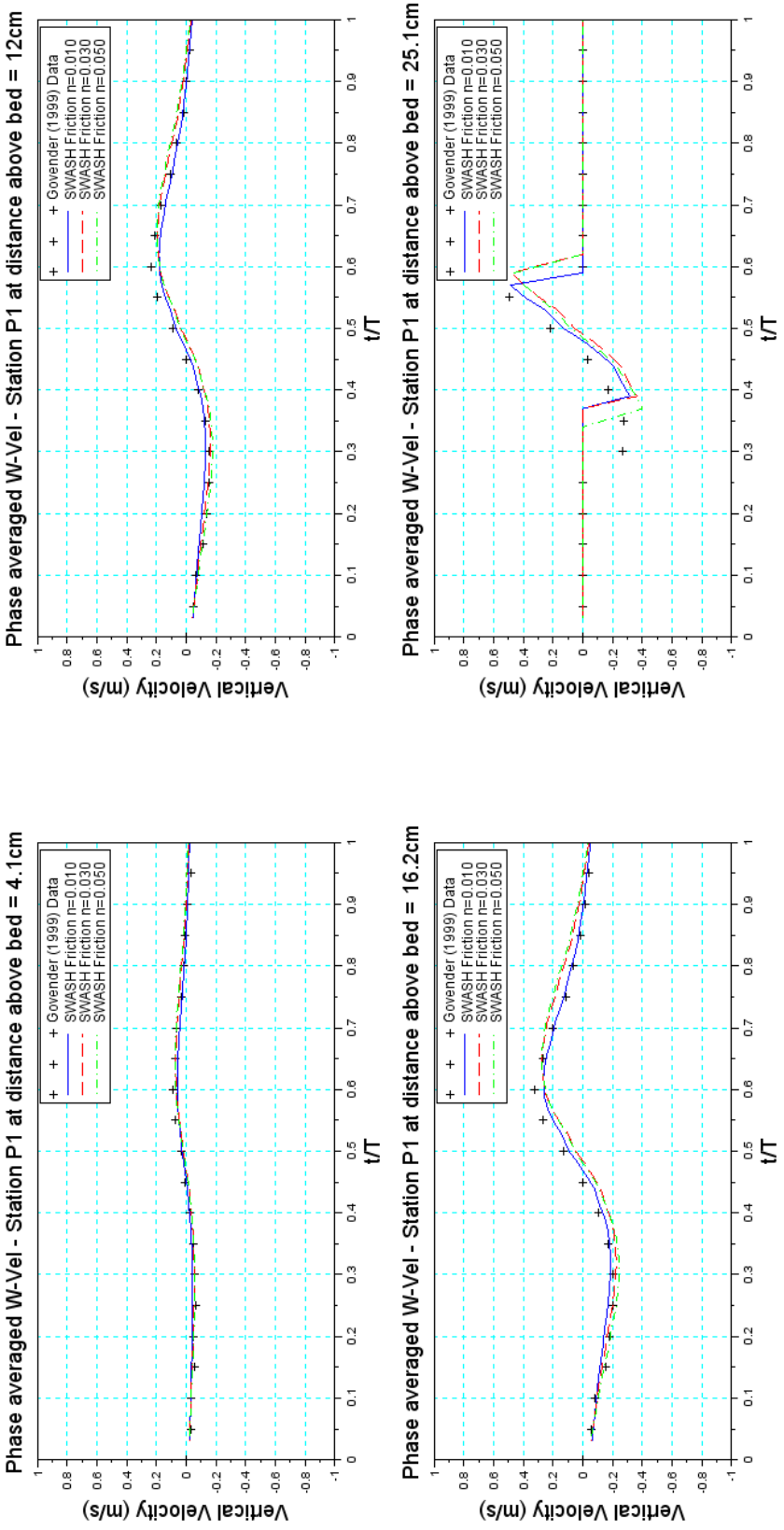

Figure A.45: Phase averaged vertical velocity in the recorded Govender (1999) and SWASH modelled time series for various Manning friction values at measuring Station P1 - Momentum not explicitly conserved

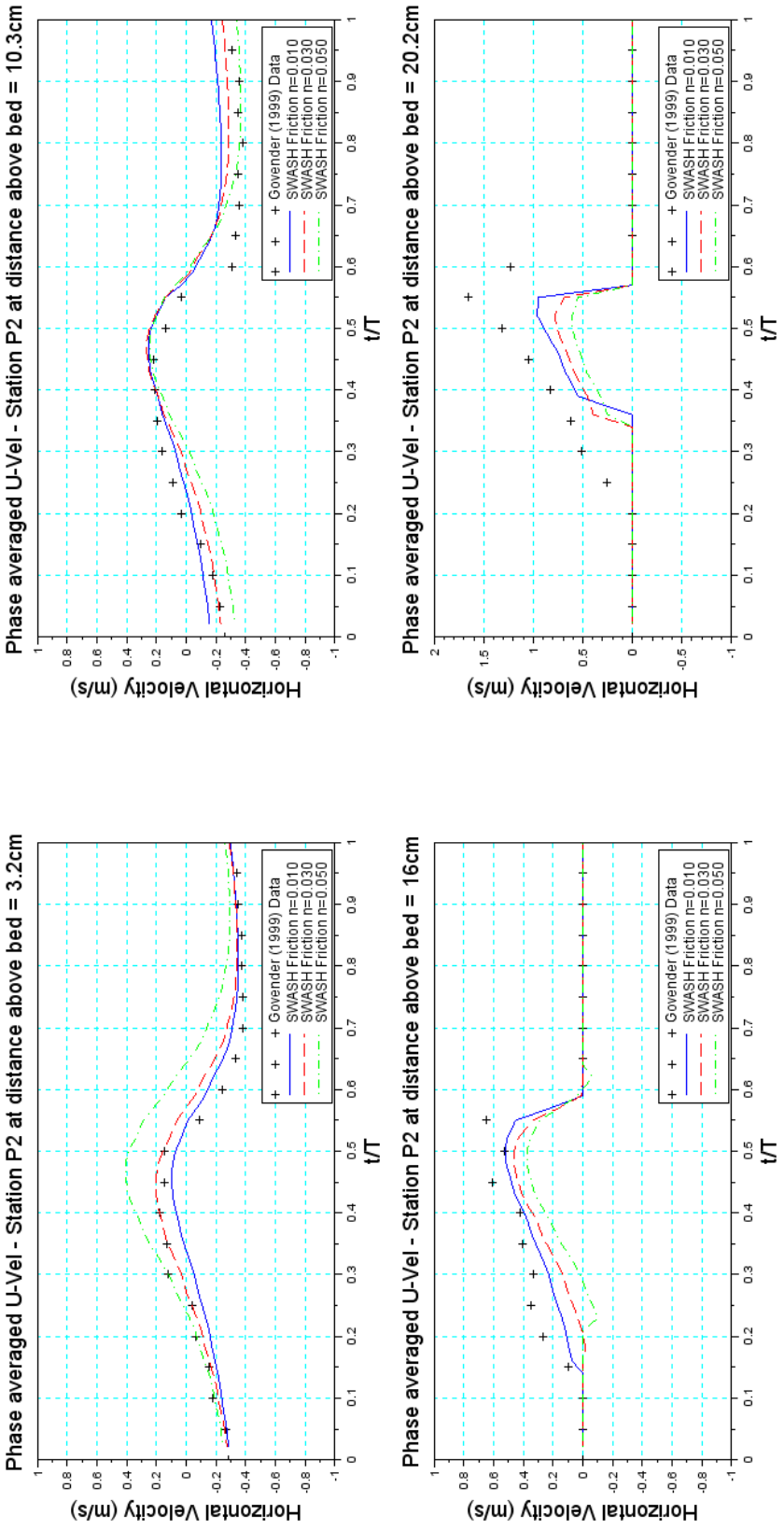

Figure A.46: Phase averaged horizontal velocity in the recorded Govender (1999) and SWASH modelled time series for various Manning friction values at measuring Station P2 - Momentum conserved

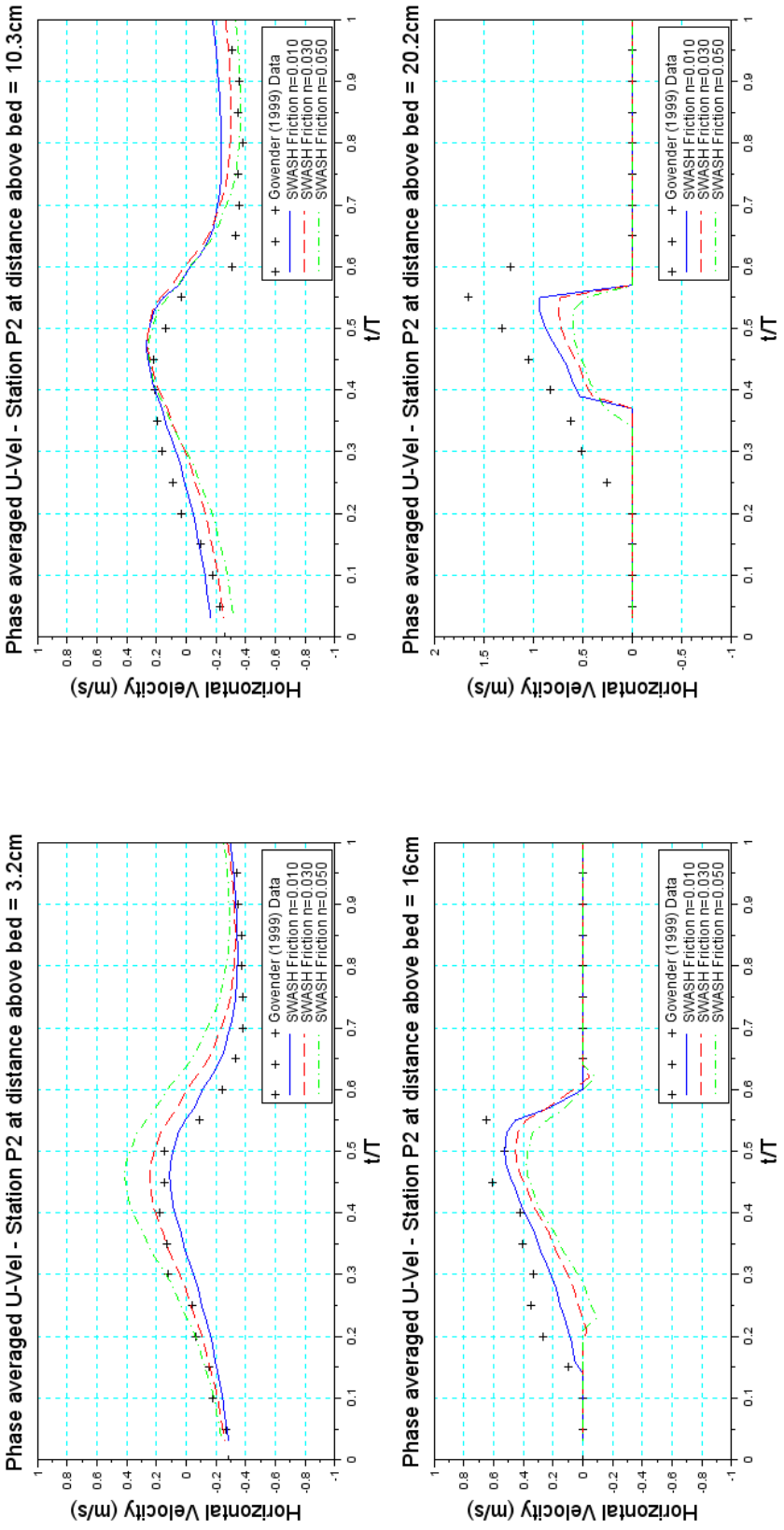

Figure A.47: Phase averaged horizontal velocity in the recorded Govender (1999) and SWASH modelled time series for various Manning friction values at measuring Station P2 - Momentum not explicitly conserved

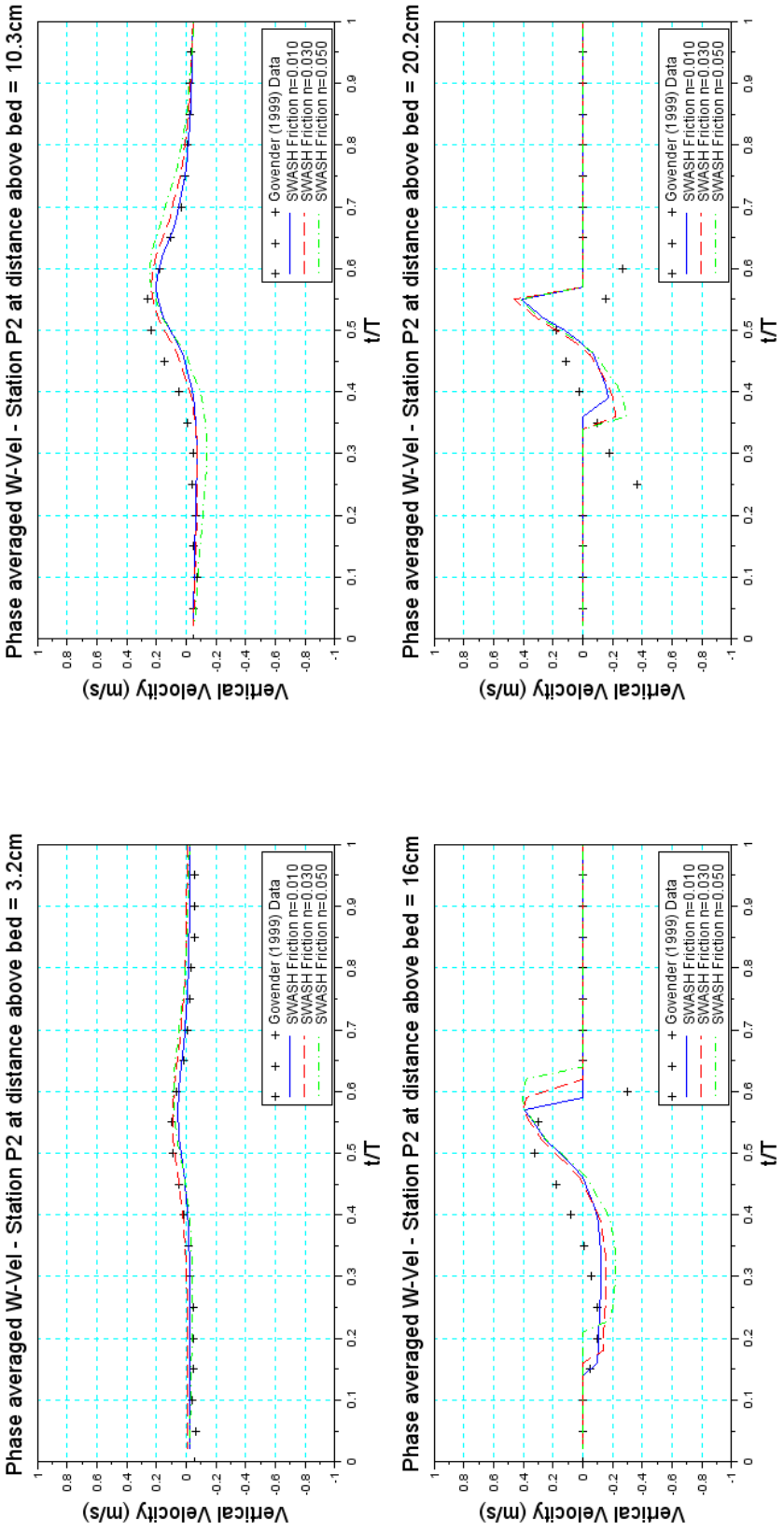

Figure A.48: Phase averaged vertical velocity in the recorded Govender (1999) and SWASH modelled time series for various Manning friction values at measuring Station P2 - Momentum conserved

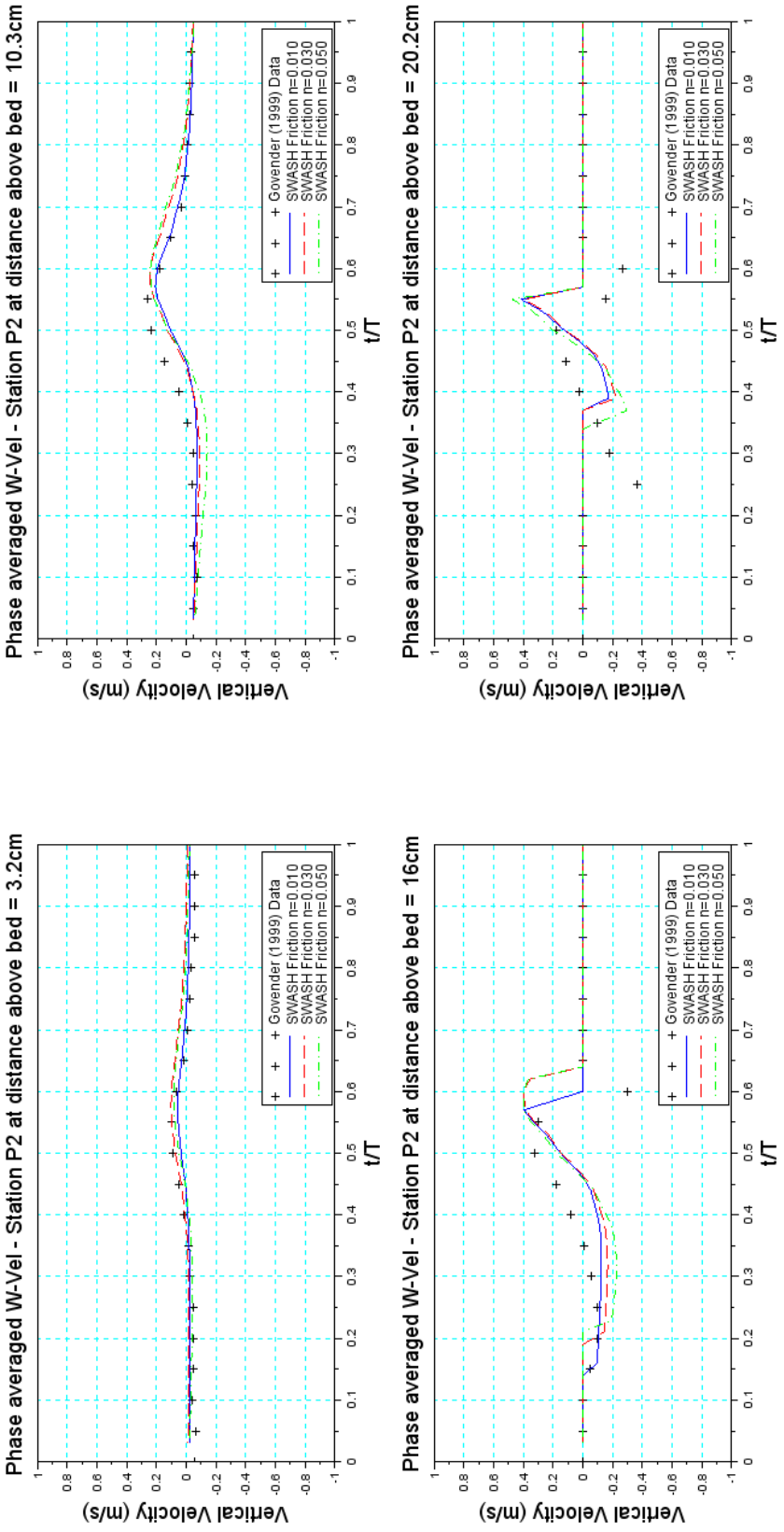

Figure A.49: Phase averaged vertical velocity in the recorded Govender (1999) and SWASH modelled time series for various Manning friction values at measuring Station P2 - Momentum not explicitly conserved

A.2.3 Horizontal and vertical advection terms of the momentum equation

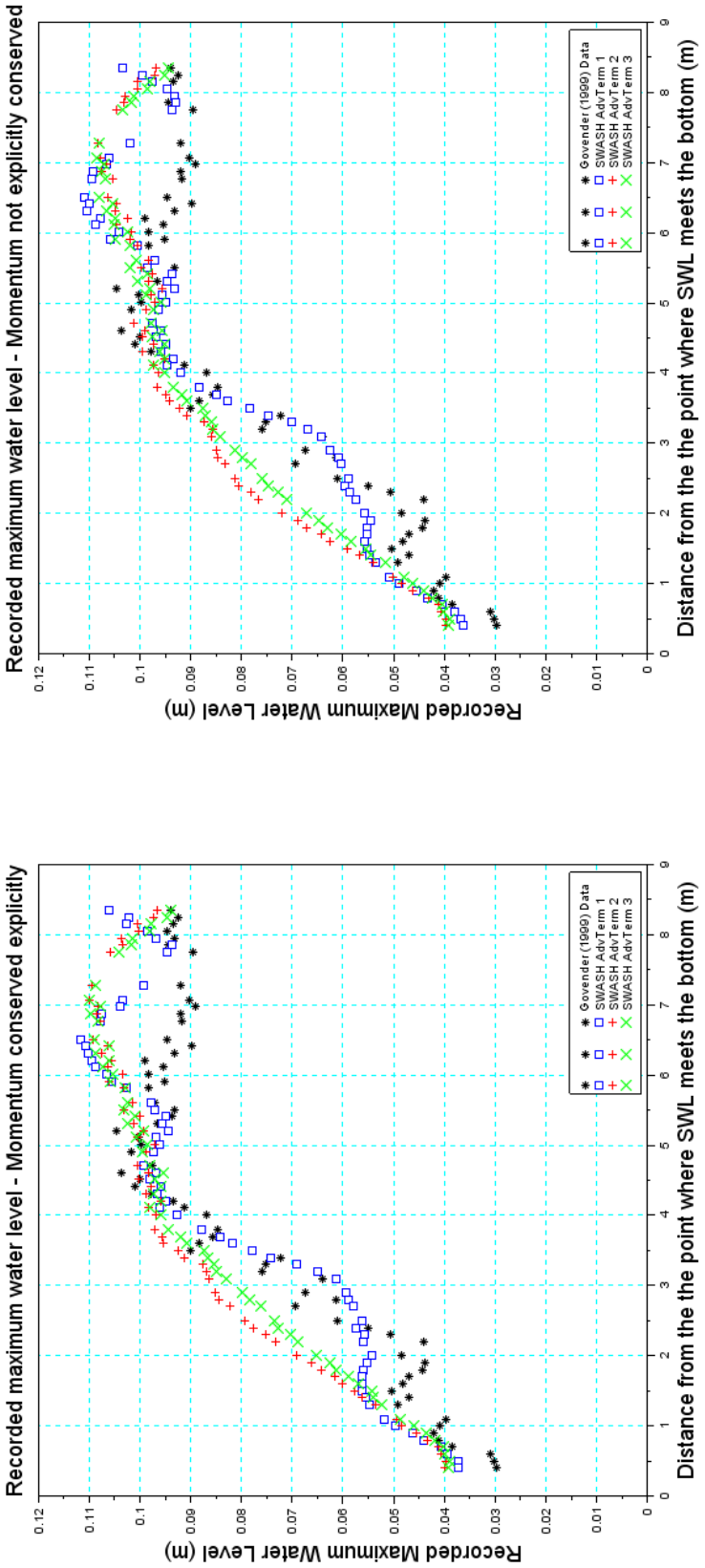

Figure A.50: Maximum wave heights in the recorded Govender (1999) and SWASH modelled time series for various advection term discretisation schemes measured in points cross-shore of the flume. Left panel shows wave heights with momentum conserved while the right panel shows wave heights without momentum conserved explicitly.

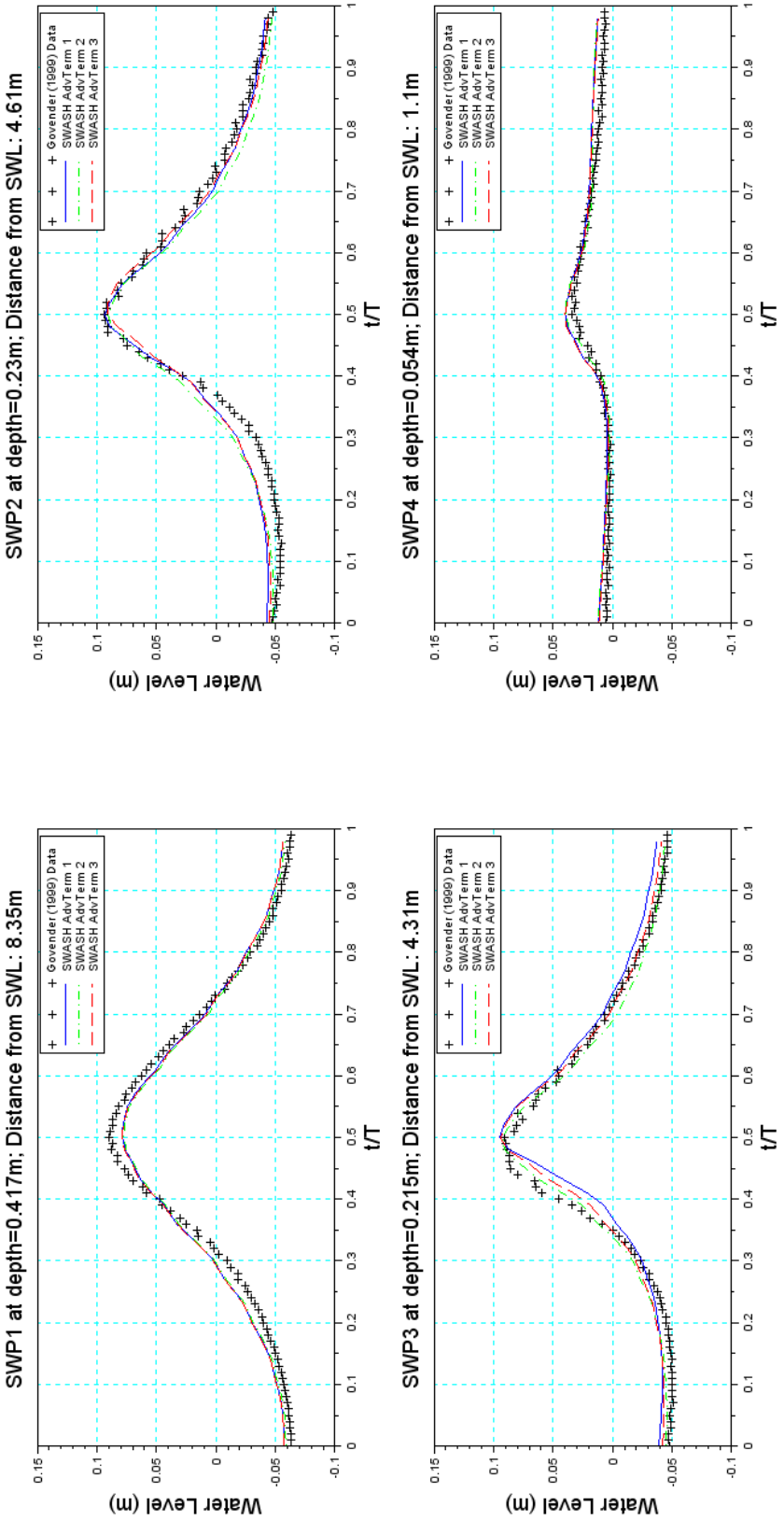

Figure A.51: Phase averaged wave heights in the recorded Govender (1999) and SWASH modelled time series for various discretisation schemes at four measuring points in the flume - Momentum conserved

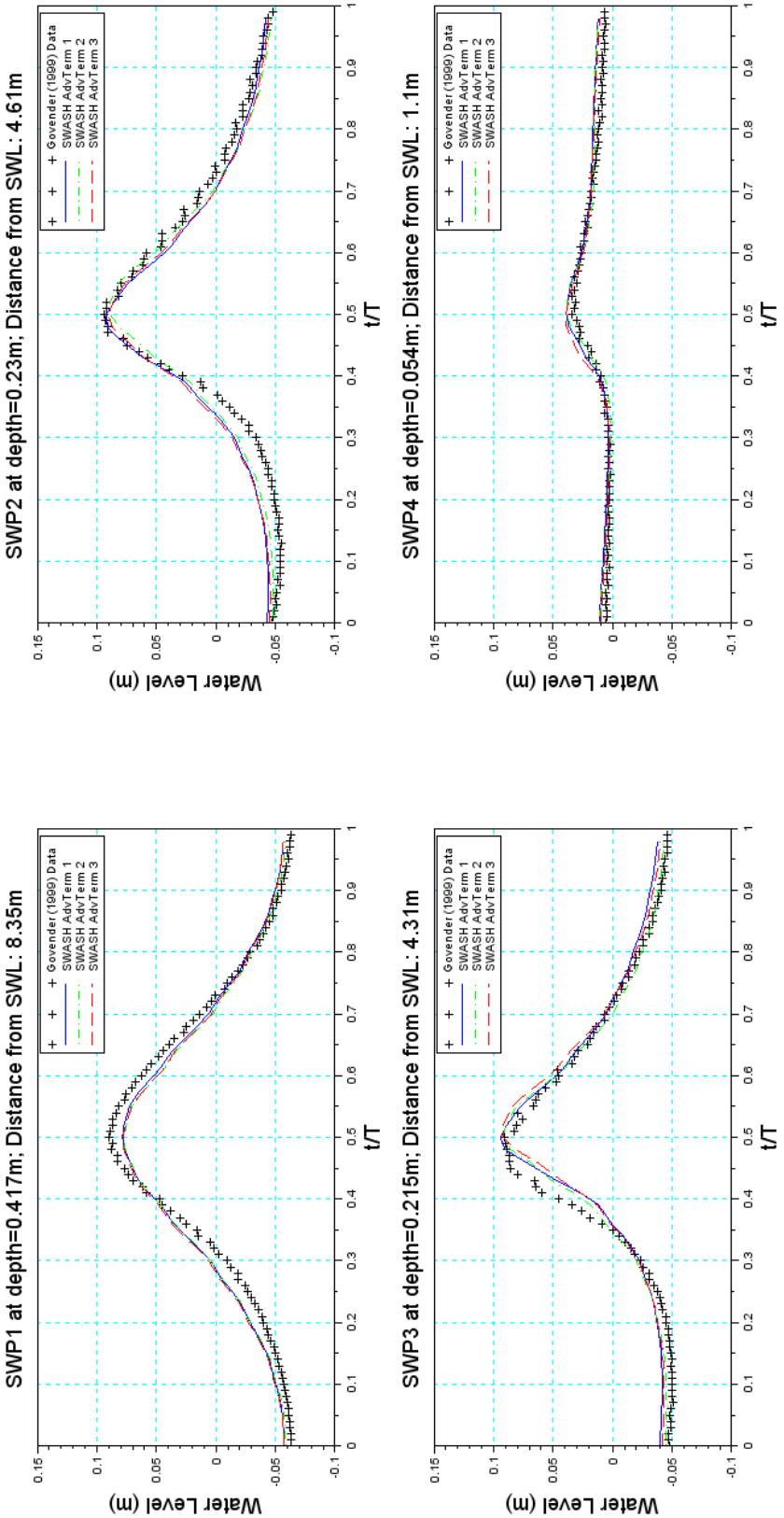

Figure A.52: Phase averaged wave heights in the recorded Govender (1999) and SWASH modelled time series for various discretisation schemes at four measuring points in the flume - Momentum not explicitly conserved

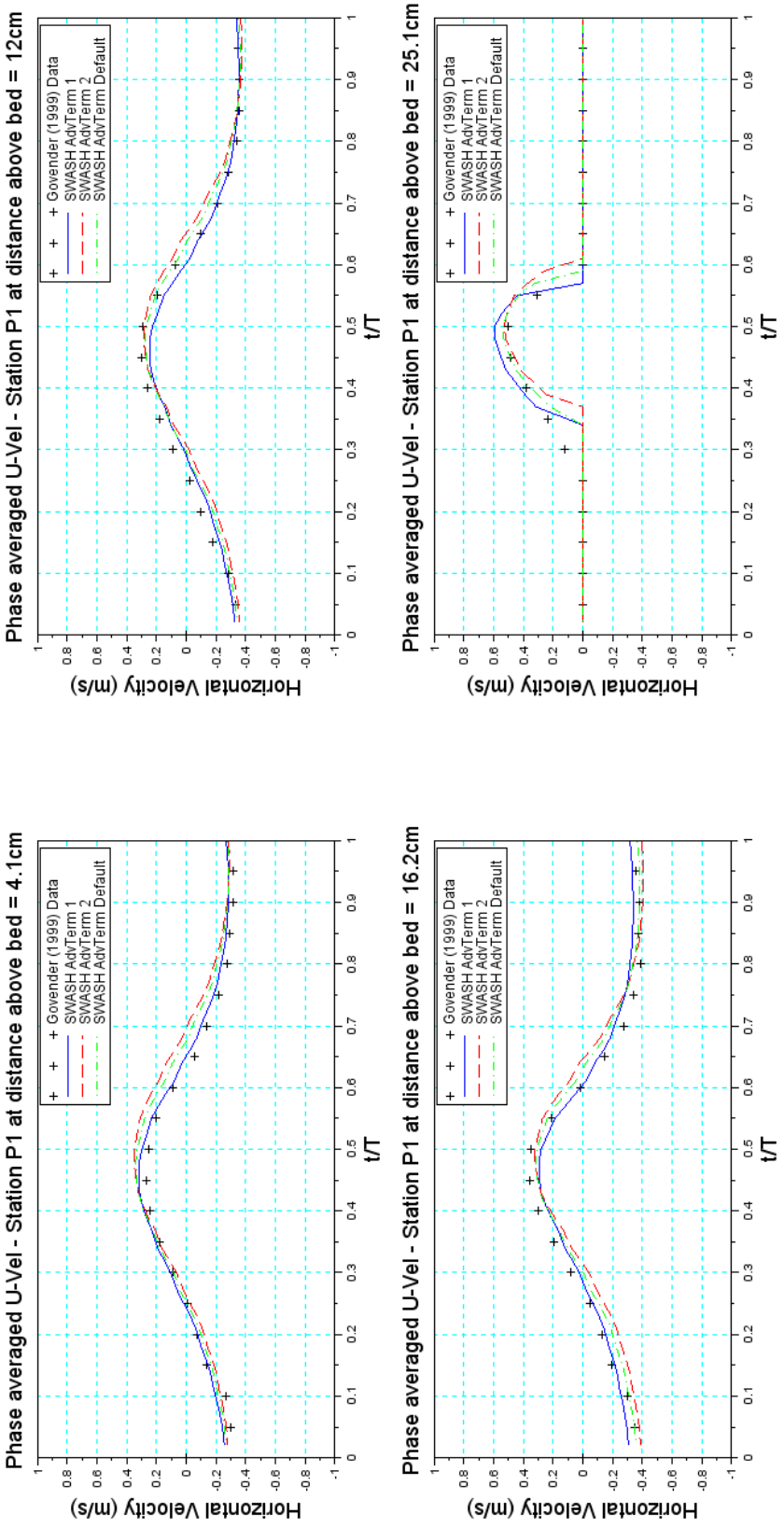

Figure A.53: Phase averaged horizontal velocity in the recorded Govender (1999) and SWASH modelled time series for various discretisation schemes at measuring Station P1 - Momentum conserved

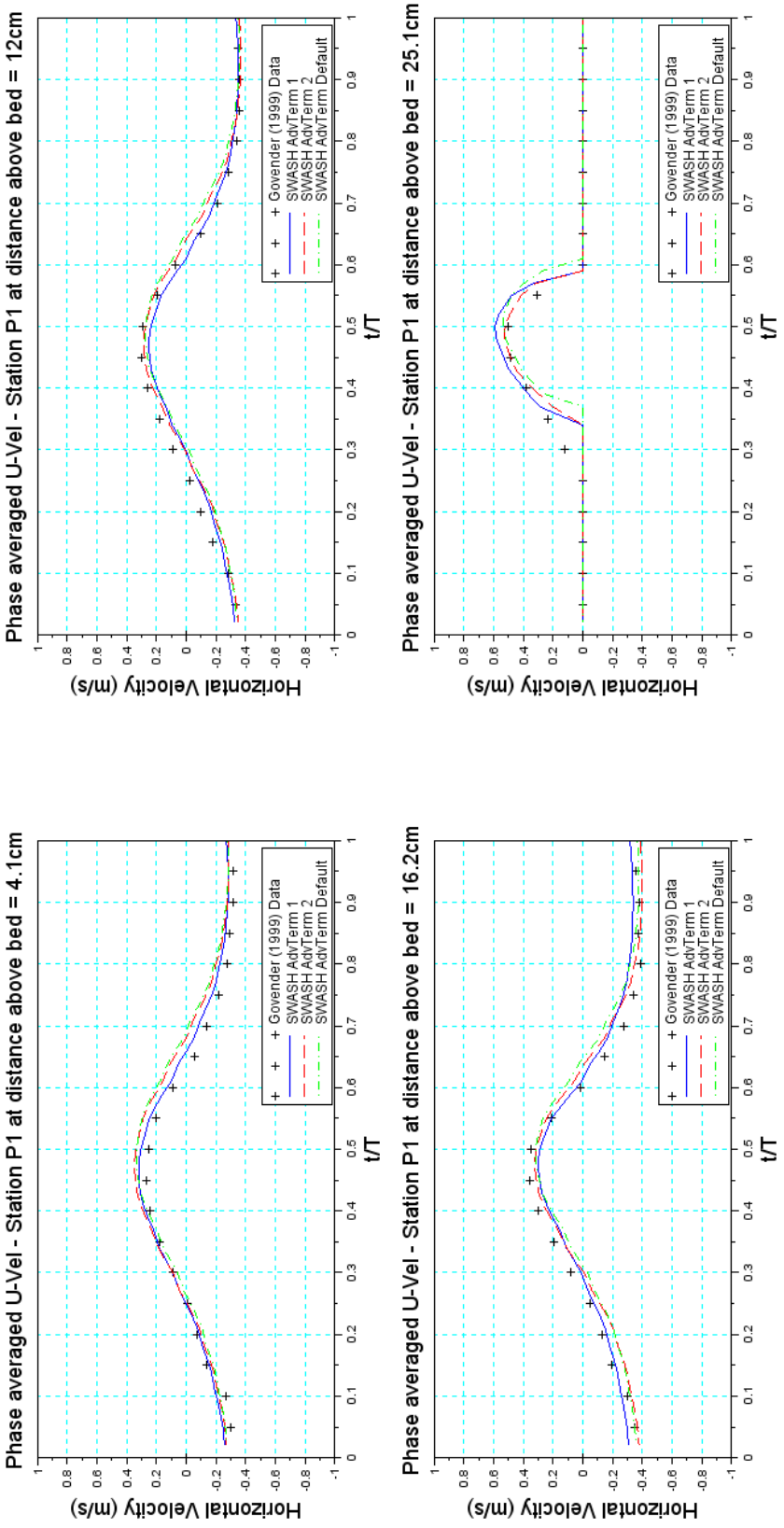

Figure A.54: Phase averaged horizontal velocity in the recorded Govender (1999) and SWASH modelled time series for various discretisation schemes at measuring Station P1 - Momentum not explicitly conserved

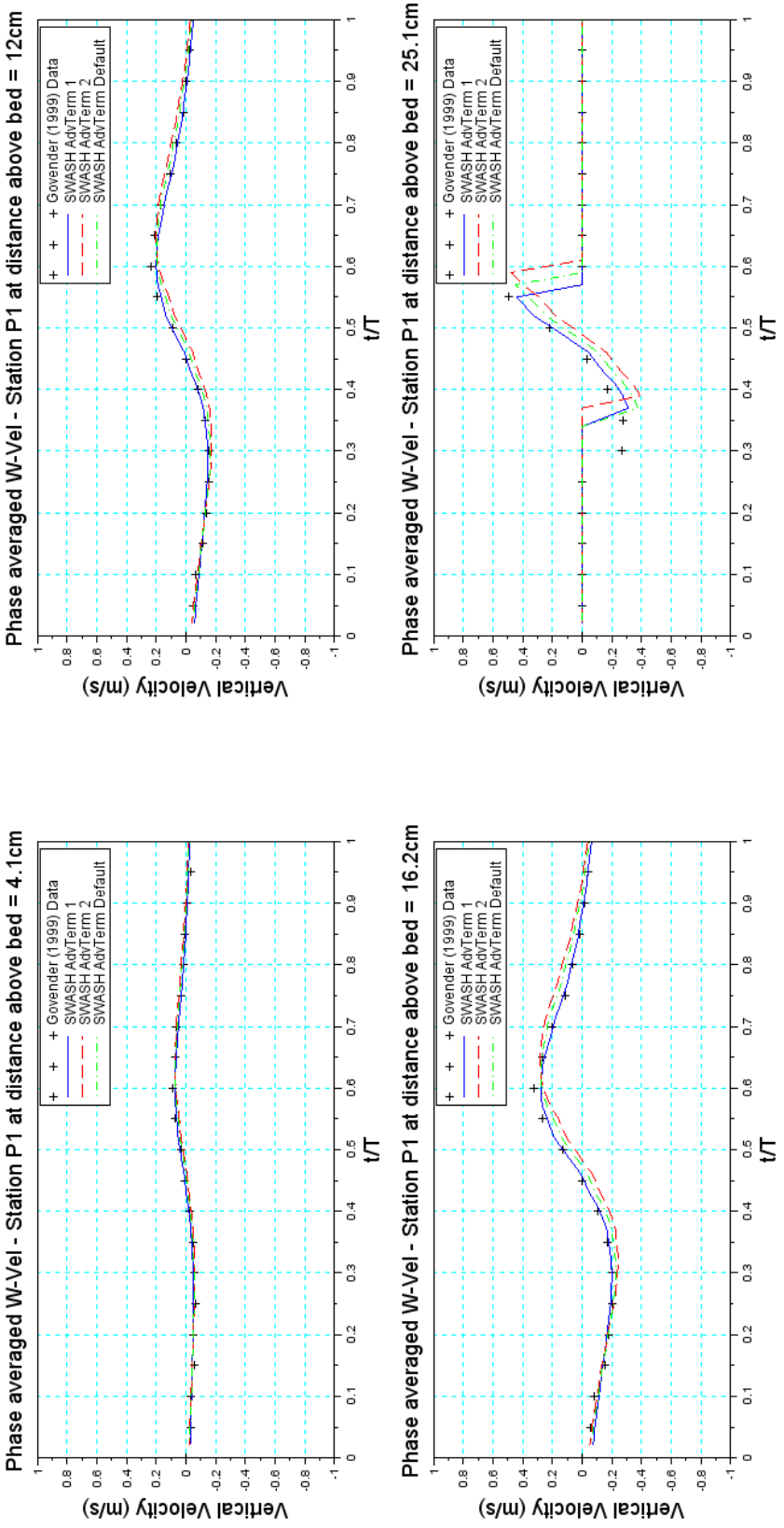

Figure A.55: Phase averaged vertical velocity in the recorded Govender (1999) and SWASH modelled time series for various discretisation schemes at measuring Station P1 - Momentum conserved

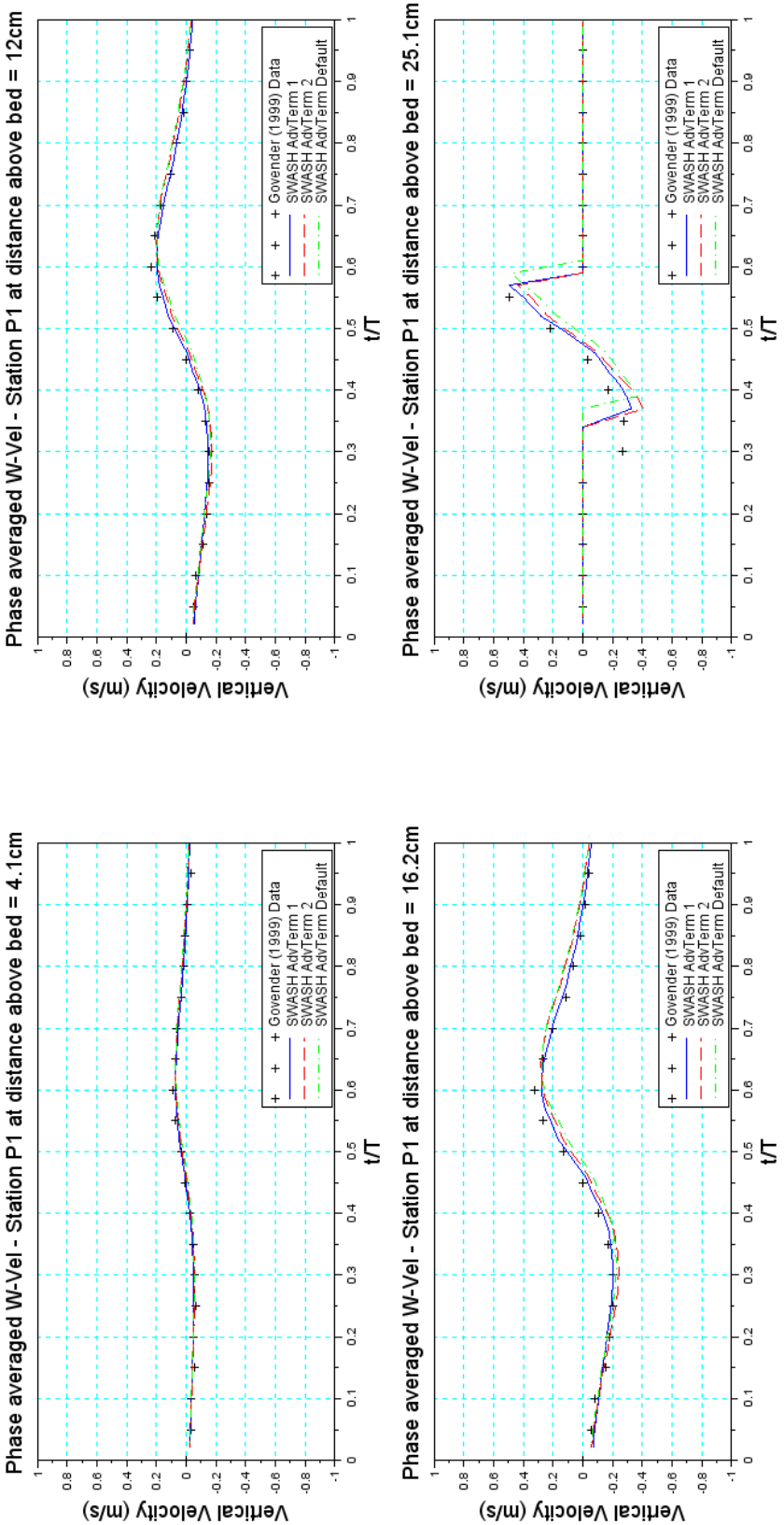

Figure A.56: Phase averaged vertical velocity in the recorded Govender (1999) and SWASH modelled time series for various discretisation schemes at measuring Station P1 - Momentum not explicitly conserved

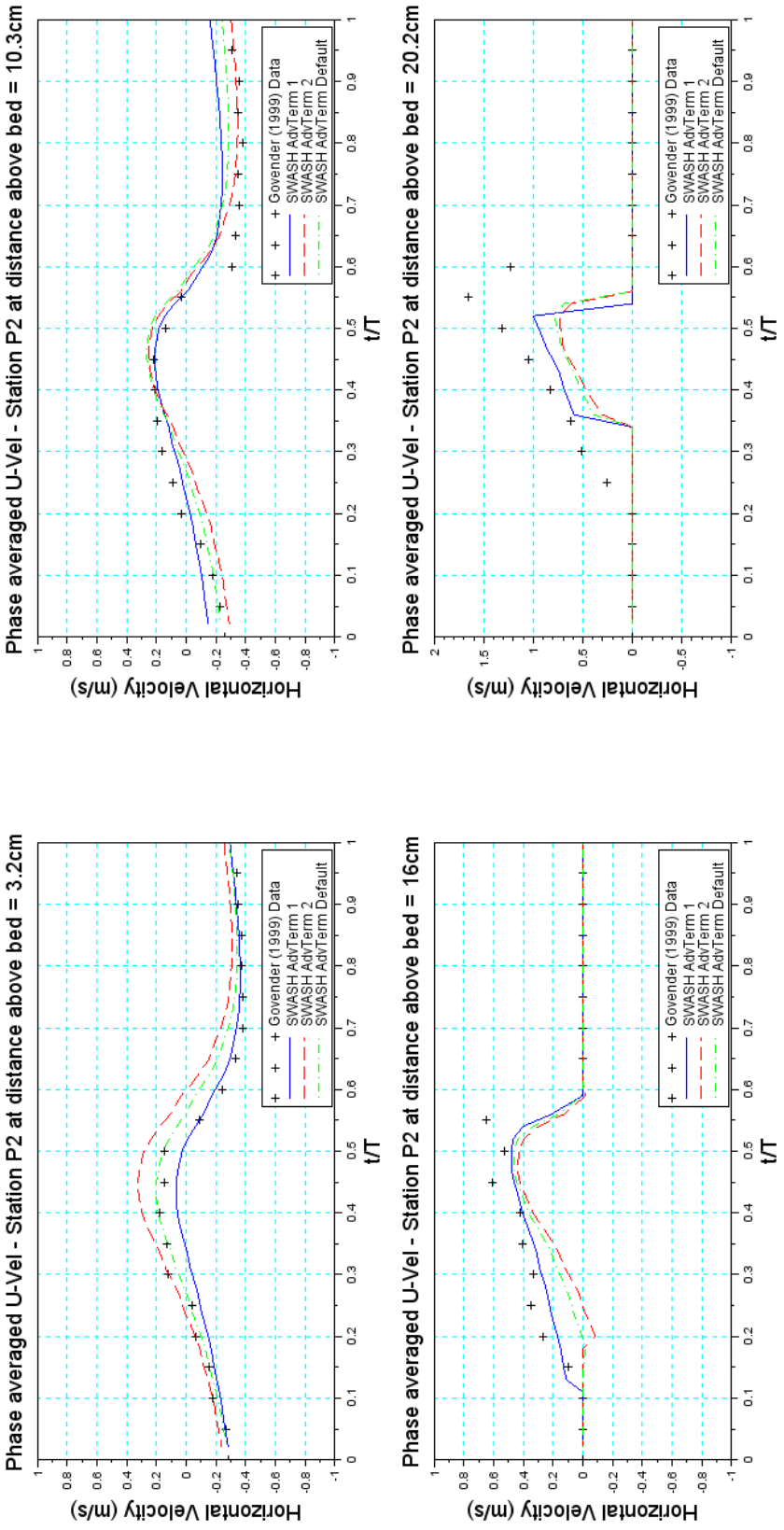

Figure A.57: Phase averaged horizontal velocity in the recorded Govender (1999) and SWASH modelled time series for various discretisation schemes at measuring Station P2 - Momentum conserved

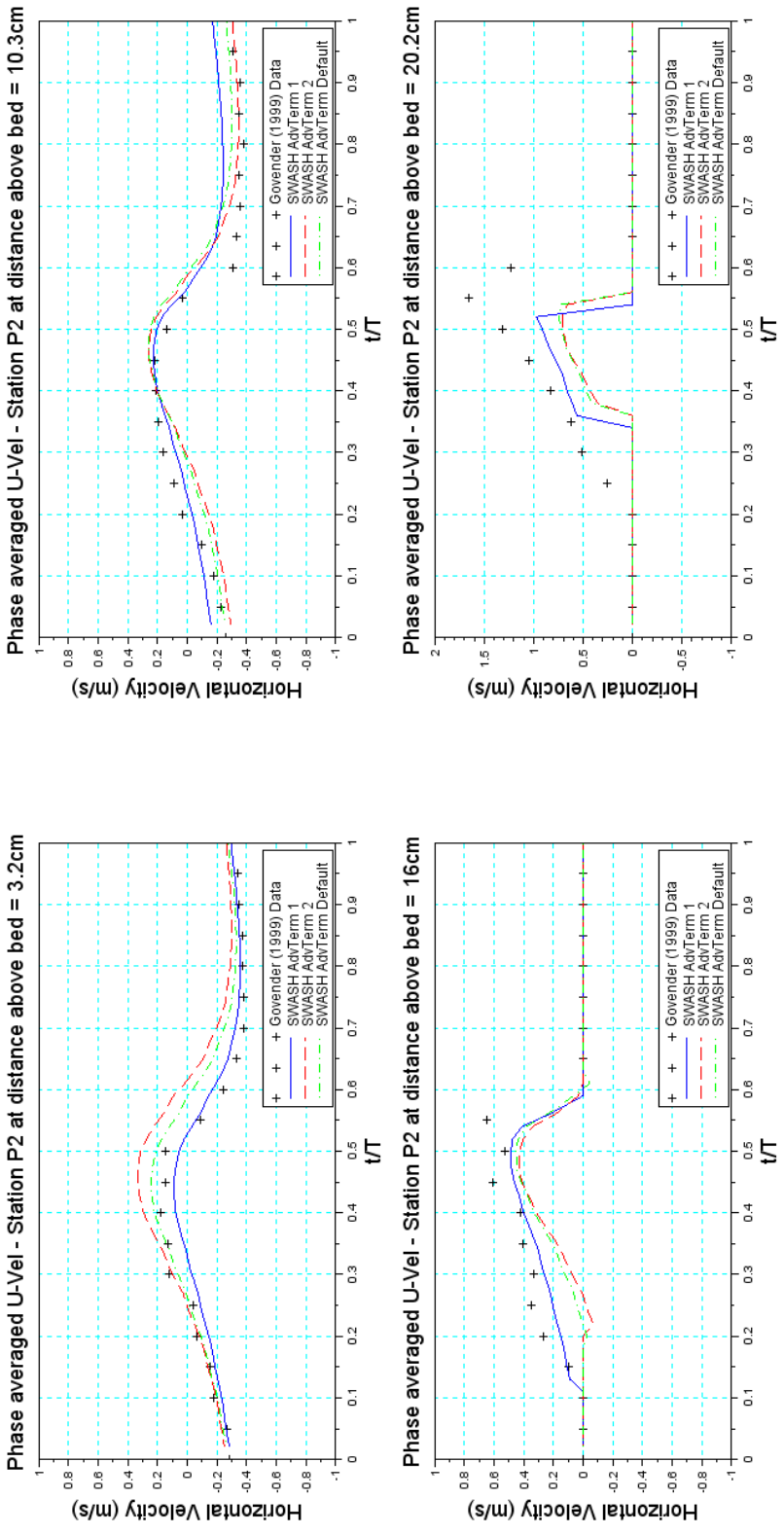

Figure A.58: Phase averaged horizontal velocity in the recorded Govender (1999) and SWASH modelled time series for various discretisation schemes at measuring Station P2 - Momentum not explicitly conserved

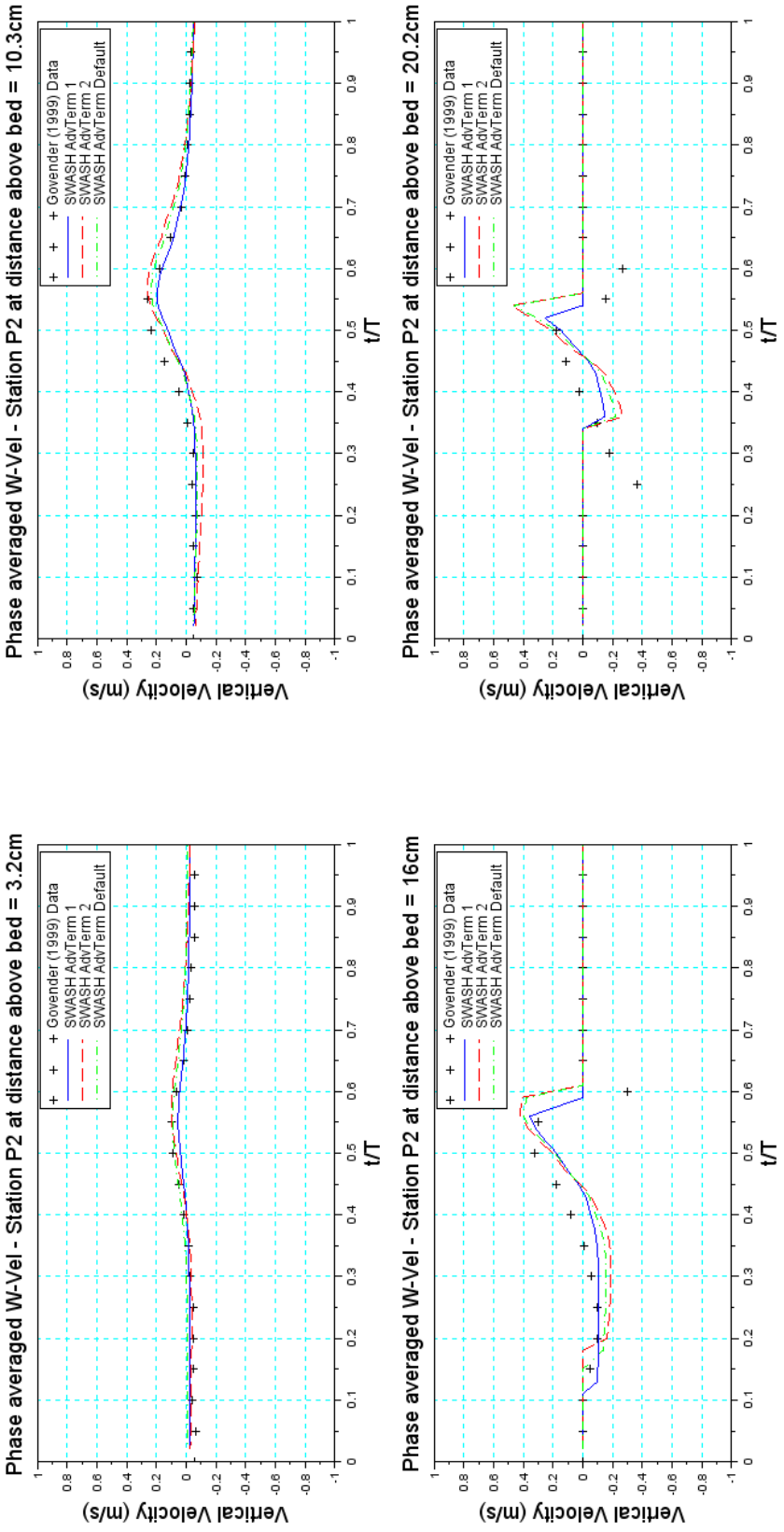

Figure A.59: Phase averaged vertical velocity in the recorded Govender (1999) and SWASH modelled time series for various discretisation schemes at measuring Station P2 - Momentum conserved

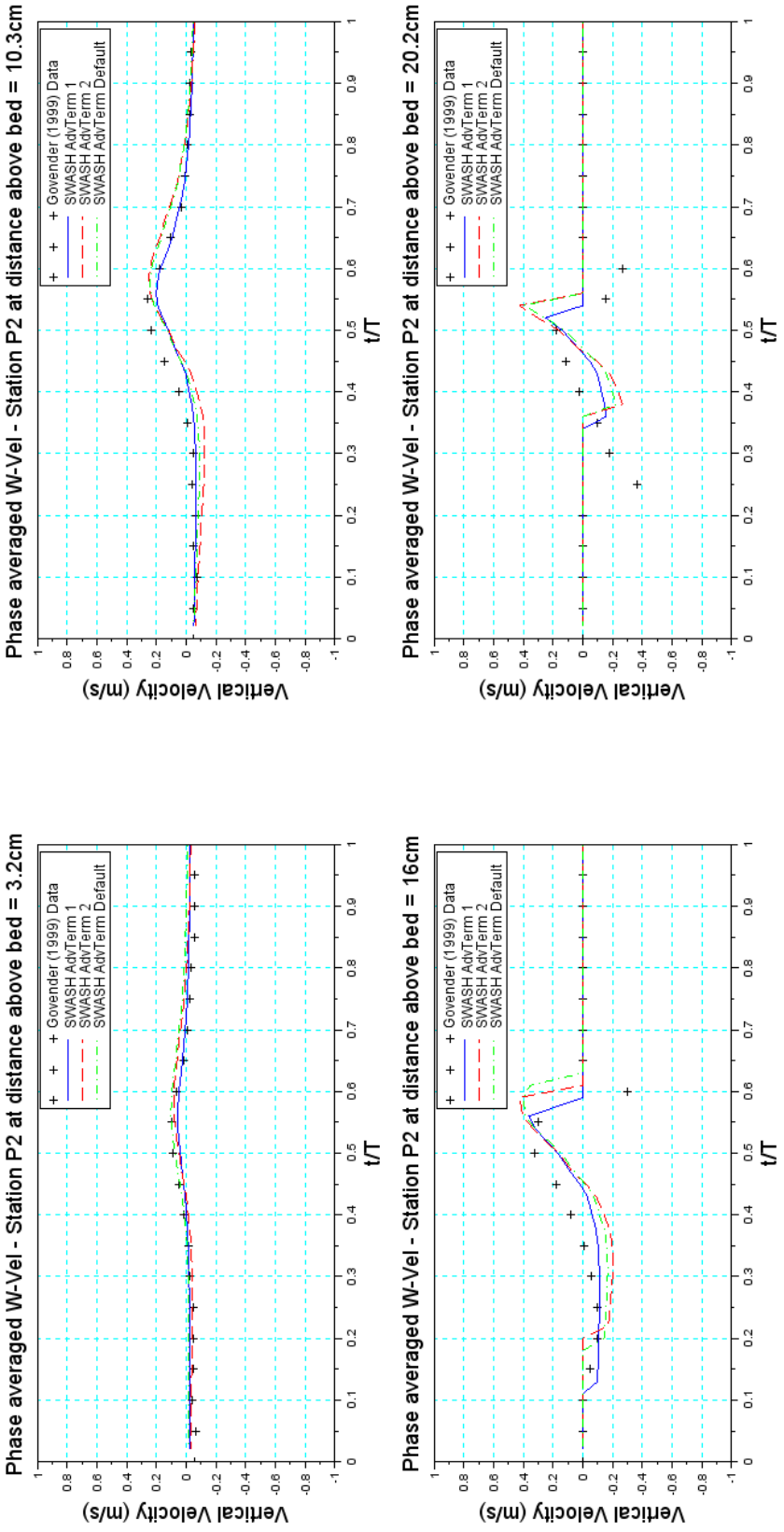

Figure A.60: Phase averaged vertical velocity in the recorded Govender (1999) and SWASH modelled time series for various discretisation schemes at measuring Station P2 - Momentum not explicitly conserved

A.2.4 Water depth in velocity points

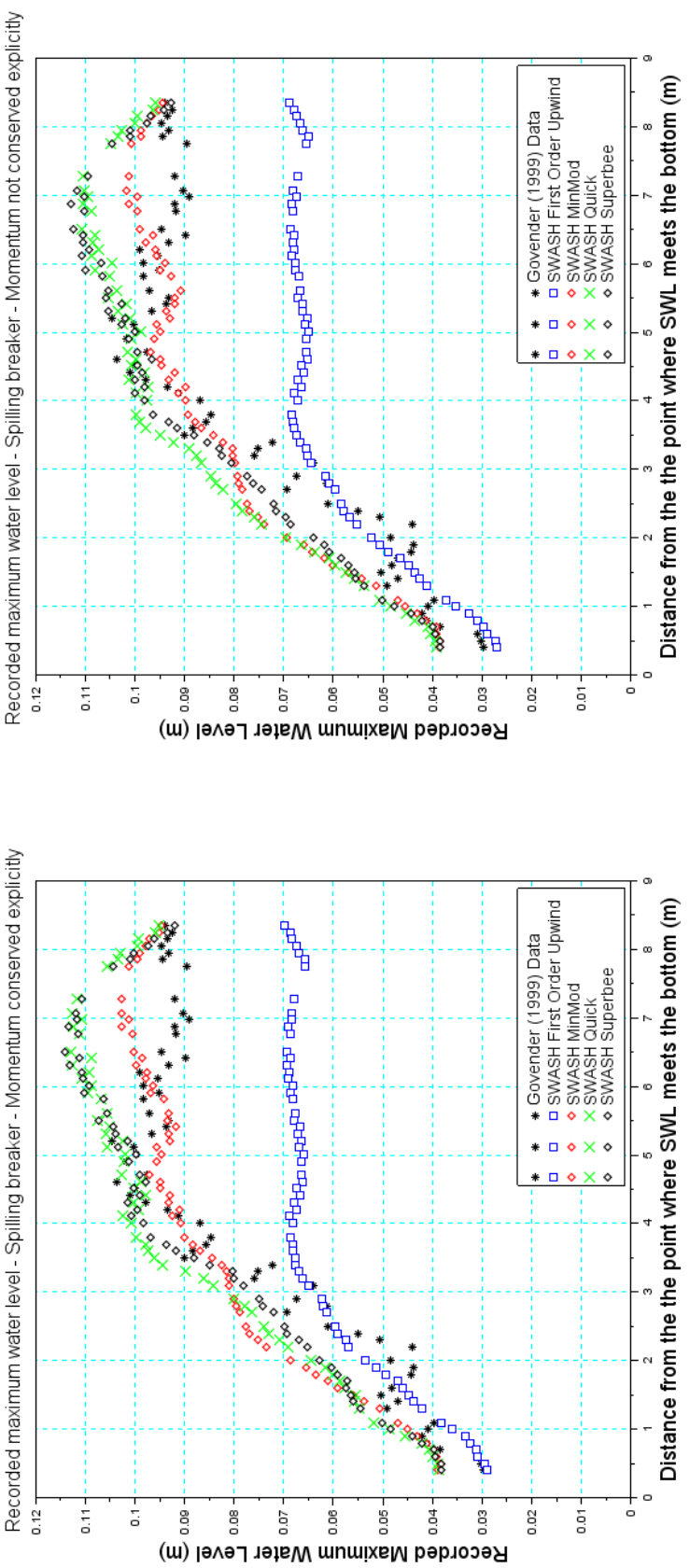

Figure A.61: Maximum wave heights in the recorded Govender (1999) and SWASH modelled time series for various higher order interpolation schemes measured in points cross-shore of the flume. Left panel shows wave heights with momentum conserved while the right panel shows wave heights without momentum conserved explicitly.

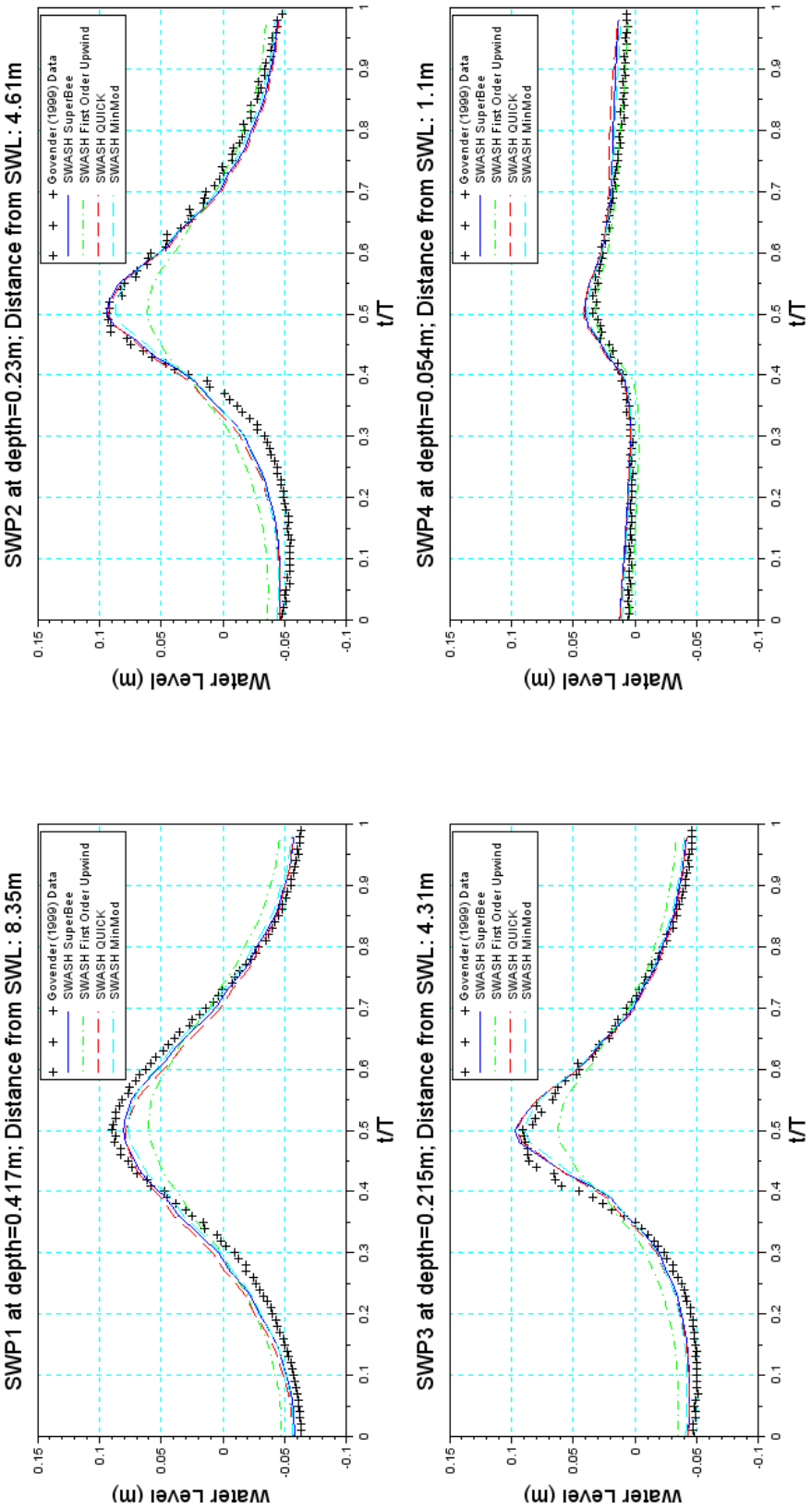

Figure A.62: Phase averaged wave heights in the recorded Govender (1999) and SWASH modelled time series for various higher order interpolation limiter schemes at four measuring points in the flume - Momentum conserved

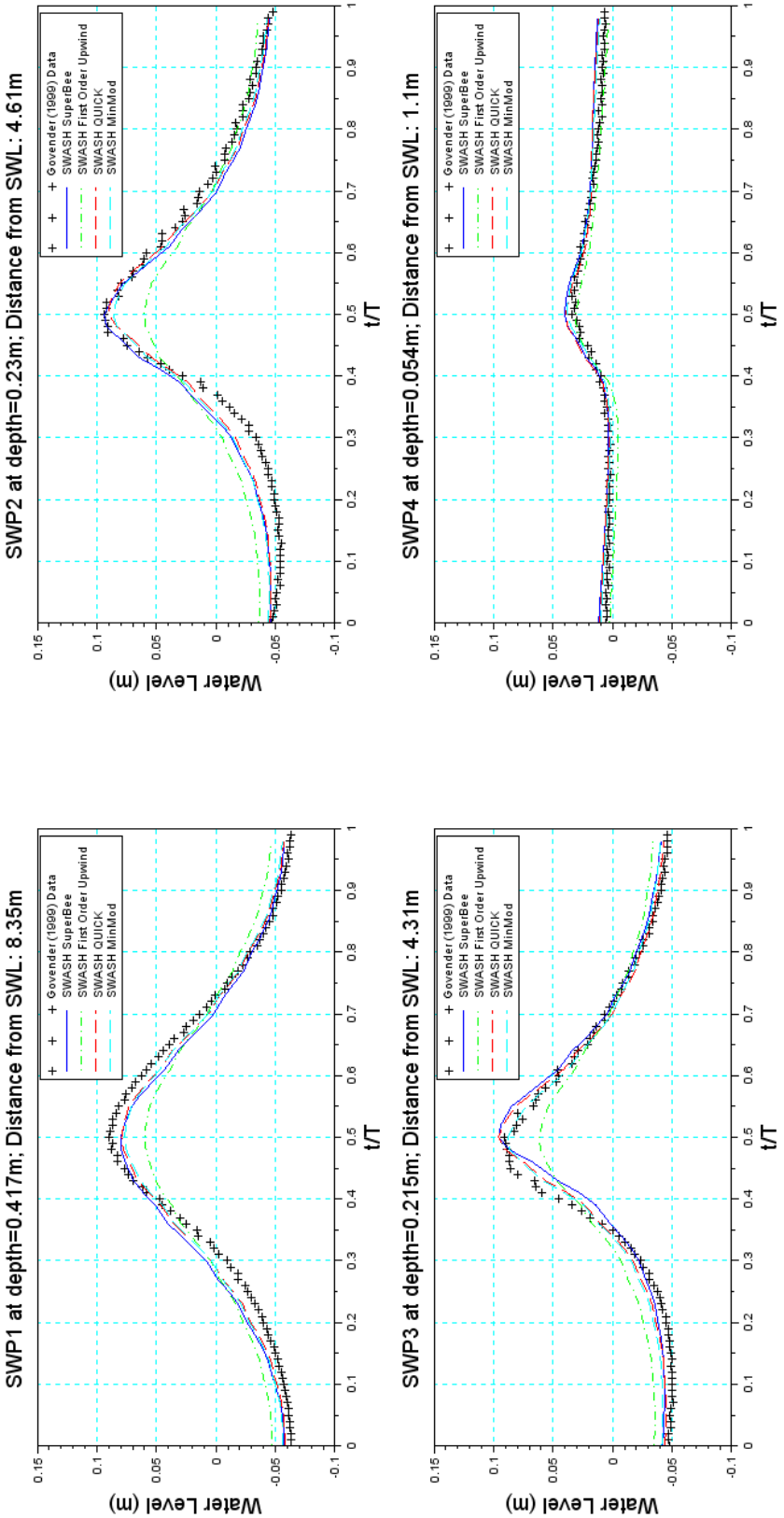

Figure A.63: Phase averaged wave heights in the recorded Govender (1999) and SWASH modelled time series for various higher order interpolation limiter schemes at four measuring points in the flume - Momentum not explicitly conserved

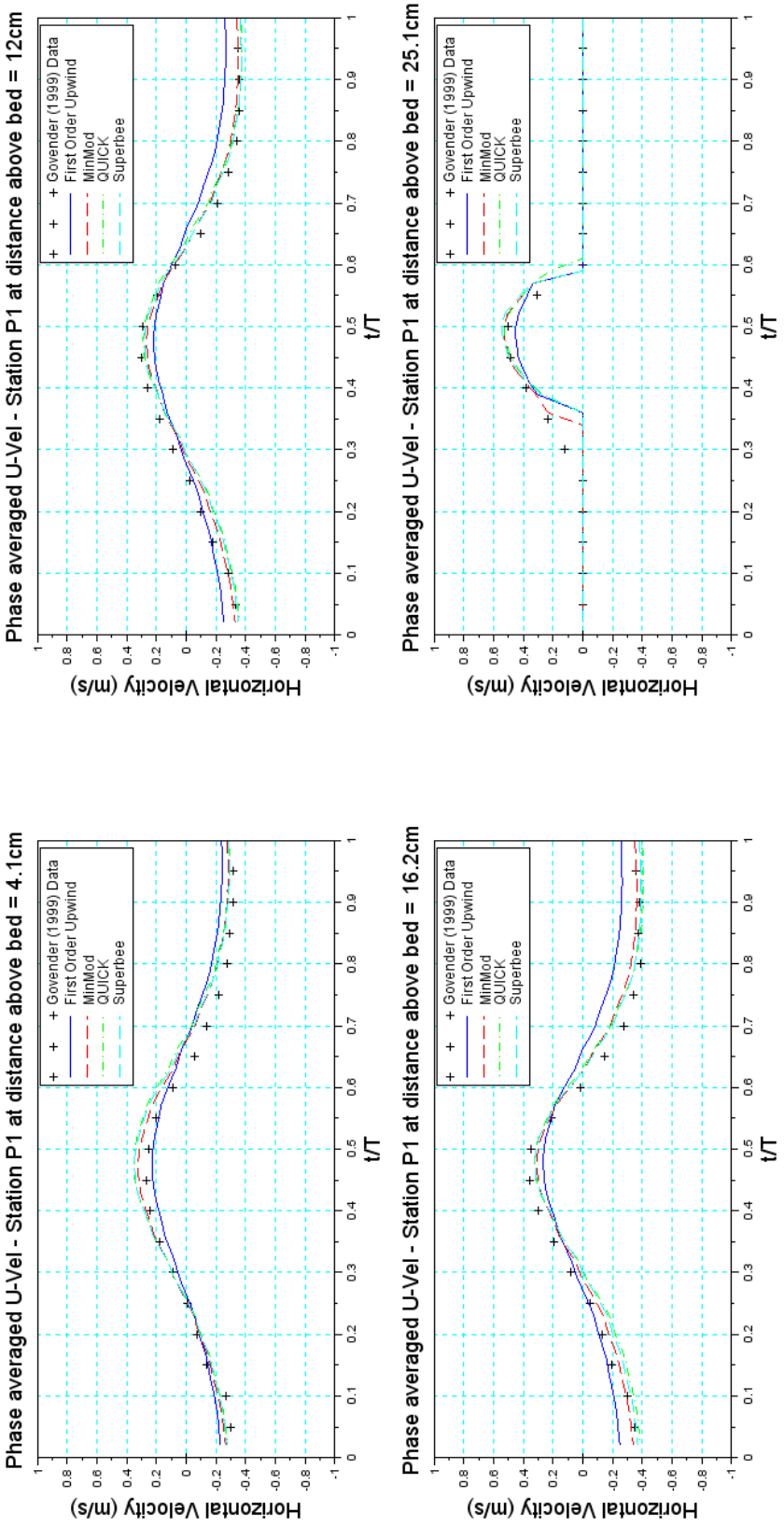

Figure A.64: Phase averaged horizontal velocity in the recorded Govender (1999) and SWASH modelled time series for various higher order interpolation limiter schemes at measuring Station P1 - Momentum conserved

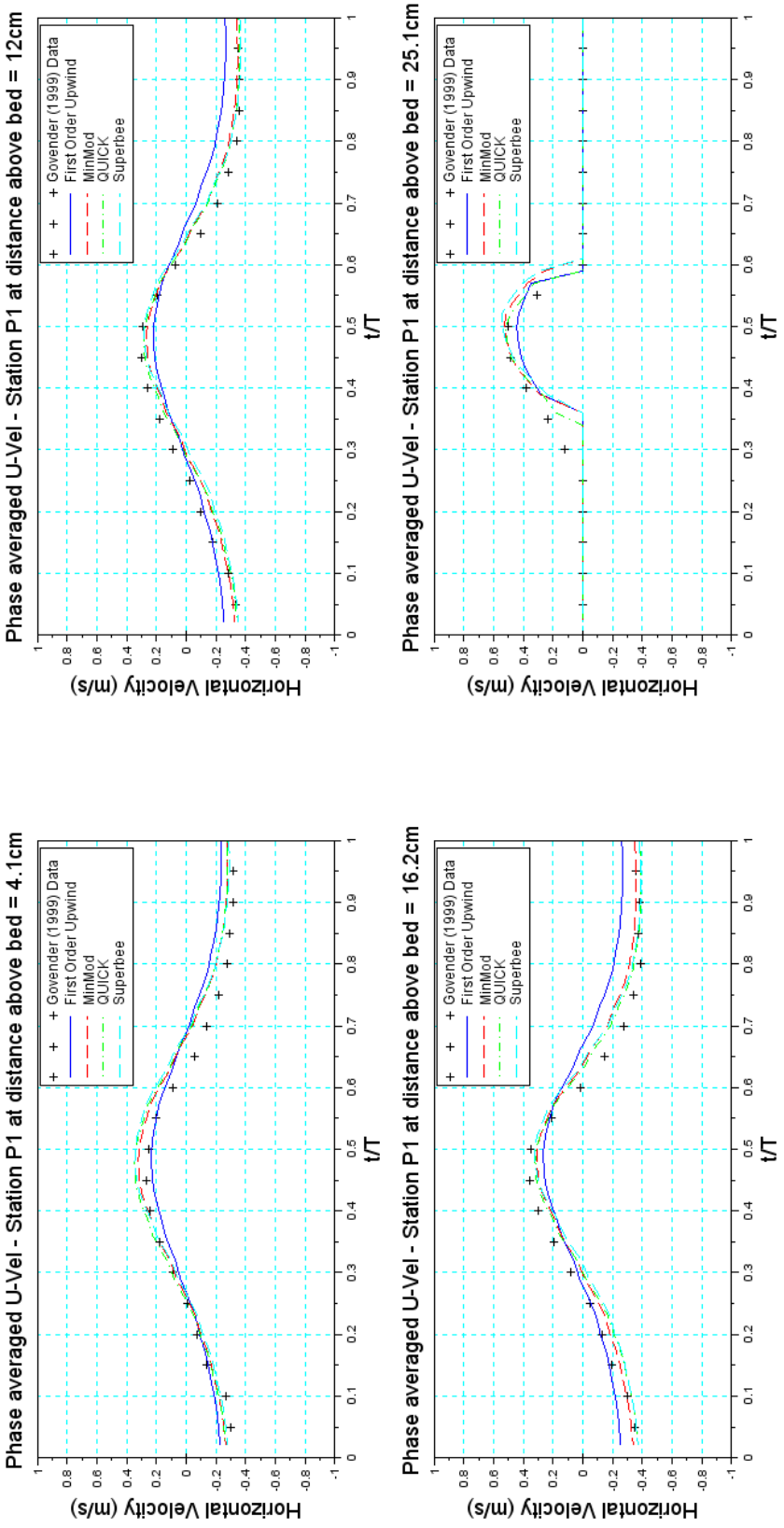

Figure A.65: Phase averaged horizontal velocity in the recorded Govender (1999) and SWASH modelled time series for various higher order interpolation limiter schemes at measuring Station P1 - Momentum not explicitly conserved

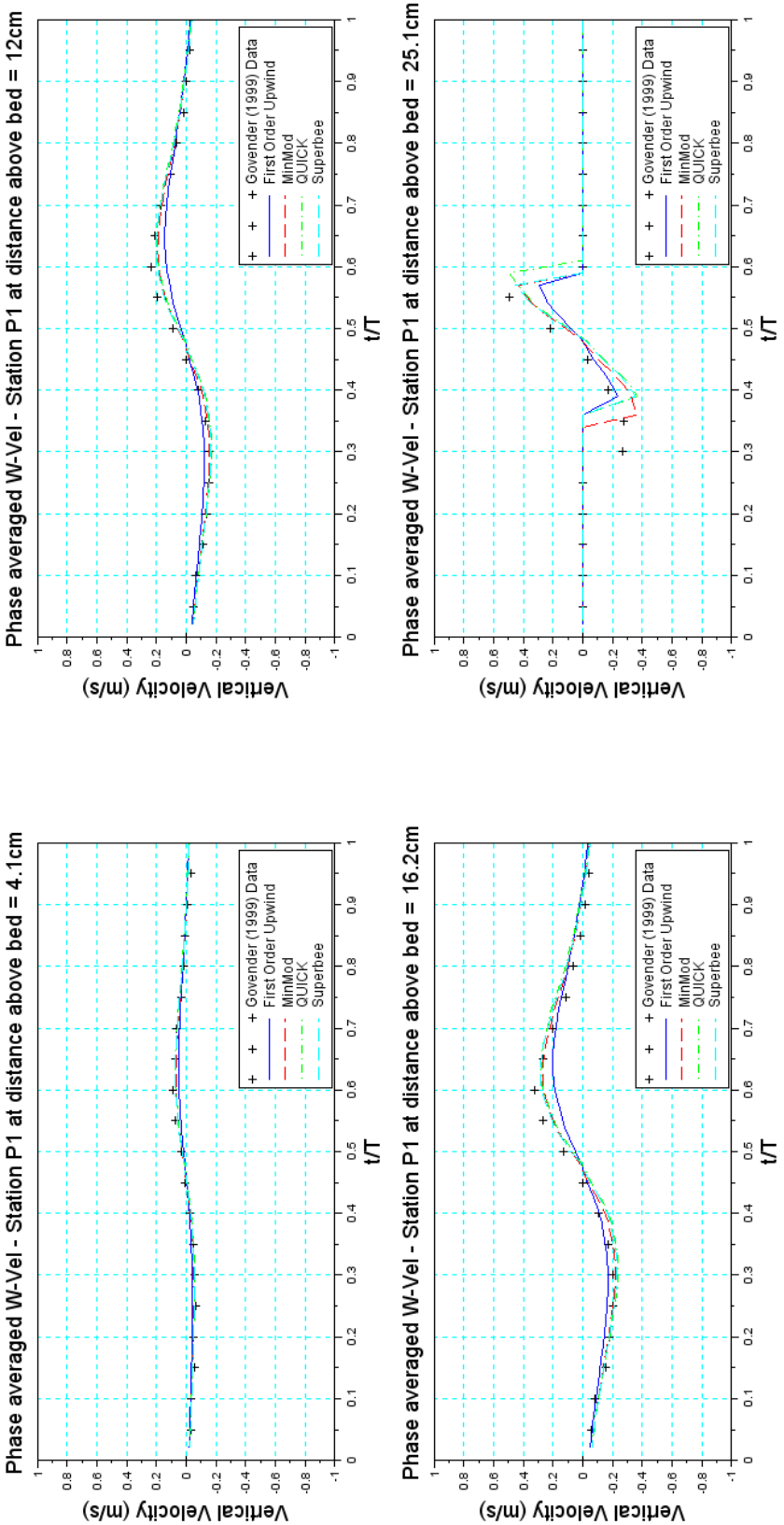

Figure A.66: Phase averaged vertical velocity in the recorded Govender (1999) and SWASH modelled time series for various higher order interpolation limiter schemes at measuring Station P1 - Momentum conserved

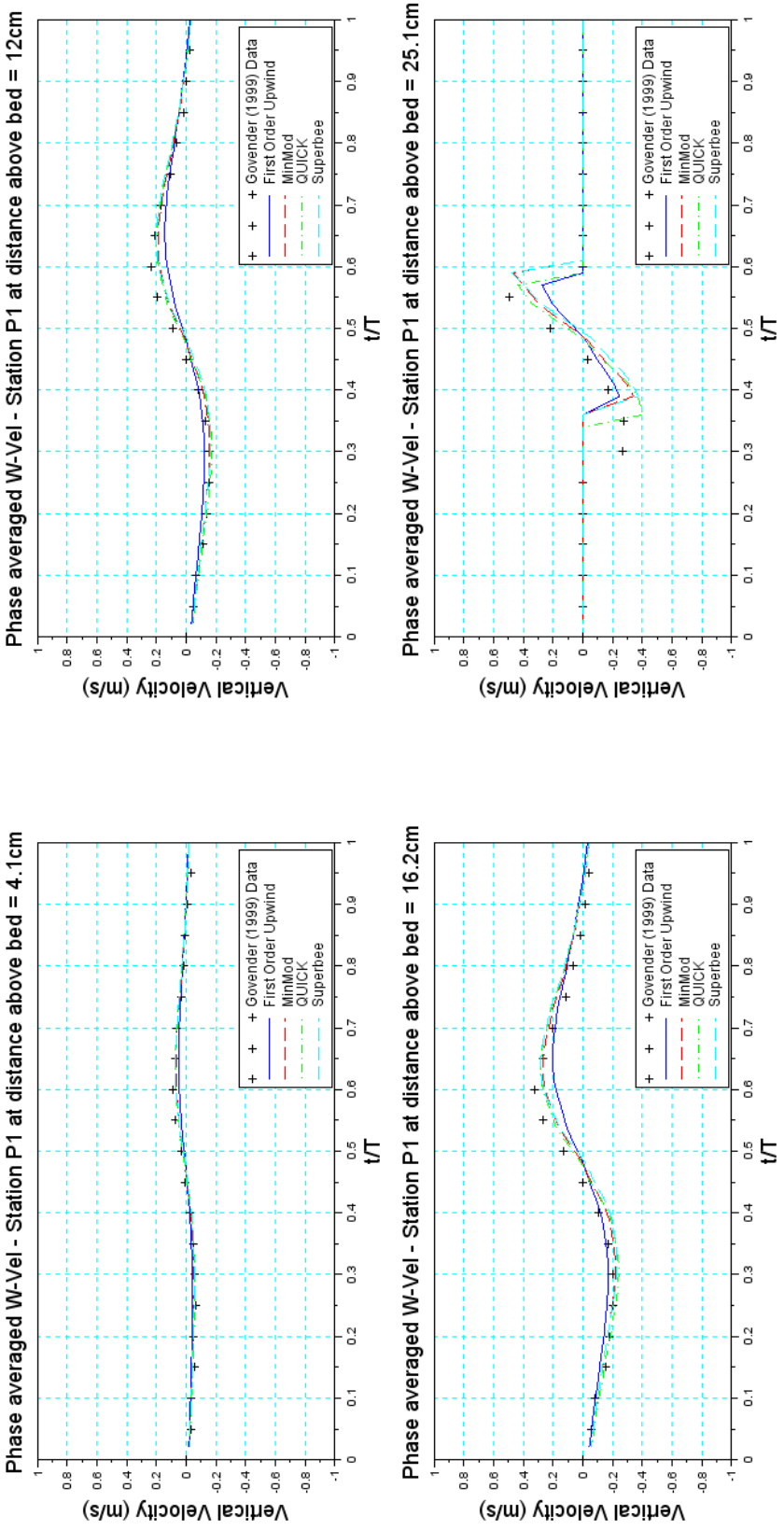

Figure A.67: Phase averaged vertical velocity in the recorded Govender (1999) and SWASH modelled time series for various higher order interpolation limiter schemes at measuring Station P1 - Momentum not explicitly conserved

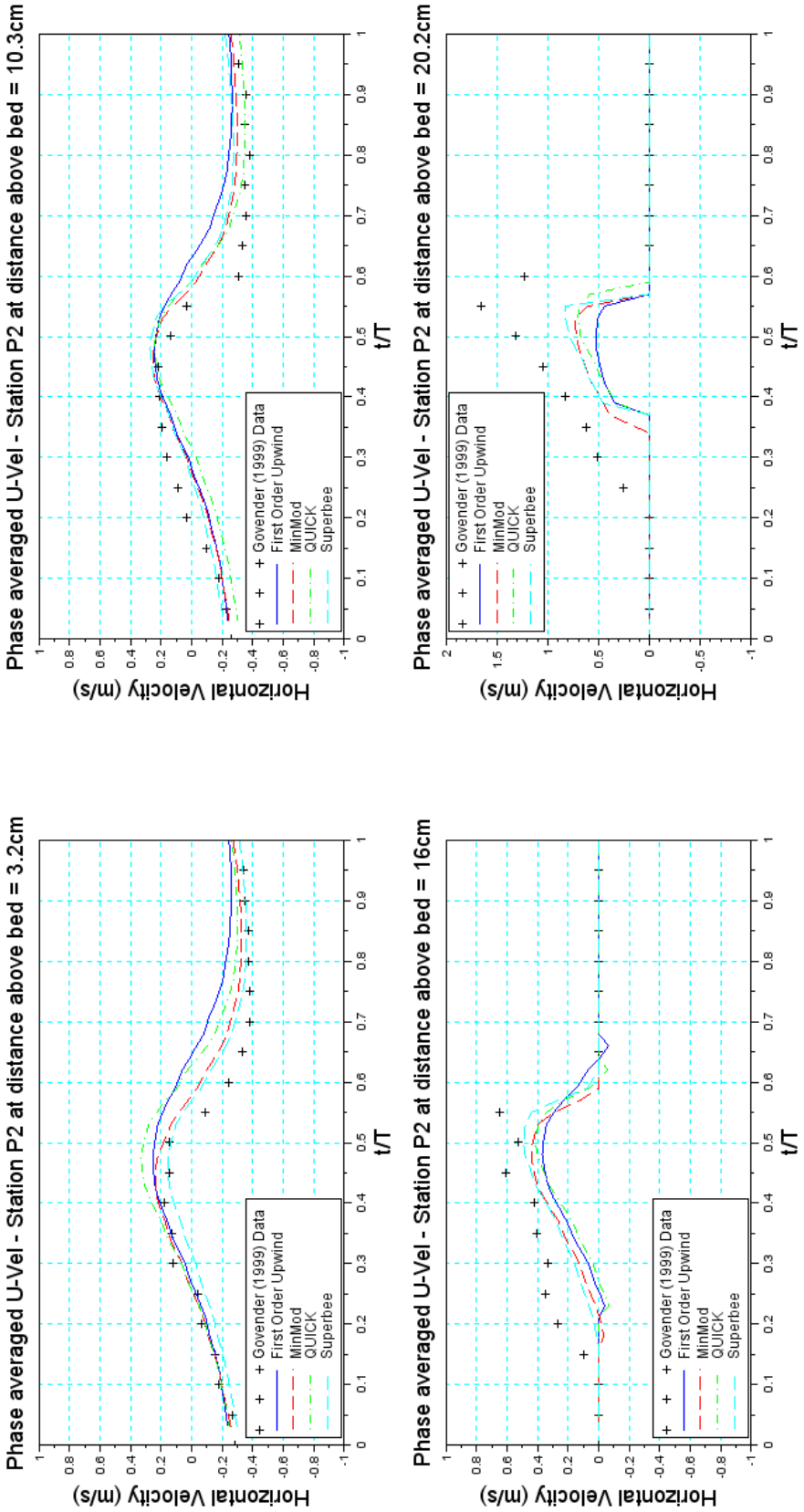

Figure A.68: Phase averaged horizontal velocity in the recorded Govender (1999) and SWASH modelled time series for various higher order interpolation limiter schemes at measuring Station P2 - Momentum conserved

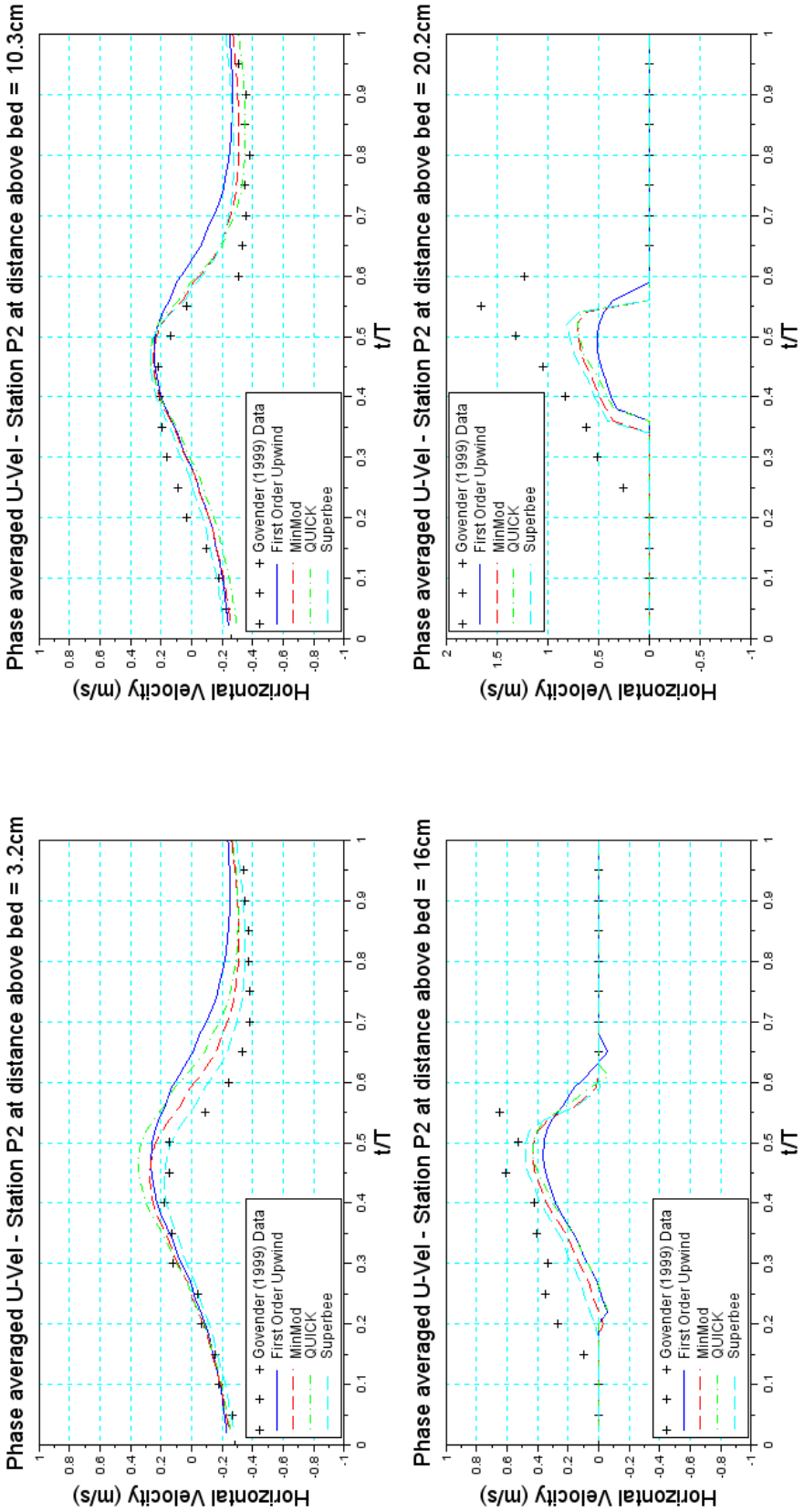

Figure A.69: Phase averaged horizontal velocity in the recorded Govender (1999) and SWASH modelled time series for various higher order interpolation limiter schemes at measuring Station P2 - Momentum not explicitly conserved

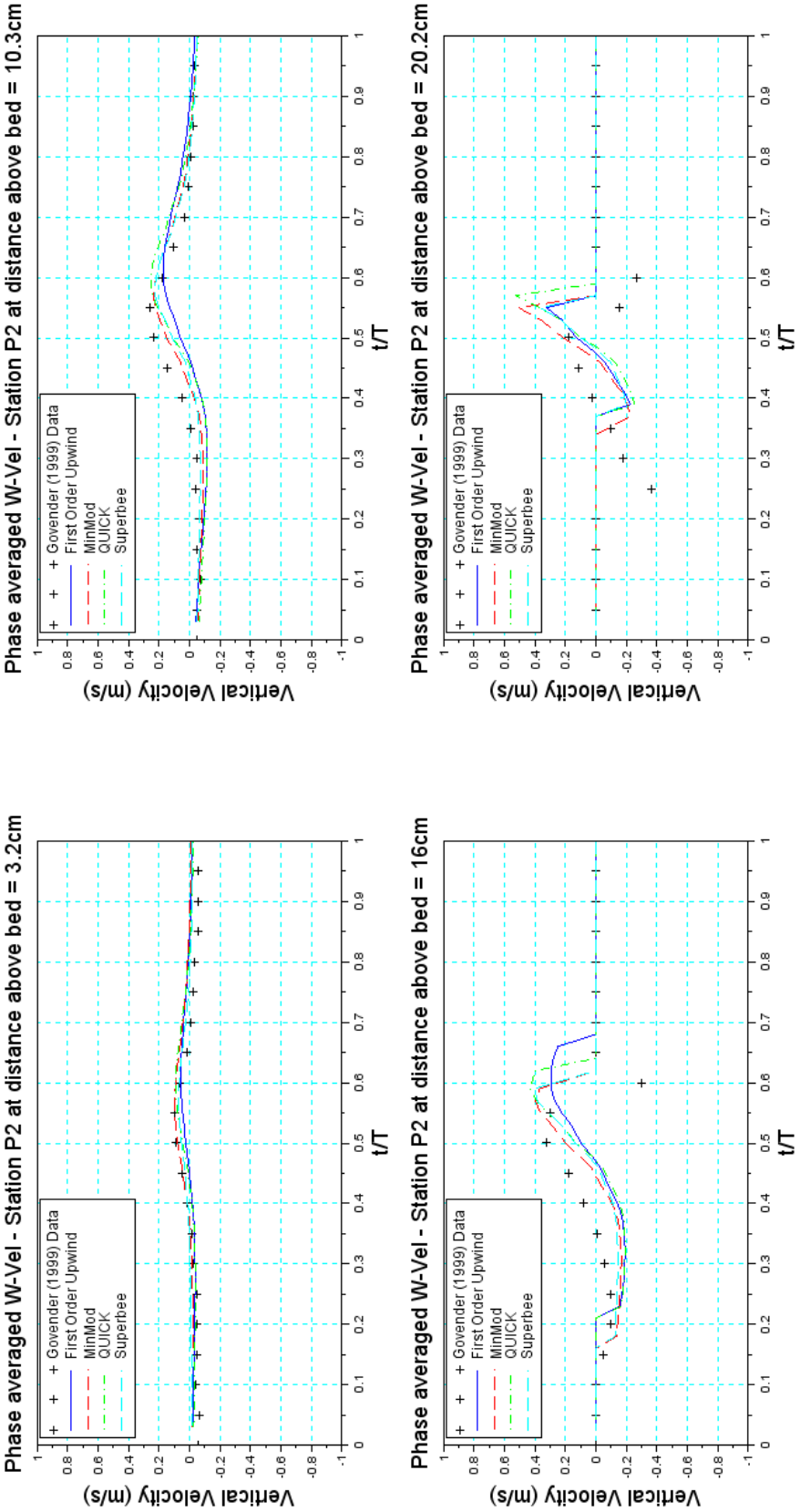

Figure A.70: Phase averaged vertical velocity in the recorded Govender (1999) and SWASH modelled time series for various higher order interpolation limiter schemes at measuring Station P2 - Momentum conserved

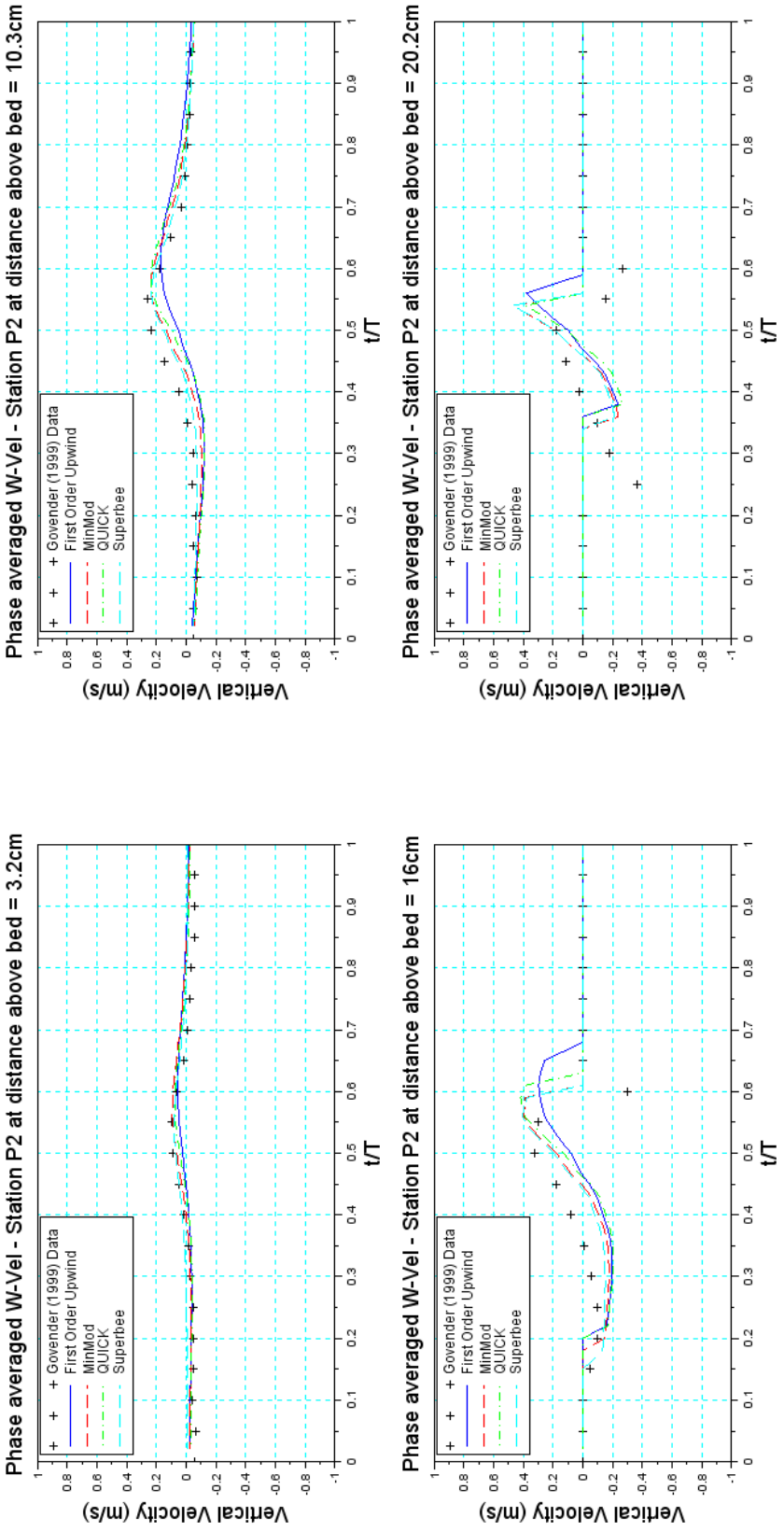

Figure A.71: Phase averaged vertical velocity in the recorded Govender (1999) and SWASH modelled time series for various higher order interpolation limiter schemes at measuring Station P2 - Momentum not explicitly conserved

Appendix B

Figures: Chapter 6

B.1 Simulation results: Water levels

B.1.1 Incipient breaking point

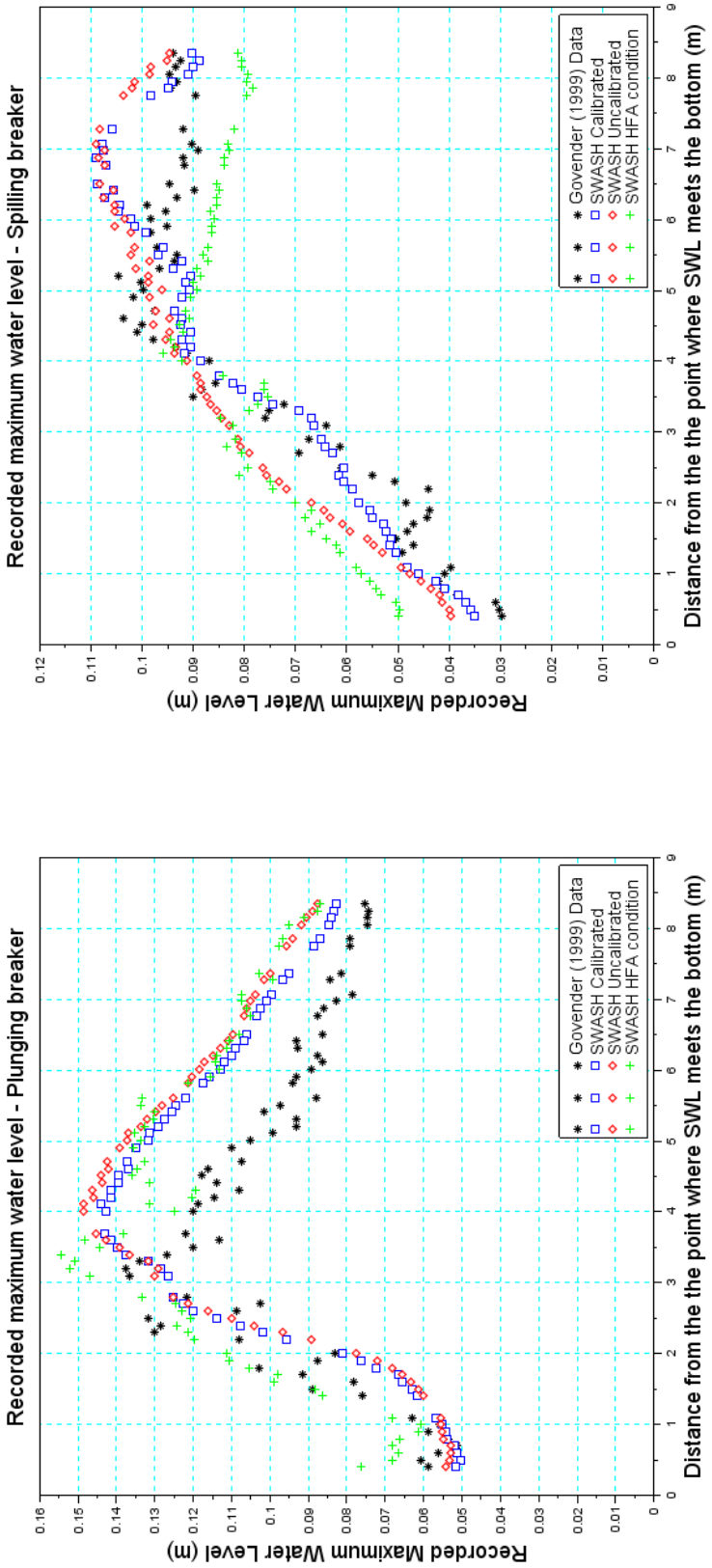

Figure B.1: Measured Govender (1999) maximum water level data compared to the SWASH numerical models

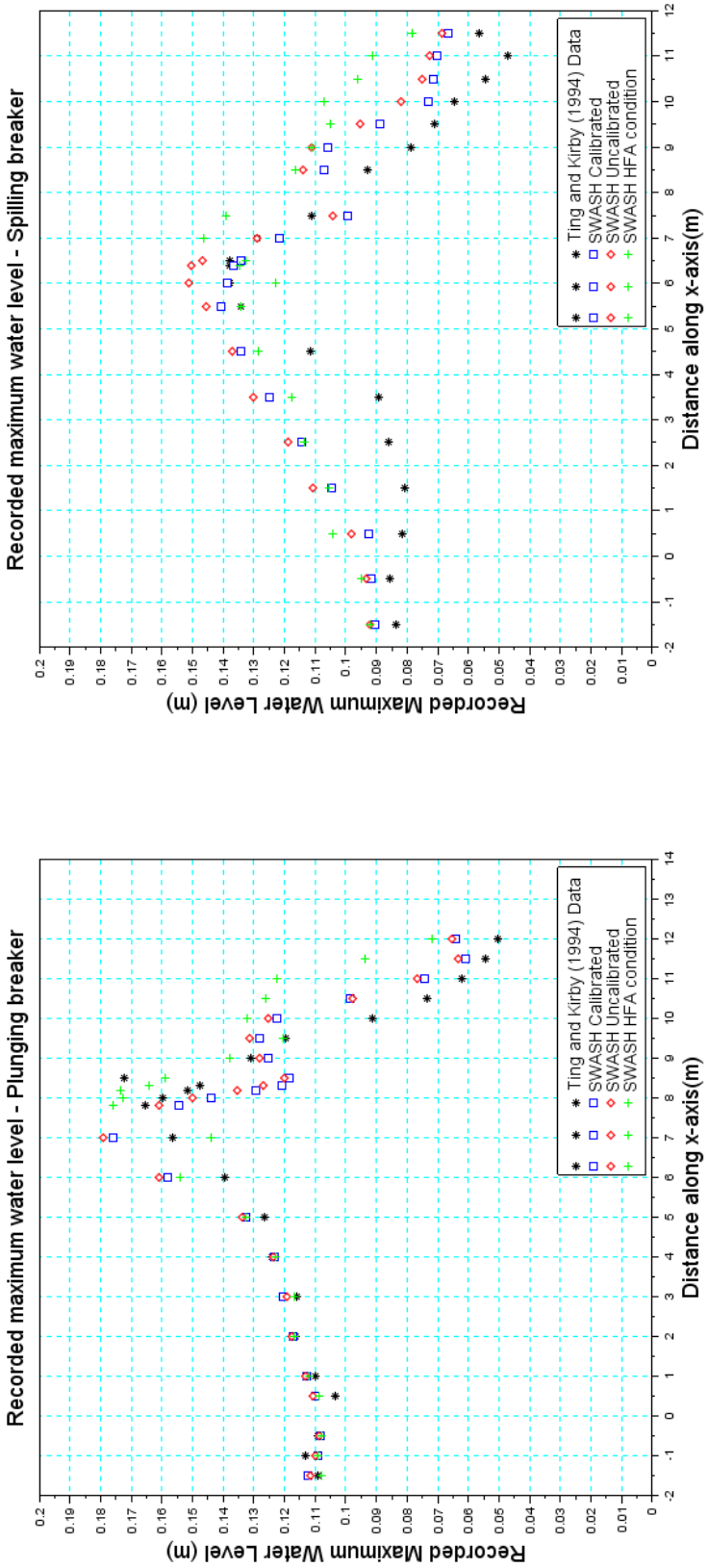

Figure B.2: Measured Ting and Kirby (1994) maximum water level data compared to the SWASH numerical models

B.1.2 Breaker depth Index

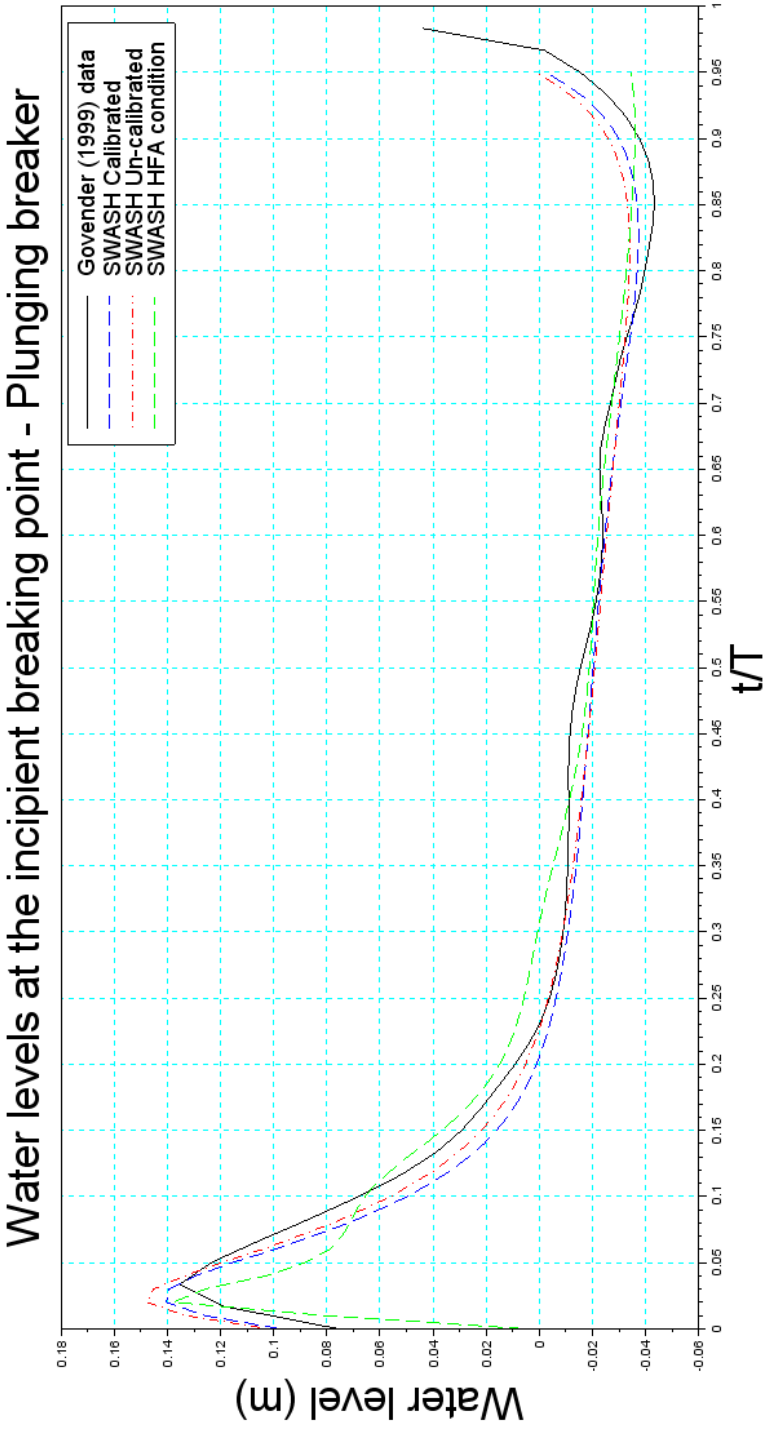

Figure B.3: Measured Govender (1999) water level data compared to the SWASH numerical models for a single plunging wave at incipient breaking.

B.1.3 Phase averaged water levels

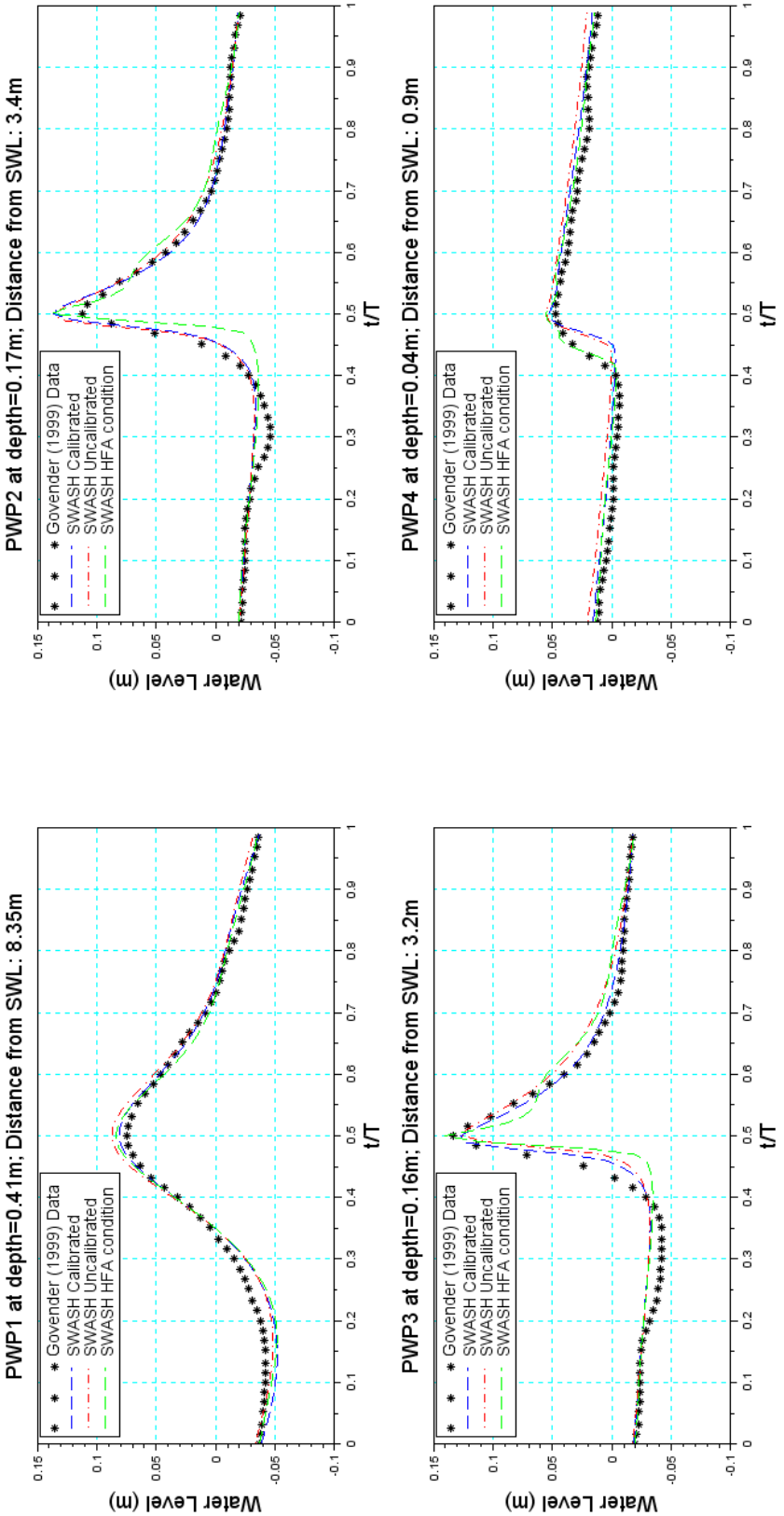

Figure B.4: Phase averaged plunging wave heights in the recorded Govender (1999) and SWASH modelled time series at four measuring points in the flume

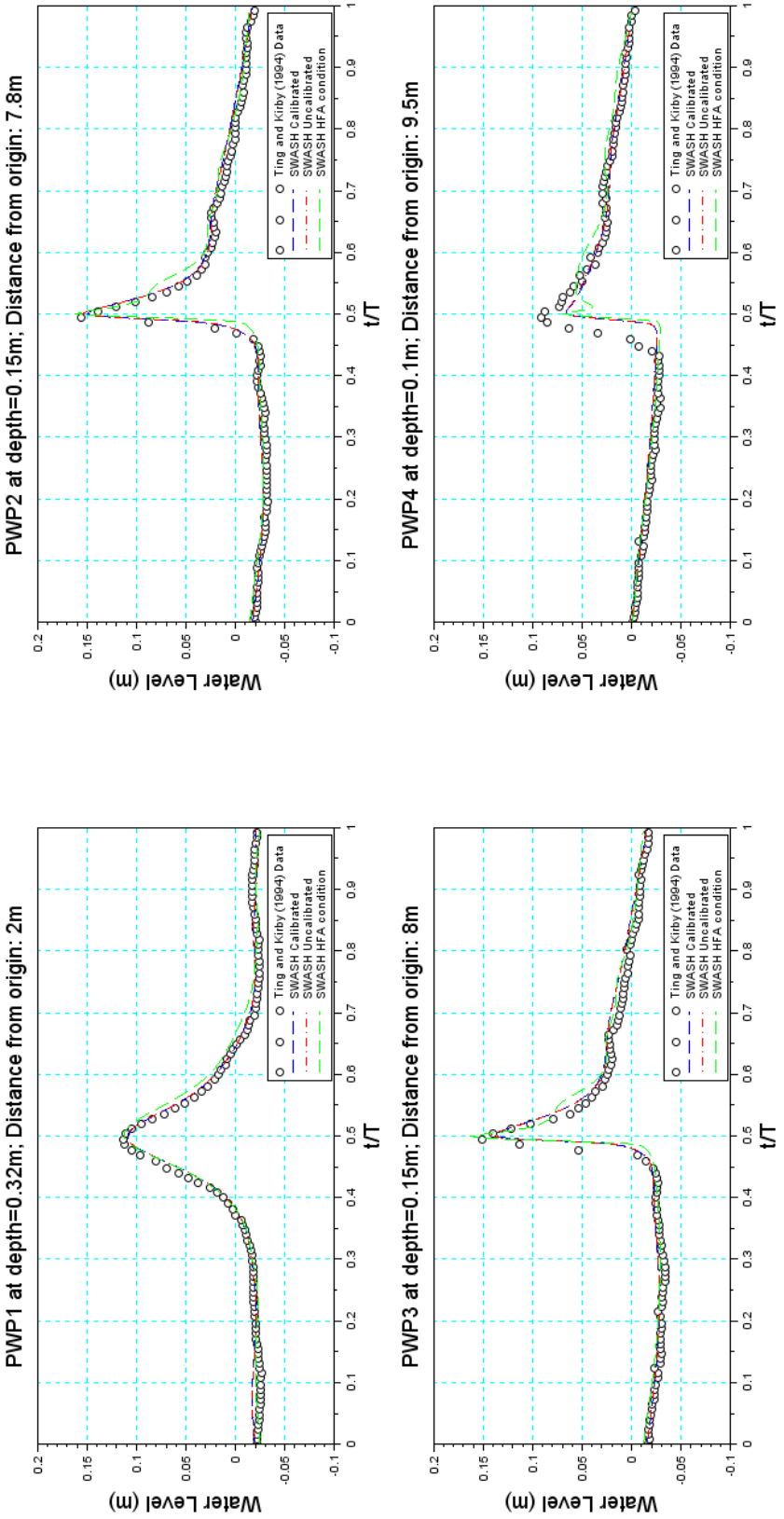

Figure B.5: Phase averaged plunging wave heights in the recorded Ting and Kirby (1994) and SWASH modelled time series at four measuring points in the flume

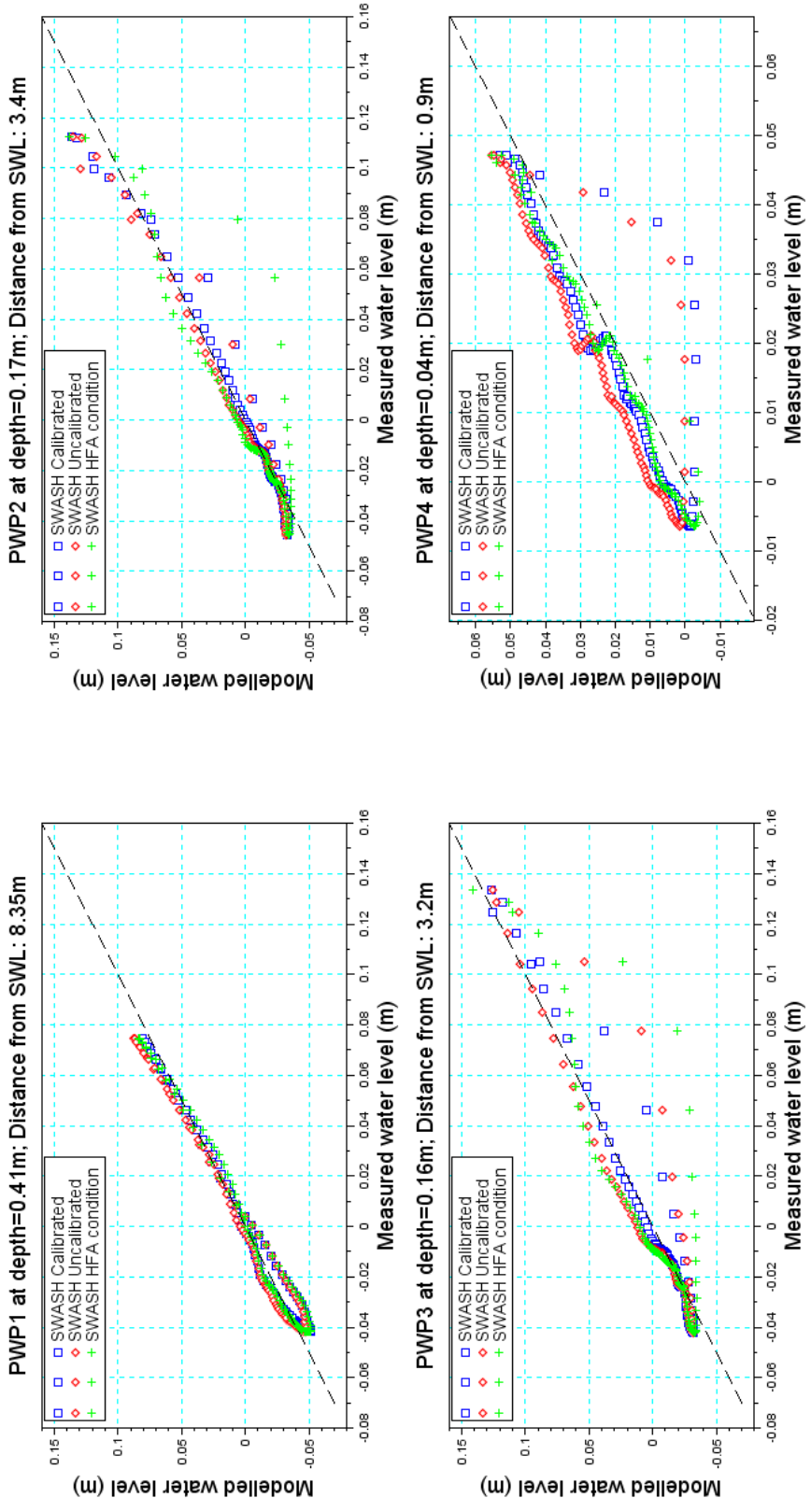

Figure B.6: Measured vs. modelled plunging wave heights in the recorded Govender (1999) and SWASH modelled time series at four measuring points in the flume

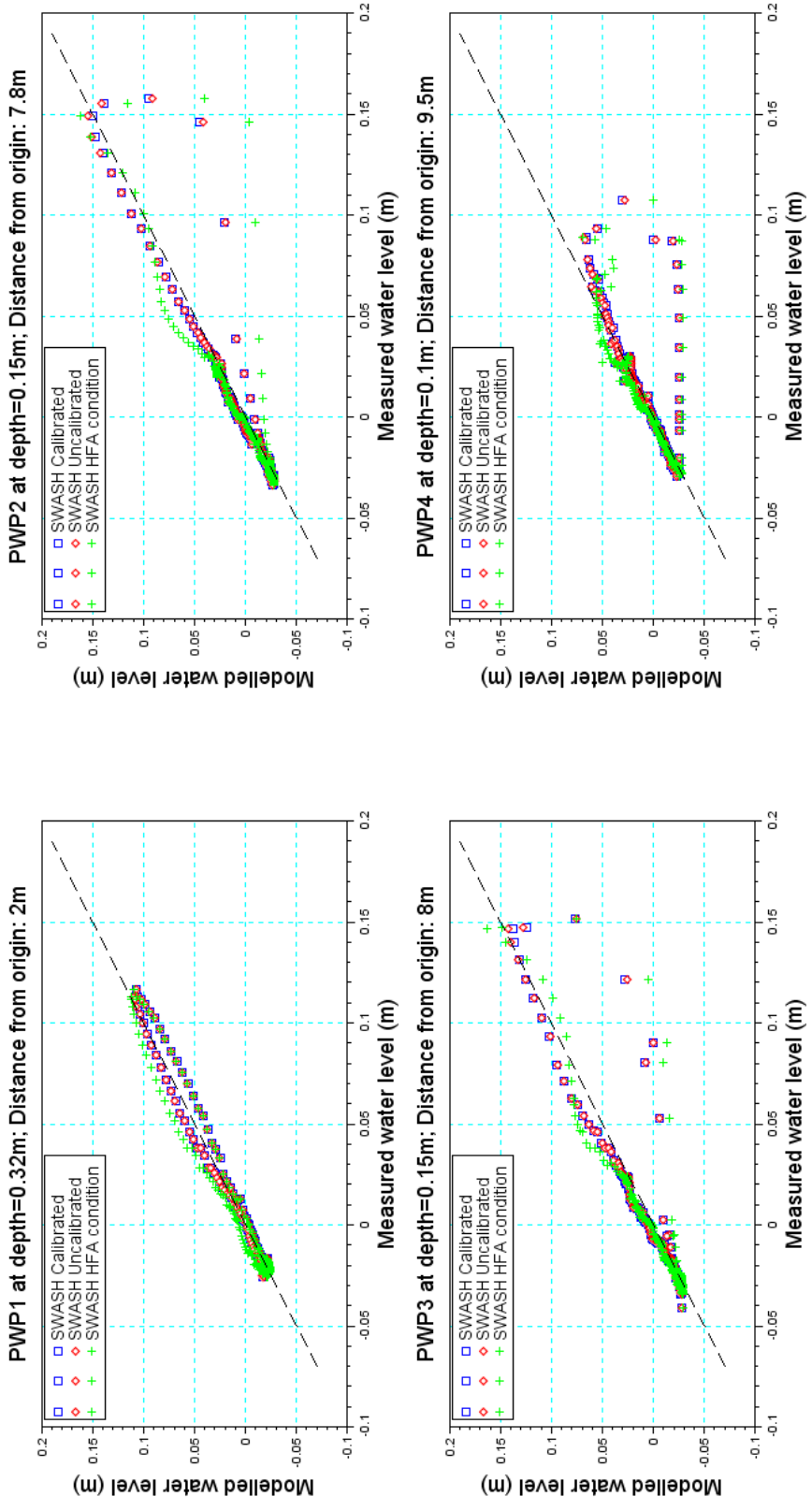

Figure B.7: Measured vs. modelled plunging wave heights in the recorded Ting and Kirby (1994) and SWASH modelled time series at four measuring points in the flume

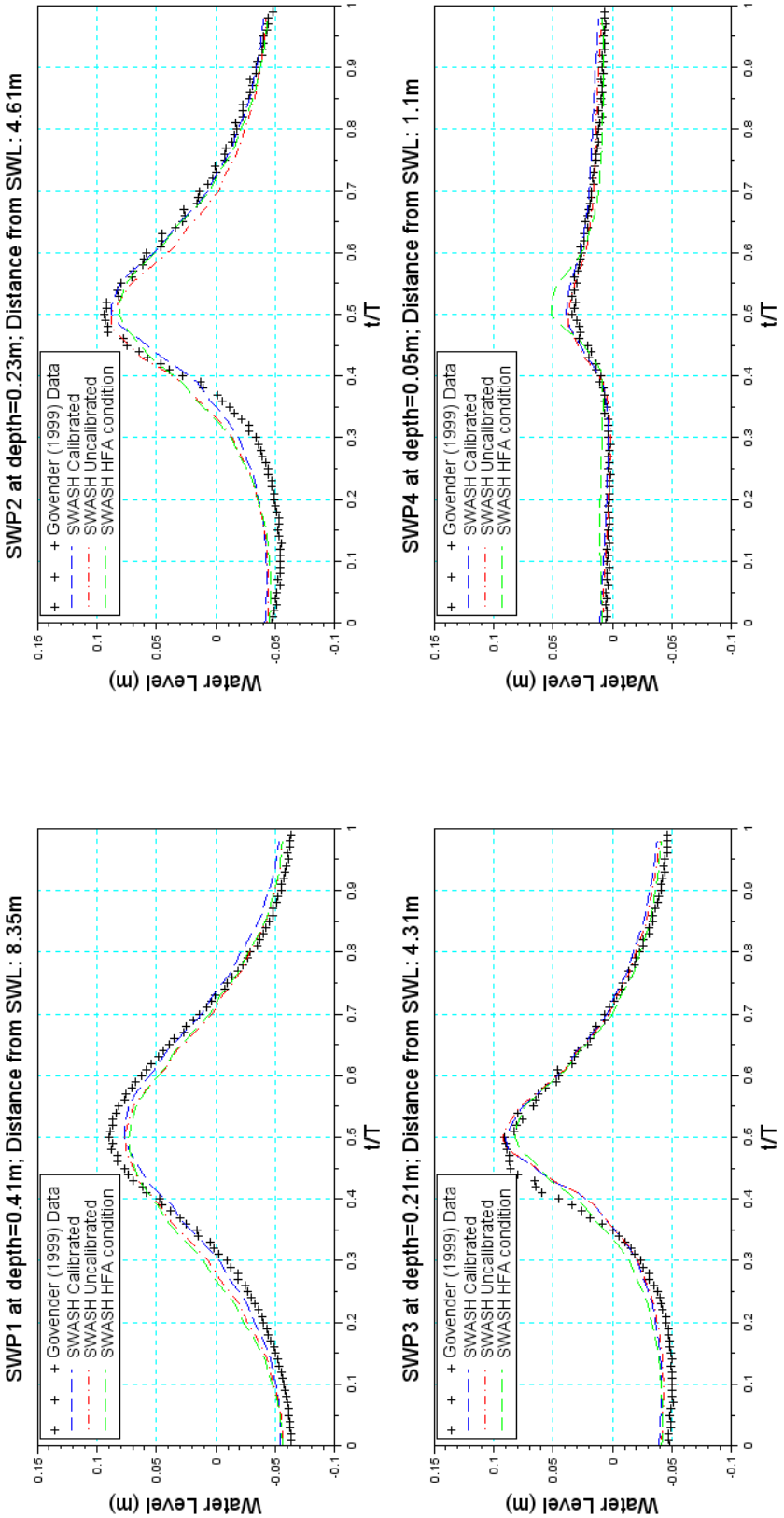

Figure B.8: Phase averaged spilling wave heights in the recorded Govender (1999) and SWASH modelled time series at four measuring points in the flume

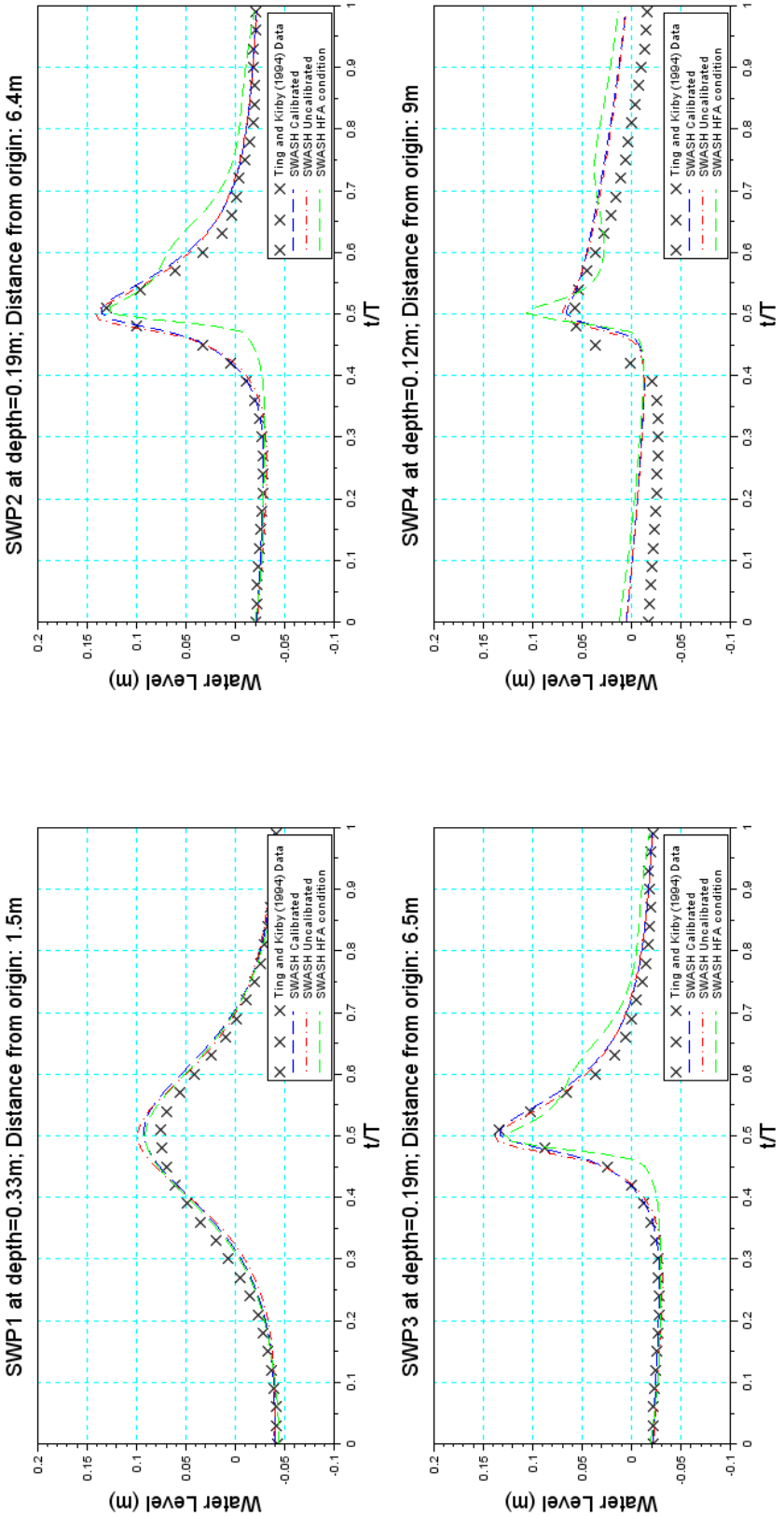

Figure B.9: Phase averaged spilling wave heights in the recorded Ting and Kirby (1994) and SWASH modelled time series at four measuring points in the flume

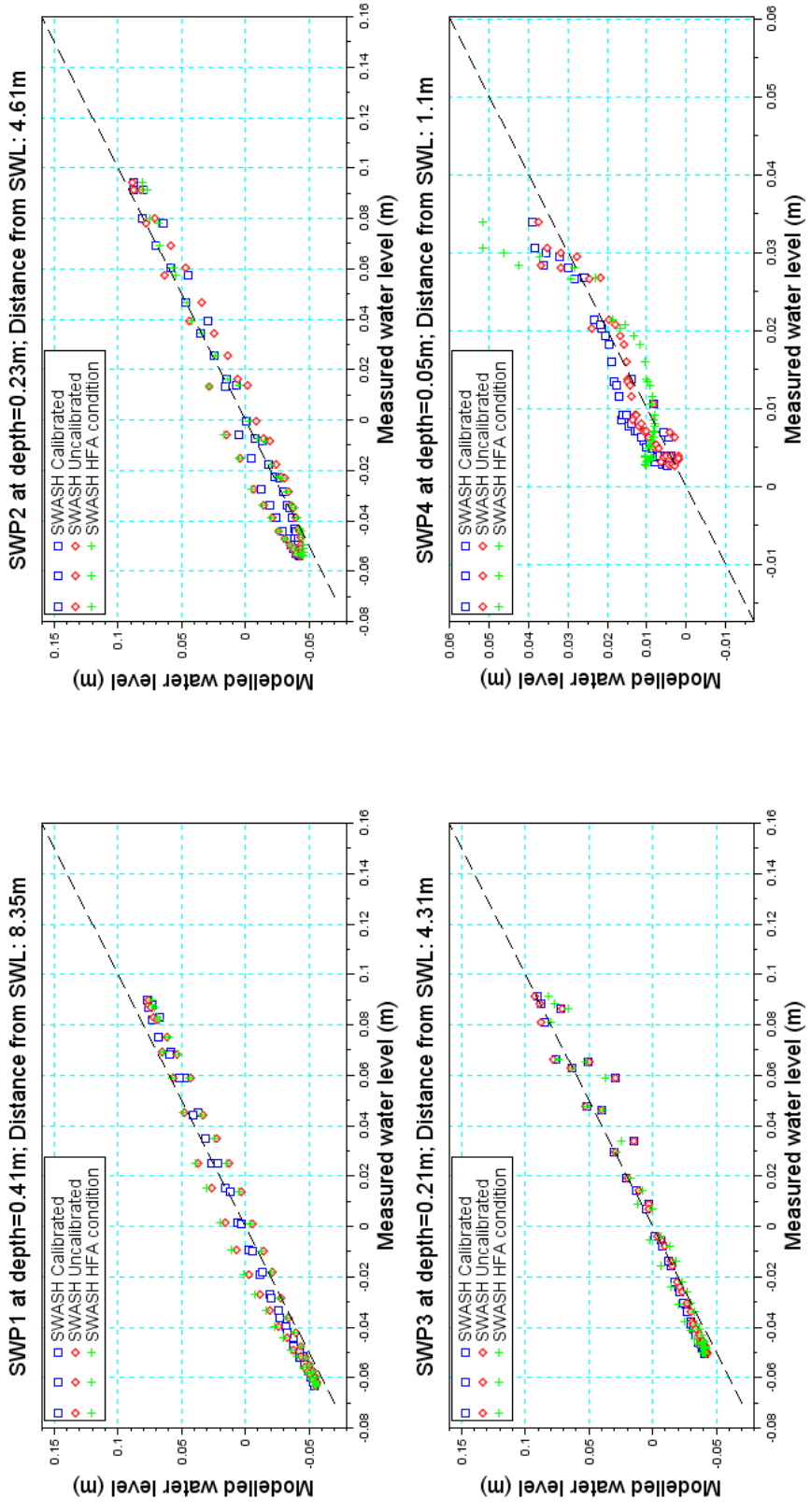

Figure B.10: Measured vs. modelled spilling wave heights in the recorded Govender (1999) and SWASH modelled time series at four measuring points in the flume

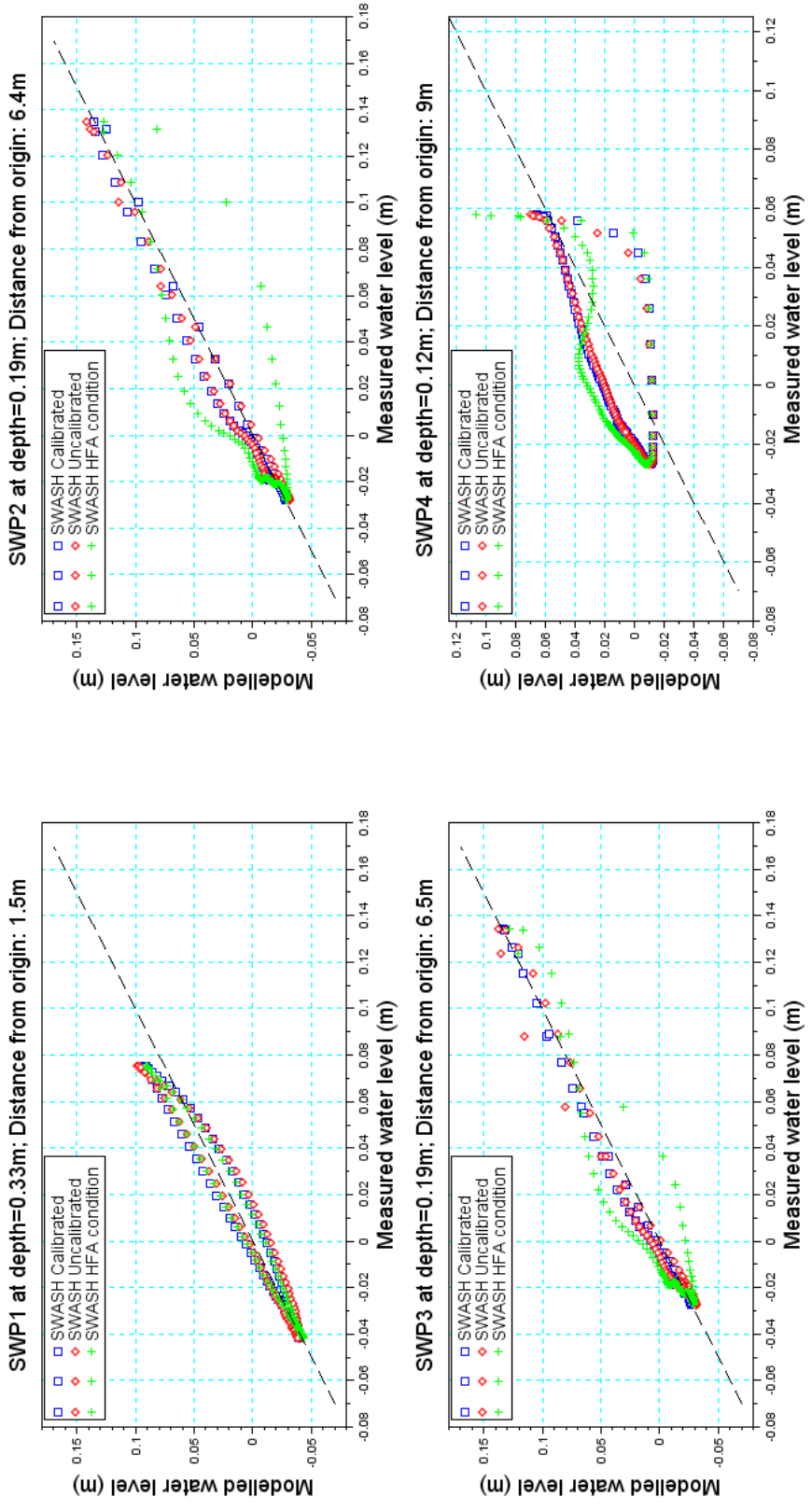

Figure B.11: Measured vs. modelled spilling wave heights in the recorded Ting and Kirby (1994) and SWASH modelled time series at four measuring points in the flume

B.1.4 Wave Setup and Setdown

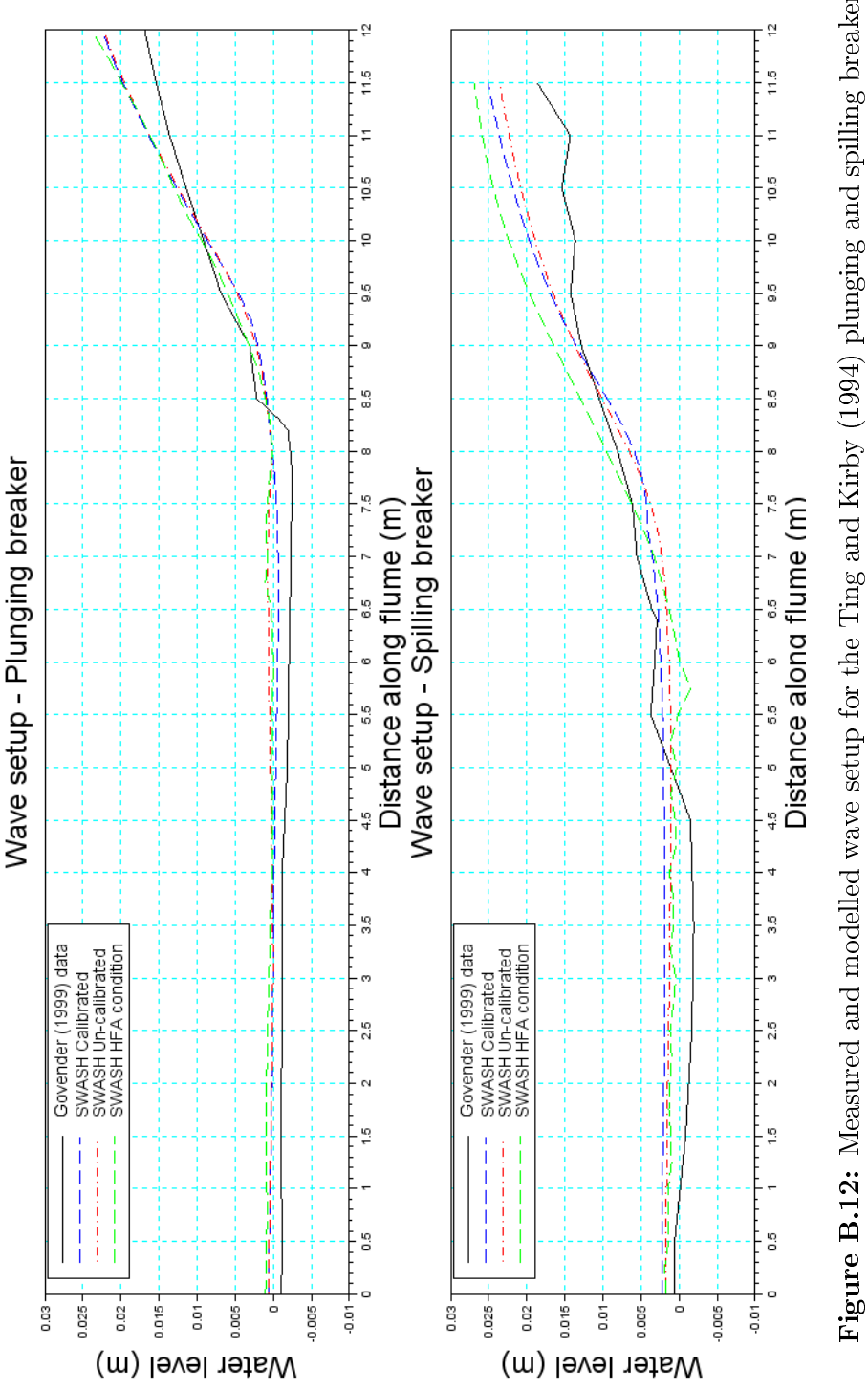

Figure B.12: Measured and modelled wave setup for the Ting and Kirby (1994) plunging and spilling breakers

B.2 Simulation results: Velocity

B.2.1 Phase averaged plunging wave comparison

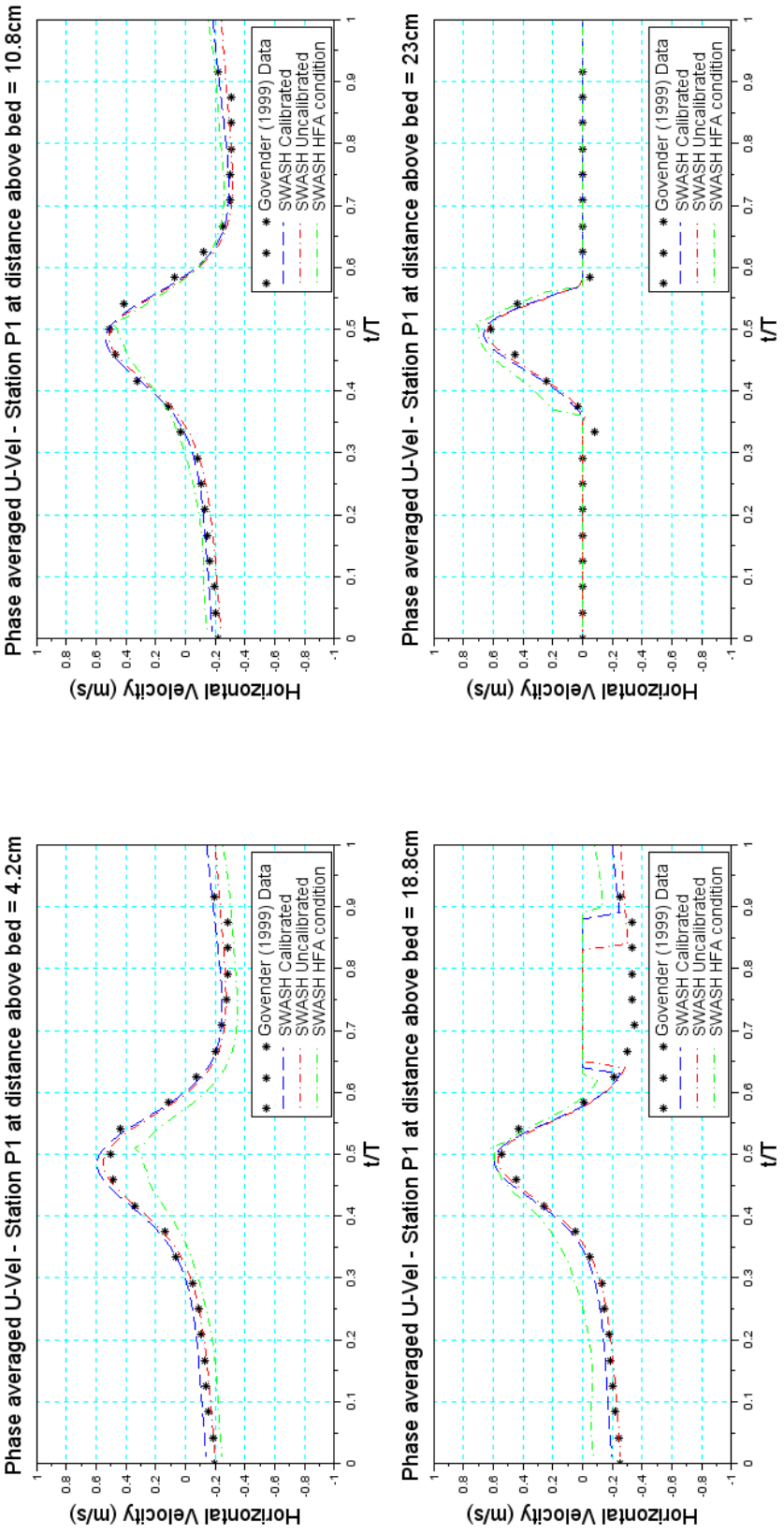

Figure B.13: Govender (1999) vs. SWASH modelled phase averaged horizontal velocity before plunging wave breaking

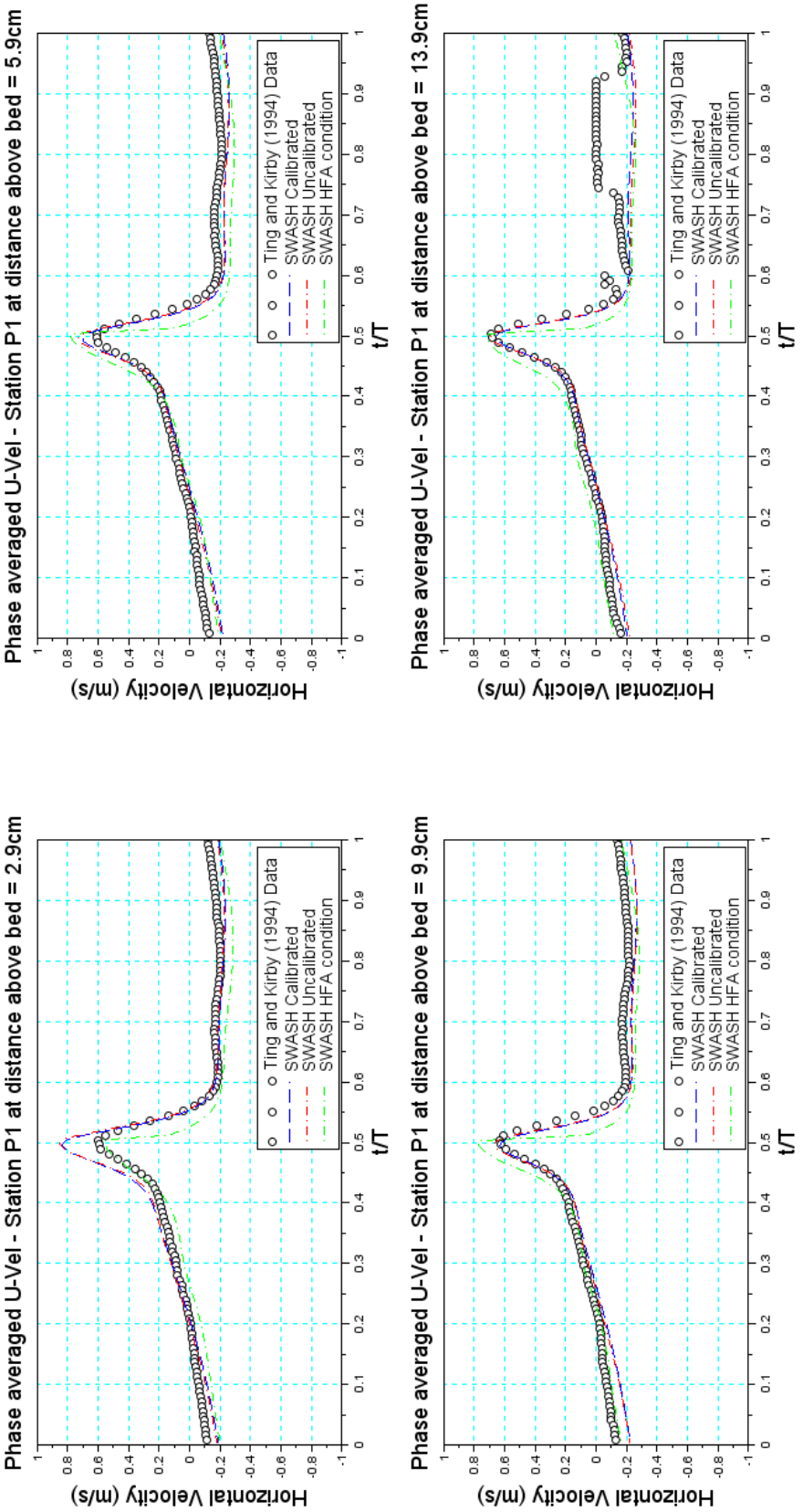

Figure B.14: Ting and Kirby (1994) vs. SWASH modelled phase averaged horizontal velocity before plunging wave breaking

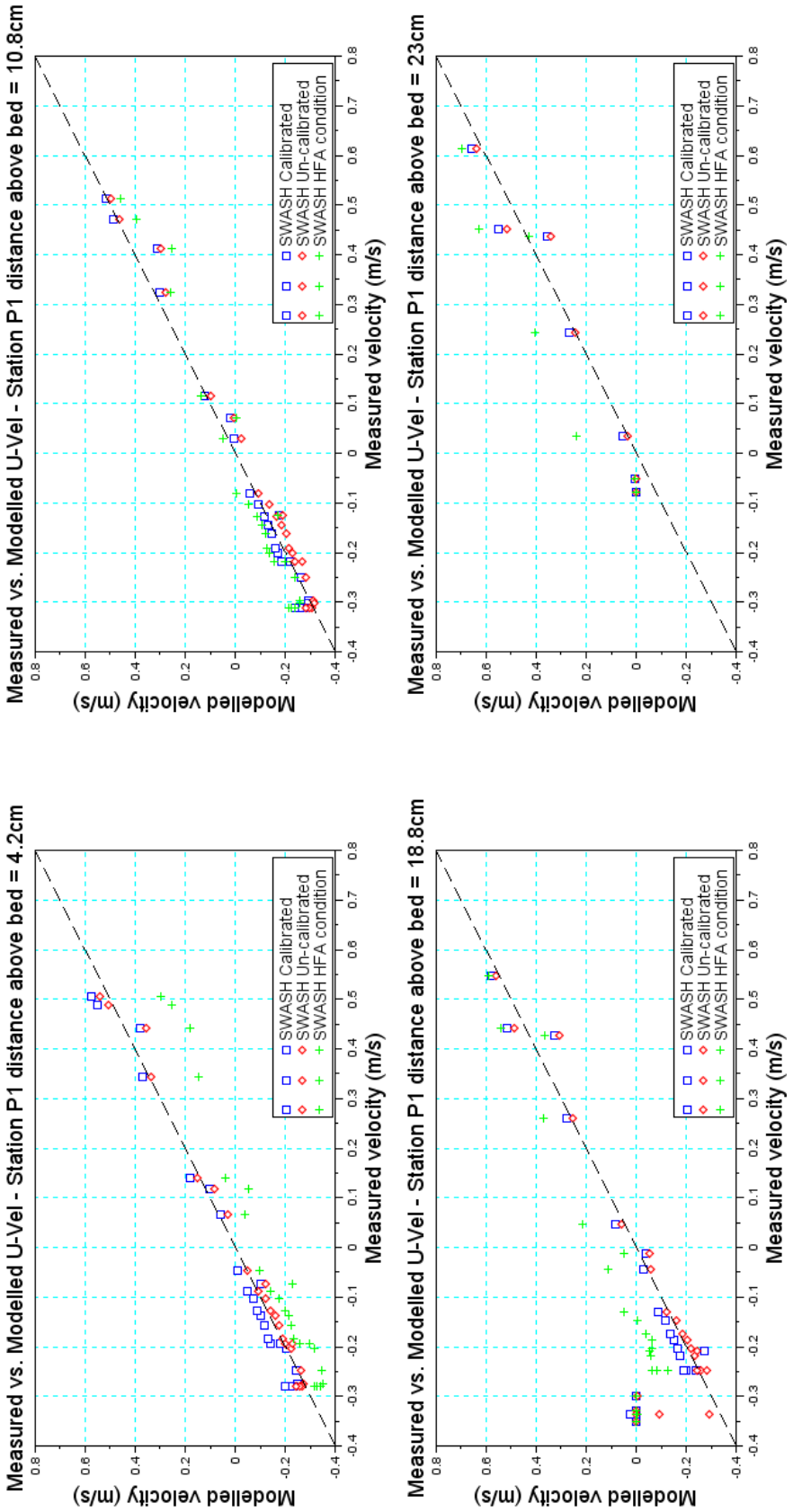

Figure B.15: Measured vs. modelled horizontal velocity before plunging wave breaking for the Govender (1999) and SWASH modelled time series

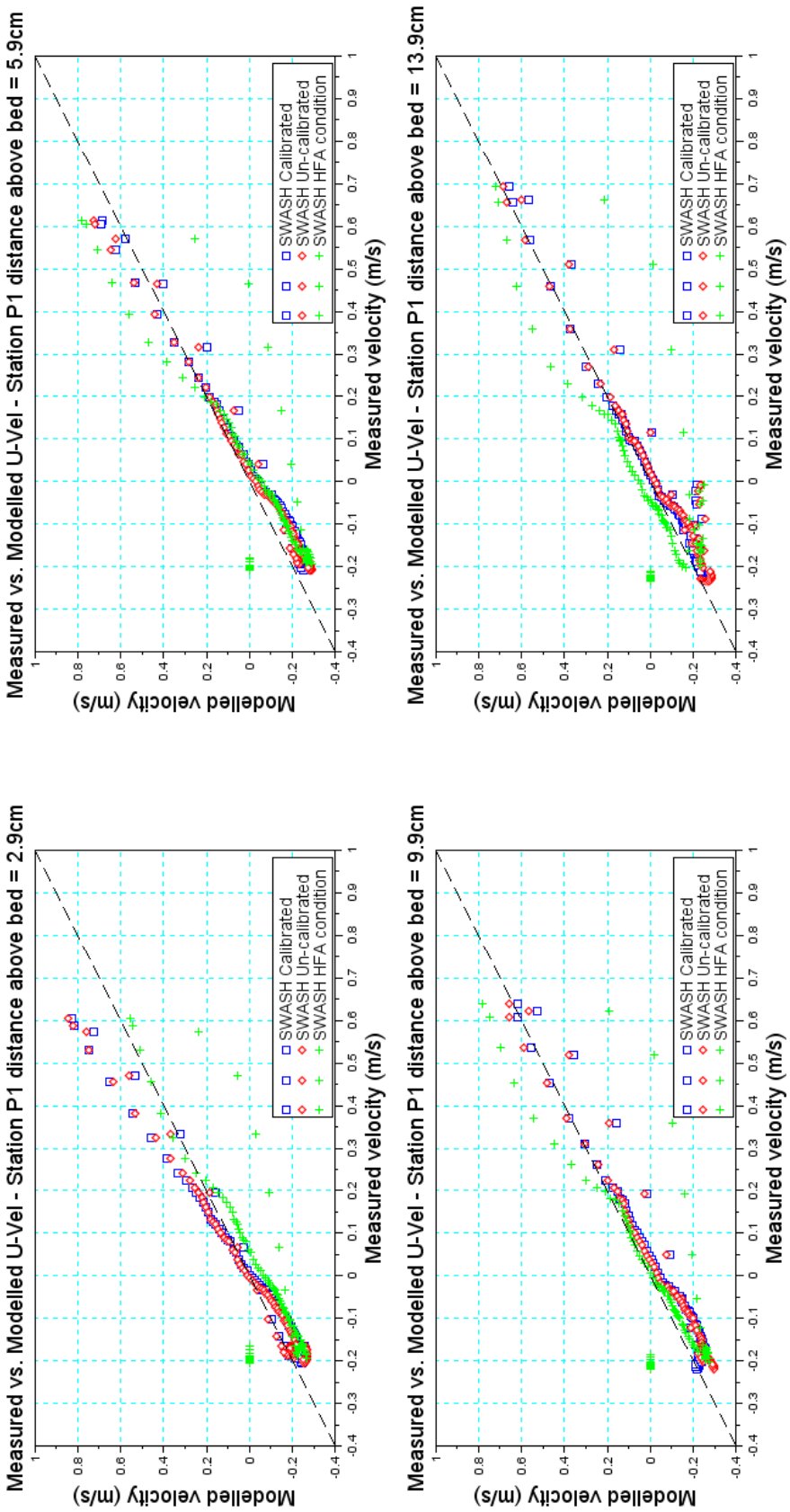

Figure B.16: Measured vs. modelled horizontal velocity before plunging wave breaking for the Ting and Kirby (1994) and SWASH modelled time series

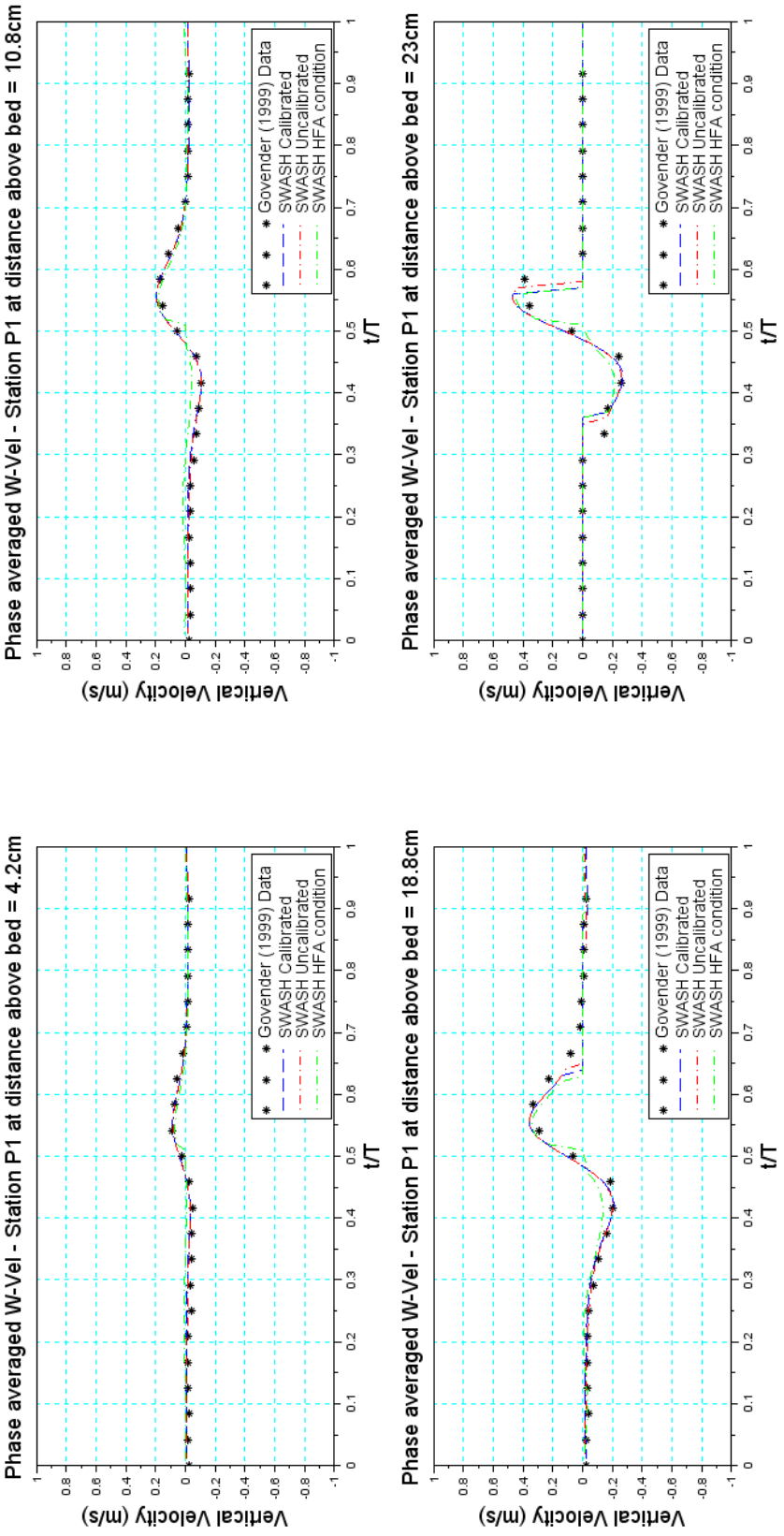

Figure B.17: Govender (1999) vs. SWASH modelled phase averaged vertical velocity before plunging wave breaking

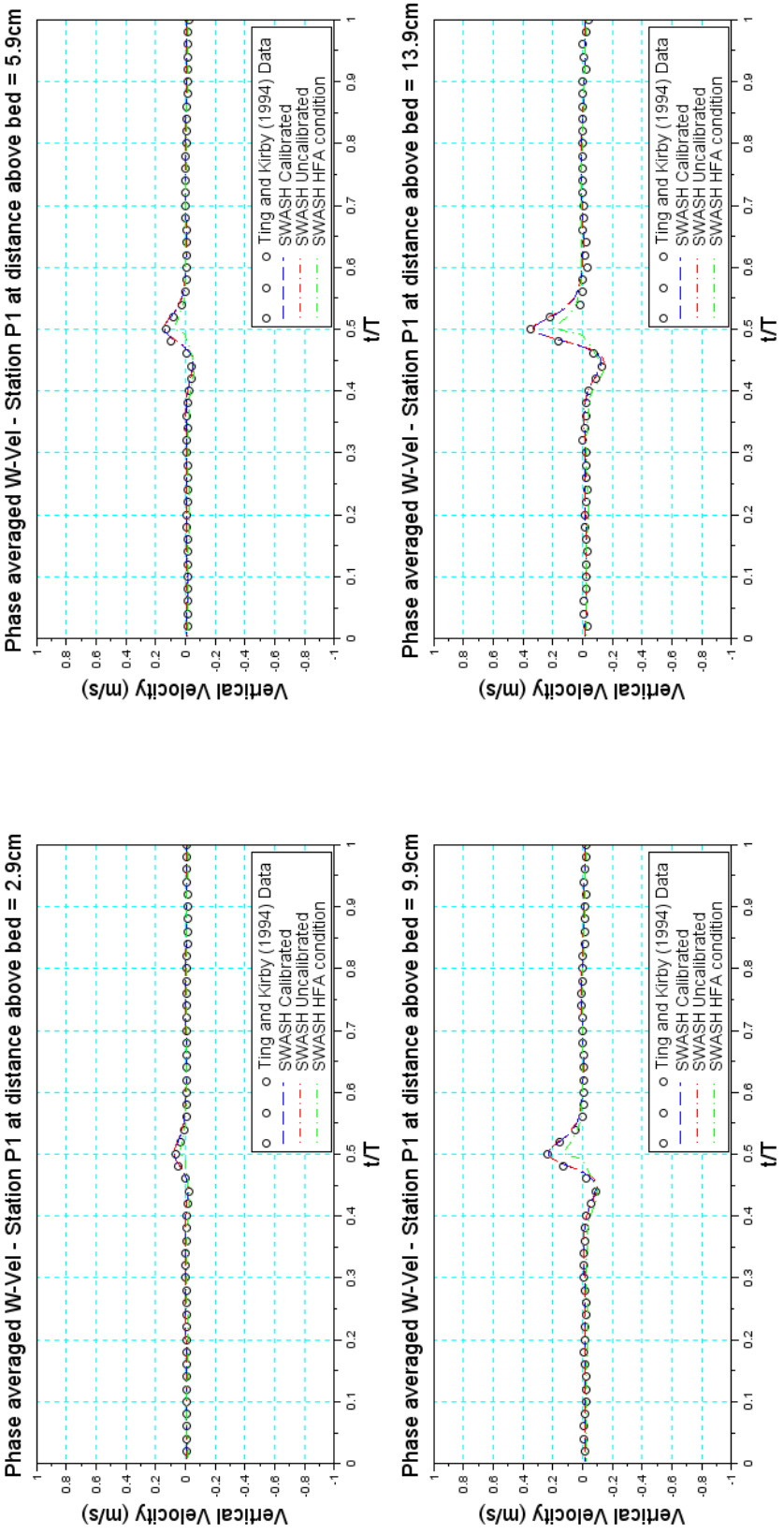

Figure B.18: Ting and Kirby (1994) vs. SWASH modelled phase averaged vertical velocity before plunging wave breaking

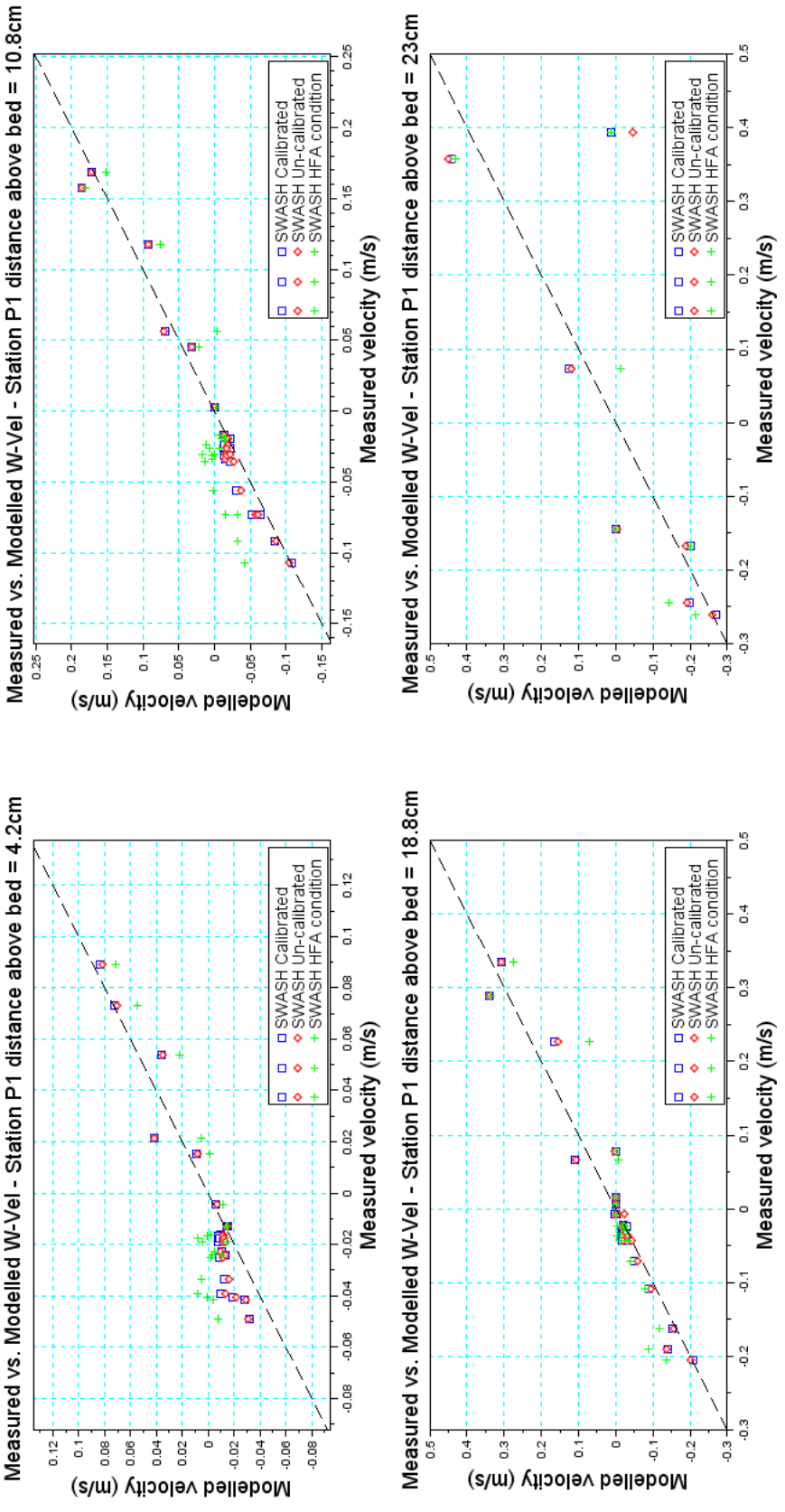

Figure B.19: Measured vs. modelled vertical velocity before plunging wave breaking for the Govender (1999) and SWASH modelled time series

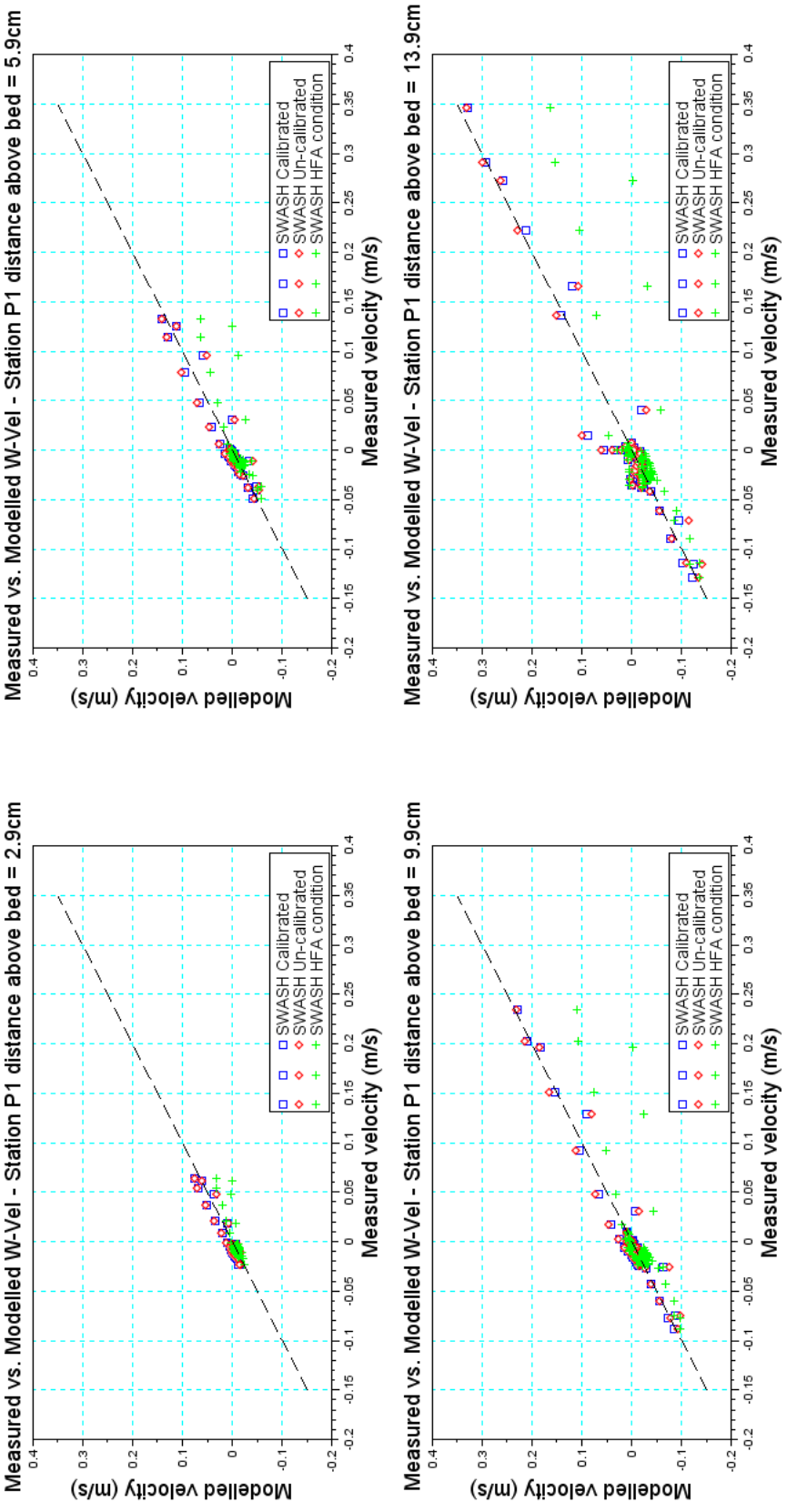

Figure B.20: Measured vs. modelled vertical velocity before plunging wave breaking for the Ting and Kirby (1994) and SWASH modelled time series

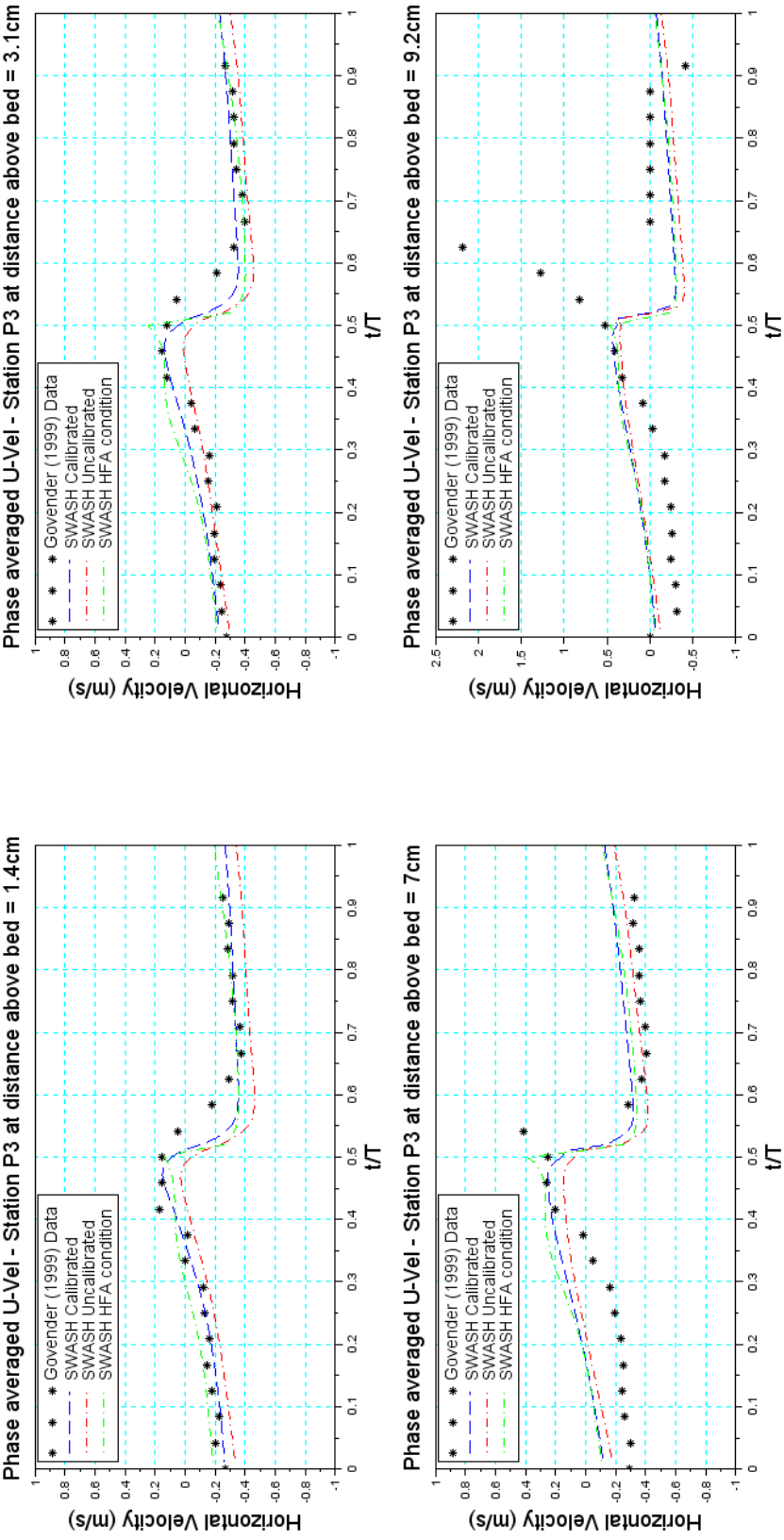

Figure B.21: Govender (1999) vs. SWASH modelled horizontal velocity after plunging wave breaking

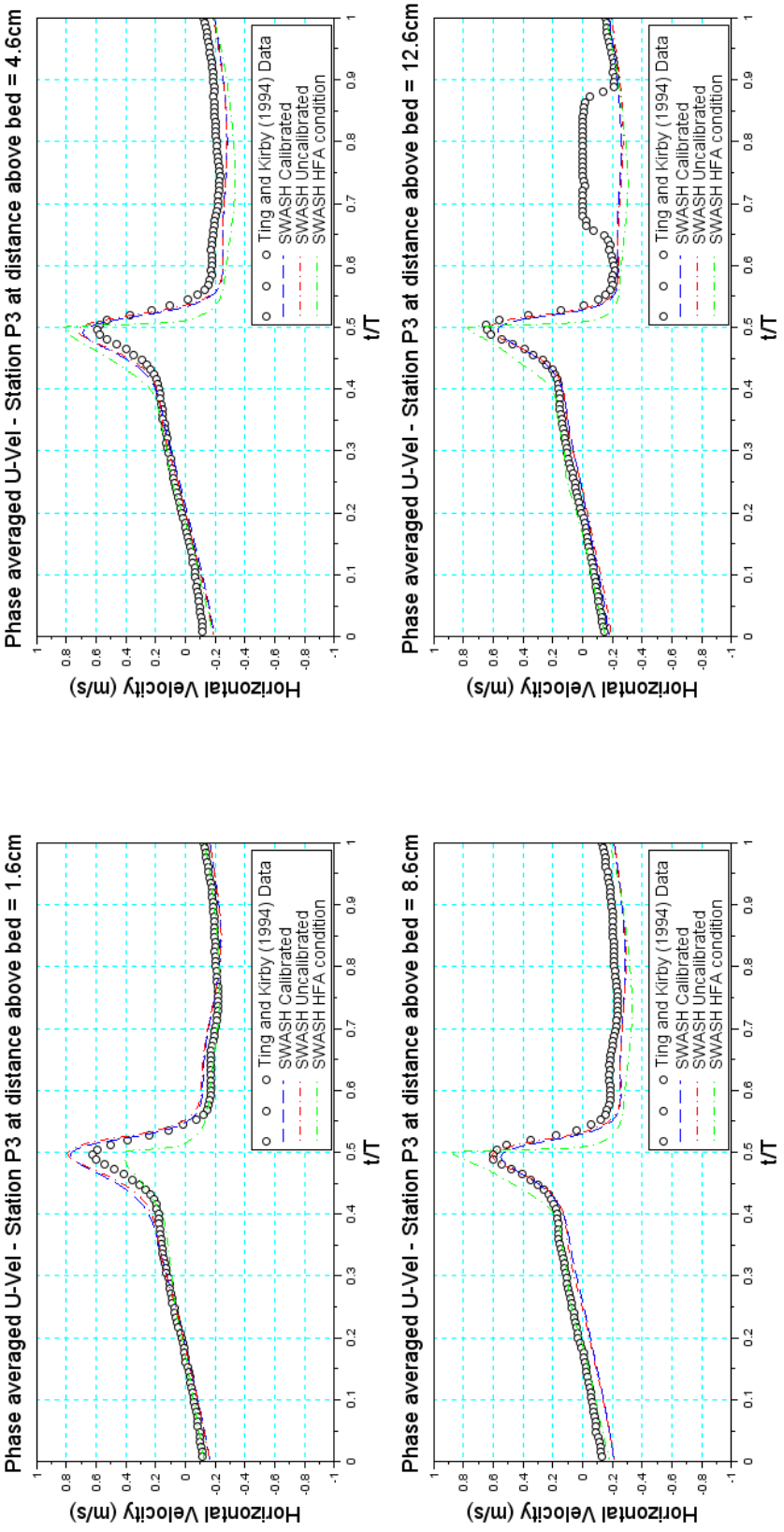

Figure B.22: Ting and Kirby (1994) vs. SWASH modelled horizontal velocity after plunging wave breaking

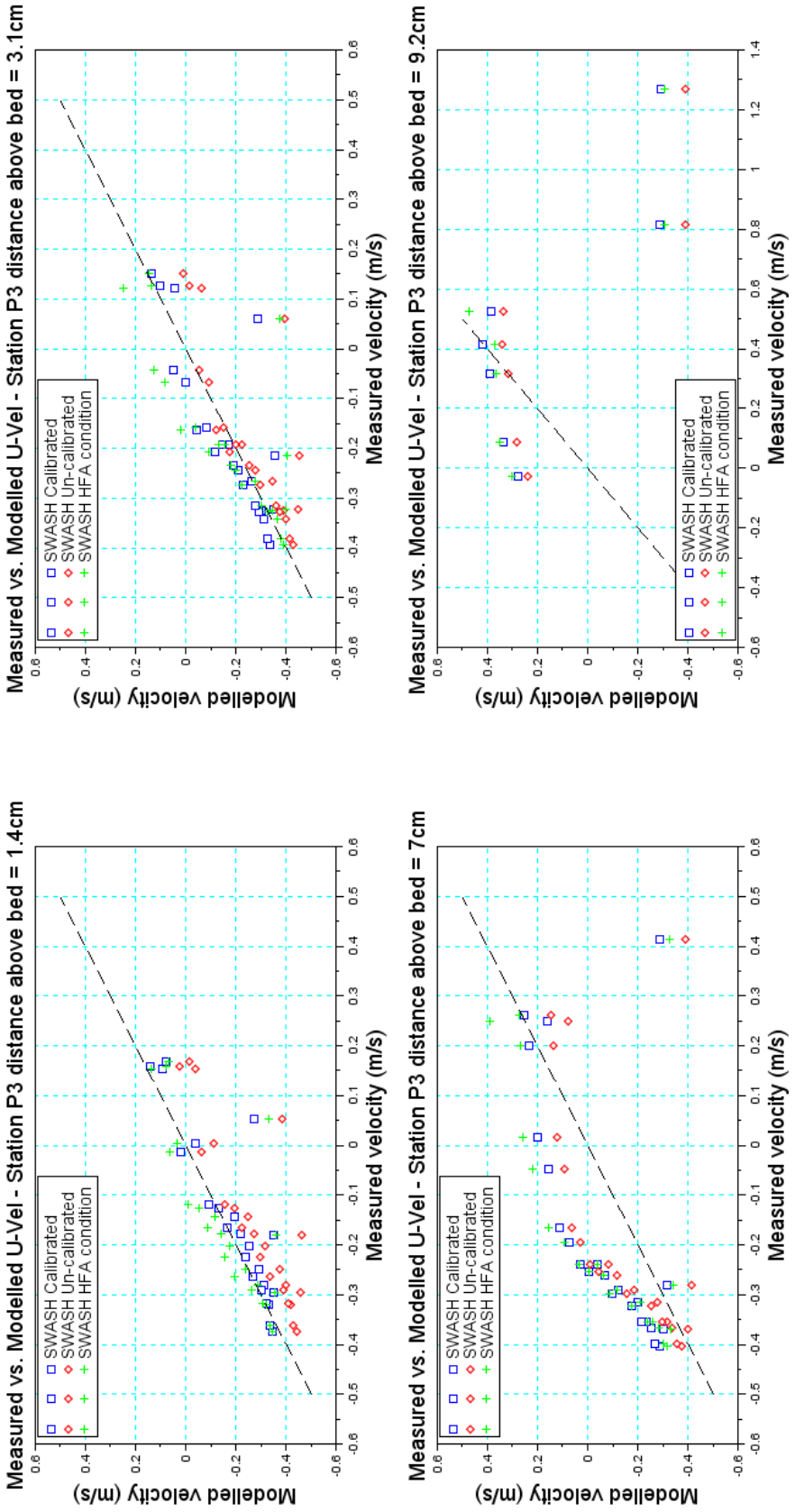

Figure B.23: Measured vs. modelled horizontal velocity after plunging wave breaking for the Govender (1999) and SWASH modelled time series

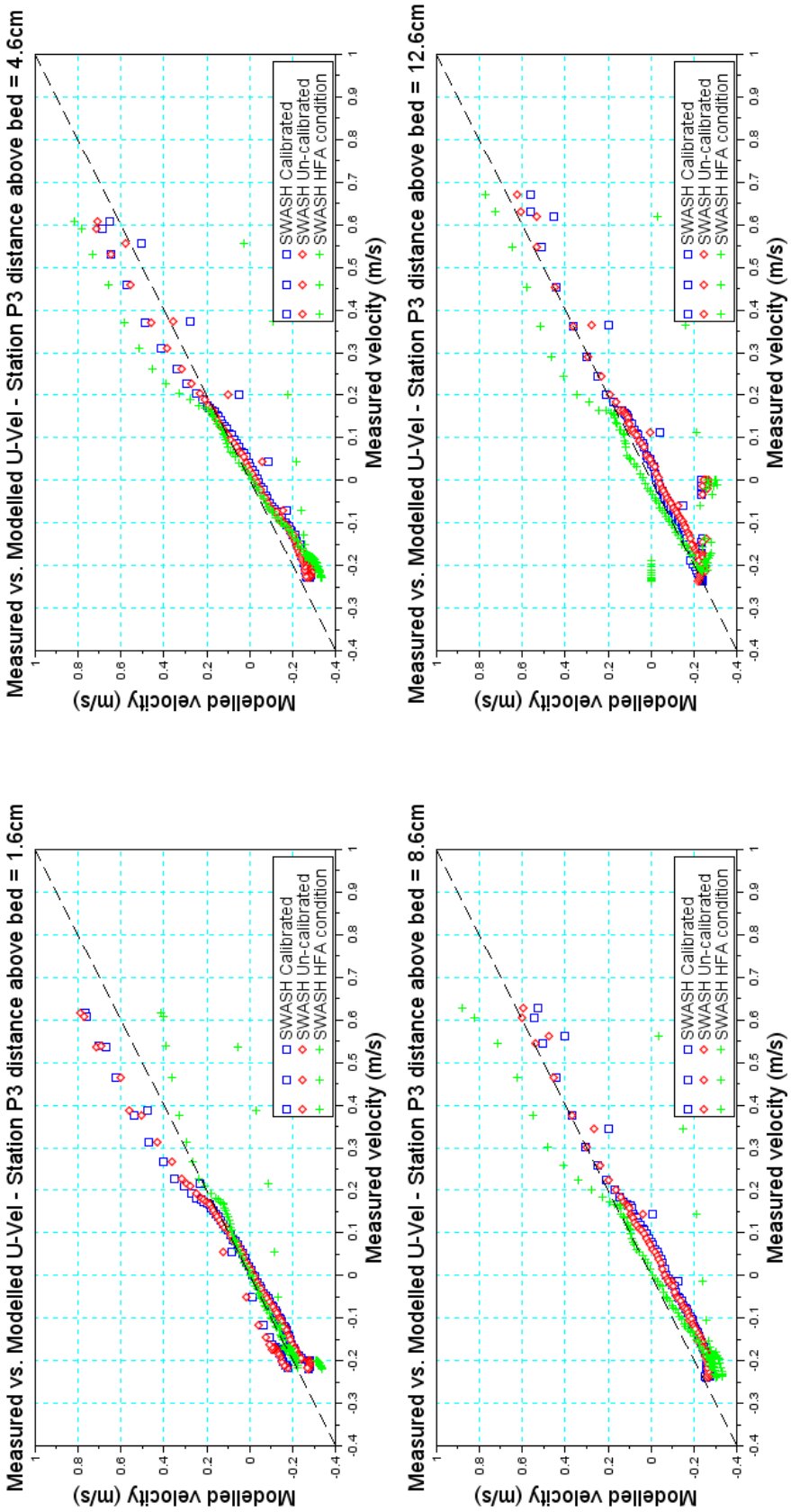

Figure B.24: Measured vs. modelled horizontal velocity after plunging wave breaking for the Ting and Kirby (1994) and SWASH modelled time series

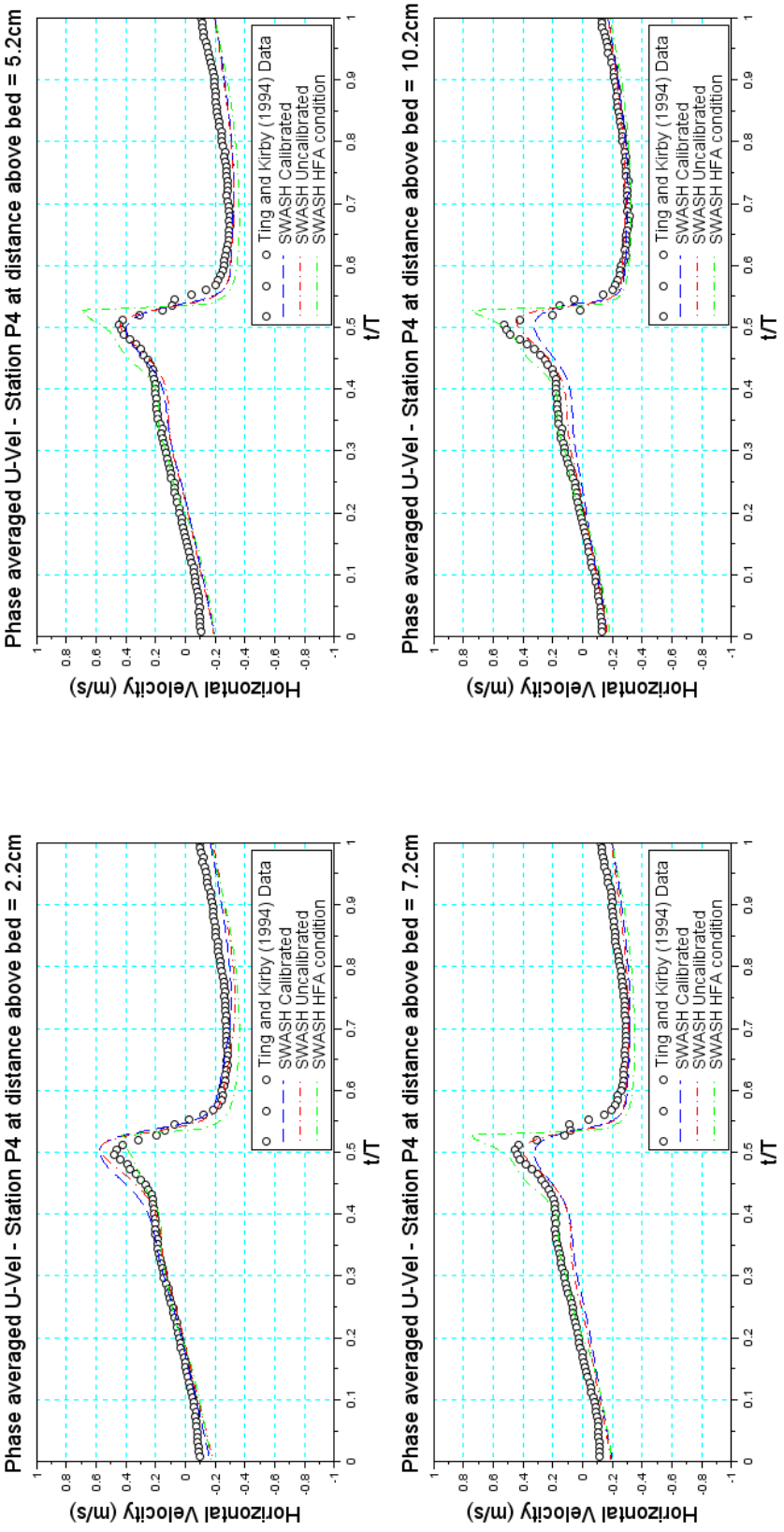

Figure B.25: Ting and Kirby (1994) vs. SWASH modelled horizontal velocity after plunging wave breaking (0.55m from break point)

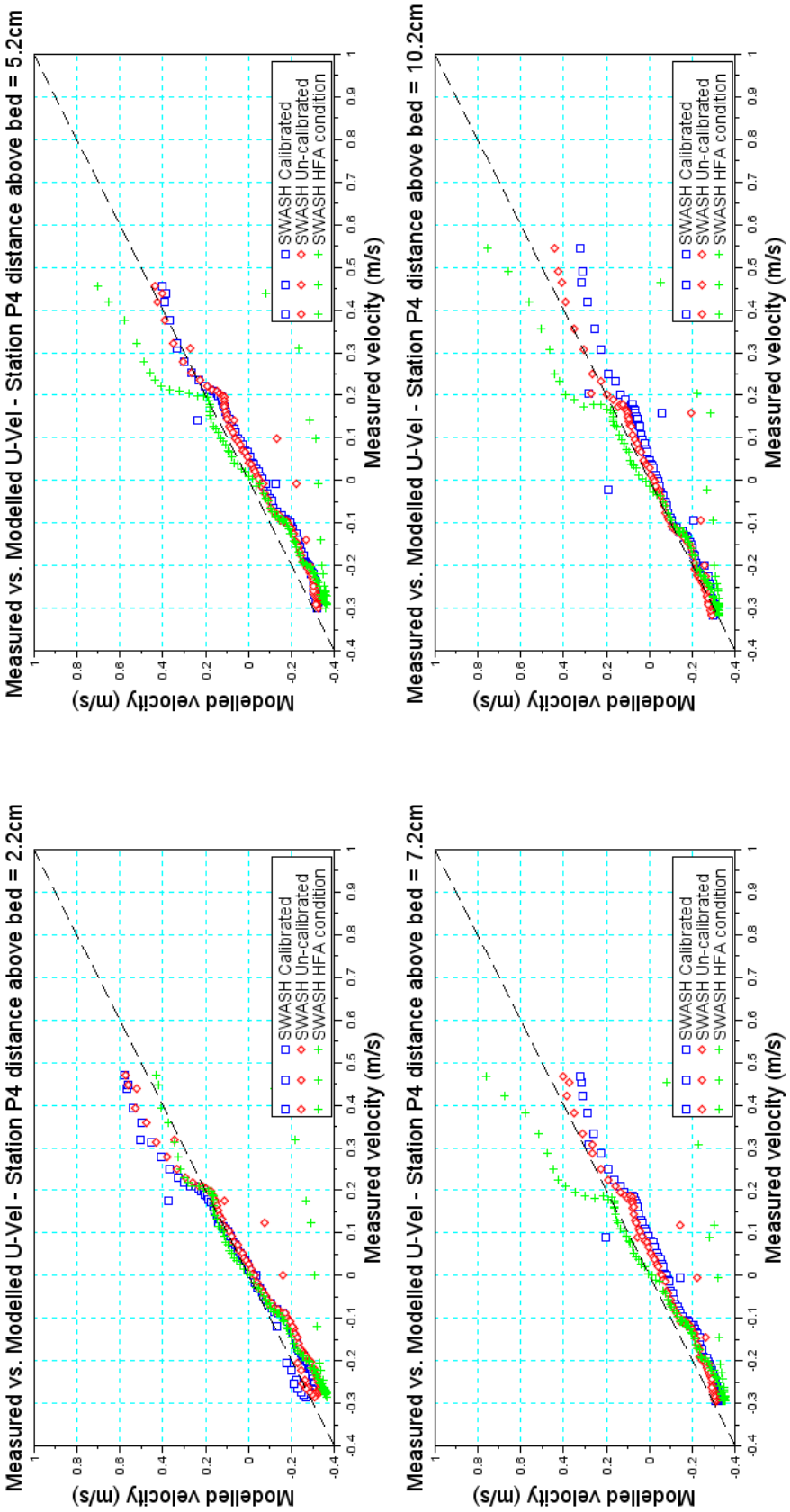

Figure B.26: Measured vs. modelled horizontal velocity after plunging wave breaking for the Ting and Kirby (1994) and SWASH modelled time series (0.55m from break point)

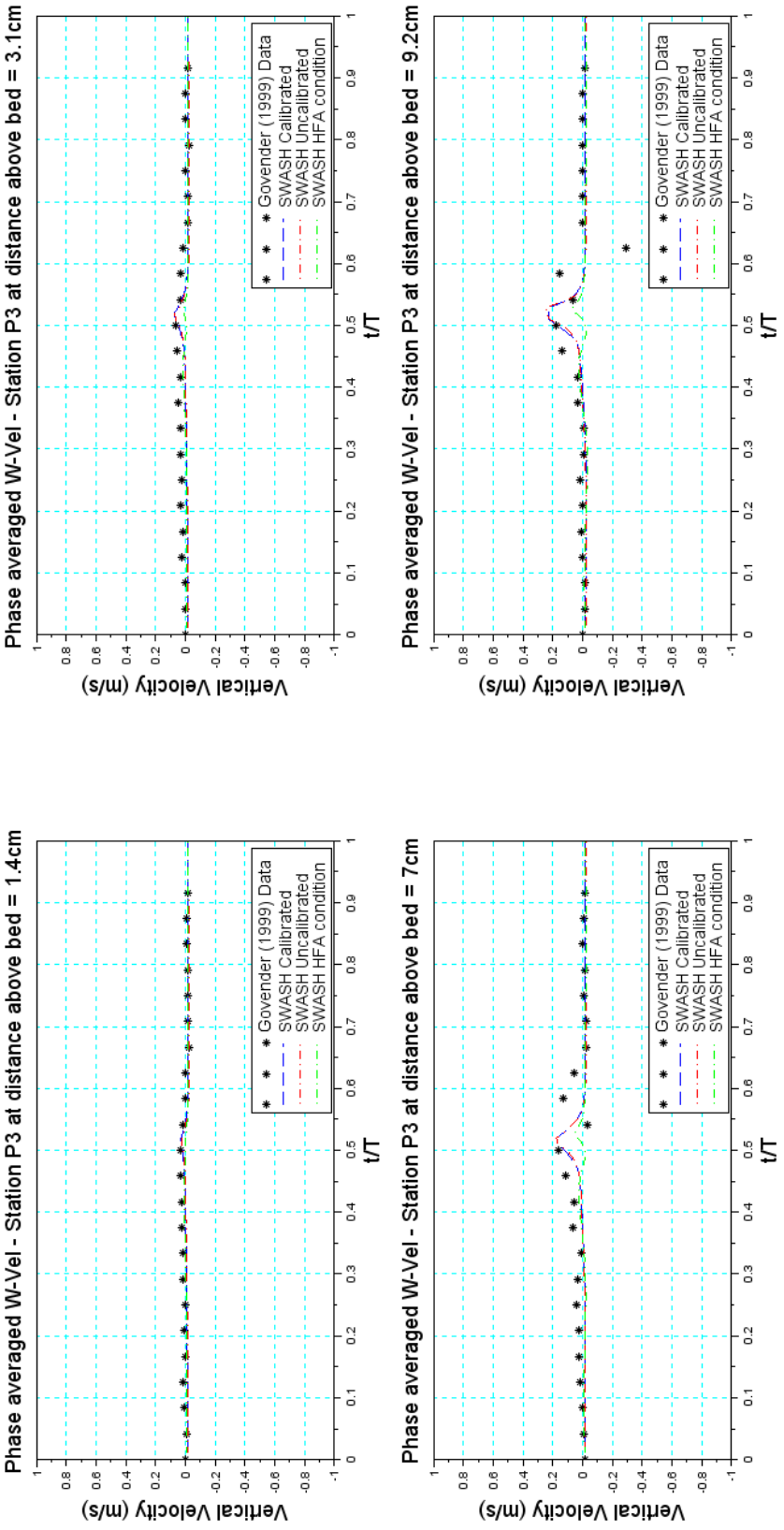

Figure B.27: Govender (1999) vs. SWASH modelled vertical velocity after plunging wave breaking

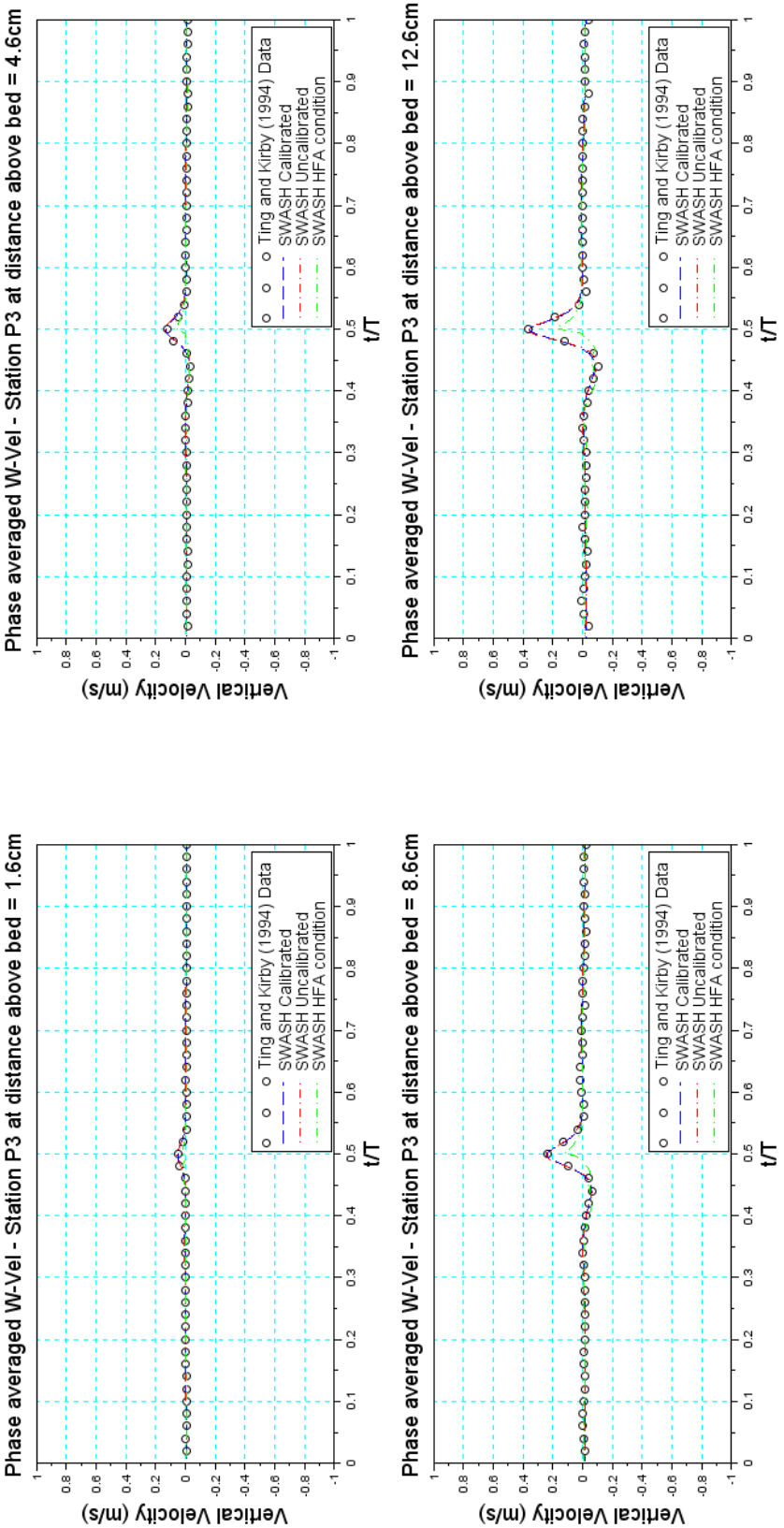

Figure B.28: Ting and Kirby (1994) vs. SWASH modelled vertical velocity after plunging wave breaking

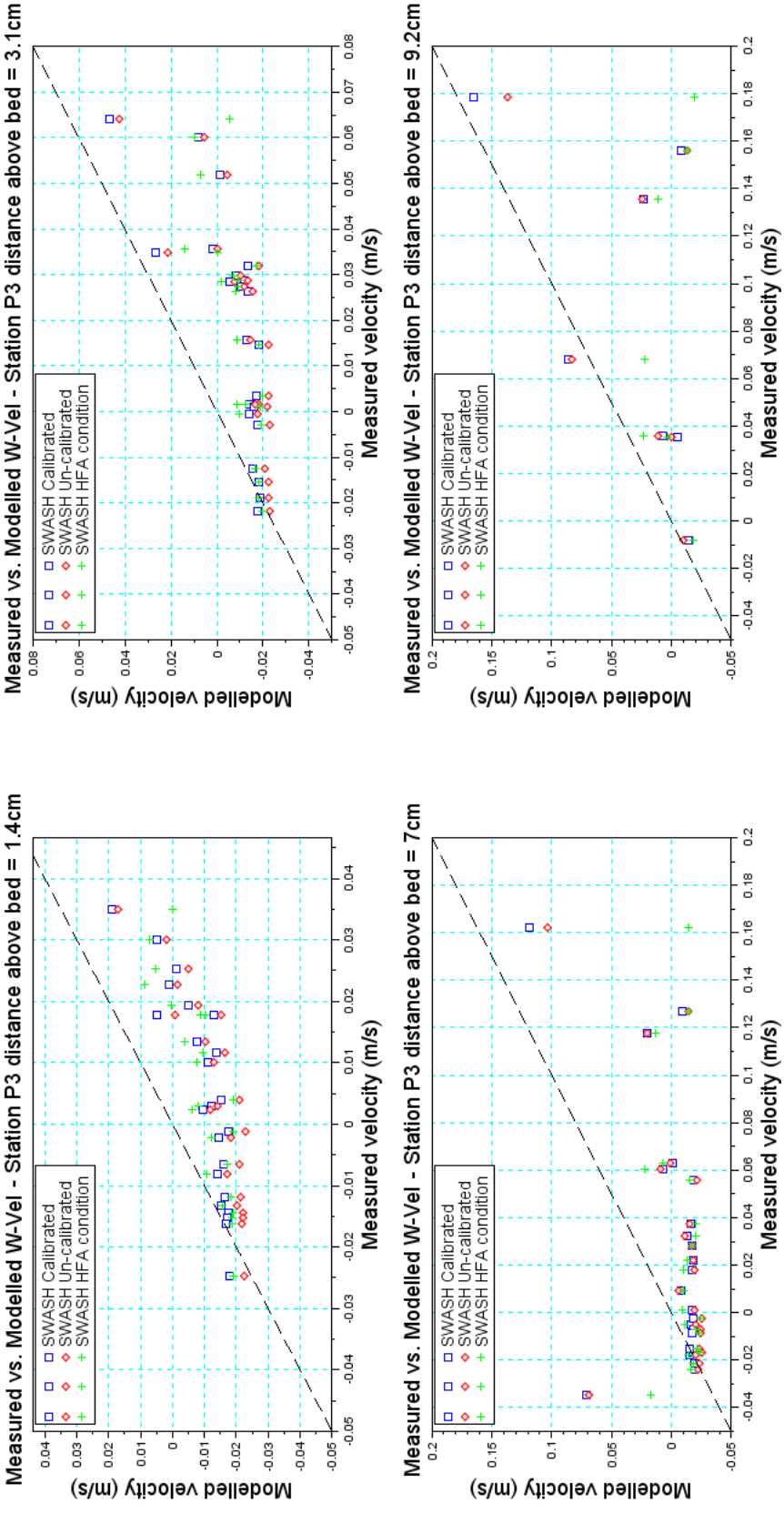

Figure B.29: Measured vs. modelled vertical velocity after plunging wave breaking for the Govender (1999) and SWASH modelled time series

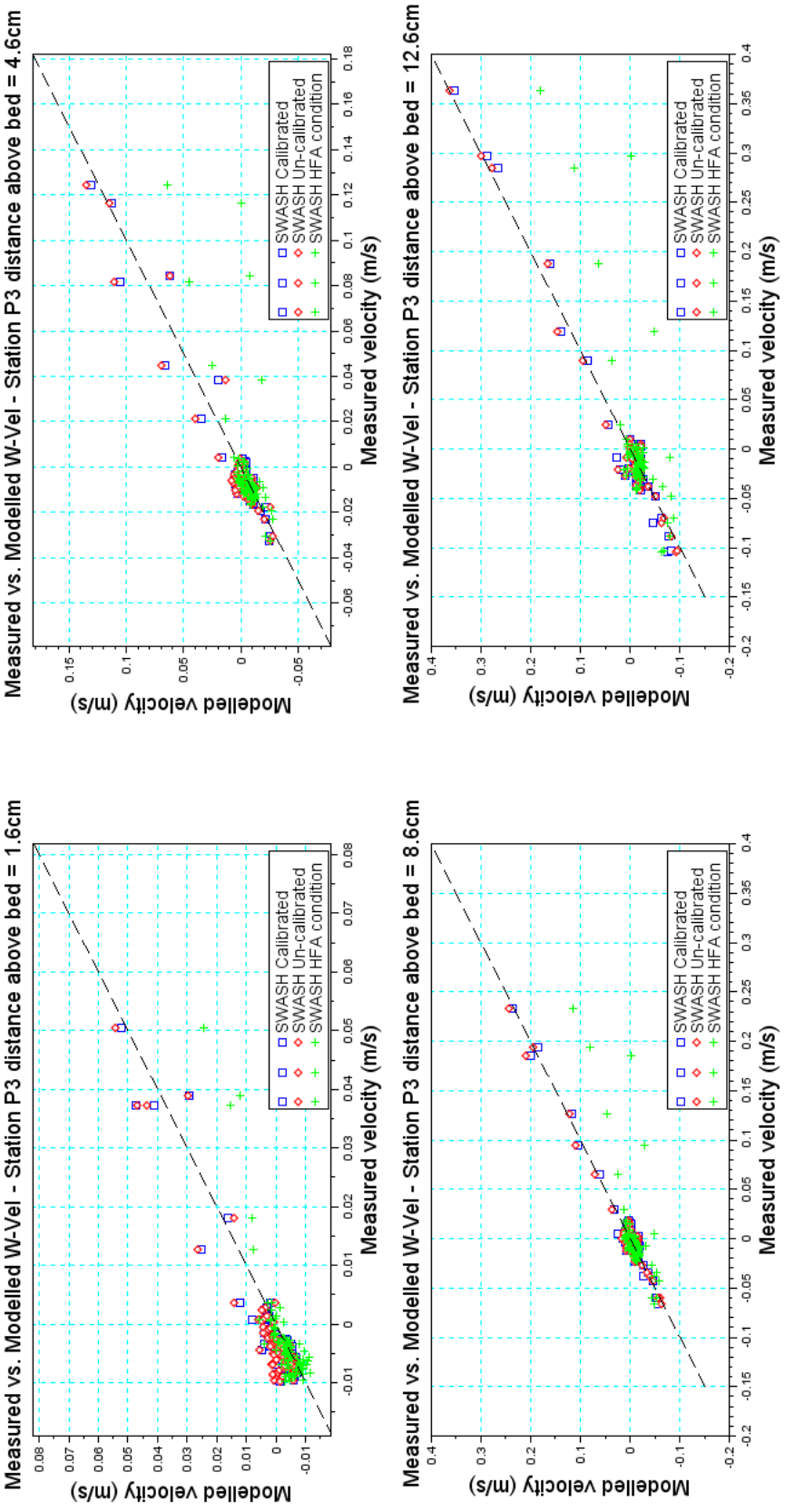

Figure B.30: Measured vs. modelled vertical velocity after plunging wave breaking for the Ting and Kirby (1994) and SWASH modelled time series

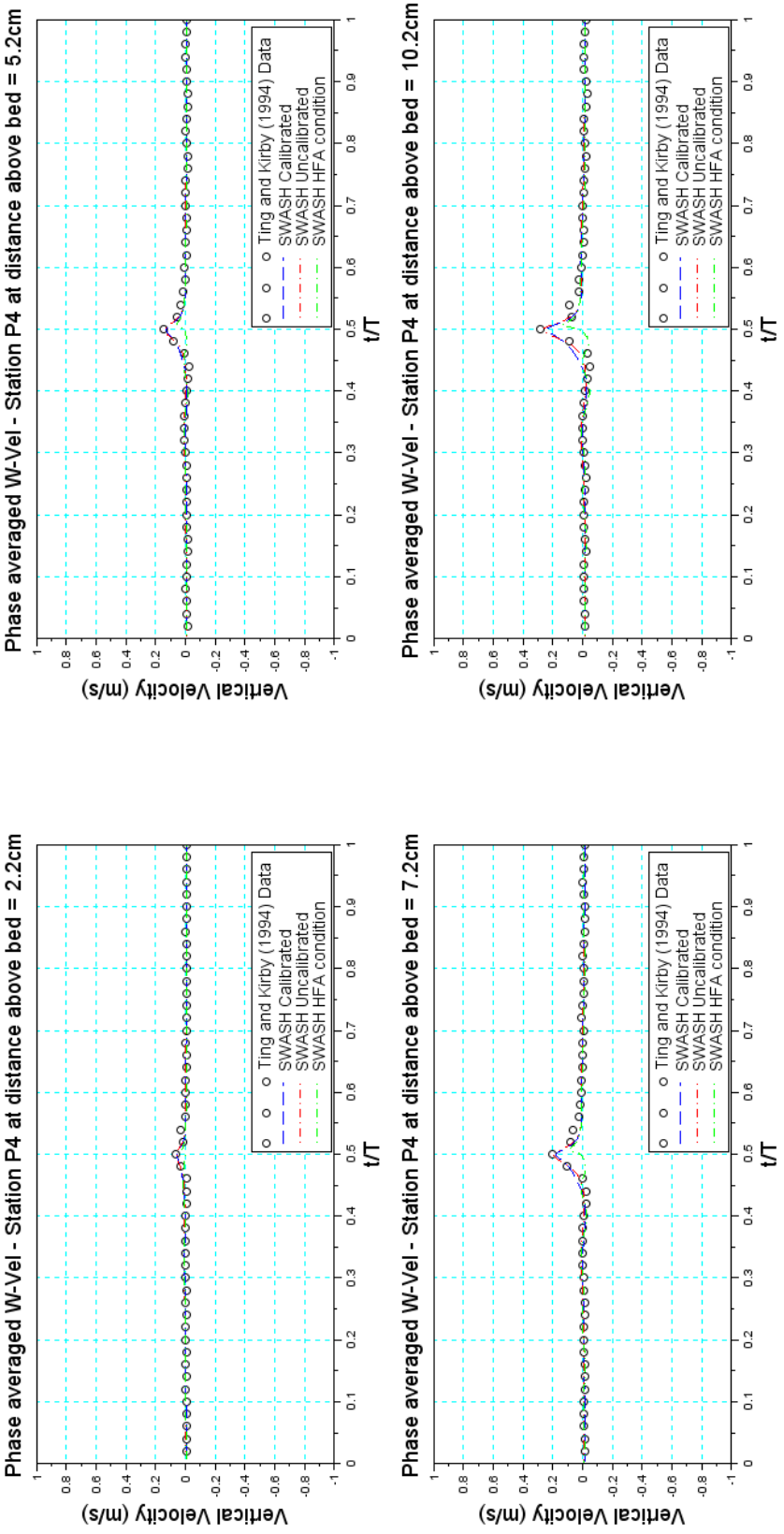

Figure B.31: Ting and Kirby (1994) vs. SWASH modelled vertical velocity after plunging wave breaking (0.55m after break point)

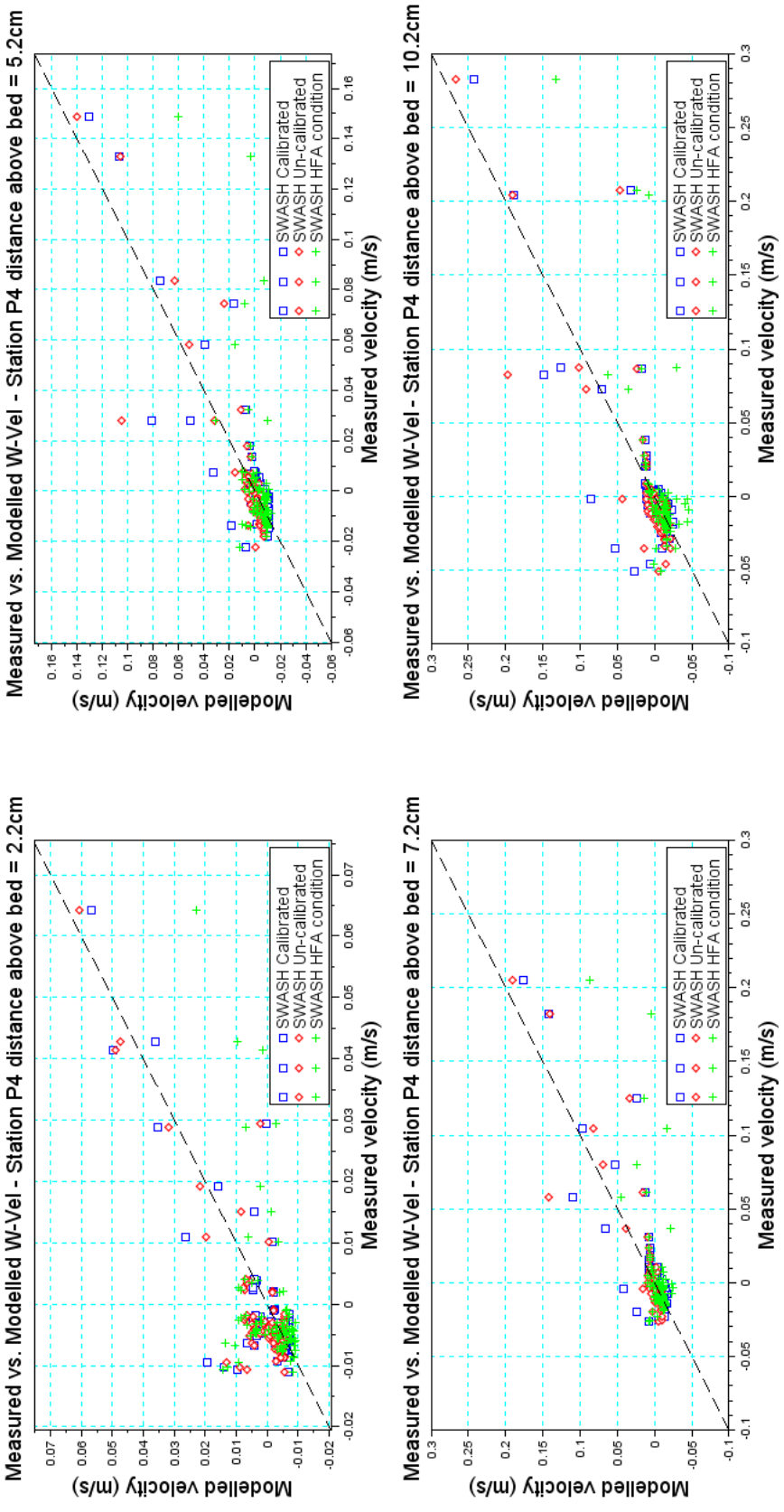

Figure B.32: Measured vs. modelled vertical velocity after plunging wave breaking (0.55m after break point) for the Ting and Kirby (1994) and SWASH modelled time series

B.2.2 Phase averaged spilling wave comparison

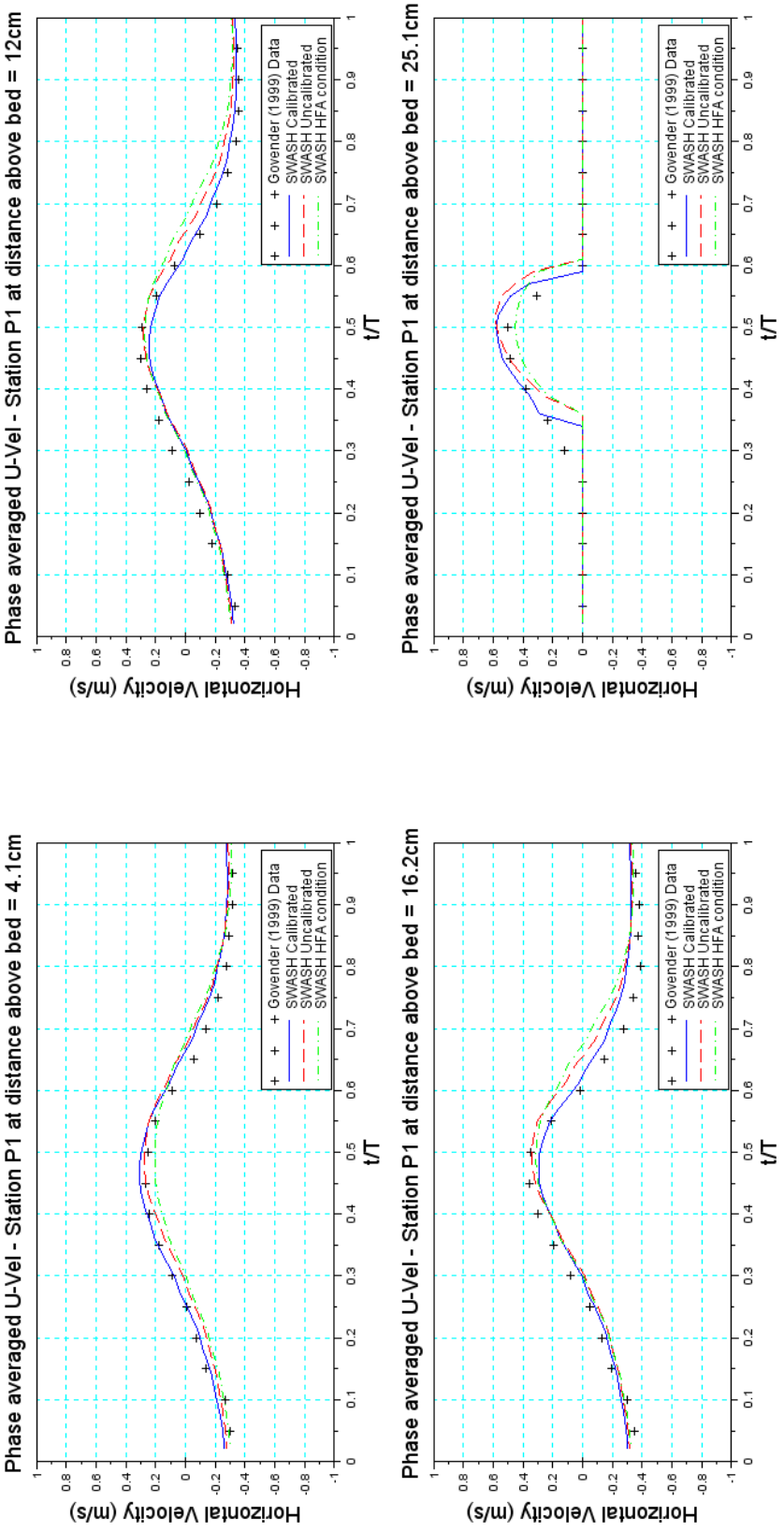

Figure B.33: Govender (1999) vs. SWASH modelled phase averaged horizontal velocity before spilling wave breaking

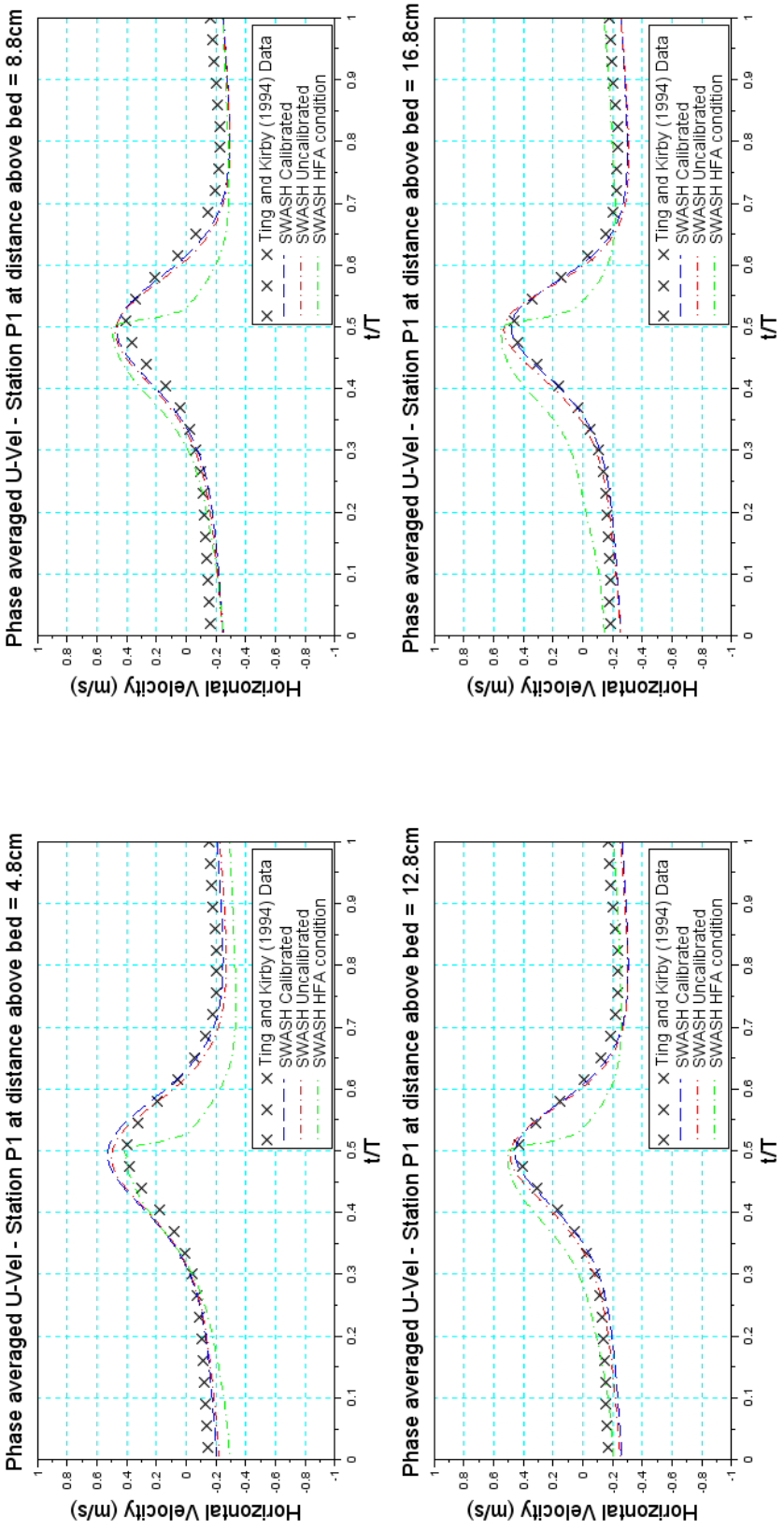

Figure B.34: Ting and Kirby (1994) vs. SWASH modelled phase averaged horizontal velocity before spilling wave breaking

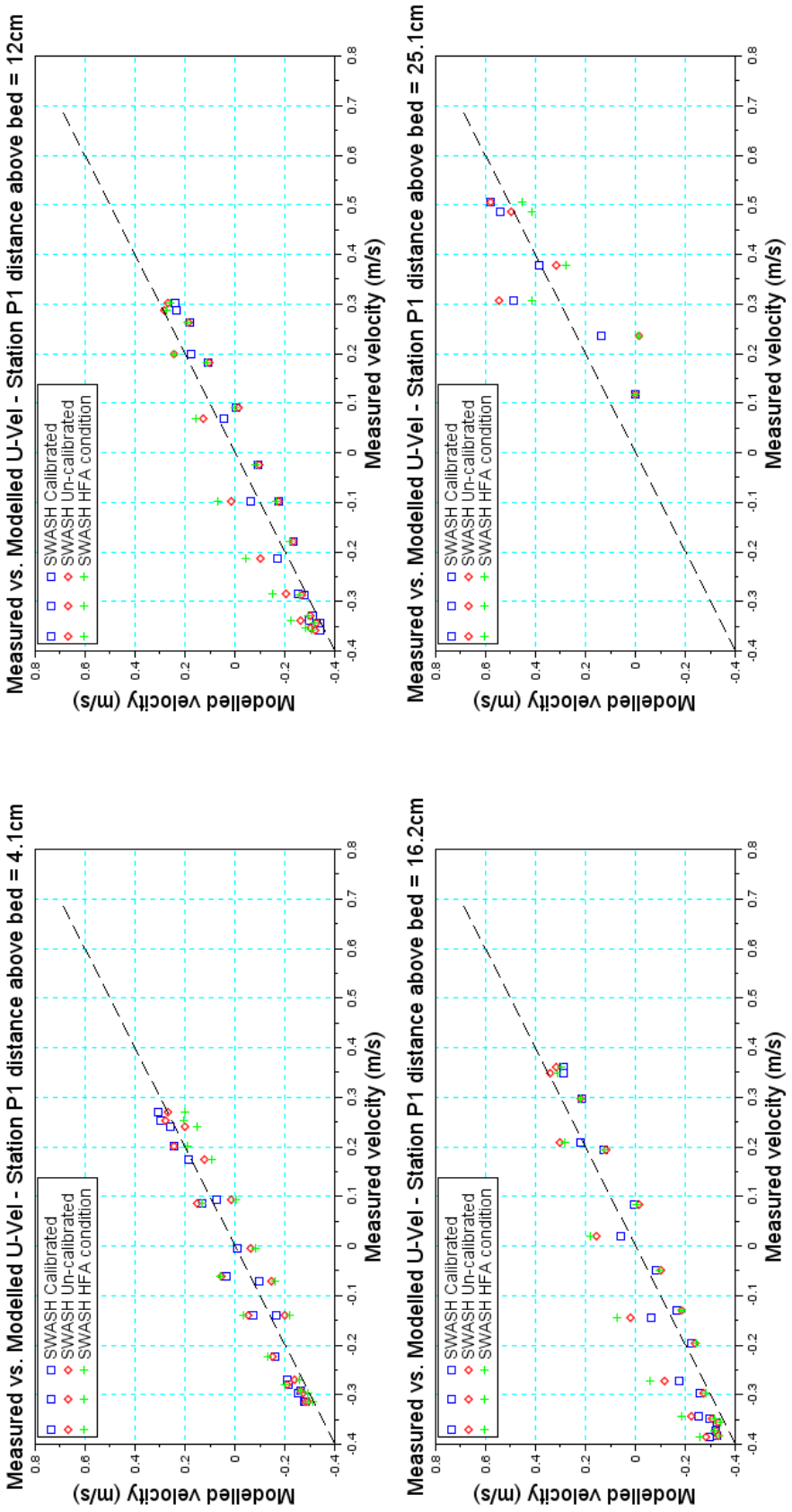

Figure B.35: Measured vs. modelled horizontal velocity before spilling wave breaking for the Govender (1999) and SWASH modelled time series

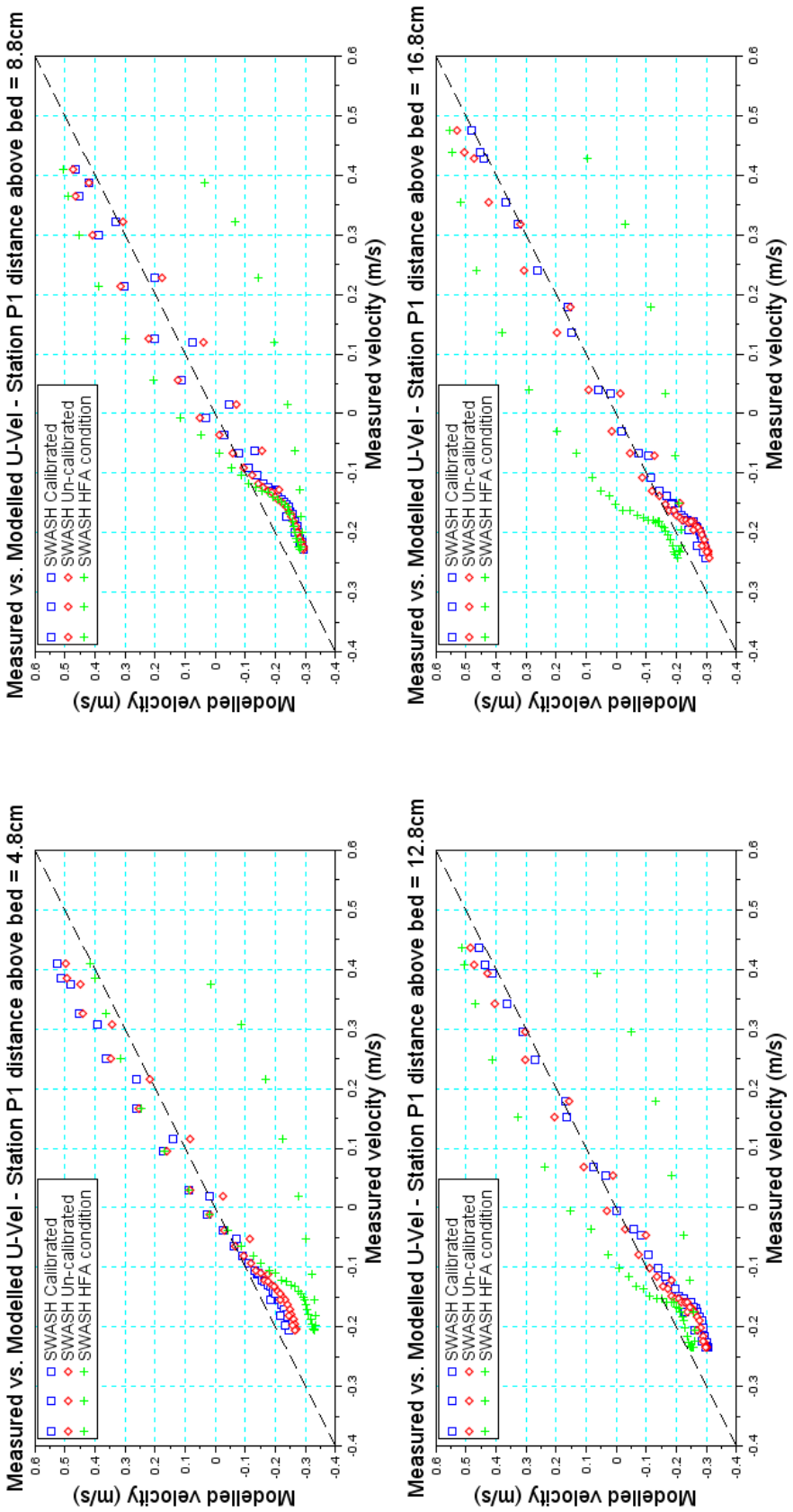

Figure B.36: Measured vs. modelled horizontal velocity before spilling wave breaking for the Ting and Kirby (1994) and SWASH modelled time series

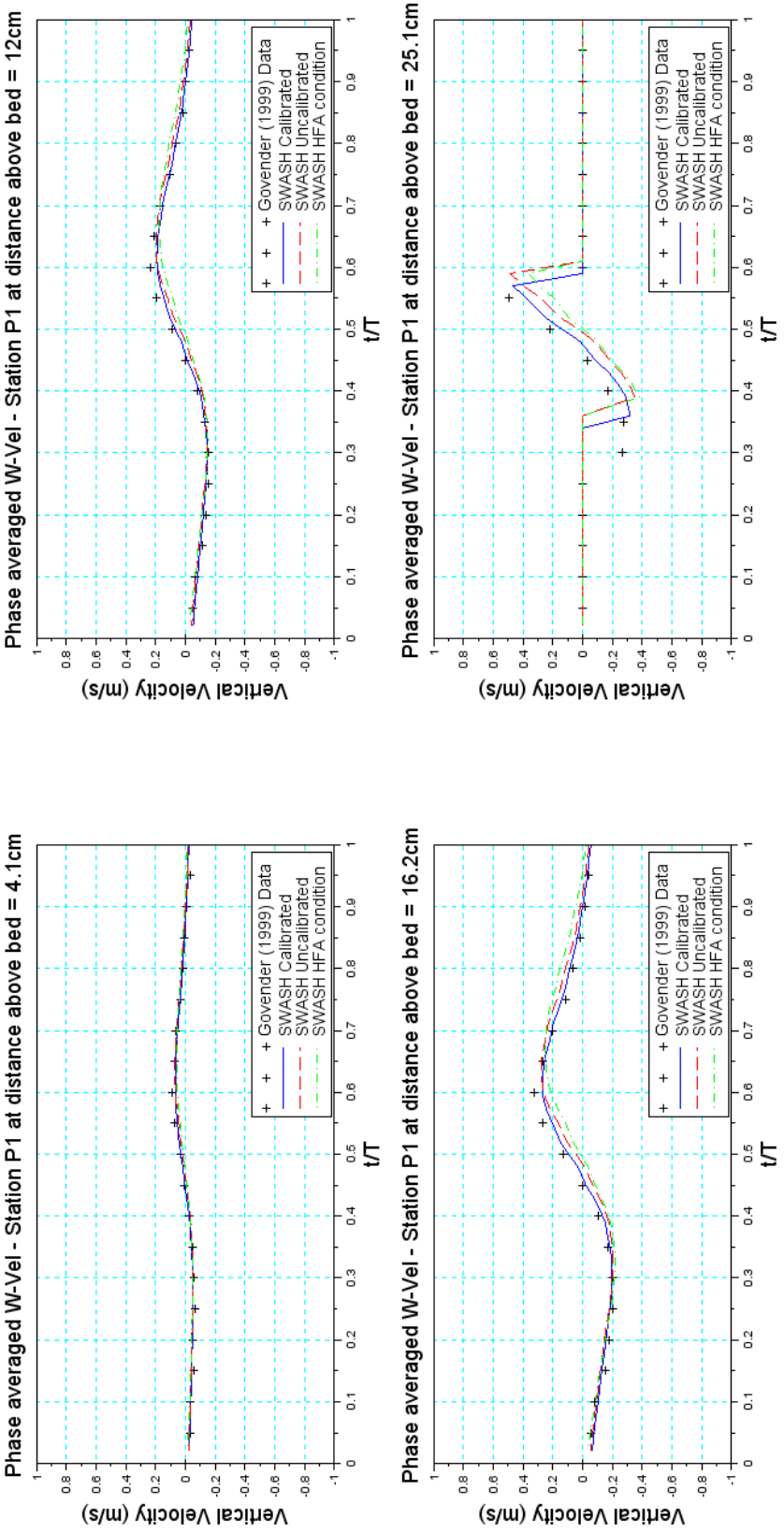

Figure B.37: Govender (1999) vs. SWASH modelled phase averaged vertical velocity before spilling wave breaking

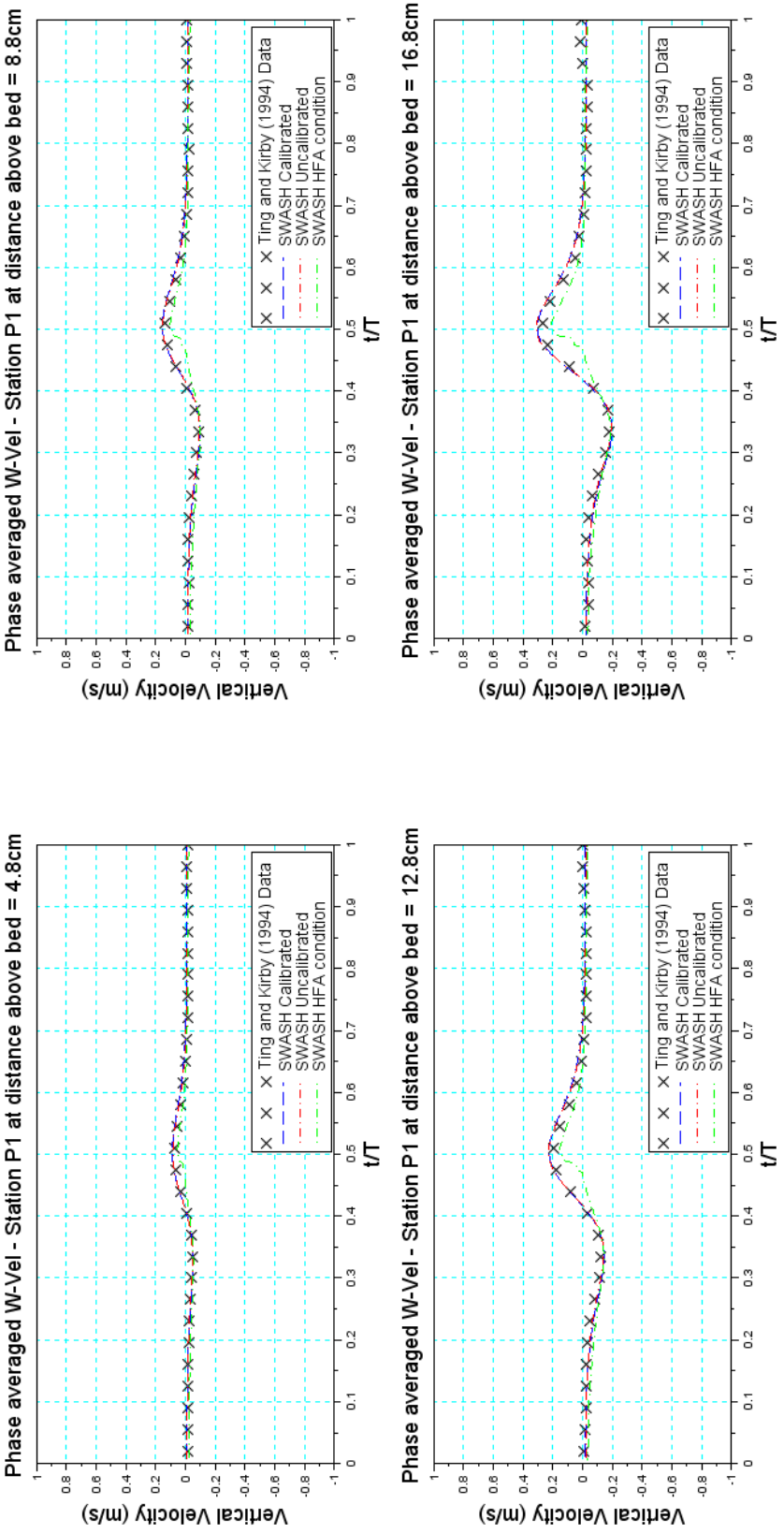

Figure B.38: Ting and Kirby (1994) vs. SWASH modelled phase averaged vertical velocity before spilling wave breaking

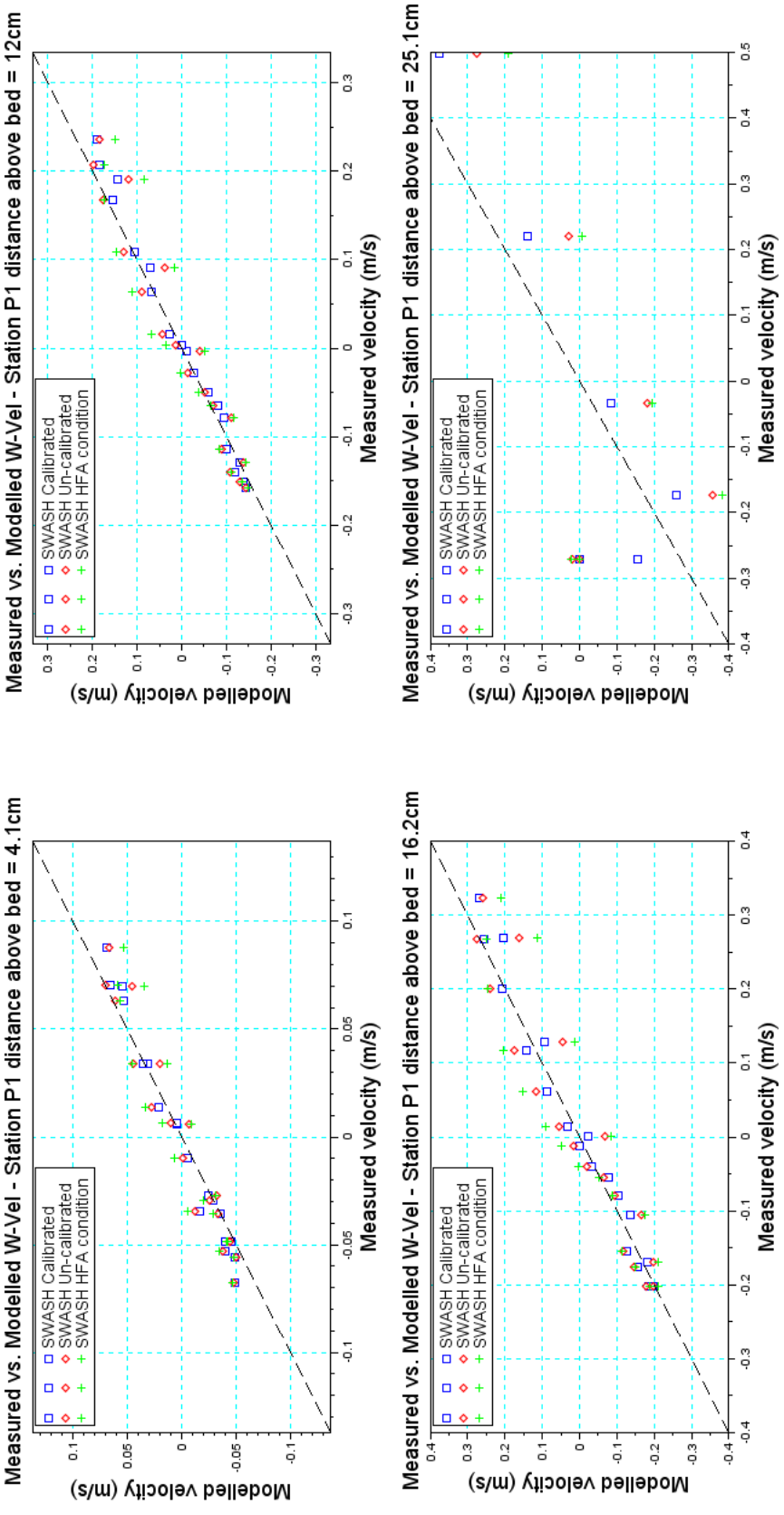

Figure B.39: Measured vs. modelled vertical velocity before spilling wave breaking for the Govender (1999) and SWASH modelled time series

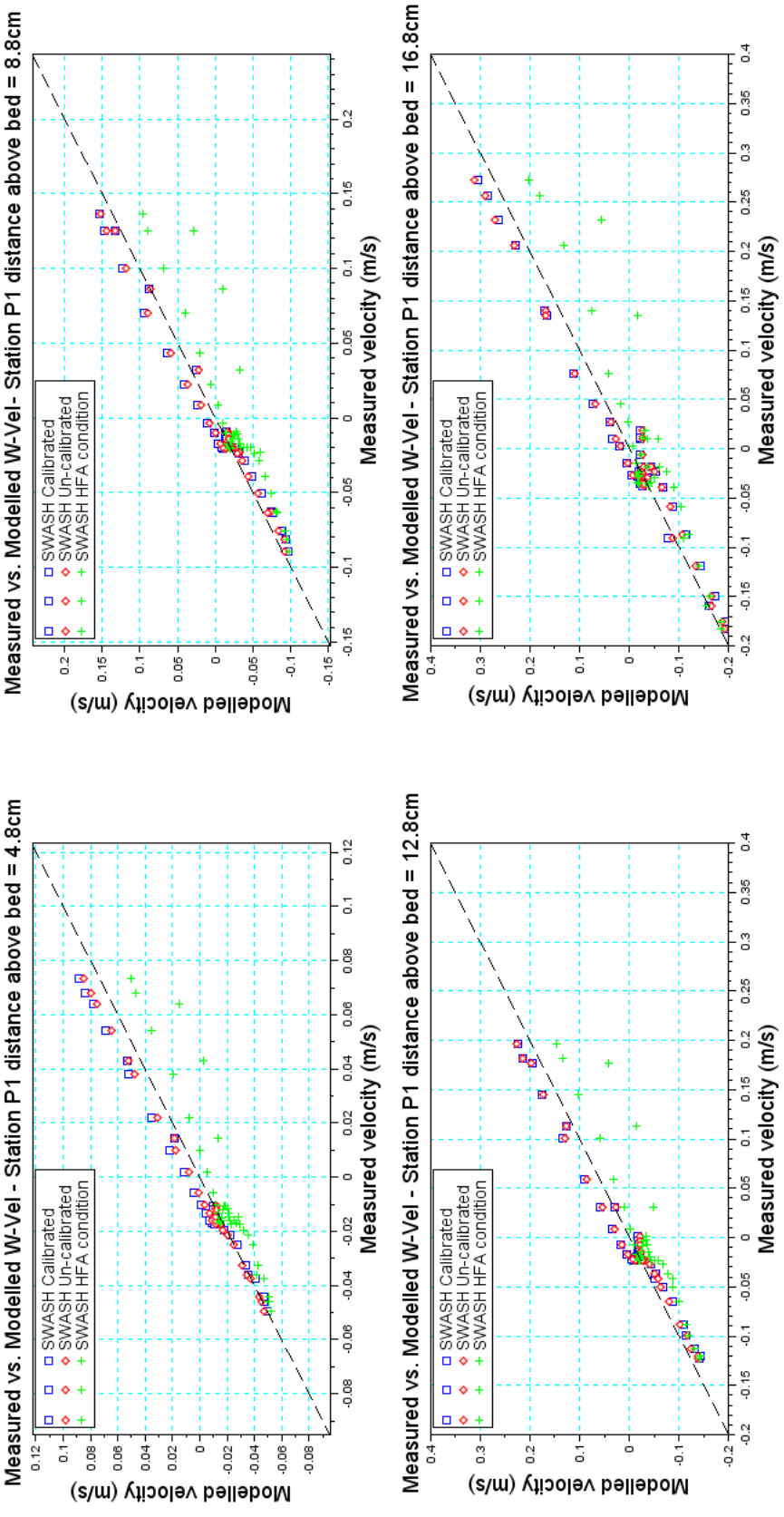

Figure B.40: Measured vs. modelled vertical velocity before spilling wave breaking for the Ting and Kirby (1994) and SWASH modelled time series

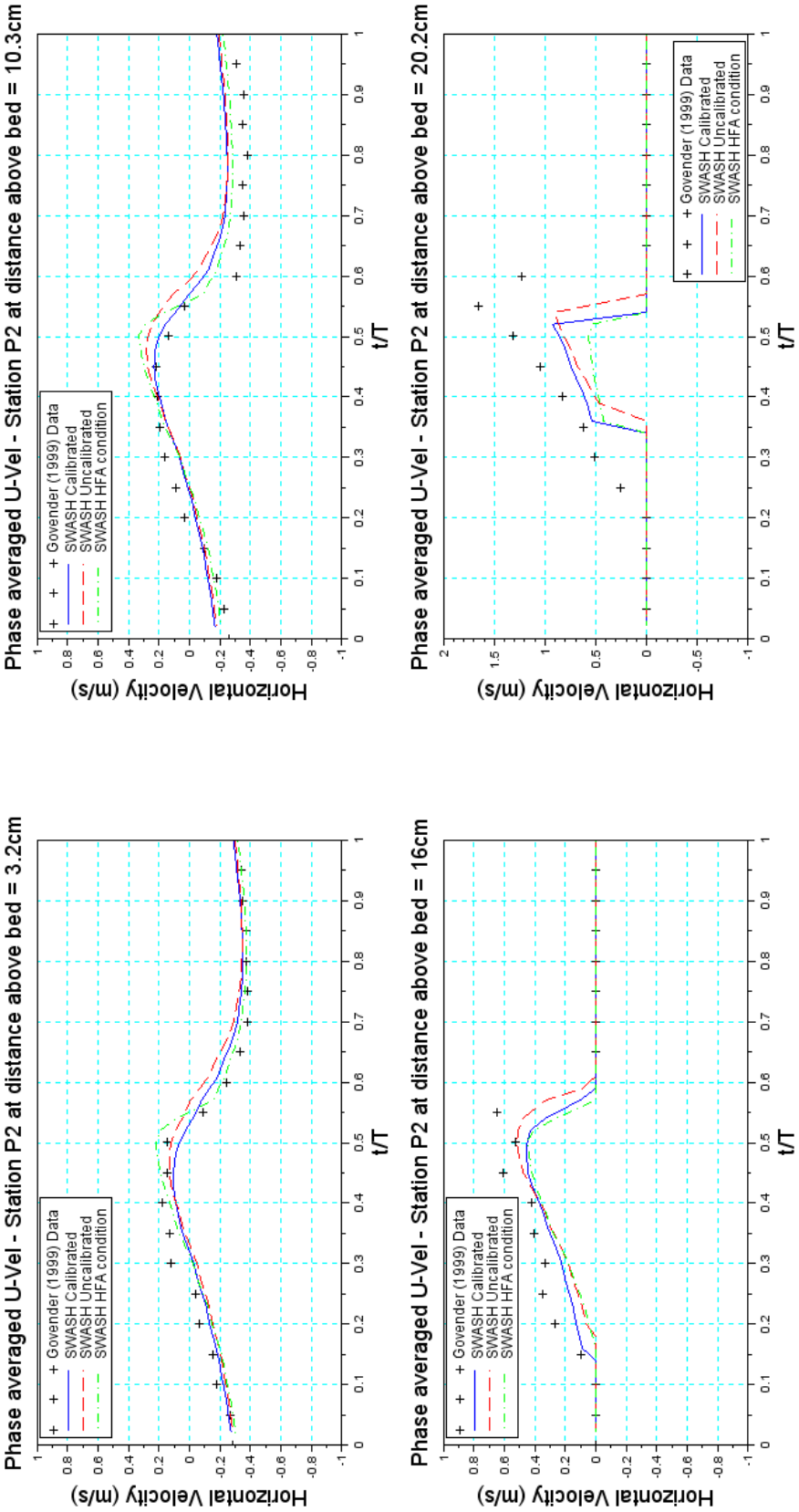

Figure B.41: Govender (1999) vs. SWASH modelled phase averaged horizontal velocity after spilling wave breaking (Note the increase in scale of the y-axis).

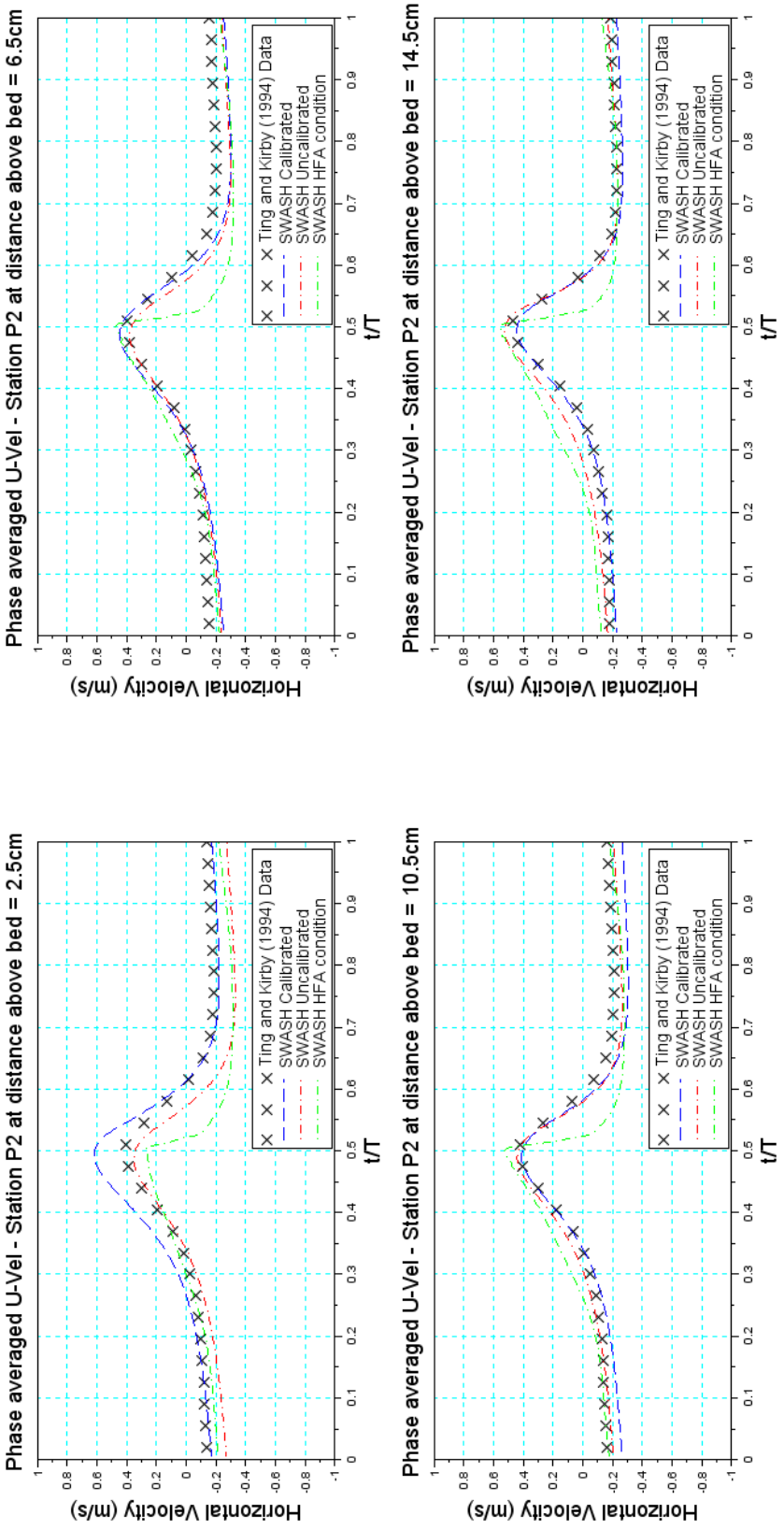

Figure B.42: Ting and Kirby (1994) vs. SWASH modelled phase averaged horizontal velocity after spilling wave breaking

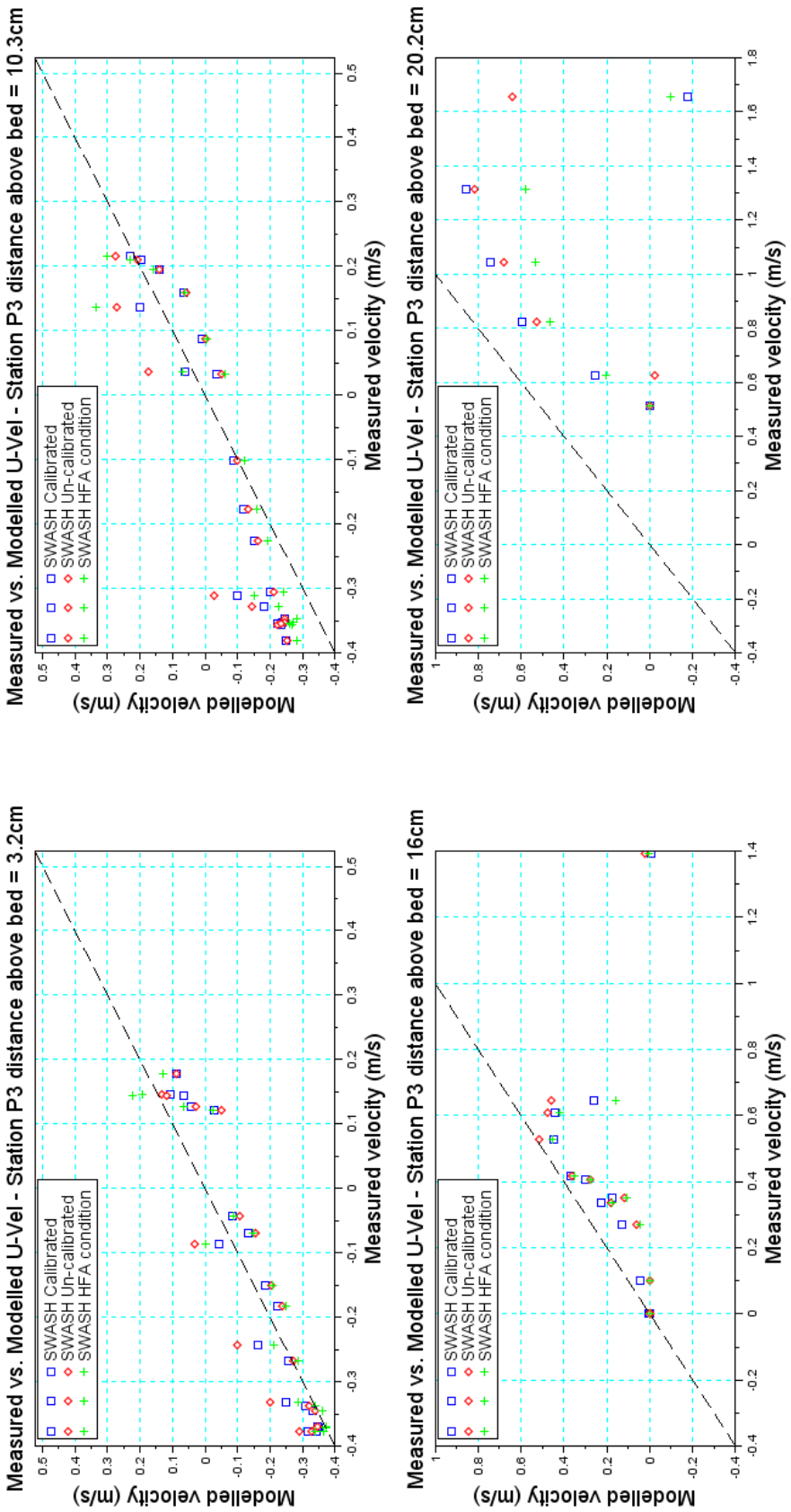

Figure B.43: Measured vs. modelled horizontal velocity after spilling wave breaking for the Govender (1999) and SWASH modelled time series

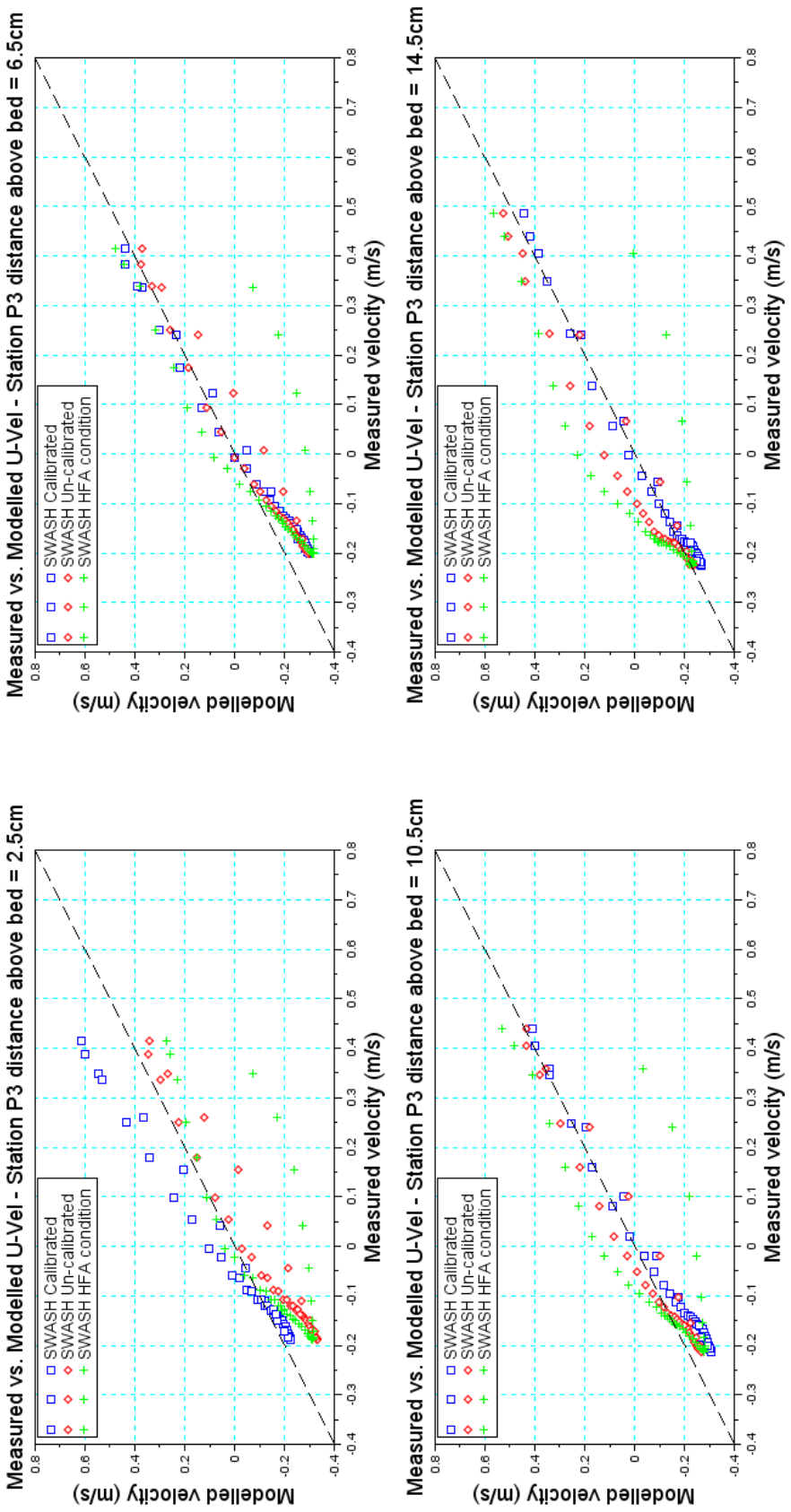

Figure B.44: Measured vs. modelled horizontal velocity after spilling wave breaking for the Ting and Kirby (1994) and SWASH modelled time series

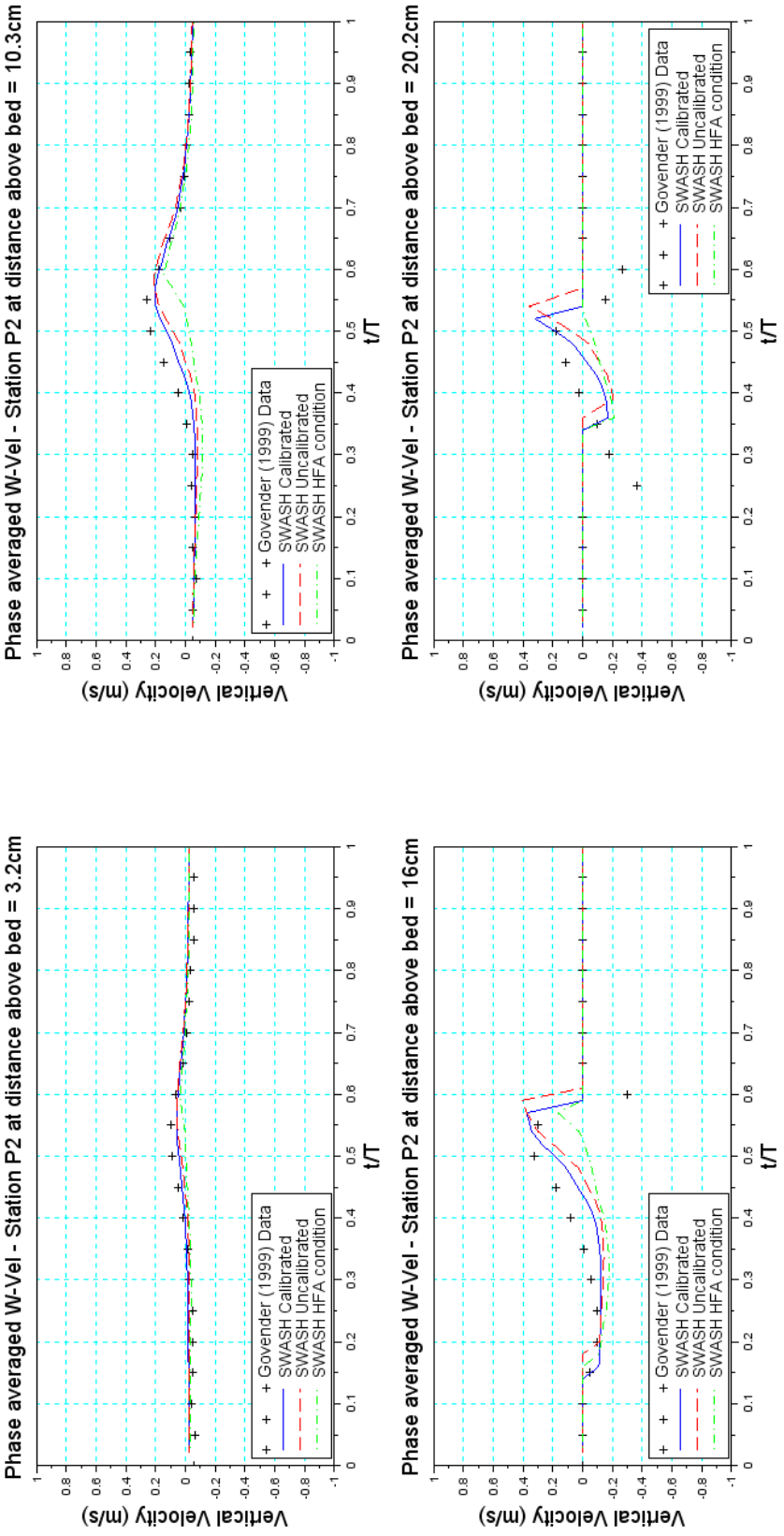

Figure B.45: Govender (1999) vs. SWASH modelled phase averaged vertical velocity after spilling wave breaking

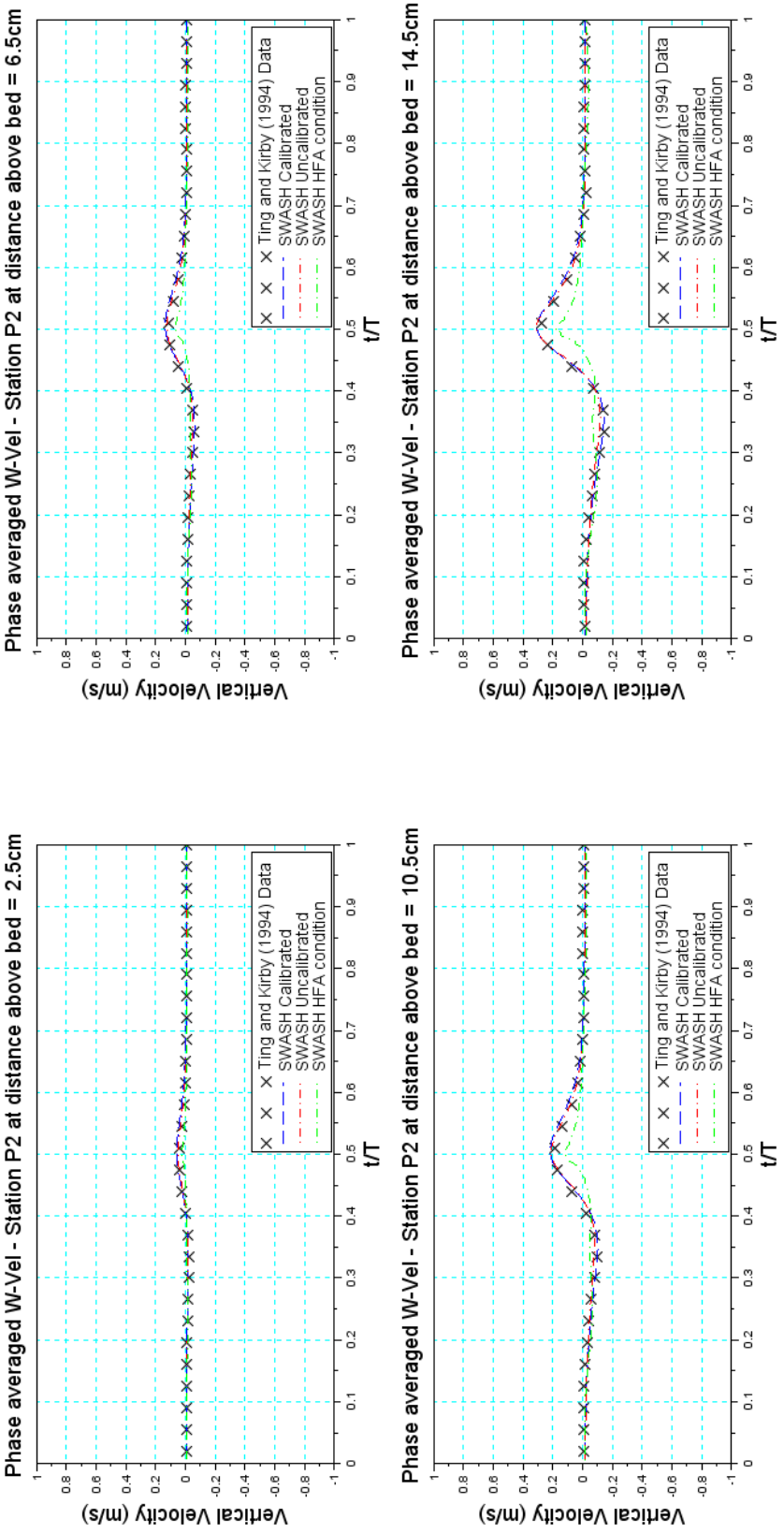

Figure B.46: Ting and Kirby (1994) vs. SWASH modelled phase averaged vertical velocity after spilling wave breaking

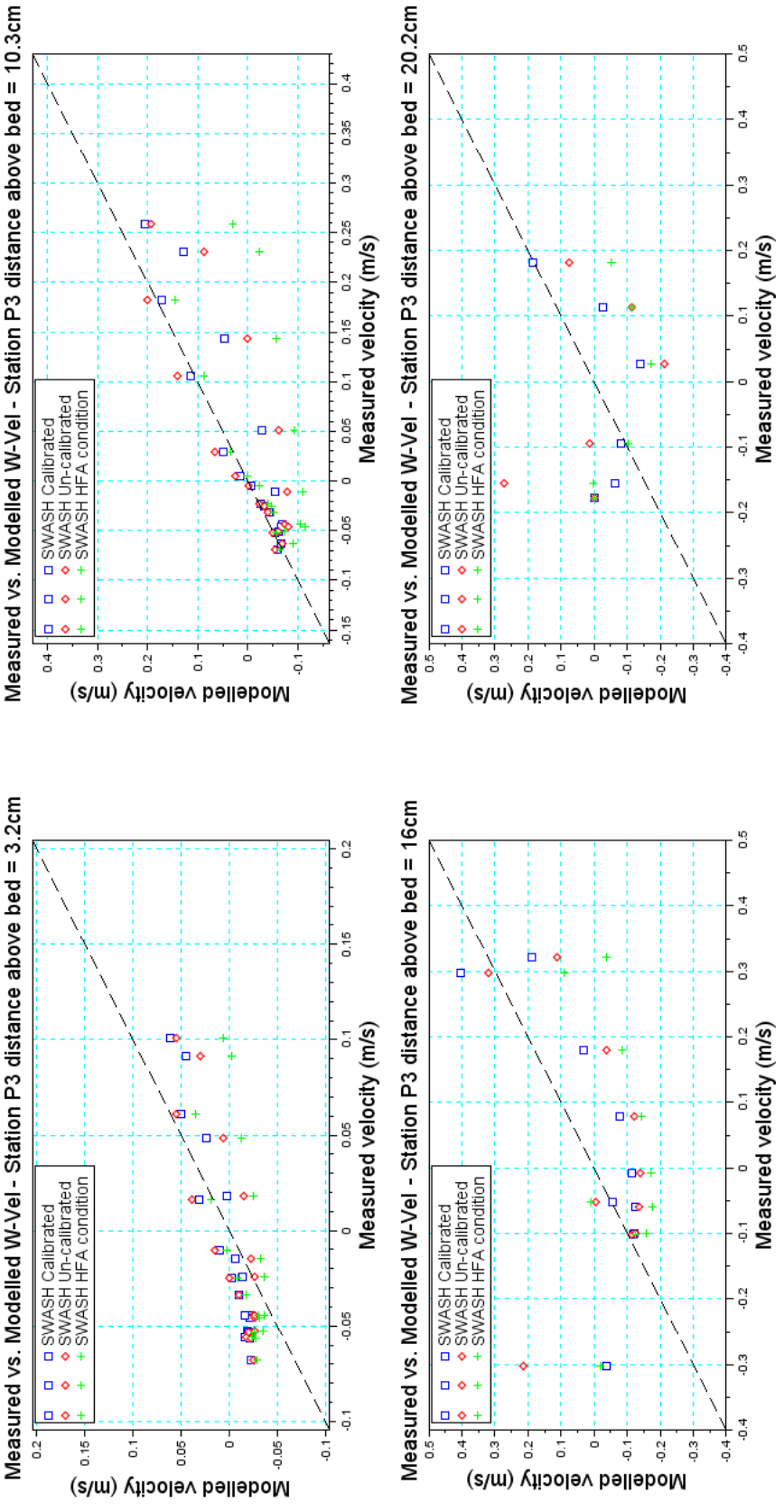

Figure B.47: Measured vs. modelled vertical velocity after spilling wave breaking for the Govender (1999) and SWASH modelled time series

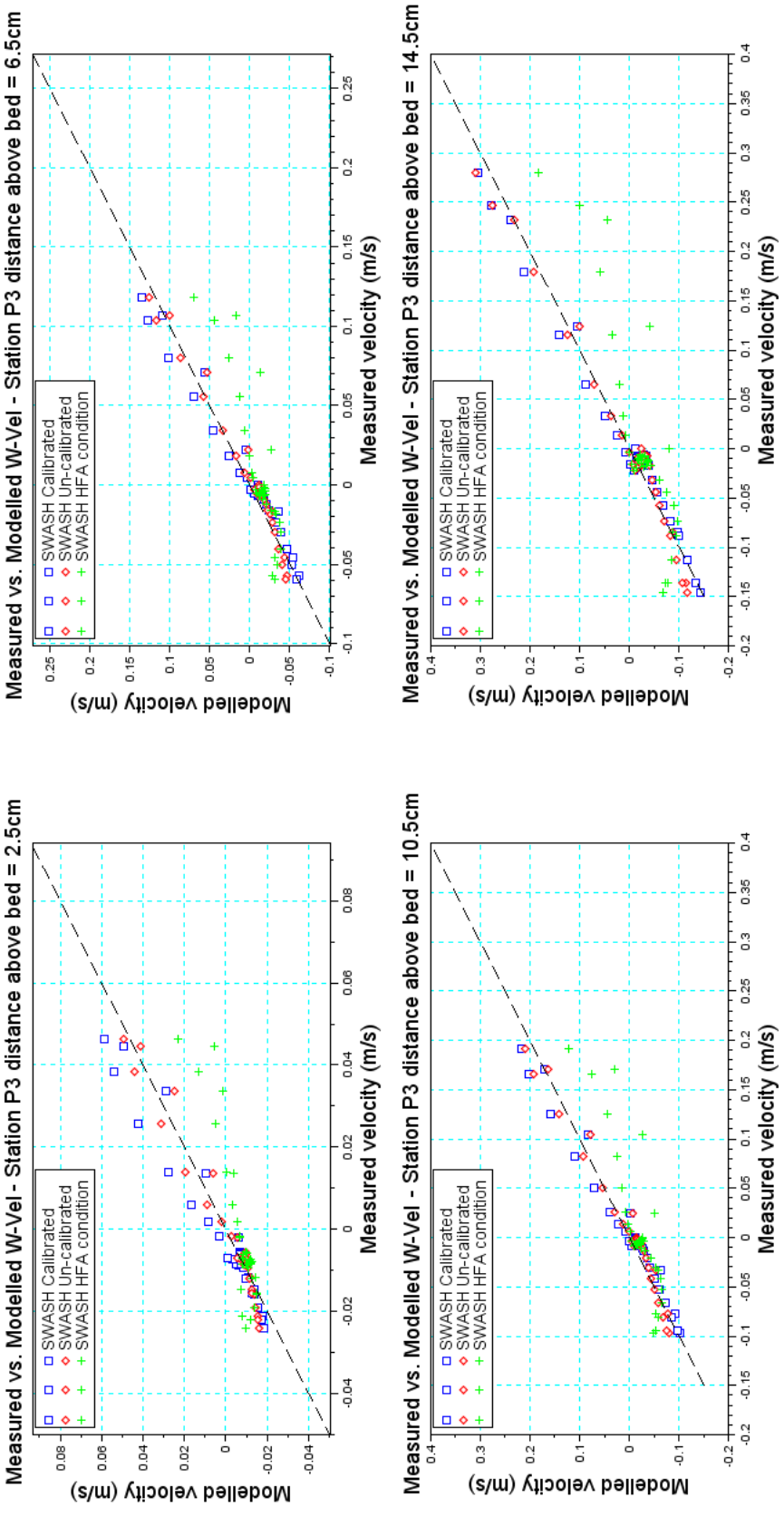

Figure B.48: Measured vs. modelled vertical velocity after spilling wave breaking for the Ting and Kirby (1994) and SWASH modelled time series

B.3 Turbulence results

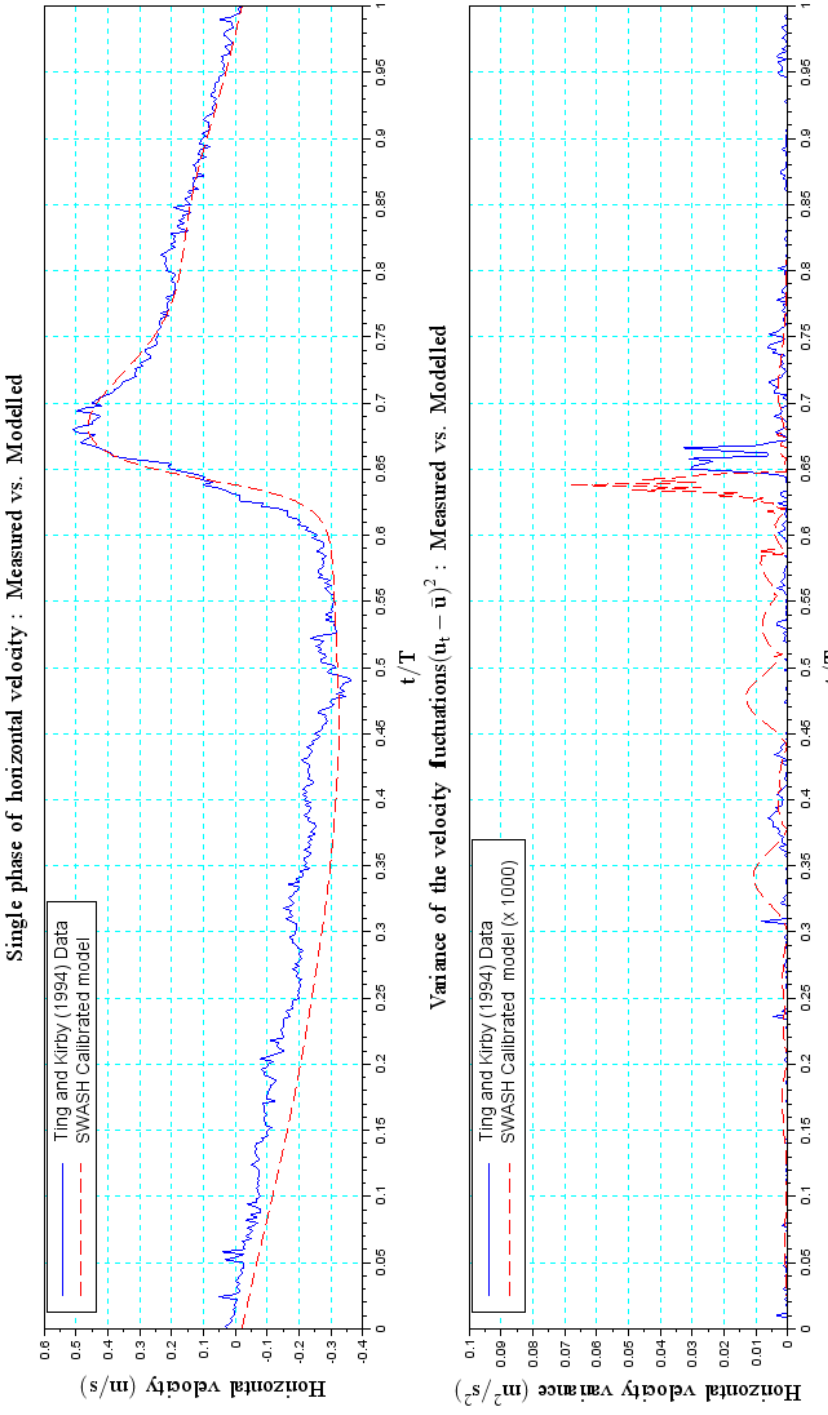

Figure B.49: Ting and Kirby (1994) vs. calibrated SWASH modelled instantaneous horizontal velocity for one plunging wave phase (upper panel). Variance in the horizontal velocity fluctuations (lower panel). Note that the SWASH data is magnified by a factor of 1000.

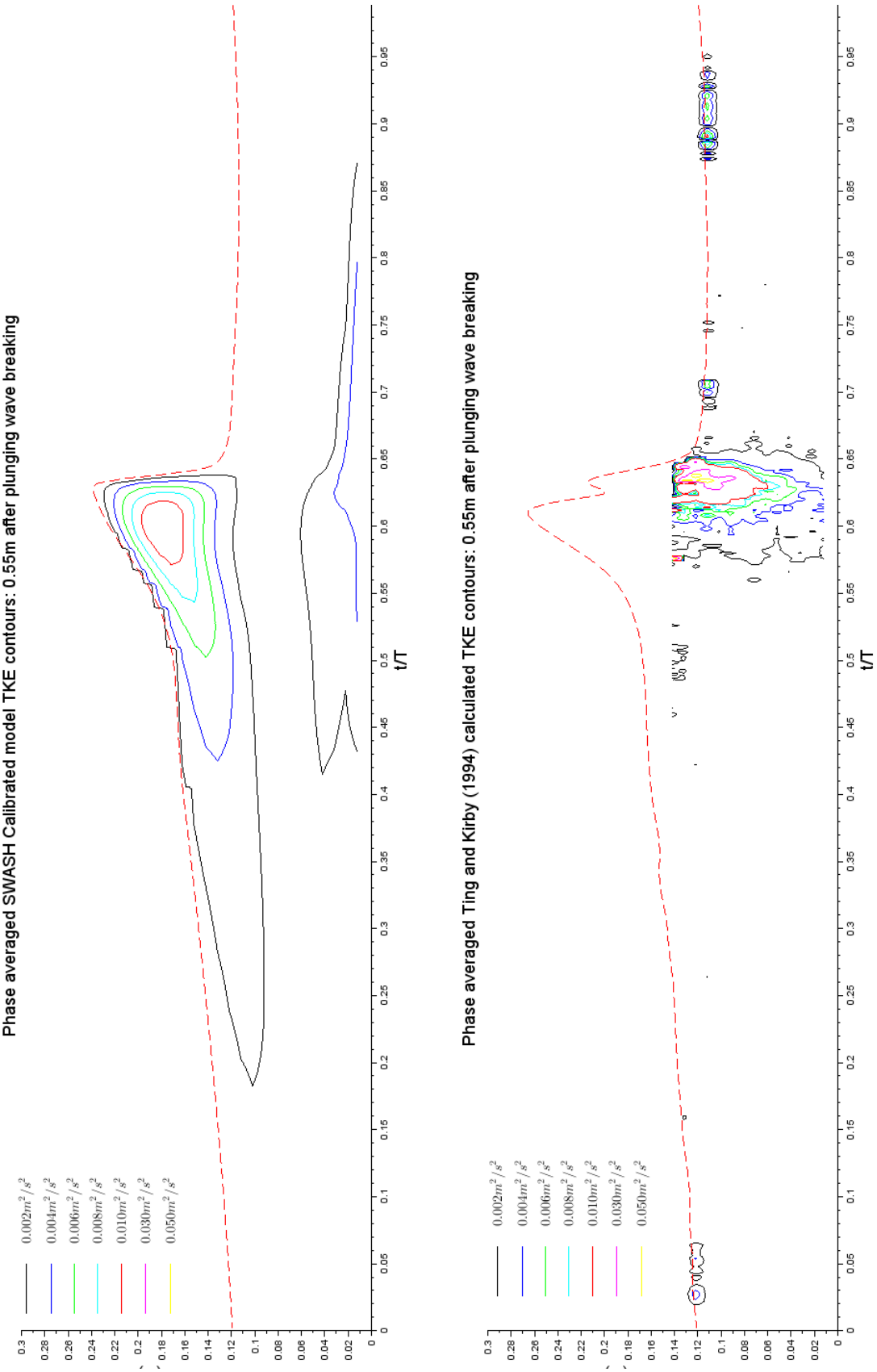

Figure B.50: SWASH modelled phase averaged TKE contours for the plunging wave approximately 0.55m after the breaking point (top panel) and the calculated TKE from the Ting and Kirby (1994) data (bottom panel).

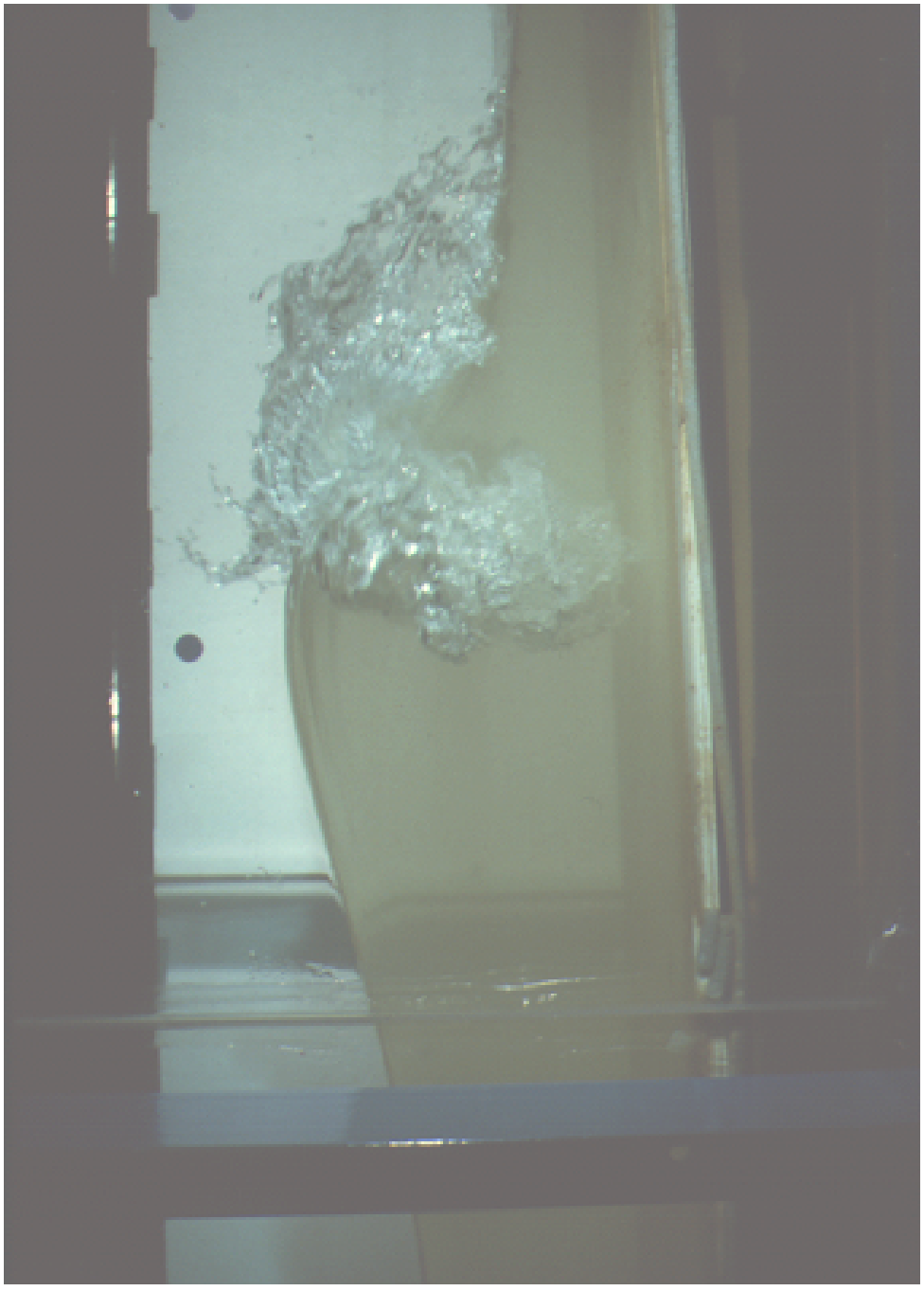

Figure B.51: Photographic image of the plunging wave taken during the Ting and Kirby (1994) laboratory experiments. The image is taken approximately 0.55m from the breaking point. The image was supplied by the authors

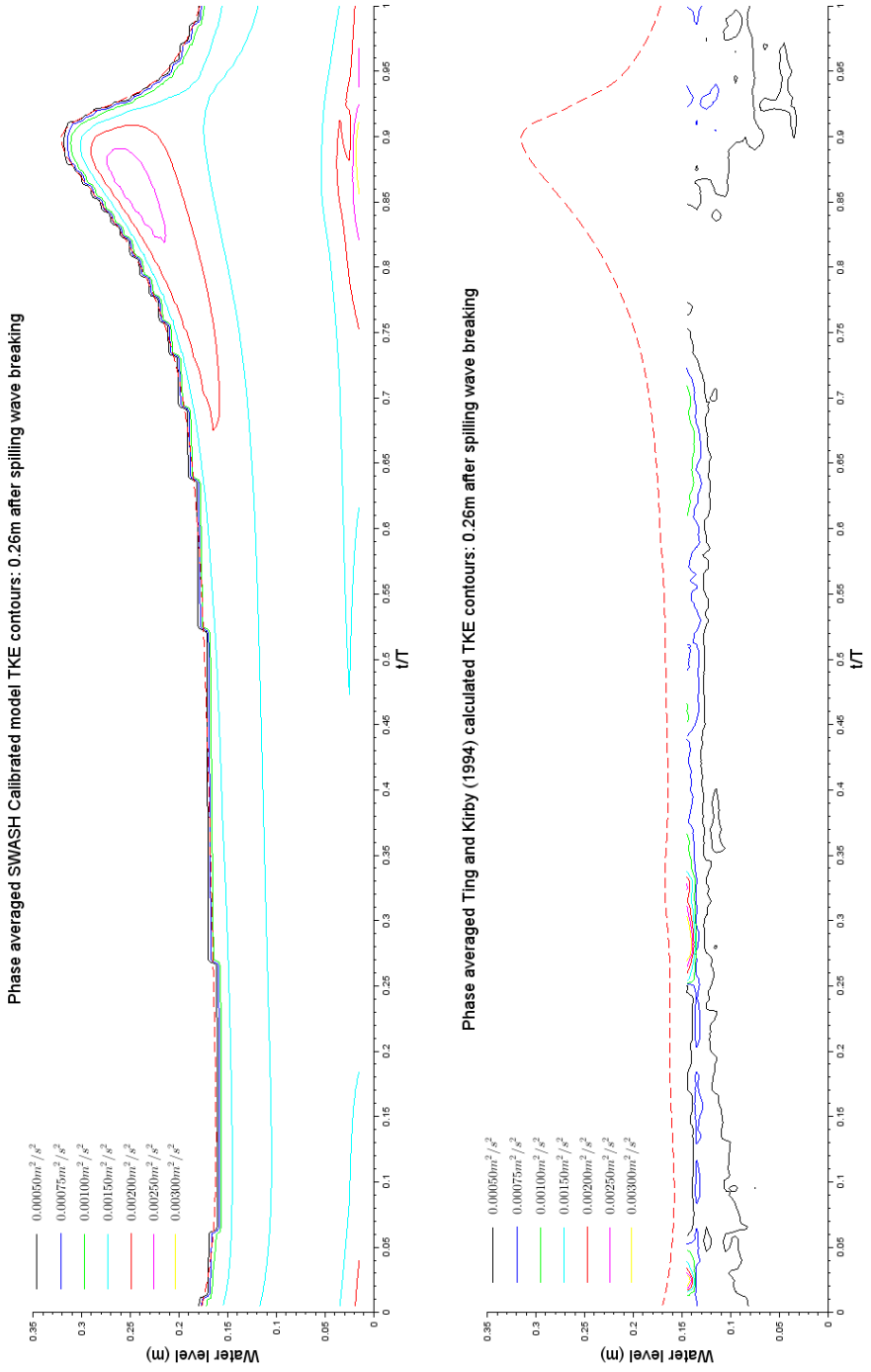

Figure B.52: SWASH modelled phase averaged TKE contours for the spilling wave approximately 0.26m after the breaking point (top panel) and the calculated TKE from the Ting and Kirby (1994) data (bottom panel).

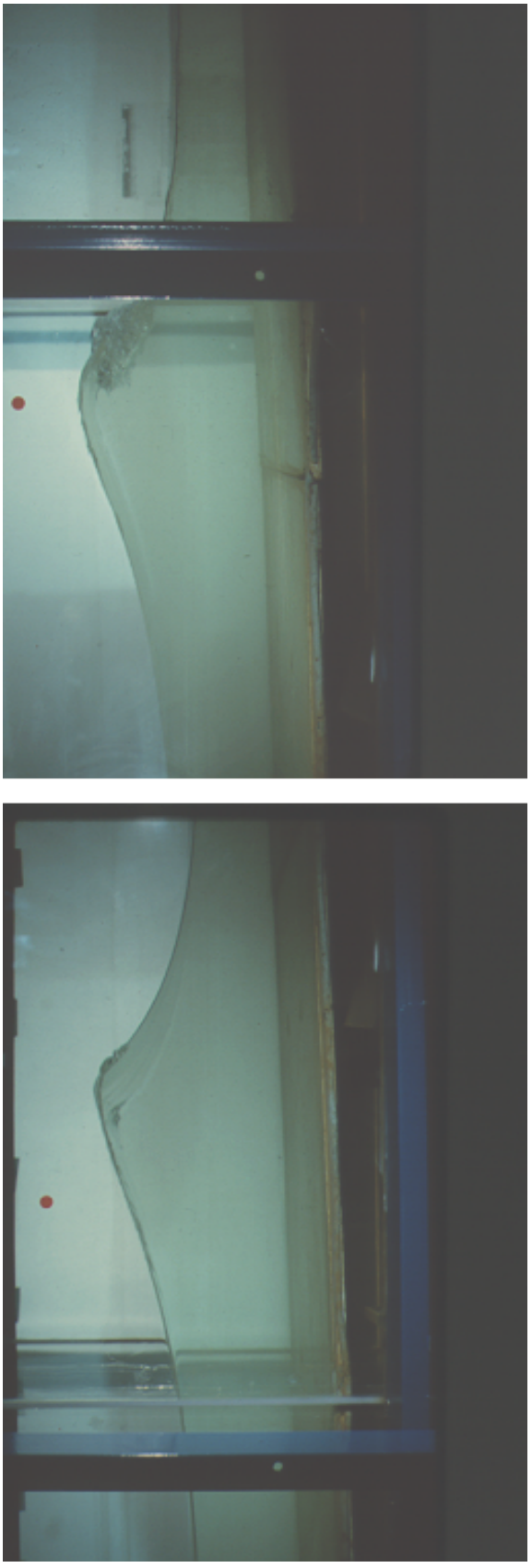

Figure B.53: Photographic images of the spilling wave taken during the Ting and Kirby (1994) laboratory experiments. The images are taken at the breaking point (left image) and at approximately 0.55m from the breaking point (right image). The images are supplied by the authors.

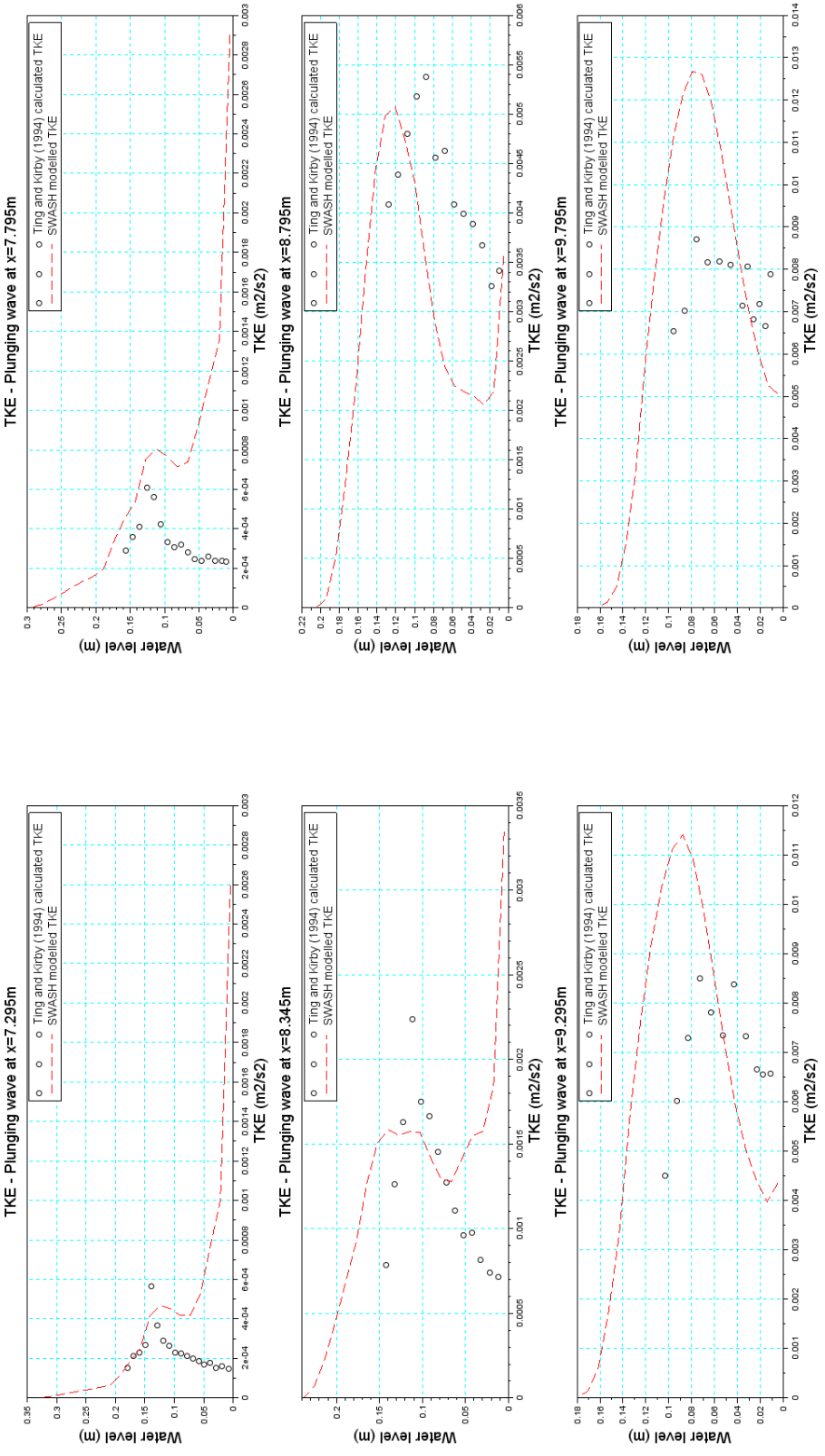

Figure B.54: Time averaged SWASH modelled TKE plotted against the Ting and Kirby (1994) data TKE calculated from the instantaneous velocities for various cross-shore positions in the flume - plunging wave

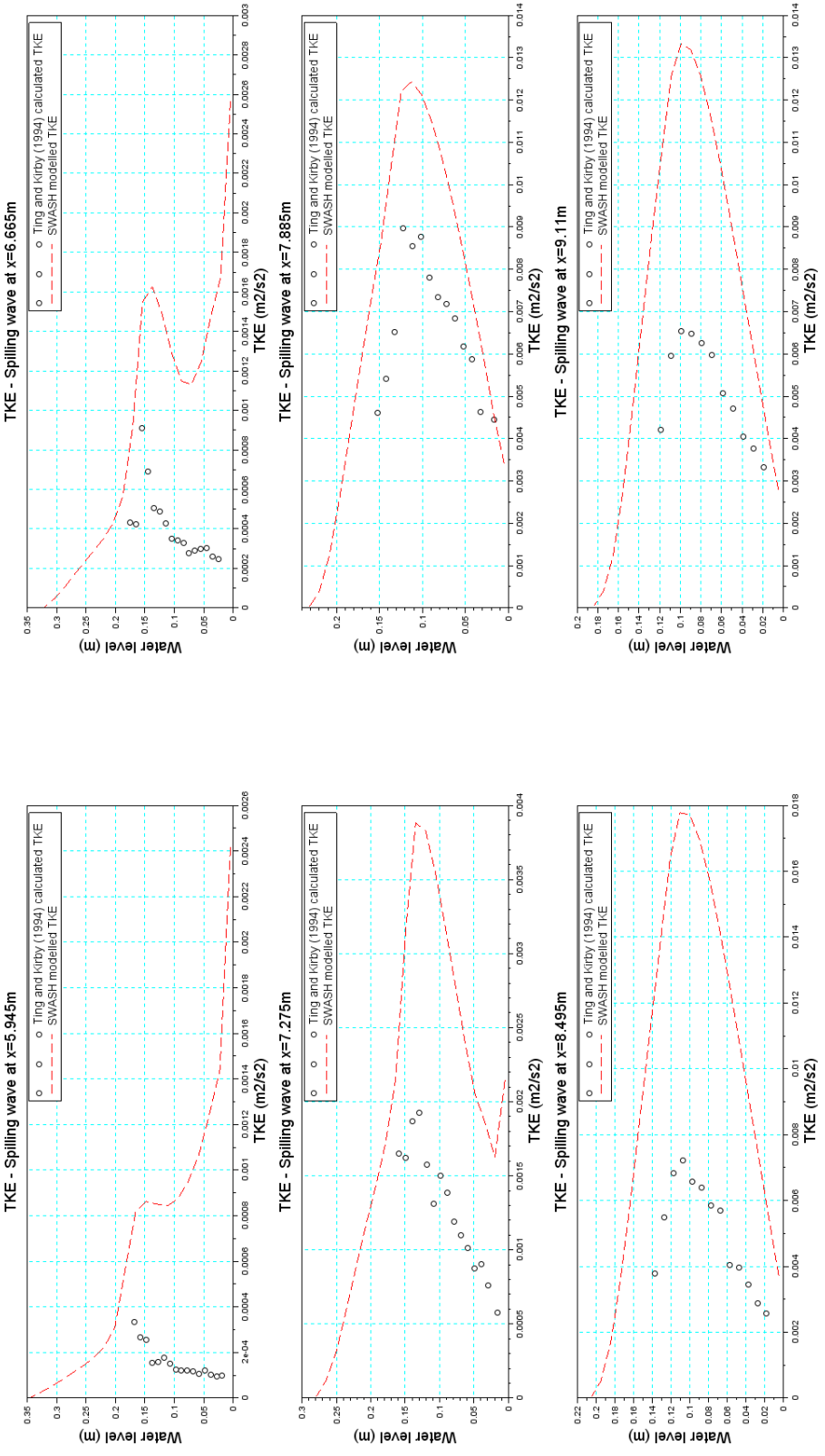

Figure B.55: Time averaged SWASH modelled TKE plotted against the Ting and Kirby (1994) data TKE calculated from the instantaneous velocities for various cross-shore positions in the flume - spilling wave